ENZYME IMMOBILISATION AND CATALYSIS IN ORDERED MESOPOROUS SILICA

Graham Michael Smith

A Thesis Submitted for the Degree of PhD
at the
University of St. Andrews

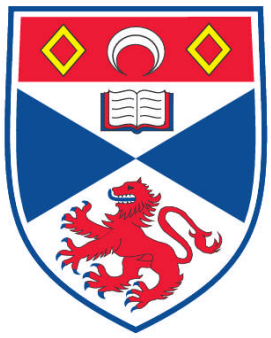

2008

Full metadata for this item is available in
Research@StAndrews:FullText
at:
https://research-repository.st-andrews.ac.uk/

Please use this identifier to cite or link to this item:
http://hdl.handle.net/10023/573

This item is protected by original copyright

Enzyme Immobilisation and Catalysis in Ordered Mesoporous Silica

A thesis presented for the degree of Doctor of Philosophy in the Faculty of Science of the University of St. Andrews

by

Graham Michael Smith

November 2007

~

Supervisors:

Dr. N. P. Botting and Dr. P. A. Wright

Declarations

(i) I, Graham M. Smith, hereby certify that this thesis, which is approximately 48000 words in length, has been written by me, that it is the record of work carried out by me and that it has not been submitted in any previous application for a higher degree.

Date …… Signature of Candidate …….

(ii) I was admitted as a research student in October, 2003 and as a candidate for the degree of PhD in January, 2004; the higher study for which this is a record was carried out in the University of St. Andrews between 2003 and 2007.

Date …… Signature of Candidate …….

(iii) I hereby certify that the candidate has fulfilled the conditions of the Resolutions and Regulations appropriate for the degree of PhD in the University of St. Andrews and that the candidate is qualified to submit this thesis in application for that degree.

Date …… Signature of Supervisor …….

(iv) In submitting this thesis to the University of St Andrews I wish access to it to be subject to the following conditions: for a period of 1 year from the date of submission, the thesis shall be withheld from use. I understand, however, that the title and abstract of the thesis will be published during this period of restricted access; and that after the expiry of this period the thesis will be made available for use in accordance with the regulations of the University Library for the time being in force, subject to any copyright in the work not being affected thereby, and a copy of the work may be made and supplied to any bona fide library or research worker, that my thesis will be electronically accessible for personal or research use, and that the library has the right to migrate my thesis into new electronic forms as required to ensure continued access to the thesis. I have obtained any third-party copyright permissions that may be required in order to allow such access and migration.

Date …… Signature of Candidate …….

Acknowledgements

I would like to thank everybody who has helped me during the course of this PhD, especially my supervisors Nigel and Paul for their excellent support and guidance. Thanks to all of the NPB and PAW group members past and present, particularly Robbie and Lyndsey. Thanks to Sylvia Williamson, for the excellent materials analyses. Thanks to everyone who made my time at St. Andrews special, especially Huanyu. Thanks to Dr C. Reeve and Dr. D. Pears of Avecia, and Dr. K. Treacher, formerly of Reaxa for their support. Thanks to Dr. D. Apperley of the EPSRC Solid State NMR facility at Durham University for the solid state NMR analyses. Thanks also to Prof E. Duguet and research workers at the ICMCB, Bordeaux for facilities and assistance with zeta potential measurements. Finally, thanks to EPSRC and Avecia for funding.

Dedication

This thesis is dedicated to my parents, Mike and Carol.

Abstract

A range of mesoporous materials based on SBA-15 have been prepared and characterised. The materials were templated by neutral block copolymer P123, and typically have a hexagonal (p6mm) pore structure, with high surface areas and narrow pore size distributions. The removal of the surfactant template by calcination and solvent extraction has been investigated. The aqueous stability of this material, and the hydrolysis of the surface was studied.

Organic functional groups were incorporated into the silica surface by co-condensation, or by post synthesis grafting. A range of functional groups were incorporated, including amine, carboxy, allyl and thiol groups. The pore size of the materials was controlled by the addition of trimethoxybenzene during synthesis, which significantly increased the pore size and uptake capacity of the materials.

The adsorption of CALB by SBA-15 was investigated, with support materials extracted by calcination or solvent extraction. Rapid uptake at high loading was observed, with a maximum loading of 450 mg g^{-1} measured. The leaching of the enzyme from the support was investigated, and found to be high with unfunctionalised supports. The leaching from functionalised supports incorporating sulfur groups was significantly reduced.

The activity of the immobilised CALB was measured by tributyrin hydrolysis in aqueous media, and by enantioselective transesterification of (R)-1-phenylethanol in organic media. The effect of surface functionalisation for reusability and thermal stability in aqueous systems was investigated.

Preliminary studies of supported CALB for dynamic kinetic resolution were carried out, with an investigation of acidic zeolites and a mesoporous supported catalyst for 1-phenylethanol racemisation. The encapsulation of immobilised CALB was investigated, and the activity and reusability of these systems studied.

Abbreviations

3-MPTES	3-Mercaptopropyltriethoxysilane
Å	Angstrom (1 x 10^{-10} m)
°C	Degree Celsius
µL	Microlitre (1 x 10^{-6} L)
BET	Brunauer-Emmett-Teller Surface Area Calculation
BJH	Barrett-Joyner-Halenda Pore Size Distribution Calculation
CALB	Candida Antarctica Lipase B
CCD	Charge Coupled Device
CLEA	Cross-linked Enzyme Aggregate
CLEC	Cross-linked Enzyme Crystal
CMC	Critical Micelle Concentration
DFT	Density Functional Theory
DKR	Dynamic Kinetic Resolution
DIPEA	Diisopropylethylamine
ESR	Electron Spin Resonance
FSM	Folded Sheet Material
GC	Gas Chromatography
GI	Glucose Isomerase
GOx	Glucose Oxidase
HTEABr	Hexadecylriethylammonium Bromide
IPPA	Isopropenyl Acetate
IUPAC	International Union of Pure and Applied Chemistry
L	Litre
m	Metre
MCF	Mesostructured Cellular Foam
MCM	Mobil Composition of Matter
mg	Milligram (1 x 10^{-3} g)
mL	Millilitre (1 x 10^{-3} L)
MPS	Mesoporous Silica
MTBE	Methyl Tert-Butyl Ether
nm	Nanometre (1 x 10^{-9} m)
NMR	Nuclear Magnetic Resonance
PEO	Polyethylene Oxide
PMO	Periodic Mesoporous Organosilane
PPL	Porcine Pancreatic Lipase
PPO	Polypropylene Oxide
PSD	Pore Size Distribution
SAXS	Small Angle X-ray Spectroscopy
SBA	Santa Barbara Material Series
SBF	Simulated Body Fluid
SEC	Size Exclusion Chromatography
TEM	Transmission Electron Microscopy
TEOS	Tetraethoxysilane
TGA	Thermo-Gravimetric Analysis
TMB	Trimethylbenzene
XRD	X-ray Diffraction

Contents

1. Literature Review

2. Characterisation of Mesoporous Materials

3. Mesoporous Silica Supports

4. Enzyme Assays

5. Immobilisation Within Mesoporous Supports

6. Catalysis With Immobilised CALB

7. Preliminary Studies on 2nd Generation Catalysts

8. General Conclusion and Further Work

1. Literature Review

1.1 Introduction

The use of immobilised enzymes offers many advantages over free enzyme systems for catalysis, including increased stability and simplified separation, resulting in greater re-usability, facile handling, easier purification, increased purity of product and reduced costs. The immobilisation of enzymes is of significant industrial importance as it facilitates the use of continuous processing of materials on a large scale. During large scale industrial applications, it is then possible to control this process stream for product quality and yield optimisation.[1]

There has been significant use within industry of nanostructured silica-based materials, with applications ranging from catalysts for fine chemical synthesis and petrochemical refinement,[2] to sorbants for chromatographic and environmental applications.[3] To date, the majority of these systems have been microporous silica based zeolites, with average pore sizes below 10 Å. The development of larger pore silica based materials, with average pore sizes on the mesoscale, well defined structures and narrow pore size distributions, offer the opportunity to develop a new range of catalysts with well-defined silica based support materials and immobilised enzymes.

1.2 Ordered Mesoporous Materials

1.2.1 Mesoporous Materials

Porous materials are classified, according to the IUPAC definition, into three categories: microporous materials, which have pore sizes below 20 Å, mesoporous materials, which have pore sizes between 20 – 500 Å, and macroporous materials with pore diameters larger than 500 Å.[4]

Prior to the development of ordered mesoporous silica, the availability of highly ordered mesoporous materials with a narrow pore size distributions and facile synthesis were limited. A material with a relatively narrow pore size distribution, anodic alumia, was

available, but difficult to synthesise as a bulk material, as well as having lower surface areas than the mesoporous silica materials described below.[5] An alternative, controlled pore glasses, can be produced easily on a commercial scale but have wide pore size distributions.[6]

1.2.2 Kanemite and the Mobil M41S Materials

The development of mesoporous materials began with the intercalation of alkyltrimethylammonium species into the layers of kanemite, a layered polysilicate material. The intercalation causes the condensation of the silica layers, resulting in the formation of three dimensional silicon dioxide networks.[7, 8] These materials were then calcined to produce silica networks with pore systems of 20 – 40 Å in diameter, with large surface areas of ~ 900 $m^2 g^{-1}$. The series of materials produced by this method are known as FSM-n (Folded Sheet Materials), where n is the number of carbon atoms in the surfactant used during preparation.

The development of mesoporous materials was initiated by work published by scientists working for Mobil, in which a series of mesoporous materials were produced under alkaline conditions, using surfactants as templates for the condensation of a series of silicate and aluminosilicate materials, known as M41S materials.[9] The morphology of the resultant material was found to be highly dependent upon the surfactant used during the synthesis and several different phases were produced, mirroring to some extent the mesostructural arrangement of the surfactant micelles.

MCM-41 (Mobil Composition of Matter No. 41) is composed of a hexagonal array of mesopores of uniform orientation (figure 1.1). The materials have a narrow pore size distribution that can be tailored to between 18 and 100 Å, in a controlled and continuous manner, depending on the cationic surfactant used as template. The materials have large surface areas, of over 700 $m^2 g^{-1}$ for the larger pore materials, and show good sorption properties, with over 0.7 $cm^3 g^{-1}$ for hydrocarbon uptake.[10]

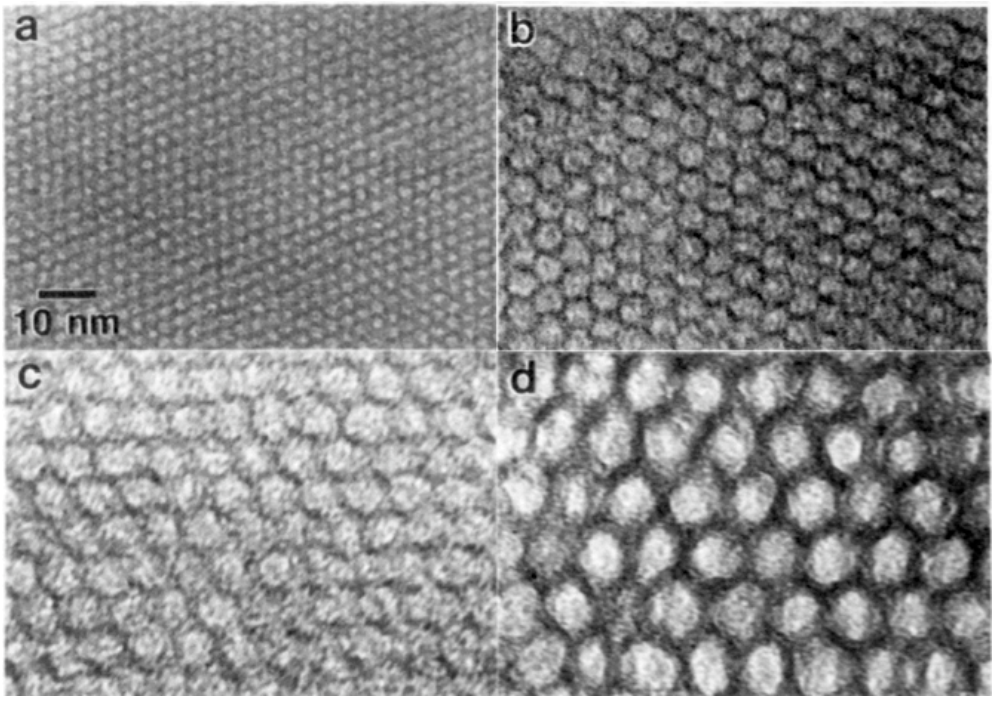

Figure 1.1: TEM images of MCM-41 with Different Pore Sizes - (a)20,(b)40,(c)65 and (d)100Å[10]

The proposed mechanisms of formation of MCM-41 are illustrated in Figure 1.2 below. There are two proposed mechanisms, the first of these via liquid crystal phase initiation, in which the silicate anions form around pre-assembled hexagonal arrays of micelles (reaction pathway 1). The second is silicate anion initiated, in which the silicate anion causes the assembly of individual micellar rods (reaction pathway 2). Of the two pathways the second is generally accepted as correct, particularly for the alkyltrimethylammonium cationic surfactants used for the synthesis of MCM-41, as the concentrations of surfactant used are unlikely to form liquid crystal phases without the presence of the silicate anion.[11]

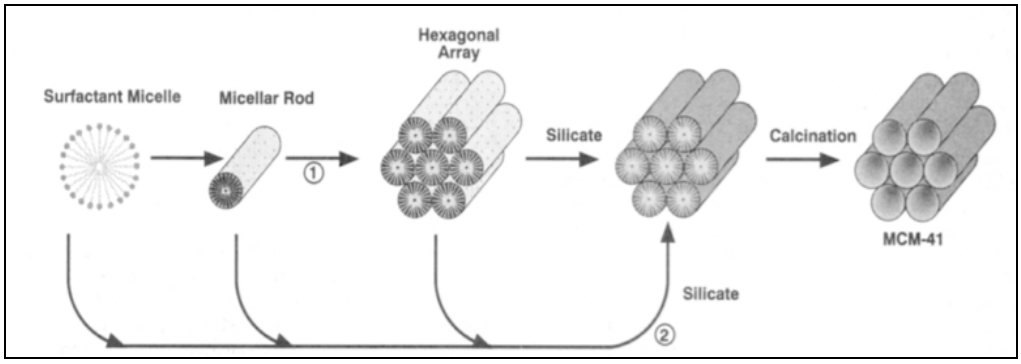

Figure 1.2: Proposed Mechanism For MCM-41 Formation[10]

In a comparison between liquid crystal templated MCM-41 and intercalation derived FSM-n materials it was found that MCM-41 has a much narrower pore size distribution, as well as much higher total pore volume, and higher hydrocarbon sorption capacity.[12] This is most likely due to incomplete conversion of the polysilicate layers of kanemite, contrasted with initial condensation of silicate anions to form a homogenous material as with MCM-41.

As the morphology of surfactant templated mesoporous materials mimics that of the surfactant liquid crystal phase, it is possible to obtain M41S family materials with different structural motifs by altering the silicon / surfactant ratio. The most significant of these is MCM-48, a material with a cubic structural motif.[11] MCM-48 is obtained when the surfactant / silica ratio is greater than one, a result that can be explained by examining the molecular packing ratio of surfactant micelles.[13]

MCM-41 and MCM-48 materials have been converted into useful catalytic materials by the incorporation of various elements into the silica structure. There are two approaches to the incorporation of metal elements into the material, one in which the elements are added to the synthesis solution and another in which the elements are incorporated after the formation of the material. A diverse range of metals have been incorporated by the co-condensation method, including titanium, chromium, vanadium, platinum, manganese, iron, copper, zinc, niobium and gallium.[14, 15] Elements that have been incorporated post-synthetically include vanadium, titanium, platinum and zirconium.[16] The incorporation of trivalent cationic elements (Al^{3+}, Ge^{3+}, Fe^{3+}) results in a negatively charged framework, which is balanced by protons, generating a material that can be used as a solid phase acid, either as a dispersion or packed for use as an ion exchange column.[17]

1.2.3 Silicate Cation Condensation

In addition to the condensation of silicate anions at high pH, a mesoporous material may also be synthesised via silicate cations in acidic media. The first material prepared by this method was SBA-1 (Santa Barbra), a mesoporous material with a cubic caged structure.[18] SBA-1 can be prepared with a hexadecyltriethylammonium bromide (HTEABr) surfactant and tetraethylorthosilicate (TEOS) in acidic aqueous media.[19, 20] The

pore size of SBA-1 can be controlled by the use of cationic surfactants of different chain lengths, with average pore sizes between 14 - 27 Å. An aluminosilicate form of SBA-1 was prepared by washing the material with aluminium chloride after calcination.[21] A mesoporous material with a hexagonal structure, denoted SBA-3, was prepared under similar conditions by changing either the condensation temperature or the acid used, with H_2SO_4 and HCl resulting in SBA-1 and with HBr and HNO_3 resulting in SBA-3.[21]

The development of mesoporous materials templated by non-ionic polymers was an important step toward the development of larger pore mesoporous materials.[22] The templating of silica by non-ionic polymers relies on hydrogen bonding interactions rather than electrostatic interactions, and as a consequence, the surfactant is typically not integrated into the structure as would a charged template and can be removed more readily.[23] For materials templated by this method it is possible to remove a substantial proportion of the template by solvent extraction.[24] Non-ionic polymers that were initially used as templates include polyethylene oxide surfactants,[25] and Tergitol[26] (a polyethylene glycol derived surfactant produced by Dow Chemical Co.).

An important development in the field of larger pore mesoporous materials was the development of SBA-15 by researchers at Santa Barbra.[27] The template used during the preparation was Pluronic P123 (BASF), a neutral triblock copolymer, with the formula $(CH_2CH_2O)_{20}(CH_2CH_2CH_2O)_{70}(CH_2CH_2O)_{20}$. The polyethylene oxide (PEO) blocks of the polymer are hydrophilic, and the polypropylene oxide (PPO) blocks are hydrophobic, resulting in the formation of micelles in aqueous media. In an acidic solution it is expected that several oxygen atoms comprising part of the P123 polymer will become protonated, increasing the strength of the interactions between polymer strands during micelle formation.[28]

The material is prepared by the addition of a silica source, typically tetraethylorthosilicate (TEOS), to an acidic aqueous solution. The silica cations that are formed in acidic media will be localised in the hydrophilic region of the micelles, and condense to form a silica matrix templated by the P123 surfactant micelles. Typically the materials obtained by this method are well ordered mesoporous materials of hexagonal symmetry (*p6mm*). A TEM micrograph showing the hexagonal structure of SBA-15 is shown below (figure 1.3).

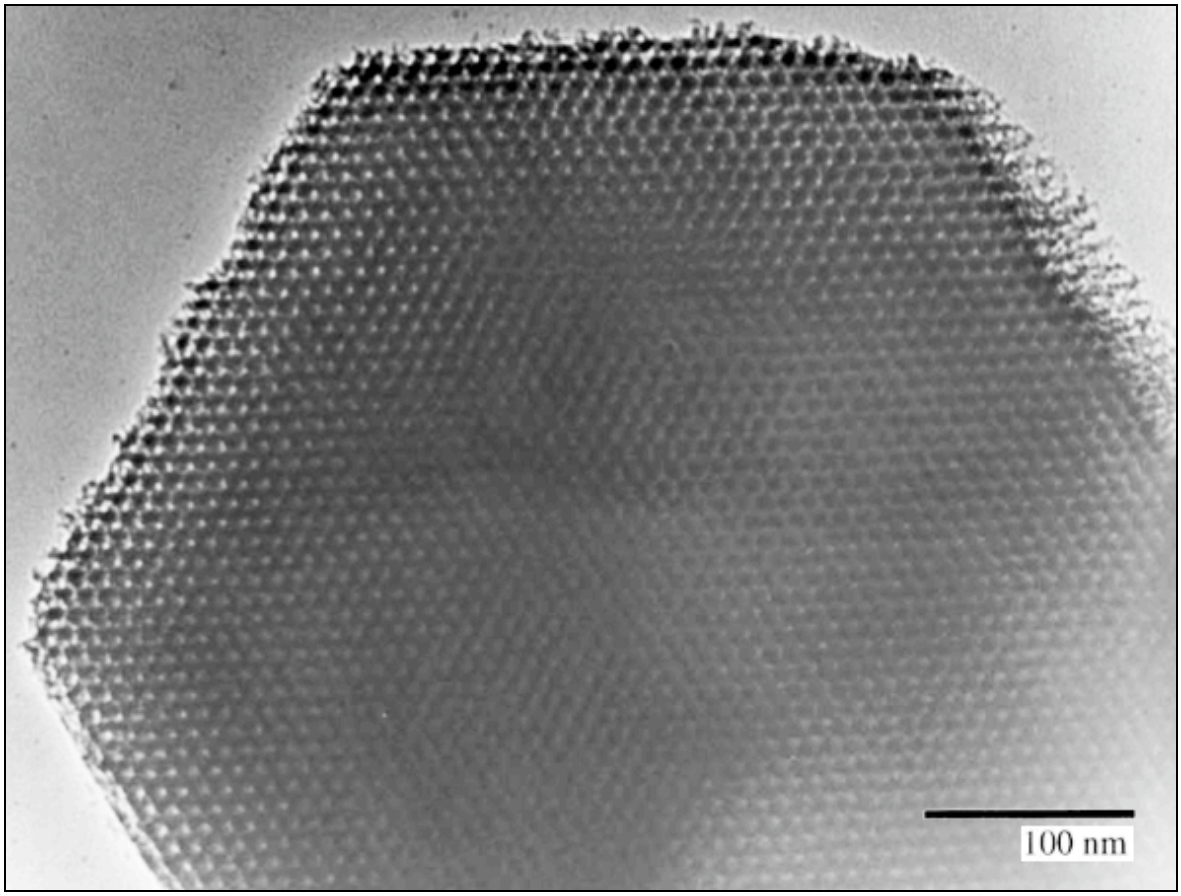

Figure 1.3: SBA-15 TEM Image[29]

The pore system of SBA-15 consists of a mixture of mesopores and micropores, the relative composition of which is determined by the synthesis conditions, including temperature of condensation and aging temperature.[30] This microporosity was investigated by nitrogen adsorption and inverse platinum imaging by electron microscopy.[31] By increasing the synthesis temperature the degree of microporosity is reduced, and the mesopore size is increased.[32] There is evidence that the microporous regions are due to the incorporation of P123 polymers within the walls of the condensed silica phase, that when removed leave micropores perpendicular to the mesopores.[33] This is supported by the structural stability of inverse carbon images of SBA-15 that have been produced once the silica has been removed (see section 1.2.7). The pore size of the materials obtained by this method can be controlled, with average pore size diameters between 46 - 300 Å, either by controlling synthesis properties[27] or by the addition of micelle swelling agents (see section 1.2.4). The TEOS : Surfactant ratio is typically 60:1 for the formation of SBA-15, but if

the ratio is increased, the material is not templated completely, and constrictions are formed within the pore system.[34]

SBA-15 is extremely thermally stable, with calcination temperatures up to 1173 K retaining the porosity of the material.[31] In addition, unlike several other mesoporous materials including MCM-41 and MCM-48,[35] SBA-15 also has high hydrothermal stability,[36] and has been shown to be thermally stable in boiling water (6 h).[28] This has been attributed to the thickness of the silica walls between the pores,[36] which are much thicker for SBA-15[30, 37] than for M41S materials.[38, 39] Studies have shown that there is an increase in hydrothermal stability after the wall thickness of MCM-41 has been increased.[40] The *in vitro* stability of SBA-15 has been studied, by measuring the formation of hydroxyapatite in simulated body fluid (SBF), which formed around SBA-15 particles after 30 days.[41]

The ratio of hydrophobic and hydrophilic regions for a Pluronic surfactant will change the morphology of the micelle that is produced.[42] This in turn, will have a direct effect on the structure of the silica matrix that is formed by condensation in the hydrophilic part of that micelle. Increasing the ratio of PEO / PPO favours formation of cubic phase materials, while reducing this ratio favours formation of lamellar phase materials (which are often not stable after removal of the template).[28]

1.2.4 Expansion of the Surfactant Micelle

Control of the morphology of the mesoporous material requires control of the morphology of the surfactant template micelle. By controlling the dimensions of the micelle the material's pore size diameter and surface area can be altered to produce the desired material properties. To use this approach to increase the average pore size of a material an organic co-solvent can be added to the synthesis mixture, which intercalates the hydrophobic portion of the micelle, increasing the size of the micelle. However, the addition of this co-solvent may also disrupt the micelle and result in amorphous silica, so the ratio of surfactant to co-solvent must be carefully controlled to avoid synthesis of amorphous silica.

This approach was used to increase the pore size of SBA-15, in which 1,3,5-trimethylbenzene (TMB) was added to the synthesis mixture, resulting in larger pore sizes

(figure 1.4).[28] The average pore size was increased dramatically with up to 300 Å diameter pore sizes after calcination. This approach was also used to expand the pore size diameter of SBA-1, when prepared with the cationic surfactant HTEABr.[21]

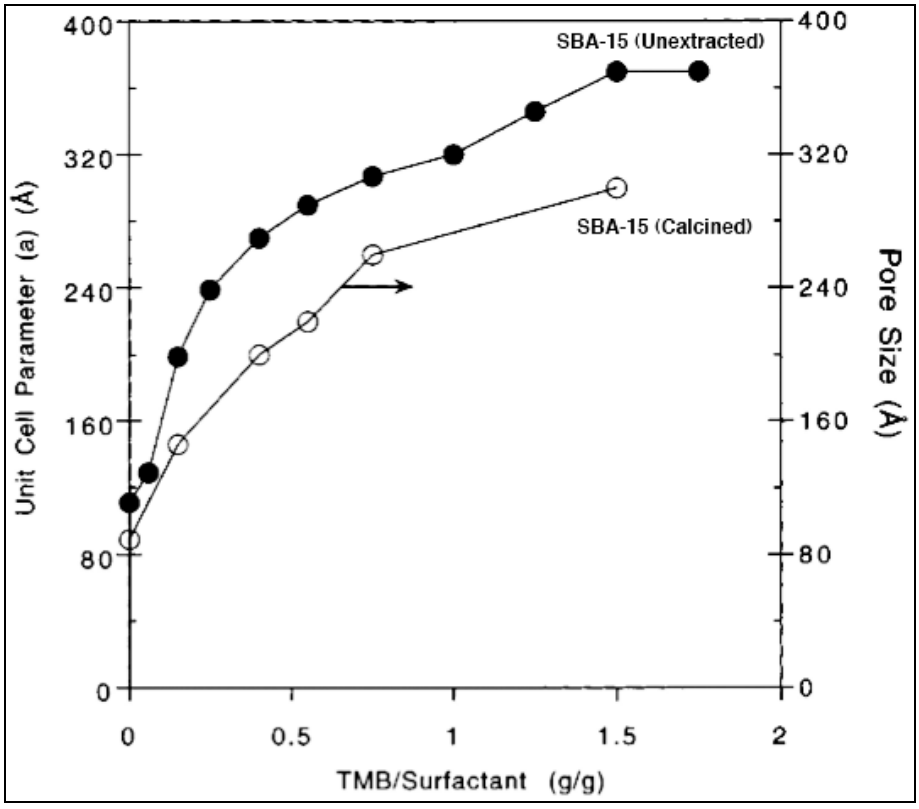

Figure 1.4: The Effect of TMB / Surfactant Ratio on Pore Size[28]

By increasing the TMB / Surfactant ratio the formation of microemulsions can provide an alternate template for the condensation of silica.[43] The materials produced via this approach are known as mesostructured cellular foams (MCFs).[44] These materials have a uniform array of spherical cells, with openings between spheres to form porous channels.[45] The phase transition to microemulsions has been reported to be between values of 0.2 - 0.3 for the co-solvent / surfactant ratio for SBA-15.[46] Figure 1.5 shows the changes in structure as the co-solvent / surfactant ratio increases, with a transition from a hexagonal array of pores to a more disordered array of spherical cells with interconnecting windows.

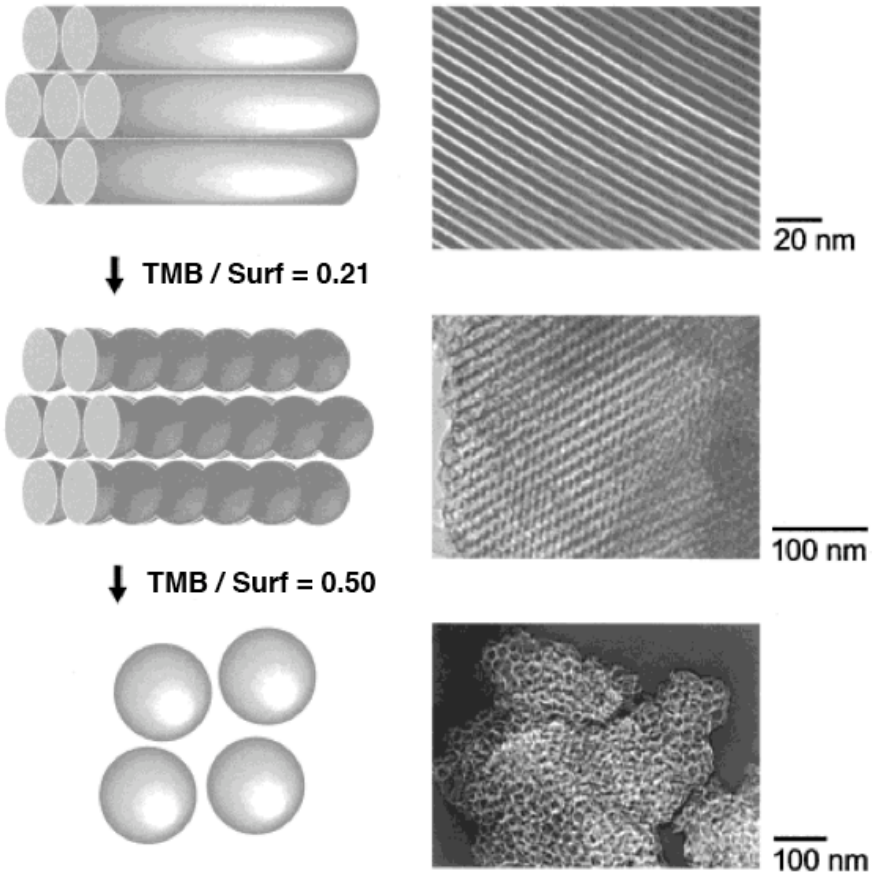

Figure 1.5: Effect of Micelle Structure on Solid Morphology by TEM[46]

Other studies in this area have investigated the effects of different organic co-solvents upon the morphology of the silica materials produced. Several solvents have been studied, as well as mixtures of solvents, including alkanes.[47] Good results were obtained using decane as a swelling agent and also with various functionalised benzenes, although TMB was found to have the greatest effect upon the pore size and morphology of the resulting material.[48]

1.2.5 Incorporation of Organic Functional Groups

The incorporation of organic functional groups is a method of controlling the surface properties of a silica matrix. By changing both the hydrophilicity of the surface and by incorporating materials that are likely to exhibit localised charges materials can be prepared for specific applications. For example, a material may be made more or less polar to be used as a selective adsorbent,[49] or the surface may be tailored to a particular protein amino acid for support applications.[29]

There are three main routes to the incorporation of organic functional groups into a material, illustrated below (figure 1.6). These are either, addition during synthesis (co-condensation), addition of an organic containing reactive group after synthesis (grafting), or by using bridged alkoxysilane precursors as the silica source, generating periodic mesoporous organosilicas (PMOs).

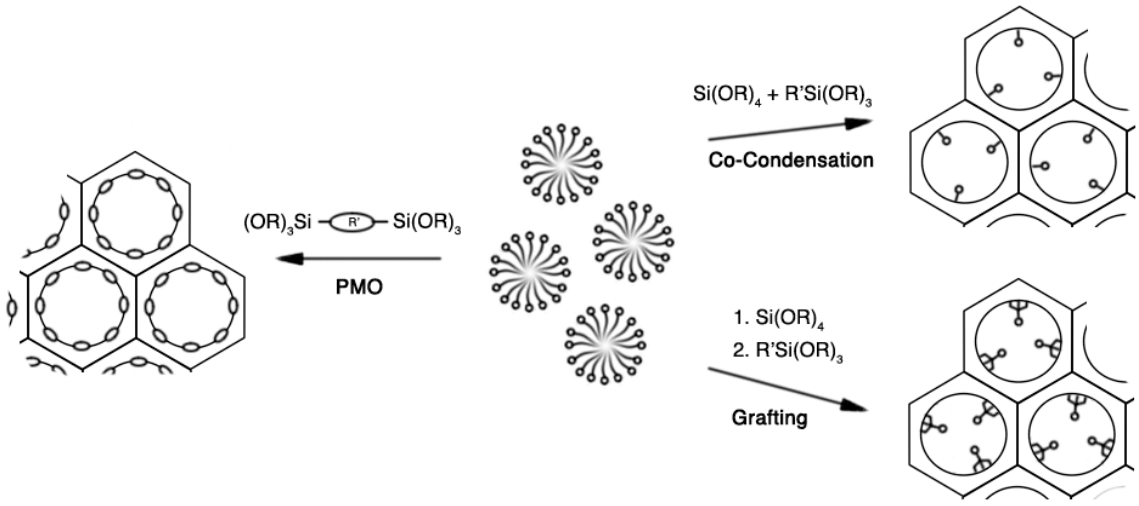

Figure 1.6: Approaches to Organic Functional Group Incorporation

Co-condensation is a facile route to the incorporation of organic functional groups into a mesoporous material. In this method an organic group is added, typically as a trialkyloxysilane, in the desired ratio to the silica source (generally TEOS). The advantages of this route are that the organic group is well integrated into the material, and generally well dispersed, depending on the functional group, and the material is prepared in a one-pot synthesis (figure 1.7). A disadvantage of co-condensation is that the addition of organoalkoxysilane to the synthesis mixture may disrupt the formation of the material, resulting in a less ordered structure, or can even cause the mesostructure of the material to change. This can be observed when the addition of 3-mercaptopropyltriethoxysilane is increased from 2 to 7 molar percent in the synthesis of SBA-15, the morphology of the structure changes from a hexagonal phase to a cubic phase.[50]

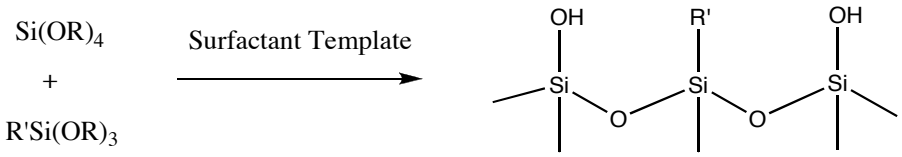

Figure 1.7: Co-condensation Approach to Organic Functional Group Incorporation

The second method of organic functional group incorporation is post-synthesis modification, also called grafting. The surface of a condensed silica material is generally composed of free silanol groups, which are available to react with several species allowing the introduction of organic functionality into the material. The silanol groups will react with alkoxysilanes of structure $R'Si(OR)_3$ (figure 1.8), chlorosilanes of structure $ClSiR'_3$, or less commonly, silazines of structure $HN(SiR_3)_3$. The advantage of this approach is that the mesostructure of the material is retained, although the pore size is reduced by the addition of a layer of material within the pores. A potential disadvantage of this approach is that the grafted species may not react completely (only one or two Si-O-Si linkages) or may react preferentially at the entrances of the pore openings, which may hinder diffusion of species into the pore system resulting in poor dispersal of organic groups through the material, and may even block access to the pore system depending on the size of the organic group introduced.[51]

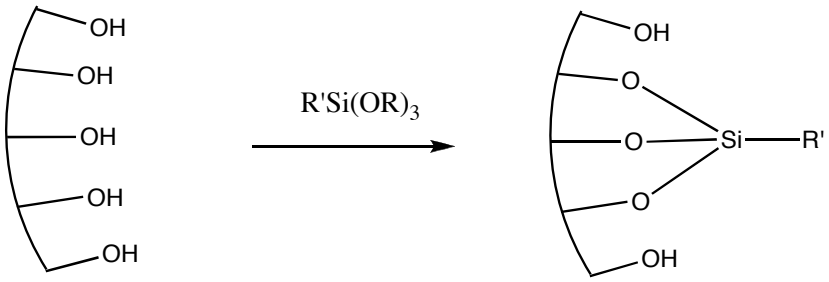

Figure 1.8: Grafting Approach to Organic Functional Group Incorporation

In sol-gel chemistry the use of bridged organosilanes of structure $(RO)_3Si\text{-}R'\text{-}Si(OR)_3$ is well established as a route to obtain organic-inorganic hybrid materials.[52] This approach can be used to prepare hybrid mesoporous materials by addition of a suitable surfactant, in either acidic or basic media (figure 1.9). The materials prepared by this method are called periodic mesoporous organosilicas (PMOs). The first examples of

materials of this type were prepared independently by three research groups.[53-55] The advantage of this approach is that the organic groups are incorporated homogeneously into the silica matrix, although the range of functional groups that can be used is limited.

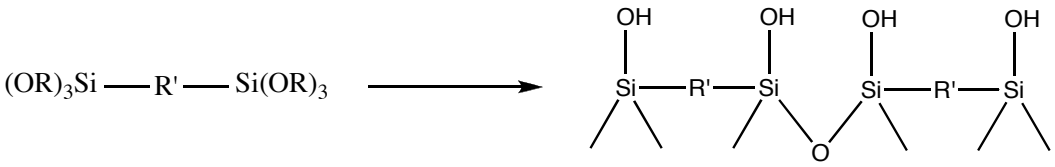

Figure 1.9: General Route to Periodic Mesoporous Organosilane Synthesis

1.2.6 Removal of the Surfactant Template

The use of surfactants as templates to prepare well ordered mesoporous materials results in a material in which the pore system is filled by surfactant after preparation of the material. This surfactant must therefore be removed from the materials if they are to be used for any sort of application. From thermogravimetric analysis, about 40% of the weight of unextracted SBA-15 is comprised of surfactant.[30] There are many different methods for removal of this surfactant, depending on the degree of surfactant removal required and the elemental composition of the material.

The most widely used method for surfactant removal is calcination,[56] in which the material is heated to a high temperature, typically greater than 400 ºC, with a flow of an oxygen containing gas. This can be either an oxygen / nitrogen mixture, or can be two temperature cycles, firstly heating with a flow of nitrogen gas, followed by a temperature cycle with a flow of oxygen or oxygen containing gas. This method of surfactant removal is very efficient, and gravimetric analysis and elemental analysis show no residual surfactant. One disadvantage to calcination is that the average pore size of the material will shrink, due to silanol condensation, with shrinkage of up to 20% average pore diameter after calcination.[30] There are some materials in which the presence of the template is integral to the stability of the material, and removal of the template causes the pore structure to collapse, this can be observed with some of the lamellar phase materials such as MCM-50, which are not stable after calcination as the silicate layers collapse to give amorphous silica.[57]

However, if the material contains organic functionalisation, or other elements that may be affected by calcination, then there are several alternative methods for surfactant removal. Solvent extraction is the most widely used of these, with conventional lab solvents, generally ethanol, used to extract the surfactant. This can be carried out efficiently by the use of a Soxhlet extraction setup. The advantage of this method of surfactant removal is that the surfactant is not destroyed and can be easily recovered and reused to template new material. Typically, 70 - 80% of the surfactant can be removed by conventional solvent extraction. An alternative to conventional solvents is the use of supercritical carbon dioxide as the extracting solvent, which was used to extract up to 93% of the cetyltrimethylammonium hydroxide template from MCM-41.[58]

Another method is microwave assisted template decomposition, using strong nitric acid and hydrogen peroxide as the solvent to remove about 95% of the surfactant from SBA-15 (Figure 1.10).[59] From nitrogen adsorption measurements on the microwave extracted sample, it can be observed that the pore size does not shrink to the same extent as with a calcined sample, most likely due to a lower degree of silanol condensation. This can be observed by comparing the solid-state silicon NMR spectra for the two samples which shows the presence of a Q^3 peak due to the silanol group, observed with the microwave treated sample, yet not for the calcined sample.

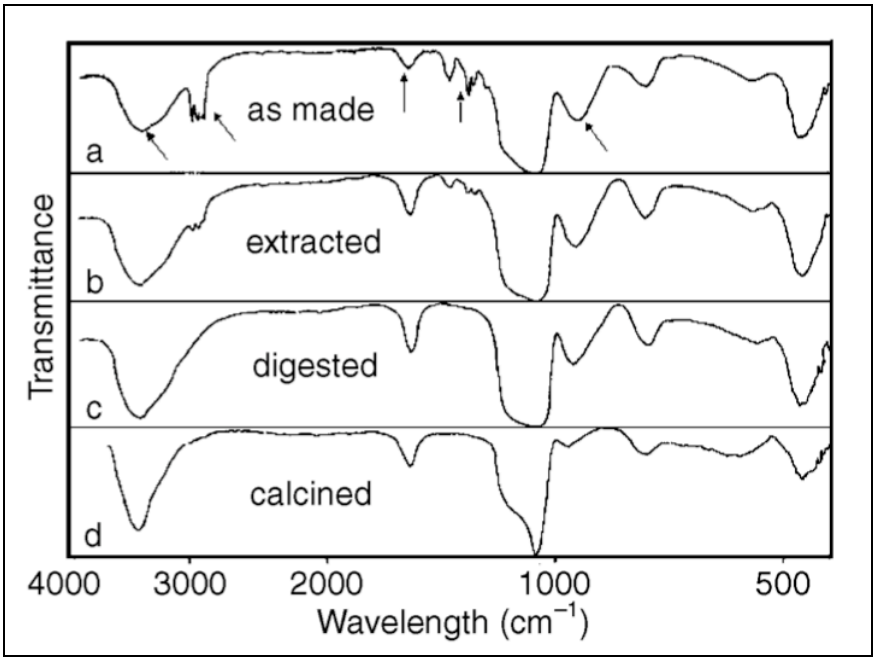

Figure 1.10: Residual Surfactant Analysis by IR Spectroscopy

Another method of surfactant removal is that of treatment with ozone.[60] The degradation of ether linkages by ozone through an oxidative mechanism can be achieved with high concentrations of ozone over a short time period,[61] or by lower concentrations of ozone over a longer period.[62] The second approach is straightforward, as the sample is placed under a 20W UV lamp (180 and 254 nm), which generates ozone from oxygen in the atmosphere. The mechanism for the breakdown of surfactant is not clear, but it has been suggested that the formation of a radical species is responsible for the decomposition of ether linkages within the surfactant.[63]

With SBA-15 and other large pore materials templated by neutral block copolymers there is a significant degree of microporosity present in the material. The surfactant within the microporous channels can be removed after removal from the mesoporous channels using a two step extraction process (figure 1.11).[64] The first step is the removal of surfactant from the mesopores with a strong acid followed by the removal of surfactant from the micropores by calcination. The decomposition of the surfactant was found to be much slower for the PEO blocks than for the PPO blocks of the P123 copolymer, which was attributed to the incorporation of the PEO ends of the template within the silica wall.[65] This supports previous studies showing the presence of a corona of micropores perpendicular to the mesopore after calcination.[33]

Figure 1.11: Two Step Surfactant Template Extraction

1.2.7 Inversion of the Pore System

An inverse image of a mesoporous material, similar to a photographic negative, can be produced from mesoporous materials by a process known as nanocasting. The first carbon nanocast of a mesoporous material was denoted CMK-1, and was prepared by the polymerisation of sucrose within the pore system of MCM-48, followed by the removal of

the silica network using sodium hydroxide in ethanol.[66] The material underwent appreciable structural shrinkage after removal of the silica framework, and retained an inverse pore system to that of MCM-48 (figure 1.12).

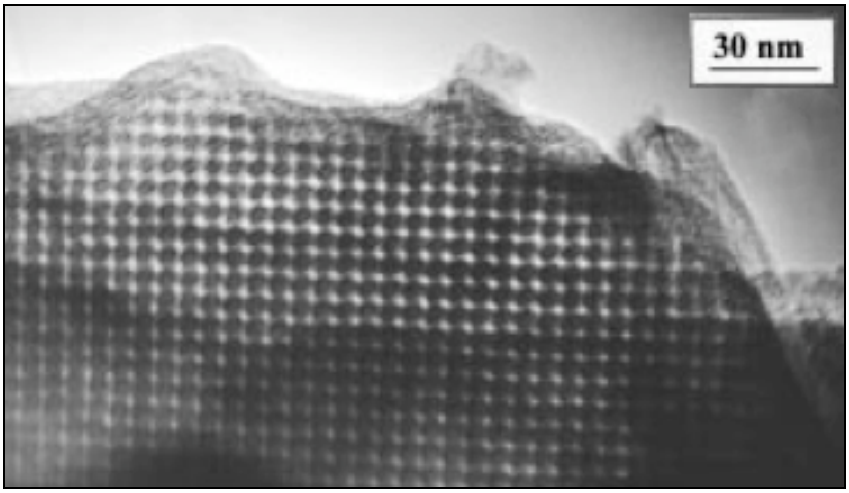

Figure 1.12: TEM Image of CMK-1 Nanocast[66]

The nanocasting process is applicable to a wide range of mesoporous materials and several different carbon monomers can be used, including furfuryl alcohol, acrylonitrile and acetylene. A nanocast of SBA-15, denoted CMK-3 (figure 1.13), was produced in which an exact inverse of the hexagonal structure was retained.[67] That the structure was retained intact, without collapse of the ordered cylindrical pores, is indirect proof that the micropores are perpendicular to the mesoporous channels, and must be bridging separate mesopores in SBA-15.

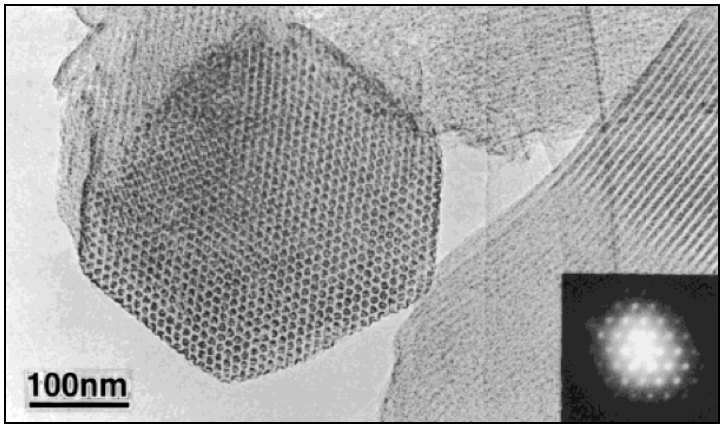

Figure 1.13: TEM Image of CMK-3 after Silica Removal[67]

1.3 Enzyme Immobilisation

1.3.1 Advantages of Enzyme Immobilisation

Enzymes are remarkable catalysts, with high turnovers at mild conditions when compared to transition metal catalysts.[68] However, the reduced stability of enzymes in solution can be a problem, as is separation and purification of the product of a reaction. These disadvantages can be reduced by the immobilisation of enzymes, which has several advantages.[1]

The primary reason for binding enzymes to support materials is to improve their stability, and binding can prevent or reduce the effect of several deactivation routes. The most important of these is deactivation by aggregation, in which the protein macromolecules agglomerate and precipitate from solution. This is the primary reason for deactivation by organic solvents, and is greatly reduced when an enzyme is immobilised, as there is little mobility of the enzyme. This separation is also an important reason for the increased stability of proteases when immobilised, as autolysis (self-splitting) is greatly reduced.[69] Another important deactivation route of enzymes is unfolding, in which the tertiary structure of the protein is lost, and is generally an irreversible process.[70, 71] Prior to isolation, proteins exist in crowded environments within a cell, and the confinement of proteins can significantly improve the stability.[72, 73]

Other advantages of immobilised enzymes that are of significant importance to industrial chemists are the reduced costs of catalysis with immobilised enzymes. This is a combination of several factors, including increased reusability of bound enzymes,[74] low temperature and pressure conditions,[75] simplified separation without use of chromatography,[76] low contamination of the product with protein impurities,[77] and heterogeneous catalysts for continuous flow reaction systems.[78] Another advantage is the ability to catalyse enantioselective reactions in aqueous media, which is difficult to achieve with traditional metal catalysts.[76]

1.3.2 Methods of Enzyme Immobilisation

There are five conceptual approaches to the immobilisation of enzymes, the method used depends on the application for which the enzyme will be used, and the stability of the

particular enzyme toward the immobilisation method. These methods are covalent attachment, surface adsorption, protein cross-linking, gel / polymer entrapment and encapsulation (figure 1.14).[79]

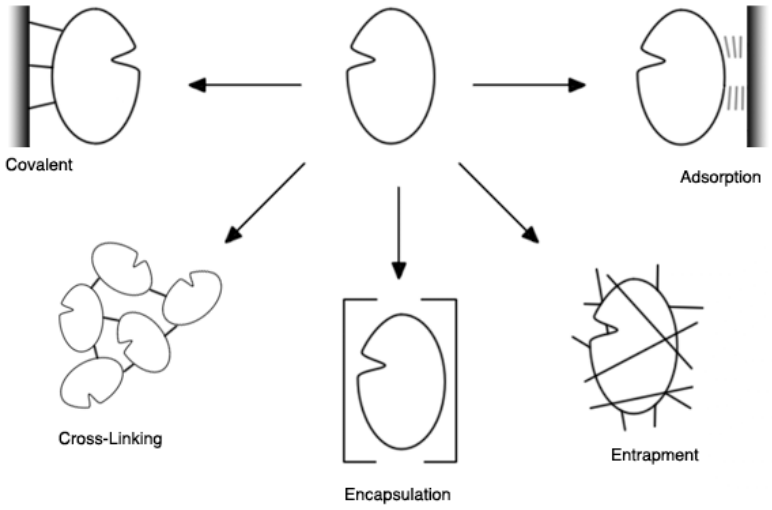

Figure 1.14: Approaches to Enzyme Immobilisation

Covalent attachment of an enzyme to a support material is a method of immobilisation that can be used to prepare a very stable biocatalyst. The advantages of this method are that the leaching of protein from the support into solution during reaction are minimised, reducing contamination of the product, and increasing the life of the catalyst. However, the protein must be stable toward the binding process, as conformational changes can be induced that can denature an active enzyme. An enzyme can also be bound in an orientation in which the active site is not accessible to substrate, which can reduce overall catalytic activity.

The adsorption of a protein onto a support material is a route to immobilisation that is suitable for many different applications. The choice of support material is decided by several factors, including stability, interaction with the desired protein, as well as solubility properties in the solvent used for catalysis. The main advantage of this approach is that it is widely applicable to many types of enzymes, and the activity of those enzymes is usually retained, as the forces on the enzyme are very mild when compared to covalent attachment and cross-linking.

The cross-linking of enzymes via intermolecular covalent bonds is a method to produce an immobilised enzyme without the use of a carrier material. Cross-linked enzymes (CLEs), have been produced by the use of glutaraldehyde.[80] This method was not ideal however, and resulted in low activities, as well as low stability and problems with handling of the gel-like material that was obtained. The method was improved by the development of cross-linked enzyme crystals (CLECs) and cross-linked enzyme aggregates (CLEAs).[81] However, the lack of a support material tends to produce a material that is unsuitable for column packing without an additional support material. In addition, the enzyme activity is often significantly reduced, as the enzyme active sites within the aggregate / crystal are rendered inaccessible to substrate.

The entrapment of an enzyme within a polymer matrix or gel can lead to stable catalysts, usually with very few preparation steps when compared to other methods. Alginate gels have been used to prepare immobilised biocatalysts, with α-amylase entrapment retaining the enzyme activity and giving good improvements in stability.[82] The entrapment of enzymes in silica sol-gel materials has been extensively studied in the literature,[83, 84] with good retention of enzyme activity and increases in enzyme stability.[85] The stability of the support material is largely dependent upon the drying method, with evaporation yielding more dense xerogels and drying with supercritical carbon dioxide yielding very low density aerogels.[86]

Encapsulating enzymes within a support material is a method in which the enzymes are isolated and trapped within a host material, which reduces aggregation and autolysis (for proteases), without modification of the enzyme. As with adsorption systems, the encapsulation methods that have been developed are widely applicable to many enzymes, with the additional benefit that leaching is greatly reduced. However, the accessibility of the enzyme may be reduced, and catalytic rates can be limited by diffusion of substrate through the support.

A polymer membrane encapsulation system was used to encapsulate bovine serum albumin (BSA) and horseradish peroxidase (HRP) with significant improvements in enzyme stability compared to the free proteins.[87] An array of polymeric microcapsules was prepared and used for the immobilisation of enzymes, including glucose oxidase, subtilisin and alcohol dehydrogenase, with retention of activity.[88]

1.3.3 Industrial Applications of Immobilised Enzymes

Immobilised enzymes are attractive catalysts for industrial application due to their high selectivity and low running costs when compared to traditional metal catalysts.[89] The applications of both whole cell systems and isolated enzymes are well established in industry,[90] with lipases,[91] nitrilases, amidases and acylases currently used in production.[80]

A well known application of immobilised enzymes for industrial catalysis is that of glucose isomerase (GI), which catalyses the conversion of D-glucose to D-fructose, and is currently the most widely used enzyme in terms of tonnage for industrial applications.[92] It is typically used for the production of high fructose corn syrup for the food industry. Glucose isomerase is a relatively expensive enzyme for applications, as a high concentration of enzyme is required to reach an acceptable rate of glucose conversion, the use of GI for industrial catalysis would not be cost-effective without immobilisation. There have been several methods of enzyme immobilisation used for glucose isomerase, either as isolated enzymes or as whole cells.[93] The encapsulation of GI within functionalised mesoporous silica was recently reported.[94]

An example of covalent immobilisation for an industrial application is the binding of penicillin G acylase to Eupergit C®, an epoxy functionalised polymer. Penicillin G acylase is a serine hydrolase, used for the production of 6-aminopenicillanic acid, an important intermediate in the production of β-lactam antibiotics.[95] The enzyme is attached by lysine residues on the surface to the epoxide groups on the surface of the polymer. The bound enzyme is reported to be highly reusable, with 60% retention of activity after 800 operations.[96]

1.4 Supporting Proteins on Mesoporous Materials

1.4.1 Adsorption of Protein by Mesoporous Supports

The adsorption of proteins on silica supports has been of considerable scientific interest, in particular with controlled pore glasses and sol-gel materials.[97] The use of controlled pore glass (pore sizes between 20 - 200 Å) as a support for biological molecules is well established in the literature.[98] However, controlled pore glass is not an ideal choice as a support material, as it is of relatively high cost and the surface area decreases

significantly as the pore size increases.[99] The use of sol-gels as protein supports has also been extensively studied.[85] However, sol-gels materials have a broad pore size distribution as well as reduced aqueous stability when compared to thick walled mesoporous materials.

The development of mesoporous materials has led to significant interest in their application as supports for amino acids and proteins.[100] The adsorption of amino acids onto mesoporous materials in aqueous media was studied using MCM-41 as an adsorbent.[101] It was found that the uptake of single amino acids was highly dependent on the pKa of the amino acid, with more acidic amino acids showing poor uptake versus basic amino acids, such as lysine. Above pH 2, the surface of MCM-41 is negatively charged, resulting in strong electrostatic attraction with positively charged amino acids.

Researchers were quick to realise the possibility of using mesoporous silicas, including MCM-41, as support materials for proteins. Shortly after the publication by the Mobil group, results on the immobilisation of small globular proteins on MCM-41 were published.[102] The study involved the adsorption of four small globular proteins - cytochrome c, papain, trypsin and horseradish peroxidase on MCM-41. There was found to be a clear relationship between the size of the protein and uptake by MCM-41, with no uptake of horseradish peroxidase, the largest of the proteins studied, and complete uptake of the smallest, cytochrome c.

Cytochrome c is a small globular protein, of molecular weight 12.4 kDa, and has been extensively studied[103-105] as a protein for uptake by mesoporous supports. The small size of cytochrome c (26 x 30 x 32 Å) and its spherical shape make it an ideal protein for the study of uptake in mesoporous materials with an average pore diameter at smaller end of the mesoporous scale.

The adsorption of cytochrome c on a carbon nanocast of SBA-15, CMK-3, with an average pore size between 30 - 65 Å has also been studied. The highest uptake of protein was obtained at pH 9.6, close to the 9.8 isoelectric point of cytochrome c, at a level of 222 mg g^{-1}. The authors attribute this high loading to an increase in the number of van der Waals interactions between the hydrophobic support[106] and the non-polar amino acid residues on the protein surface, coupled with reduced inter-protein repulsion.[107]

Lysozyme is an antimicrobial protein that has attractive properties for the study of protein adsorption. It is a small (30 x 30 x 45 Å) highly stable protein with four internal disulfide bonds,[108] and an isoelectric point of 11. The adsorption of lysozyme was investigated with MCM-41 and MCM-48.[109] However, the uptake of protein by these materials is very slow, taking several days to reach maximal loadings of 90 - 110 mg g^{-1}.[110] This may be related to the pore size, as similar studies with larger pore SBA-15 and FDU-12 have been more successful, especially with larger pore windows in the case of FDU-12.[111]

The most success with lysozyme has been with a SBA-15 material that was prepared with a short pore length, known as Rod-SBA-15.[112] Particle morphology is normally overlooked with mesoporous materials in favour of pore diameter. Extremely rapid uptake of up to 200 mg g^{-1} within 10 minutes was reported for Rod-SBA-15 with lysozyme, with very high maximum uptake of 533 mg g^{-1}. This very rapid uptake can be attributed to the higher availability of pore entrances in Rod-SBA-15 due to the short pore length.[113] The activity and leaching of protein from this material is yet to be studied, although a high degree of leaching is to be expected at such high loading, coupled with the lack of surface functionalisation / encapsulation.

The immobilisation of trypsin on three mesoporous materials, MCM-41, MCM-48 and SBA-15 was investigated and compared to commercial silica gel.[114] The buffered trypsin solution (pH 6) was mixed with the support for 2 h at 4 °C, after which time the solid was recovered by centrifugation. The amount of trypsin adsorbed was measured by analysis of the supernatant by Bradford's assay. For each solid the uptake of trypsin was very good, with 92% uptake from the smallest pore material, MCM-41, and higher uptake with the other supports. However, leaching of trypsin into a buffered solution at pH 8 was found to be a significant problem with between 35 and 72% bound protein leached back into solution after mixing with one portion of buffer.

1.4.2 Functionalised Mesoporous Materials as Supports

The adsorption of protein on mesoporous support materials is largely due to van der Waals forces or to electrostatic attraction between the protein and the surface of the material.[115] As electrostatic interactions are much stronger than van der Waals forces, one

method of improving the adsorption of proteins is to increase the number of these interactions. Mesoporous silicas are versatile materials, and the surface of the support can be modified to promote favourable interactions between protein and surface.

By introducing organic functional groups that will interact favourably with the amino acid residues on the protein surface, the support can be tailored to a specific enzyme. When coupled with careful control and choice of the average pore size and morphology of the support, a material can be prepared that is well suited to the task of immobilising and supporting an enzyme for catalysis. By use of the methods discussed earlier, organic groups can be introduced to increase the hydrophobicity of the surface, for example incorporation of alkyl chains, saturated and unsaturated, as well as aromatic hydrocarbons such as phenyl groups. It is also possible to introduce organic groups to interact with specific amino acid residues on the surface of the protein, and carboxylic acids, thiol and amine groups have been introduced with the aim of increasing the strength of electrostatic attractions.

The immobilisation of trypsin on functionalised SBA-15 was studied.[29] The organic functionalisation was achieved by co-condensation of an appropriate triethoxysilane and also by condensation of the triethoxysilane post-synthesis. Several organic functional groups were incorporated into the materials, with thiol, amine, phenyl, alkyl chlorides and carboxylic acids incorporated. The immobilisation of trypsin was investigated with the materials, and activity of the protease measured by the hydrolysis of *N*-α-benzoyl-DL-arganine-4-nitroanilide (BAPNA), which yields *p*-nitroaniline as a product which can be measured by UV-Vis spectroscopy at 405 nm (figure 1.15).

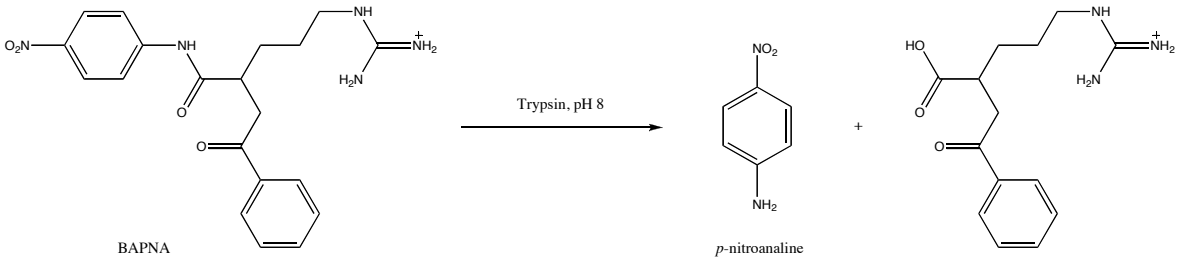

Figure 1.15: BAPNA Hydrolysis by Trypsin

The immobilisation and leaching was found to be highly dependent on the surface chemistry of the support. The maximum loading offered was 2.4 mg g^{-1}, with mixing at 4 °C for 2 h. No uptake was observed for unextracted SBA-15, indicating minimal surface adsorption for an unfunctionalised material. The uptake with calcined SBA-15 and ethanol extracted SBA-15 was good, with > 99% and 94% uptake respectively. With these solids however, leaching was a problem with over half of the enzyme leaching with one wash at pH 8. After functionalisation of the surface the leaching was vastly reduced, with some leaching of trypsin from the hydrophobic supports functionalised with phenyl, but significantly lower leaching from the thiol and alkyl chloride functionalised supports, which are more likely to interact with amino acid residues on the protein surface (such as cysteine and lysine). To demonstrate the low leaching of trypsin with isPrSH-SBA-15, the solid support was removed and the hydrolysis of BAPNA was measured, any hydrolysis after solid removal would be due to free trypsin in solution. The results from this are shown below (figure 1.16), and it can be clearly seen that there is no activity from trypsin that has leached from the support.

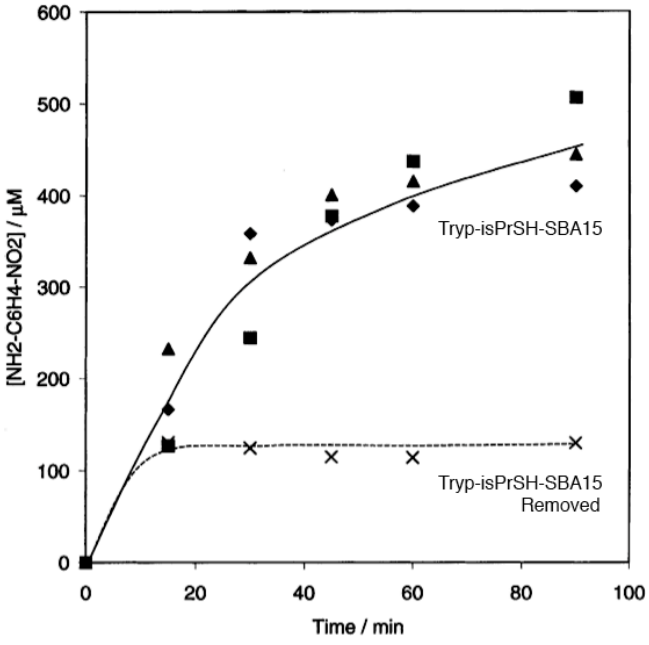

Figure 1.16: Removal of isPrSH-SBA-15 / Trypsin from BAPNA Hydrolysis[29]

Column packed silica based stationary phases for chromatographic applications are well known, and frequently used for the separation of organic molecules in gas and liquid

chromatography. Mesoporous materials can also be used as stationary phases for the separation of species that do not bind irreversibly to the silica surface. This was studied with the column packing of hydrocarbon functionalised SBA-15, using dimethyloctadecylchlorosilane to produce a reverse phase column for HPLC.[116] The capillary column prepared was used to investigate the separation of the products of trypsin digested myoglobin as well as small molecular weight proteins. The separation of these biomolecules was achieved with well defined sharp peaks, demonstrating the versatility of application for mesoporous materials that can be achieved by modifying the surface chemistry.

The effect of ionic strength on the adsorption of cytochrome c by cyano-functionalised MCM-41 (CNS) has been studied.[104] It was found that the adsorption rapidly decreases as the ionic strength of the solution is increased (figure 1.17) by the addition of ammonium sulfate or sodium chloride. It was found that the addition of salt after the immobilisation of cytochrome c did not increase the levels of leaching from the support, indicating a different mechanism of adsorption to desorption.

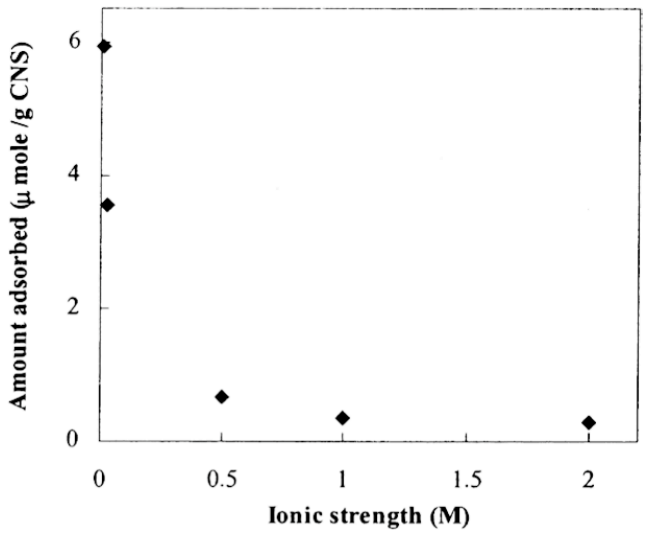

Figure 1.17: Influence of Ionic Strength on the Adsorption of Cytochrome C on CNS

The immobilisation of CALB on hydrophobic mesoporous material was achieved by high pressure packing with an HPLC column.[117] The supports compared were FDU-12 and spherical MCF particles, prepared by the addition of ammonium fluoride before autoclave condensation.[118] The surface of the materials was modified before use by the

addition of chlorodimethyloctylsilane or chlorodimethyloctadecylsilane to prepare a hydrophobic material. The materials were then packed into an HPLC column, after which a high concentration enzyme solution was cycled through the column under high pressure. The solid was then collected, washed with deionised water, and dried under vacuum. The enzyme loading, which was measured by elemental analysis of nitrogen, was between 125 - 275 mg g^{-1} after two hours, higher than for the conventionally mixed material with loadings between 40 - 90 mg g^{-1}. The catalytic activity of the immobilised protein prepared by this method was good, with 25 - 40% activity of CALB immobilised by adsorption (3.6 - 5.4 μmol min^{-1} mg^{-1}). The reusability of this material was excellent, with greater reusability and thermal stability than the commercially available Novozyme 435, demonstrating the effectiveness of the pore system in stabilising the enzyme.

As enzymes have developed to operate within the confined environment of a cell, there is evidence that with some enzymes the confined environment of the pore system enhances the catalytic rate relative to solution. Glucose isomerase and organophosphorous hydrolase immobilised within functionalised SBA-15 showed an enhancement in catalytic rate for the conversion of D-fructose to D-glucose and for the hydrolysis of paraoxon respectively.[94] The materials used in the study were expanded pore (TMB) SBA-15 with amine and carboxylic acid functionalisation. It was suggested that the increased activity was due to confinement of the protein reducing unfolding to non-active states, although this was not proven experimentally.[119]

The immobilisation of chloroperoxidase on periodic mesoporous organosilanes, prepared by condensation of bis[3-(trimethoxysilyl)propyl]amine and P123 template, was investigated.[120] The pore size was too small in all but one of the prepared PMOs (PMO PA-40 (pore size 40 - 100 Å) where 40 represents the percentage composition of silicon atoms) for chloroperoxidase to enter the pore system upon adsorption. However, leaching of chloroperoxidase was a significant problem for all materials when washed with the assay buffer (pH 2.75). Leaching from within the pore system of PA-40 material was reduced relative to the surface adsorbed materials (42% retention versus 13% for surface adsorption). The chloroperoxidase immobilised within PA-40 showed significantly better activity over multiple re-uses, as the activity decreased rapidly for the surface adsorbed enzyme due to the higher leaching.

1.4.3 Controlled Release Systems

The low biotoxicity and the amount of control over the morphology of mesoporous silicas make them attractive targets for use in biomedical applications. To this end, research has been carried out investigating the controlled release of small biological molecules and organic compounds for use in targeted drug delivery systems.

The use of MCM-41 as a carrier material for ibuprofen has been investigated.[121] Two different supports with the MCM-41 structure, templated by C_{12}-TAB and C_{16}-TAB surfactants were prepared. The analgesic / anti-inflammatory drug was introduced into the pore system of both materials by stirring the support in a concentrated ibuprofen solution in hexane.

The maximum loading achieved was 300 mg g^{-1}, with both support materials. The materials were also compressed into pellets of 0.3 g, and the total uptake was found to be the same, albeit the uptake was slower. The release profile was then measured by immersing the prepared material in simulated body fluid (SBF),[122] with the release of ibuprofen monitored by UV-Vis spectroscopy. The release of ibuprofen was fairly rapid (figure 1.18), with 60% desorbed within 24h, for all samples. For the samples which were compressed into pellets after adsorption of ibuprofen (A1 and B1), the release was not complete, most likely due to the blocking or collapse of part of the pore system under pressure during pellet formation. The pore size did not significantly effect the desorption, this was attributed to the small size of ibuprofen (10 x 6 Å) relative to the size of both pore systems (25 and 18 Å).

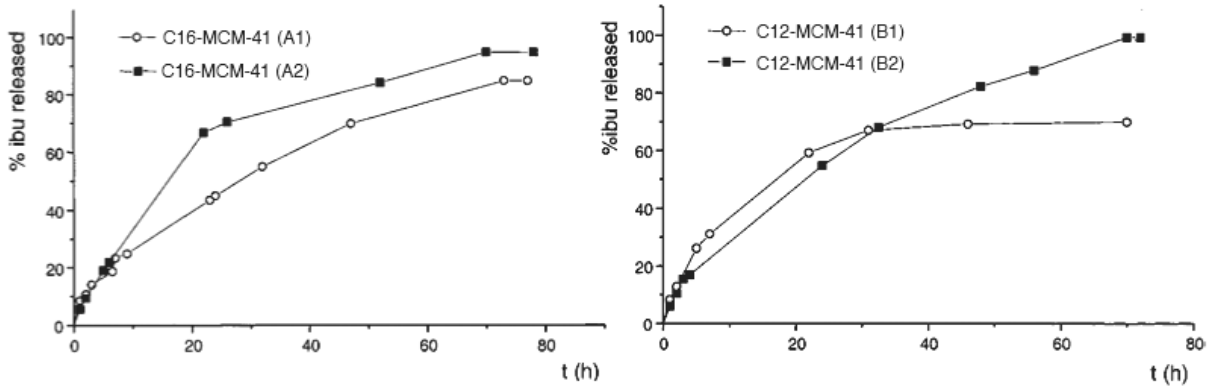

Figure 1.18: Release of ibuprofen from MCM-41[121]

An ideal drug delivery system is one in which the release of the guest molecules can be controlled, or targeted to a specific region. An elegant approach to the controlled release of a guest molecule is the modification of MCM-41 by coumarin, to produce a photochemically controlled gate to the pore system (figure 1.19).[123]

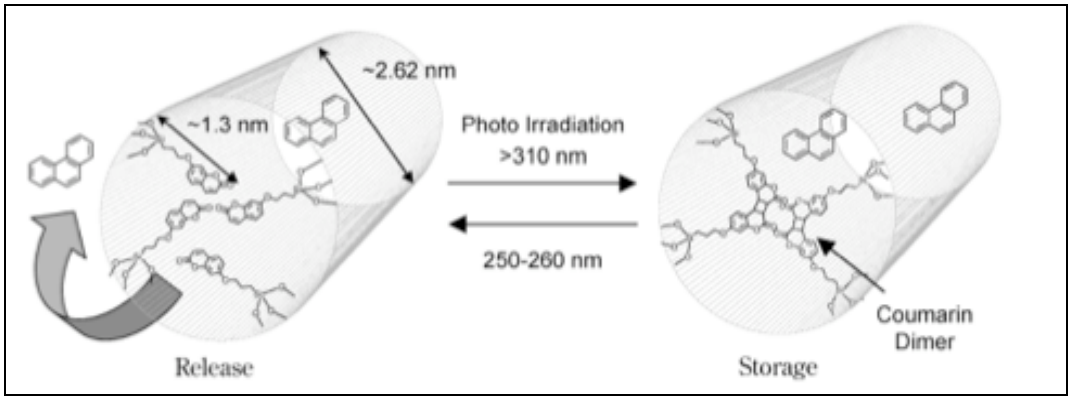

Figure 1.19: Photochemical Control of Coumarin Modified MCM-41[124]

The coumarin is grafted to the surface of MCM-41 before the surfactant template has been removed. Following removal of the surfactant template, the guest molecule is entrapped in the material by adsorption, followed by photodimerisation of the coumarin by UV radiation of wavelength greater than 310 nm (figure 1.20). This method was used to entrap phenanthrene within the pore system at a loading of 216 mg g^{-1}, after washing with n-hexane.

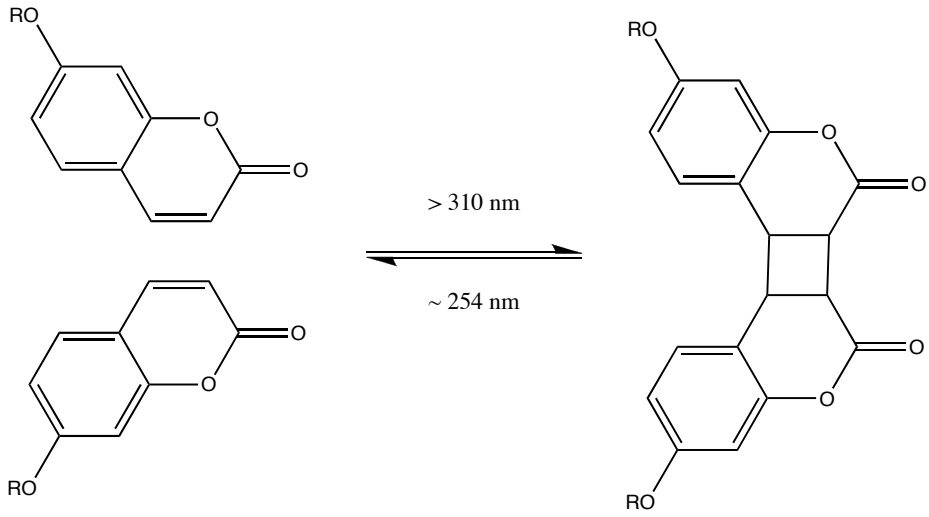

Figure 1.20: Reversible Photodimerisation of Coumarin

The entrapped guest molecules can then be released by the photocleavage of the cyclobutane dimer, with UV radiation of wavelength 254 nm. The release of the phenanthrene is rapid after the photocleavage, with 68% release after 24 hours. The entrapment was not completely reversible, with a maximum release of ~ 75% phenanthrene.

A one step co-condensation of an ibuprofen mesoporous silica release system has also been achieved, by using ibuprofen as the template for the silica matrix rather than a surfactant.[125] The material was prepared by the co-condensation of TEOS, 3-aminopropyltriethoxysilane and ibuprofen (figure 1.21). Although not as well ordered as a surfactant templated material, the material has a defined pore system with average pore size diameter of 20 Å. The material also shows a well defined release profile, from a loading of ~ 240 mg g^{-1}, with near complete release of ibuprofen after 30 h, measured by UV-Vis absorption at 222 nm.

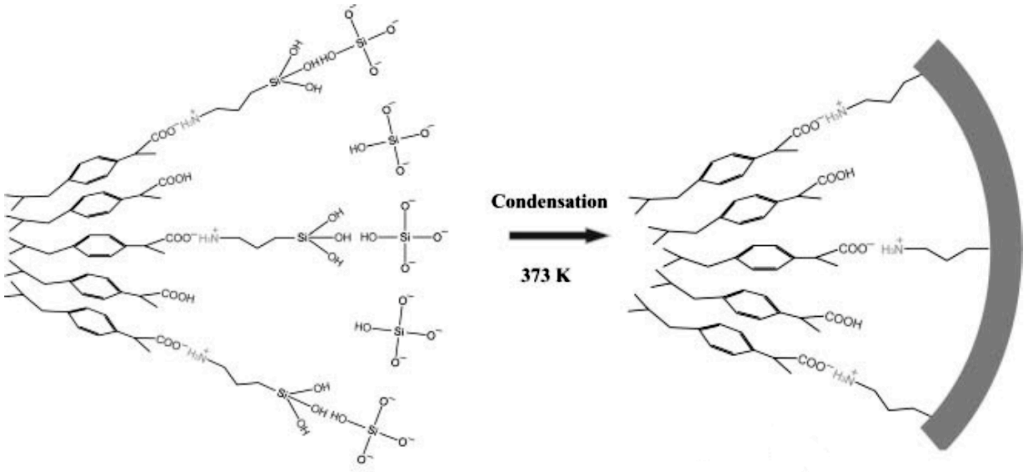

Figure 1.21: Ibuprofen Templated Mesoporous Material[125]

1.4.4 Entrapment of Protein Within Mesoporous Materials

For typical applications, the release of immobilised protein from within the pore system is not required. Retention of the protein can be enhanced by a number of different methods, such as controlling the protein environment to maintain binding with buffers or modifying the surface to increase favourable interactions between enzyme and surface.

Another approach is to physically prevent the escape of protein by either binding the protein covalently or by encapsulating the protein within the pore system.

Mesoporous solids are potentially very good systems for studying the encapsulation of protein as the narrow well defined pore systems make it straightforward to match the protein to the size of the pore, with few physical changes to the host material required to entrap the protein. For immobilised enzyme catalysts, there are some potential problems with this approach that must be considered. The encapsulating process must not destroy the activity of the enzyme, either by inhibition or denaturation. The active site of the enzyme must also remain available to substrates, so the pore system must remain accessible after encapsulation. These caveats aside, this method is potentially a route to robust systems, in which the protein is not chemically altered, yet is unable to escape from the support material.

This approach was investigated in the first report of mesoporous materials as protein supports,[102] in which 3-aminopropyltriethoxysilane (APS) was used as an encapsulating agent with immobilised trypsin on MCM-41. The immobilised trypsin was dried in air, then transferred to toluene, a large excess of 3-aminopropyltriethoxysilane was added, followed by mixing at room temperature. The solid was recovered by centrifugation and washed with toluene, ethanol and deionised water. However, this approach did not produce an active immobilised enzyme, as less than 1% activity was retained. An alternative approach in which dimethylchloride was substituted for toluene and less APS was used yielded a catalyst which retained 13% of the free enzyme activity. The reduced activity was attributed to an inaccessibility of the active site rather than deactivation of the enzyme.

A similar approach was used to entrap porcine pancreatic lipase (PPL) within MCM-41, this time using vinyltrimethoxysilane as the encapsulating agent. The procedure used was to immobilise PPL within the pore system of MCM-41, followed by washing with acetone. The solid was then transferred to toluene and an excess of vinyltrimethoxysilane added to the mixture. The mixture was then stirred for three hours, recovered by filtration and washed with acetone. The recovered solid showed good residual activity (~ 40%) and the reusability of the encapsulated enzyme was reported to be excellent (94% after 5 operations).[126]

A novel approach to protein encapsulation was reported,[127] in which catalase, a highly active enzyme for the decomposition of hydrogen peroxide, was immobilised within mesoporous spheres, followed by encapsulation by layers of polyelectrolytes and nanoparticles. The encapsulated protein was treated with proteases without significant loss of activity (98% activity retained), demonstrating the inaccessibility of the enzyme to the protease. The reusability of this material was also excellent, with 70% activity retained after 25 successive batch reactions.

1.4.5 Covalent Attachment to Mesoporous Supports

The attachment of penicillin acylase to MCM-41 has been reported using glutaraldehyde to covalently attach the protein to the surface.[128] The support was modified with 3-aminopropyltriethoxysilane, followed by addition of glutaraldehyde, which binds the protein via a lysine residue, although a reducing agent to reduce the resulting imine bond was not used (figure 1.22).

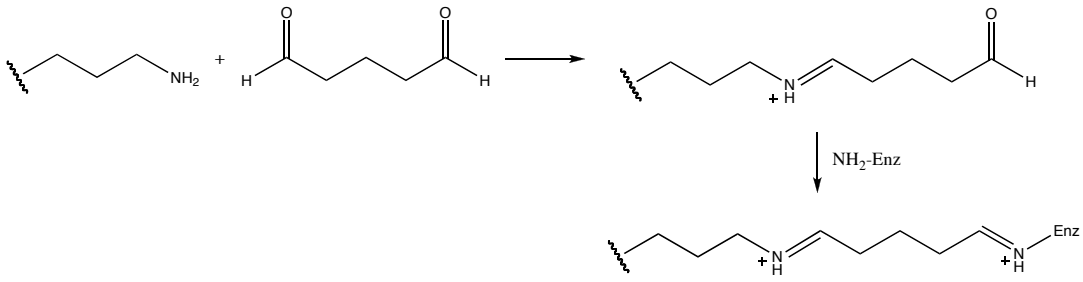

Figure 1.22: Glutaraldehyde Attachment of isPrNH$_2$-MCM41 to Penicillin Acylase

Penicillin acylase catalyses the hydrolysis of penicillin G to 6-aminopenicillic acid, and this reaction was used to measure the activity of the bound enzyme. The activity of the material in which the enzyme was bound by covalent attachment was 25% when compared to the material in which the protein was adsorbed. This was attributed to lower uptake of protein in the glutaraldehyde modified support due to the smaller pore size after modification (the uptake was not measured directly). The covalent attachment did not improve the reusability of the enzyme, with 48% activity loss after 4 uses, when compared to 29% loss for the adsorbed enzyme.

The covalent attachment of glucose oxidase (GOx) and bovine serum albumin (BSA) to an amino-functionalised mesostructured cellular foam has been reported.[129] In the study, amino-functionalised MCF (grafted) was first activated by addition of glutaraldehyde to the material, followed by mixing with the protein solution. The amount of protein incorporated into the material was measured by Bradford's analysis of the solution after immobilisation, with loadings of up to 210 mg g^{-1} GOx and 360 mg g^{-1} BSA reported. The catalytic activity of the proteins after immobilisation was not reported.

1.5 Catalysis with Mesoporous Silica Supported Enzymes

Often the primary aim of protein immobilisation is to prepare a material for catalysis with the added advantages of a heterogeneous system. The catalytic activity of an immobilised enzyme can be reduced relative to the activity of the free enzyme by deactivation, inaccessibility or by reduced substrate diffusion. For industrial applications the reusability and stability of the bound enzyme are of critical importance. Although it may be possible to produce a material with a very high loading of enzyme, this is not advantageous if the cost is the significant reduction of activity or accessibility.

The effect of the pore size of various mesoporous materials with trypsin has been studied.[114] Three supports, MCM-41, MCM-48 and SBA-15 were investigated with immobilised trypsin for the hydrolysis of BAPNA. It was found that the activity was higher with the larger pore material, SBA-15, and was reduced with the smaller pore materials. The morphology of the pore system, with the three dimensionally accessible pore system of MCM-48 versus the two dimensional accessibility of MCM-41, was found not to be as important for reaction rate as the size of the pore entrance, indicating that reduced substrate diffusion and pore blocking are significant with the smaller pore materials.

The effect of the confined environment of SBA-15 on protein digestion was investigated by measuring the rate of proteolysis of myoglobin by trypsin.[130] Both proteins were adsorbed by the mesoporous material at pH 6.5, the pH was then adjusted to pH 8.2 to initiate the proteolysis. The rate of digestion was compared to trypsin and myoglobin in solution, and was found to be much quicker to reach equilibrium with SBA-15, with 8

peptides and 58% sequence coverage within 10 minutes, compared to 3 peptides and 27% sequence coverage after 12 hours in solution. This was attributed to an increased relative concentration of proteins within the pore system when compared to solution phase. This also indicates a degree of mobility for at least one protein within the mesoporous system, as the rapid decomposition of myoglobin would not be observed if both proteins were tightly bound to the silica surface.

The immobilisation of α-chymotrypsin on MCM-41 has been studied.[131] The immobilisation consists of two steps, firstly the immobilisation of α-chymotrypsinogen A, followed by the activation of the immobilised protein with trypsin to yield α-chymotrypsin. The loading obtained was 170 mg g^{-1}, after stirring for 2 h at pH 7.2.The catalytic activity was measured by the kinetic resolution of (±)-trans-p-methoxy-3-phenylglycidic acid (figure 1.23).

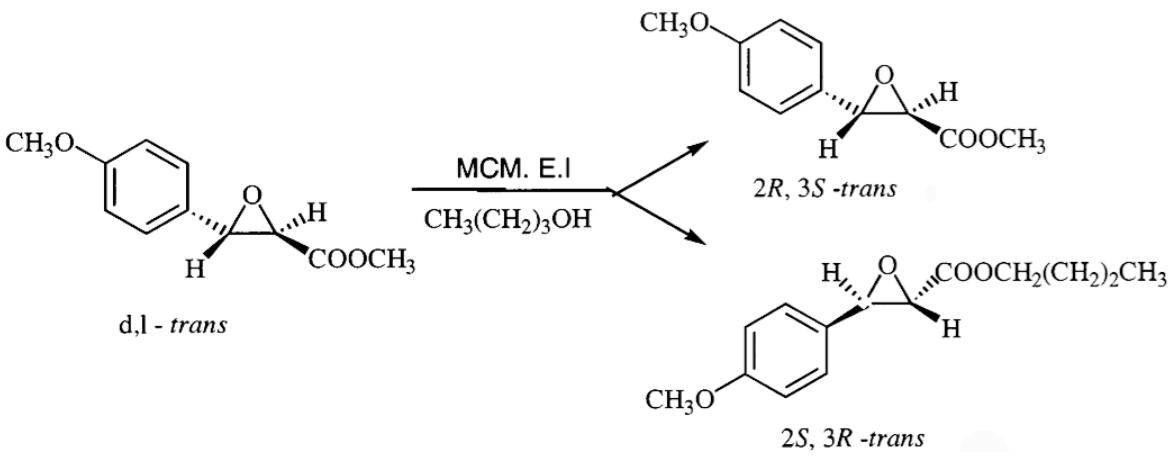

Figure 1.23: Kinetic Resolution of (±)-trans-p-methoxy-3-phenylglycidic acid[131]

The kinetic resolution was specific toward the 2R, 3S enantiomer with an e.e. of 65% at 45% conversion. The reusability was investigated, with no loss of activity after five reuses reported.

1.6 Conclusion

Mesoporous materials are a promising set of materials to study templating effects and materials chemistry, as well as to study the uptake of proteins for transport and catalysis. They can be tailored very easily with good control of pore size, morphology and surface properties. Mesoporous materials are particularly promising for the immobilisation of enzymes, as control of the pore size and the surface chemistry of the support is essential to study the adsorption / desorption properties of proteins. Mesoporous materials are also ideal for the study of confinement effects and encapsulated enzyme systems.

The industrial advantages of enzymes as alternatives to traditional metal catalysts have been recognised, and there are many applications now being brought into production. There is considerable interest in improving the engineering properties of enzymes with much work being done to prepare enzymes for processing applications. There are several examples of processes that would not be cost effective without the significant benefits afforded by immobilisation procedures.

The academic study of mesoporous materials has seen rapid growth since the initial publications by the Mobil group, and is a popular subject for research. A good understanding of the fundamental properties of templated mesoporous materials has been reached, and many studies have begun on the rational design of new and interesting materials and applications.

References

[1] U. T. Bornscheuer, *Angew. Chem., Int. Ed.*, 2003, **42**, 3336.
[2] A. Corma, *Chem. Rev.*, 1995, **95**, 559.
[3] H. H. P. Yiu and P. A. Wright, *J. Mater. Chem.*, 2005, **15**, 3690.
[4] *IUPAC Manual of Symbols and Terminology, Pure. Appl. Chem.*, 1978, **31**, 578.
[5] G. E. Thompson, *Thin Solid Films*, 1997, **297**, 192.
[6] R. Schnabel and P. Langer, *J. Chromatogr.*, 1991, **544**, 137.
[7] T. Yanagisawa, T. Shimizu, K. Kuroda and C. Kato, *Bull. Chem. Soc. Jpn.*, 1990, **63**, 988.
[8] T. Yanagisawa, T. Shimizu, K. Kuroda and C. Kato, *Bull. Chem. Soc. Jpn.*, 1990, **63**, 1535.
[9] C. T. Kresge, M. E. Leonowicz, W. J. Roth, J. C. Vartuli and J. S. Beck, *Nature*, 1992, **359**, 710.
[10] J. S. Beck, J. C. Vartuli, W. J. Roth, M. E. Leonowicz, C. T. Kresge, K. D. Schmitt, C. T. W. Chu, D. H. Olson, E. W. Sheppard, S. B. McCullen, J. B. Higgens and J. L. Schlenker, *J. Am. Chem. Soc.*, 1992, **114**, 10834.
[11] J. C. Vartuli, K. D. Schmitt, C. T. Kresge, W. J. Roth, M. E. Leonowicz, S. B. McCullen, S. D. Hellring, J. S. Beck and J. L. Schlenker, *Chem. Mater.*, 1994, **6**, 2317.
[12] J. C. Vartuli, C. T. Kresge, M. E. Leonowicz, A. S. Chu, S. B. McCullen, I. D. Johnson and E. W. Sheppard, *Chem. Mater.*, 1994, **6**, 2070.
[13] J. N. Israelachvilli, D. J. Mitchell and B. W. Ninham, *J. Chem. Soc., Faraday Trans.*, 1976, **72**, 1525.
[14] K. Schumacher, M. Grun and K. K. Unger, *Microporous Mesoporous Mater.*, 1999, **27**, 201.
[15] M. Morey, A. Davidson and G. Stucky, *Microporous Mater.*, 1996, **6**, 99.
[16] G. Oye, J. Sjoblom and M. Stocker, *Adv. Colloid Interface Sci.*, 2001, **89-90**, 439.
[17] A. Tuel, *Microporous Mesoporous Mater.*, 1999, **27**, 151.
[18] Q. S. Huo, D. I. Margolese, U. Ciesla, P. Y. Feng, T. E. Gier, P. Sieger, R. Leon, P. M. Petroff, F. Schuth and G. D. Stucky, *Nature*, 1994, **368**, 317.
[19] A. Firouzi, D. Kumar, L. M. Bull, T. Besier, P. Sieger, Q. Huo, S. A. Walker, J. A. Zasadzinski, C. Glinka, J. Nicol, D. Margolese, G. D. Stucky and B. F. Chmelka, *Science*, 1995, **267**, 1138.
[20] Q. S. Huo, D. I. Margolese, U. Ciesla, D. G. Demuth, P. Y. Feng, T. E. Gier, P. Sieger, A. Firouzi, B. F. Chmelka, F. Schuth and G. D. Stucky, *Chem. Mater.*, 1994, **6**, 1176.
[21] M. J. Kim and R. Ryoo, *Chem. Mater.*, 1999, **11**, 487.
[22] F. Schueth, *Stud. Surf. Sci. Catal.*, 2004, **148**, 1.
[23] G. S. Attard, J. C. Glyde and C. G. Goltner, *Nature*, 1995, **378**, 366.
[24] P. T. Tanev and T. J. Pinnavaia, *Science*, 1995, **267**, 865.
[25] S. A. Bagshaw, E. Prouzet and T. J. Pinnavaia, *Science*, 1995, **269**, 1242.
[26] E. Prouzet and T. J. Pinnavaia, *Angew. Chem., Int. Ed.*, 1997, **36**, 516.
[27] D. Zhao, J. Feng, Q. Huo, N. Melosh, G. H. Frederickson, B. F. Chmelka and G. D. Stucky, *Science*, 1998, **279**, 548.
[28] D. Y. Zhao, Q. S. Huo, J. L. Feng, B. F. Chmelka and G. D. Stucky, *J. Am. Chem. Soc.*, 1998, **120**, 6024.
[29] H. H. P. Yiu, P. A. Wright and N. P. Botting, *J. Mol. Catal. B: Enzym.*, 2001, **15**, 81.

[30] M. Kruk, M. Jaroniec, C. H. Ko and R. Ryoo, *Chem. Mater.*, 2000, **12**, 1961.
[31] R. Ryoo, C. H. Ko, M. Kruk, V. Antochshuk and M. Jaroniec, *J. Phys. Chem. B*, 2000, **104**, 11465.
[32] A. Galarneau, H. Cambon, F. Di Renzo and F. Fajula, *Langmuir*, 2001, **17**, 8328.
[33] M. Imperor-Clerc, P. Davidson and A. Davidson, *J. Am. Chem. Soc.*, 2000, **122**, 11925.
[34] E. B. Celer, M. Kruk, Y. Zuzek and M. Jaroniec, *J. Mater. Chem.*, 2006, **16**, 2824.
[35] S. Jun, J. M. Kim, R. Ryoo, Y. S. Ahn and M. H. Han, *Microporous Mesoporous Mater.*, 2000, **41**, 119.
[36] K. Cassiers, T. Linssen, M. Mathieu, M. Benjelloun, K. Schrijnemakers, P. Van Der Voort, P. Cool and E. F. Vansant, *Chem. Mater.*, 2002, **14**, 2317.
[37] P. T. Tanev and T. J. Pinnavaia, *Chem. Mater.*, 1996, **8**, 2068.
[38] V. Y. Gusev, X. B. Feng, Z. Bu, G. L. Haller and J. A. Obrien, *J. Phys. Chem.*, 1996, **100**, 1985.
[39] P. Van Der Voort, M. Baltes and E. F. Vansant, *Catal. Today*, 2001, **68**, 119.
[40] R. Mokaya, *J. Phys. Chem. B*, 1999, **103**, 10204.
[41] M. A. Vallet-Regi, L. Ruiz-Gonzalez, I. Izquierdo-Barba and J. M. Gonzalez-Calbet, *J. Mater. Chem.*, 2006, **16**, 26.
[42] P. Alexandridis, J. F. Holzwarth and T. A. Hatton, *Macromolecules*, 1994, **27**, 2414.
[43] P. Schmidt-Winkel, C. J. Glinka and G. D. Stucky, *Langmuir*, 2000, **16**, 356.
[44] P. Schmidt-Winkel, W. W. Lukens, P. D. Yang, D. I. Margolese, J. S. Lettow, J. Y. Ying and G. D. Stucky, *Chem. Mater.*, 2000, **12**, 686.
[45] P. Schmidt-Winkel, W. W. Lukens, D. Y. Zhao, P. D. Yang, B. F. Chmelka and G. D. Stucky, *J. Am. Chem. Soc.*, 1999, **121**, 254.
[46] J. S. Lettow, Y. J. Han, P. Schmidt-Winkel, P. D. Yang, D. Y. Zhao, G. D. Stucky and J. Y. Ying, *Langmuir*, 2000, **16**, 8291.
[47] J. L. Blin and B. L. Su, *Langmuir*, 2002, **18**, 5303.
[48] S. K. Jana, R. Nishida, K. Shindo, T. Kugita and S. Namba, *Microporous Mesoporous Mater.*, 2004, **68**, 133.
[49] K. Y. Ho, G. McKay and K. L. Yeung, *Langmuir*, 2003, **19**, 3019.
[50] R. P. Hodgkins, A. E. Garcia-Bennett and P. A. Wright, *Microporous Mesoporous Mater.*, 2005, **79**, 241.
[51] F. Hoffmann, M. Cornelius, J. Morell and M. Froeba, *Angew. Chem., Int. Ed.*, 2006, **45**, 3216.
[52] D. A. Loy and K. J. Shea, *Chem. Rev.*, 1995, **95**, 1431.
[53] S. Inagaki, S. Guan, Y. Fukushima, T. Ohsuna and O. Terasaki, *J. Am. Chem. Soc.*, 1999, **121**, 9611.
[54] T. Asefa, M. J. MacLachan, N. Coombs and G. A. Ozin, *Nature*, 1999, **402**, 867.
[55] B. J. Melde, B. T. Holland, C. F. Blanford and A. Stein, *Chem. Mater.*, 1999, **11**, 3302.
[56] C. T. Kresge, M. E. Leonowicz, W. J. Roth, J. C. Vartuli and J. S. Beck, *Nature*, 1992, **359**, 710.
[57] U. Ciesla and F. Schuth, *Microporous Mesoporous Mater.*, 1999, **27**, 131.
[58] S. Kawi and M. W. Lai, *Chem. Commun.*, 1998, 1407.
[59] B. Z. Tian, X. Y. Liu, C. Z. Yu, F. Gao, Q. Luo, S. H. Xie, B. Tu and D. Y. Zhao, *Chem. Commun.*, 2002, **11**, 1186.
[60] J. Patarin, *Angew. Chem., Int. Ed.*, 2004, **43**, 3878.
[61] T. Clark, J. D. Ruiz, H. Y. Fan, C. J. Brinker, B. I. Swanson and A. N. Parikh, *Chem. Mater.*, 2000, **12**, 3879.

[62] M. T. J. Keene, R. Denoyel and P. L. Llewellyn, *Chem. Commun.*, 1998, 2203.
[63] G. Buchel, R. Denoyel, P. L. Llewellyn and J. Rouquerol, *J. Mater. Chem.*, 2001, **11**, 589.
[64] C. M. Yang, B. Zibrowius, W. Schmidt and F. Schuth, *Chem. Mater.*, 2003, **15**, 3739.
[65] C. M. Yang, B. Zibrowius, W. Schmidt and F. Schuth, *Chem. Mater.*, 2004, **16**, 2918.
[66] R. Ryoo, S. H. Joo and S. Jun, *J. Phys. Chem. B*, 1999, **103**, 7743.
[67] S. Jun, S. H. Joo, R. Ryoo, M. Kruk, M. Jaroniec, Z. Liu, T. Ohsuna and O. Terasaki, *J. Am. Chem. Soc.*, 2000, **122**, 10712.
[68] H. E. Schoemaker, D. Mink and M. G. Wubbolts, *Science*, 2003, **299**, 1694.
[69] M. R. Stoner, D. A. Dale, P. J. Gualfetti, T. Becker, M. C. Manning, J. F. Carpenter and T. W. Randolph, *Enzyme Microb. Technol.*, 2004, **34**, 114.
[70] A. Nicholls, K. A. Sharp and B. Honig, *Proteins: Struct., Funct., Genet.*, 1991, **11**, 281.
[71] K. A. Dill, *Biochemistry*, 1990, **29**, 7133.
[72] G. Ping, J. M. Yuan, M. Vallieres, H. Dong, Z. Sun, Y. Wei, F. Y. Li and S. H. Lin, *J. Chem. Phys.*, 2003, **118**, 8042.
[73] G. Ping, J. M. Yuan, Z. F. Sun and Y. Wei, *J. Mol. Recognit.*, 2004, **17**, 433.
[74] A. Manjon, J. L. Iborra and A. Arocas, *Biotechnol. Lett.*, 1991, **13**, 339.
[75] K. Faber and M. C. R. Franssen, *Trends Biotechnol.*, 1993, **11**, 461.
[76] M. Ikunaka, *Catal. Today*, 2004, **96**, 93.
[77] P. Brandi, A. D'Annibale, C. Galli, P. Gentili and A. S. N. Pontes, *J. Mol. Catal. B: Enzym.*, 2006, **41**, 61.
[78] E. Salinas, A. A. J. Torriero, M. I. Sanz, F. Battaglini and J. Raba, *Talanta*, 2005, **66**, 92.
[79] A. M. Klibanov, *Anal. Biochem.*, 1979, **93**, 1.
[80] A. Schmid, J. S. Dordick, B. Hauer, A. Kiener, M. Wubbolts and B. Witholt, *Nature*, 2001, **409**, 258.
[81] R. A. Sheldon, *Adv. Synth. Catal.*, 2007, **349**, 1289.
[82] M. G. Sankalia, R. C. Mashru, J. M. Sankalia and V. B. Sutariya, *Eur. J. Pharmaceut. Biopharmaceut.*, 2007, **65**, 215.
[83] M. T. Reetz, *Adv. Mater.*, 1997, **9**, 943.
[84] M. T. Reetz, A. Zonta and J. Simpelkamp, *Biotechnol. Bioeng.*, 1996, **49**, 527.
[85] D. Avnir, S. Braun, O. Lev and M. Ottolenghi, *Chem. Mater.*, 1994, **6**, 1605.
[86] A. C. Pierre and G. M. Pajonk, *Chemical Reviews*, 2002, **102**, 4243.
[87] S. Cohen, T. Yoshioka, M. Lucarelli, L. H. Hwang and R. Langer, *Pharm. Res.*, 1991, **8**, 713.
[88] R. V. Parthasarathy and C. R. Martin, *Nature*, 1994, **369**, 298.
[89] G. Hills, *Eur. J. Lipid Sci. Technol.*, 2003, **105**, 601.
[90] J. M. Woodley, *Biochem. Soc. Trans.*, 2006, **34**, 301.
[91] F. W. Paques and G. A. Macedo, *Quim. Nova*, 2006, **29**, 93.
[92] S. H. Bhosale, M. B. Rao and V. V. Deshpande, *Microbiol. Rev.*, 1996, **60**, 280.
[93] V. J. Jensen and S. Rugh, *Methods Enzymol.*, 1987, **136**, 356.
[94] C. H. Lei, Y. Shin, J. K. Magnuson, G. Fryxell, L. L. Lasure, D. C. Elliott, J. Liu and E. J. Ackerman, *Nanotechnology*, 2006, **17**, 5531.
[95] A. I. Kallenberg, F. van Rantwijk and R. A. Sheldon, *Adv. Synth. Catal.*, 2005, **347**, 905.
[96] E. Katchalski-Katzir and D. M. Kraemer, *J. Mol. Catal. B: Enzym.*, 2000, **10**, 157.
[97] A. C. Pierre, *Biocatal. Biotransform.*, 2004, **22**, 145.
[98] H. H. Weetall, *Appl. Biochem. Biotech.*, 1993, **41**, 157.

[99] L. D. Gelb and K. E. Gubbins, *Langmuir*, 1998, **14**, 2097.
[100] H. R. Luckarift, J. C. Spain, R. R. Naik and M. O. Stone, *Nat. Biotechnol.*, 2004, **22**, 211.
[101] E. S. Hartmann, M. Munsch and H. Thiel, *Stud. Surf. Sci. Catal.*, 2004, **154**, 2020.
[102] J. F. Diaz and K. J. Balkus, Jr., *J. Mol. Catal. B: Enzym.*, 1996, **2**, 115.
[103] J. Deere, E. Magner, J. G. Wall and B. K. Hodnett, *Chem. Commun.*, 2001, 465.
[104] J. Deere, E. Magner, J. G. Wall and B. K. Hodnett, *J. Phys. Chem. B*, 2002, **106**, 7340.
[105] M. E. Gimon-Kinsel, V. L. Jimenez, L. Washmon and K. J. Balkus, *Stud. Surf. Sci. Catal.*, 1998, **117**, 373.
[106] G. Hummer, J. C. Rasaiah and J. P. Noworyta, *Nature*, 2001, **414**, 188.
[107] A. Vinu, C. Streb, V. Murugesan and M. Hartmann, *J. Phys. Chem. B*, 2003, **107**, 8297.
[108] C. C. F. Blake, D. F. Koenig, G. A. Mair, A. C. T. North, D. C. Phillips and V. R. Sarma, *Nature*, 1965, **206**, 757.
[109] J. M. Kisler, A. Dahler, G. W. Stevens and A. J. O'Connor, *Microporous Mesoporous Mater.*, 2001, **44**, 769.
[110] J. Yang, A. Daehler, G. W. Stevens and A. J. O'Connor, *Stud. Surf. Sci. Catal.*, 2003, **146**, 775.
[111] J. Fan, C. Z. Yu, T. Gao, J. Lei, B. Z. Tian, L. M. Wang, Q. Luo, B. Tu, W. Z. Zhou and D. Y. Zhao, *Angew. Chem., Int. Ed.*, 2003, **42**, 3146.
[112] J. Fan, J. Lei, L. M. Wang, C. Z. Yu, B. Tu and D. Y. Zhao, *Chem. Commun.*, 2003, 2140.
[113] J. Lei, J. Fan, C. Z. Yu, L. Y. Zhang, S. Y. Jiang, B. Tu and D. Y. Zhao, *Microporous Mesoporous Mater.*, 2004, **73**, 121.
[114] H. H. P. Yiu, P. A. Wright and N. P. Botting, *Microporous Mesoporous Mater.*, 2001, **44**, 763.
[115] M. Matsui, Y. Kiyozumi, T. Yamamoto, Y. Mizushina, F. Mizukami and K. Sakaguchi, *Chem. Eur. J.*, 2001, **7**, 1555.
[116] J. W. Zhao, F. Gao, Y. L. Fu, W. Jin, P. Y. Yang and D. Y. Zhao, *Chem. Commun.*, 2002, 752.
[117] Y. Han, S. S. Lee and J. Y. Ying, *Chem. Mater.*, 2006, **18**, 643.
[118] Y. Han, S. S. Lee and J. Y. Ying, *Chem. Mater.*, 2007, **19**, 2292.
[119] A. K. Dunker and A. Fernandez, *Trends Biotechnol.*, 2007, **25**, 189.
[120] S. Hudson, J. Cooney, B. K. Hodnett and E. Magner, *Chem. Mater.*, 2007, **19**, 2049.
[121] M. Vallet-Regi, A. Ramila, R. P. del Real and J. Perez-Pariente, *Chem. Mater.*, 2001, **13**, 308.
[122] T. Kokubo, H. Kushitani, S. Sakka, T. Kitsugi and T. Yamamuro, *J. Biomed. Mater. Res.*, 1990, **24**, 721.
[123] N. K. Mal, M. Fujiwara and Y. Tanaka, *Nature*, 2003, **421**, 350.
[124] N. K. Mal, M. Fujiwara, Y. Tanaka, T. Taguchi and M. Matsukata, *Chem. Mater.*, 2003, **15**, 3385.
[125] F. Y. Qu, G. S. Zhu, H. M. Lin, J. Y. Sun, D. L. Zhang, S. G. Li and S. L. Qiu, *Eur. J. Inorg. Chem.*, 2006, **19**, 3943.
[126] H. Ma, J. He, D. G. Evans and X. Duan, *J. Mol. Catal. B: Enzym.*, 2004, **30**, 209.
[127] Y. J. Wang and F. Caruso, *Chem. Mater.*, 2005, **17**, 953.
[128] H. Jing, X. F. Li, D. G. Evans, X. Duan and C. Y. Li, *J. Mol. Catal. B: Enzym.*, 2000, **11**, 45.

[129] X. Zhang, R. F. Guan, D. Q. Wu and K. Y. Chan, *J. Mater. Sci.: Mater. Med.*, 2007, **18**, 877.
[130] J. Fan, W. Q. Shui, P. Y. Yang, X. Y. Wang, Y. M. Xu, H. H. Wang, X. Chen and D. Y. Zhao, *Chem. Eur. J.*, 2005, **11**, 5391.
[131] N. W. Fadnavis, V. Bhaskar, M. L. Kantam and B. M. Choudary, *Biotechnol. Prog.*, 2003, **19**, 346.

2. Characterisation of Mesoporous Materials

2.1 Introduction

The characterisation of solid materials is of vital importance to understand their chemical and physical properties. By understanding the structure of a material we can attempt to modify the properties of the material, or develop new materials with a directed approach. The characterisation of bulk materials involves not only analysis of short range structure, but of long range order as well. For mesoporous materials this involves characterisation of surface composition, charge and area as well as pore size and morphology. Many different physical methods were used in this work to investigate these properties, several of which are described below.

2.2 Nitrogen Adsorption

Nitrogen adsorption is a useful technique to investigate the porosity and surface structure of a material, giving the surface area of a material, the average pore size of a mesoporous material, the total volume of the pore system and the nature of the pore system.[1]

2.2.1 Nitrogen Adsorption Isotherms

The adsorption of gases on a material can be described as fitting one of five types of isotherm described by the Brunauer classification of isotherms.[2] These isotherm classifications are illustrated in figure 2.1.

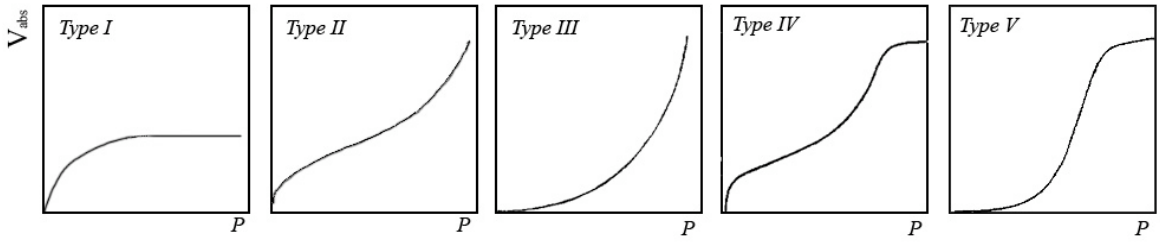

Figure 2.1: Brunauer Isotherm Classification

Adsorption of type I occurs via monolayer adsorption of a gas on a surface, commonly known as Langmuir adsorption. Adsorption types II and III are characteristic of multilayer adsorption, with greater affinity for surface and adsorbate respectively. Types IV and V are characteristic of porous systems with capillary condensation and multilayer adsorption. Type IV isotherms are typical for mesoporous materials, as the pore system is of sufficient diameter that multilayer adsorption is possible before capillary condensation. The adsorption regions of a type IV isotherm are annotated in figure 2.2.

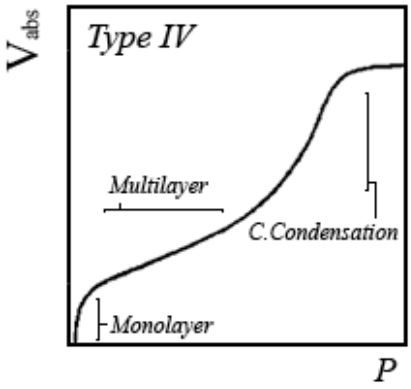

Figure 2.2: Type IV Adsorption

The nitrogen adsorption trace for SBA-15 is shown below (figure 2.3). The adsorption trace is type IV, with a hysteresis between the adsorption and desorption traces (see section 2.2.4). The monolayer, multilayer and condensation steps are very well defined, and can be used to calculate the surface area using the BET method and pore size diameter using the BJH method.

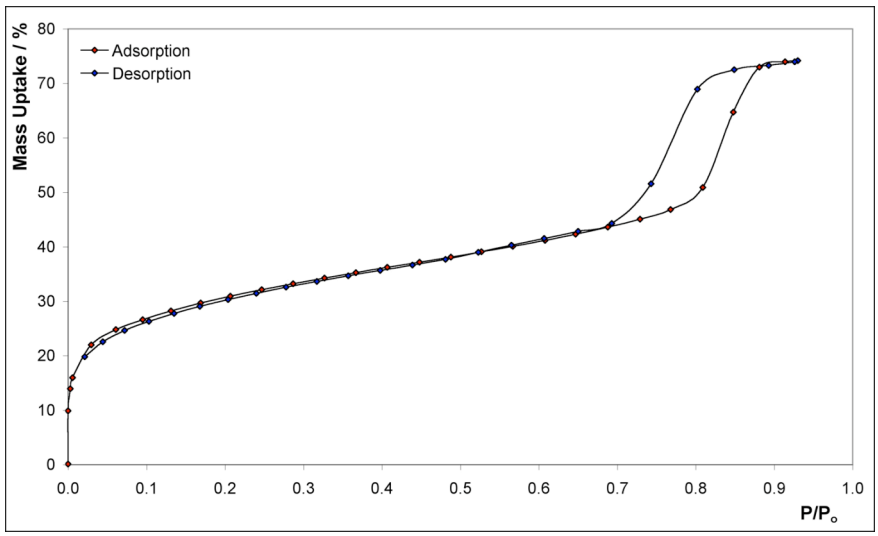

Figure 2.3: Nitrogen Adsorption Isotherm for SBA-15

2.2.2 BET Theory

BET theory, named after Brunauer, Emmett and Teller, is a modification of Langmuir's work on monolayer formation, extended to multimolecular adsorption upon a surface.[3] This is derived from the polarisation theory of DeBoer and Zwicker, which describes the induced dipole in a multilayer caused by the dipole of the layer below.[4]

$$\frac{P}{v(P-P_o)} = \left(\frac{c-1}{v_m C}\right)\left(\frac{P}{P_o}\right) + \frac{1}{v_m c} \tag{2.1}$$

The resultant BET equation (Equation 2.1) can be applied to the nitrogen adsorption of mesoporous and open surface materials to give a measurement of the surface area of a material. In the BET equation υ is the volume adsorbed, υ_m is the volume of gas adsorbed in one unimolecular layer, P and P_o are the equilibrium and saturation pressures and c is the BET constant expressed in equation 2.2, where E_1 is the adsorption of the first layer, and E_L is the adsorption of subsequent layers (this is equal to the heat of liquification).

$$c = \exp\left(\frac{E_1 - E_L}{RT}\right) \tag{2.2}$$

The nitrogen adsorption data are plotted as $P/\upsilon(P\text{-}P_o)$ versus P/P_o and the gradient and intercept are used to calculate the monolayer adsorbed gas quantity (υ_m) and the BET constant (c). This calculation is only valid for the linear region of the BET plot, when P/P_o is typically between 0.05 and 0.35. The surface area can then be calculated for the material by applying equation 2.3. Where S is the surface area, N is Avogadro's number, M is the molecular weight of the adsorbate, s is the adsorption cross-section and a is the weight of the sample.

$$S = \frac{S_{total}}{a} = \frac{v_m N s}{M} \tag{2.3}$$

There are some inherent limitations to the BET model that must be considered when the model is applied. The surface area calculation is limited to a pressure range in which the BET plot is linear, which can be quite narrow (between 0.1 and 0.3 P/P_o) for some materials, for example graphitised carbons. The average area of each molecule in the monolayer is assumed to be the volume of liquefied gas, 0.162 nm^2 for nitrogen, although alternative values have been proposed in the range of 0.13 - 0.20 nm^2.[5] Finally the BET model assumes uniform adsorption of gas, an assumption that may not be valid for materials with a high affinity between gas and surface, or with microporous materials with very narrow pores (of thickness close to the adsorption cross-section).[1] These limitations are not prohibitive for the measurement of the surface area of mesoporous silica materials, which do contain microporosity, but micropores are typically larger than the adsorption cross-section, nor is there a particularly high affinity between nitrogen and surface that may result in localised adsorption.

2.2.3 BJH Theory

BJH theory, developed by Barrett, Joyner and Halenda, is a method of measuring the pore volume and pore diameter of an adsorbate. The theory is based upon the fact that a gas will condense at a lower pressure than its saturation pressure in a confined environment. The Kelvin equation (equation 2.4) can be used to estimate the pore radii r at any given equilibrium pressure P, where γ is the surface tension.

$$\ln\frac{P_o}{P} = \frac{2\gamma V}{rRT} \tag{2.4}$$

However, the Kelvin equation does not account for the multilayer adsorption on the surface of each pore, which reduces the effective radii of each pore, and thus the volume available for condensation. This is accounted for by the factor t in equation 2.5 representing the thickness of the adsorbed monolayer. This thickness can be calculated from the BET equation, as discussed above.

$$r_p = \frac{2\gamma V}{RT\ln P_o/P} + t \tag{2.5}$$

The BJH model can be applied to the adsorption or desorption trace, with a larger value for the pore size distribution obtained for BJH analysis of the adsorption trace. Typically the BJH analysis reported in literature is for the desorption trace, the values reported (section 3) were also calculated from the desorption branch of the isotherm.

2.2.4 Hysteresis

In nitrogen adsorption experiments it is possible to observe a hysteresis loop during the capillary condensation step, that is, the amount of gas adsorbed is dependent not only on the relative pressure P/P_o, but also on the path taken to get to the data point, either adsorption or desorption.

A hysteresis loop is observed when during the desorption step, a lower relative partial pressure must be reached before the same level of gas uptake is reached, relative to the adsorption step. This can be observed in the isotherm plotted below, which was measured for calcined SBA-15 (figure 2.4).

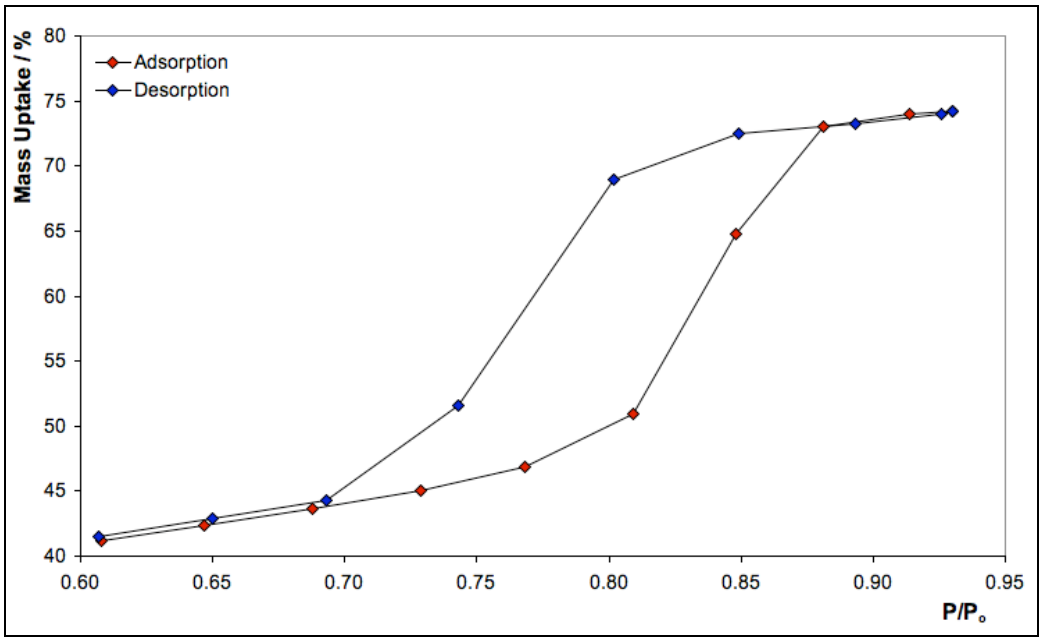

Figure 2.4: Hysteresis in SBA-15 Nitrogen Adsorption

It has been suggested that this hysteresis is due to incomplete wetting of the internal surface upon adsorption, due to adsorbed impurities coating the internal surface until sufficient pressure is reached to cause their displacement by adsorbate.[6] This does not

explain however, the reversibility of this behaviour in some systems. This reversibility may be better explained when the entrance to a pore is narrower that the internal cavity, this causes the adsorbate to fill more quickly in the neck of the pore than the cavity, followed by complete adsorption at a higher pressure than without the neck.[7] This is described by the Kelvin equation (equation 2.6) below, where r is the radius of the cavity.

$$p = p_o \exp\left(\frac{-2\gamma V}{rRT}\right) \tag{2.6}$$

The adsorbate in the neck of the pore will not desorb until the pressure has dropped to satisfy the equation below (equation 2.7).

$$p_d = p_o \exp\left(\frac{-2\gamma V}{r_c RT}\right) \tag{2.7}$$

Because the radius of the neck is lower than the radius of the cavity the adsorption pressure p_a must be greater than the desorption pressure p_d, resulting in a hysteresis loop. For capillary pores, open at both ends, a meniscus within the pore will be formed, as illustrated below (figure 2.5). The condensation step will fill according to the Kelvin equation with r_a the effective radius of the pore on adsorption, and r_d the radius of the pore upon desorption. As r_a is smaller than r_d, the adsorption pressure is higher than the desorption pressure and a hysteresis is observed.

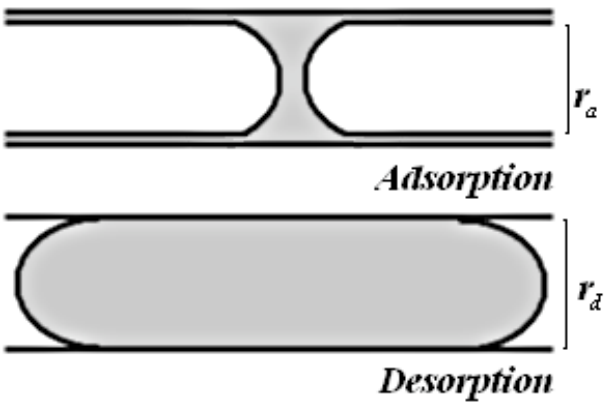

Figure 2.5: Hysteresis in Capillary Pores

From the shape of a hysteresis loop we can gain information about the morphology of the pore system. Two types of hysteresis loop are illustrated below (figure 2.6), that are observed with mesoporous materials. The first, type A, is observed with materials with one narrow opening (ink bottle type) and capillary pores, which are open at both ends, and where the internal diameter is close to the diameter of the neck. The second type, type B, is observed for pores in which the diameter of the neck is much smaller than the diameter of the internal cavity.[6] The desorption branch will always return to meet the adsorption branch at a partial pressure of 0.42, as this point is the thermodynamic limit for the stability of bulk nitrogen.[8]

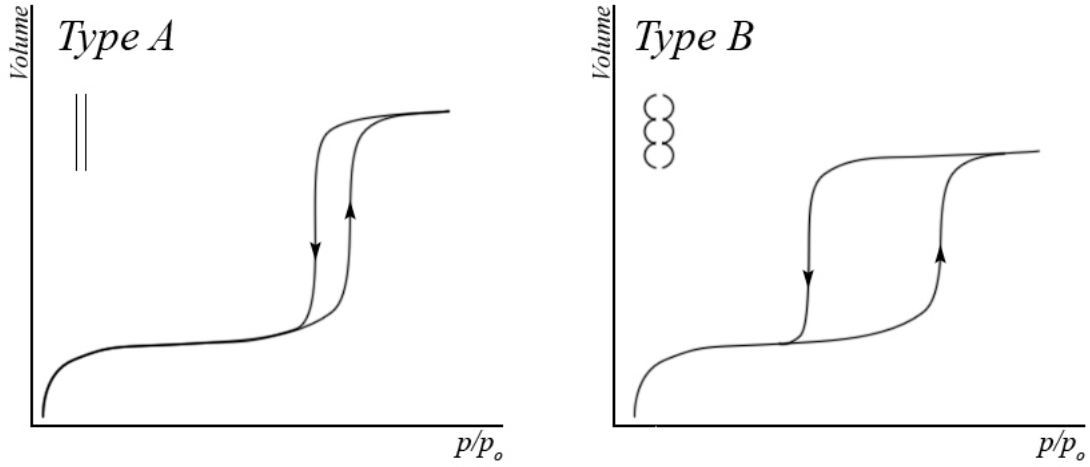

Figure 2.6: Hysteresis Loop Types for Mesoporous Materials

2.3 Thermal Gravimetric Analysis

Thermal gravimetric analysis (TGA) is a technique used to study how the weight of a sample changes with increasing temperature, usually under a gas flow, as a result of sample changes producing volatile products. This can provide useful information about thermally induced changes in the sample, such as decomposition or loss of water of crystallisation.

Modern TGA instruments use piezoelectric crystals as the detection method, in which the conductivity of the crystal changes depending with variation in mechanical stress. Attachment of a weighing arm to the crystal causes a change in the mechanical

stress when the sample weight changes, which is measured by monitoring the potential across the crystal. This is the principle upon which the TA Instruments SDT 2960 used for sample analysis operates. The furnace operates under a controlled atmosphere, with either an inert gas or oxygen containing gas flow. This gas removes volatile decomposition products, can promote decomposition (depending on the gas selected) and maintains a constant pressure within the furnace. The flow rate of the gas must be carefully controlled to ensure accurate results across the temperature gradient and between different samples.

A TGA trace for isPrSH-SBA15 (5%) is shown below (figure 2.7). The TGA trace shows the weight loss of the thermally induced conversion between three plateaus, when plotted as temperature versus weight loss. The initial temperature loss is due to evaporation of solvent. This is followed by a weight loss from the decomposition of the surfactant template (see 3.2.2), with a third weight loss due to silanol condensation (loss of H_2O) and decomposition of organic functional groups on the surface of the material. Some TGA apparatus includes an effluent gas analysis (EGA) module, which analyses the gas produced with each transition step, typically by Fourier transform infrared spectroscopy (FT-IR). This can help with identification of the intermediate products during the thermal conversion.

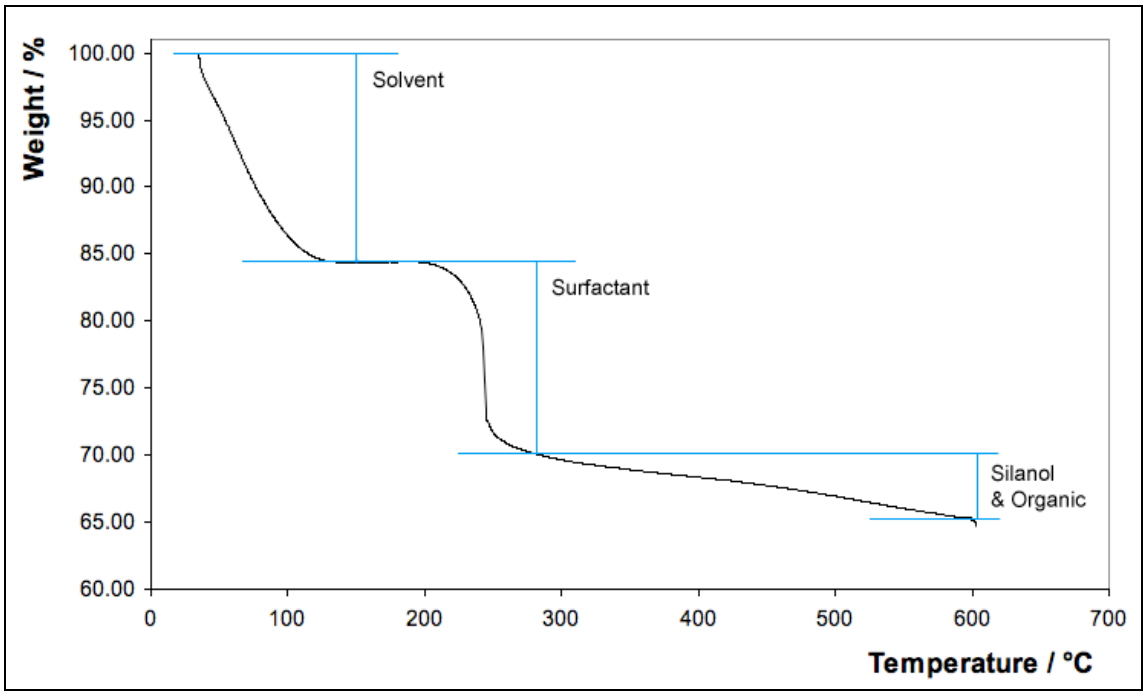

Figure 2.7: TGA Trace for isPrSH-SBA15 (5%)

A limitation of thermal gravimetric analysis is that it does not identify phase transitions or decompositions generating non-volatile products. However, it is a useful technique for mesoporous materials, as it can measure the decomposition of template molecules and incorporated organic functional groups.

2.4 Elemental Analysis

Elemental analysis is a method of quantitatively measuring the elemental composition of a material. This ratio of elements can be used to obtain an empirical chemical formula for a compound or material. This is a very useful method for characterisation, especially in organic chemistry, where the smallest integer ratio for a pure substance can be obtained and correlated with other characterisation methods, including mass spectrometry, to identify a compound. If the formula is already known then elemental analysis can be used to identify and determine the purity of a sample.

Elemental analysis consists of complete combustion of the sample material, resulting in the evolution of carbon dioxide, water, nitrogen oxides and sulfur dioxide. The gases are then separated by a chromatographic method (typically frontal chromatography, in which the gases are fed continuously onto the column) and analysed by a thermal conductivity detector. It is also possible to measure oxygen content by prior reduction to carbon monoxide and subsequent detection, originally by iodine titration[9] or recently by thermal conductivity measurement, although typically only carbon, hydrogen, nitrogen and sulfur are measured.

The analysis of mesoporous silica materials by elemental analysis is more complex than analysis of molecular compounds, as the theoretical composition for silica materials cannot be calculated accurately, due to masking by residual P123 surfactant, which is not completely removed by ethanol extraction (see section 3.2.2). The incorporation of nitrogen and sulfur containing groups within a mesoporous material can be measured by elemental analysis, and the measurement of incorporated amine, nitrile, thiol and thioether groups are discussed in section 3.3.

2.5 Ellman's Assay

The quantitative analysis of free thiol concentration can be measured using Ellman's assay.[10] The Ellman assay is based upon the cleavage of 5,5'-dithiobis(2-nitrobenzoic acid) (DNTB) and the high extinction coefficient of the 2-nitro-5-thiobenzoate anion which is produced (figure 2.8) and can be measured by UV-Visible spectroscopy at 412 nm.

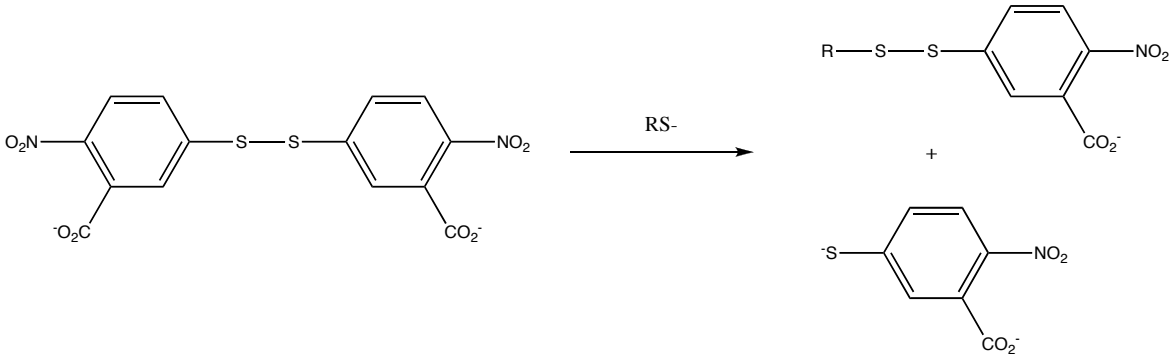

Figure 2.8: Cleavage of DNTB During the Ellman Assay

The assay was calibrated by measurement of the response of DNTB to known concentrations of cysteine, this calibration is plotted below (figure 2.9).

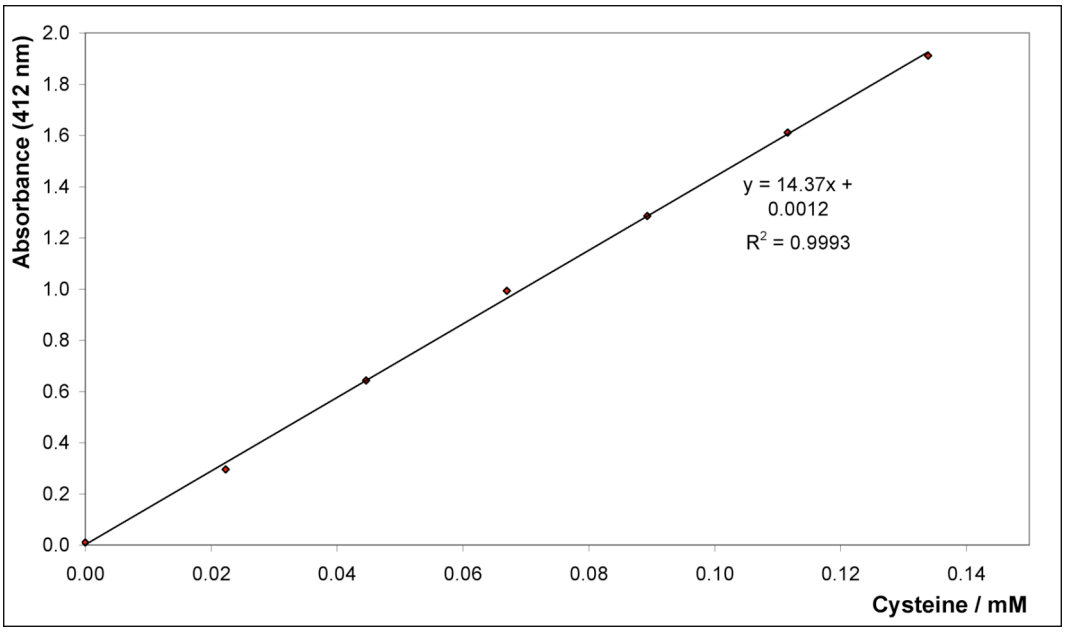

Figure 2.9: Cysteine Standard Calibration for Ellman's Assay

2.6 Zeta Potential Measurement

A charged particle in a medium will result in the generation of an electrical double layer around the particle. This double layer consists of the Stern layer, composed of strongly bound ions, and a more diffuse layer of charged particles surrounding the Stern layer (figure 2.10). There is a boundary within this diffuse layer, known as the hydrodynamic plane of shear, or slipping plane, in which particles below the shear plane will move with the charged particle as a single entity. The electric potential associated with this boundary is known as the zeta potential.

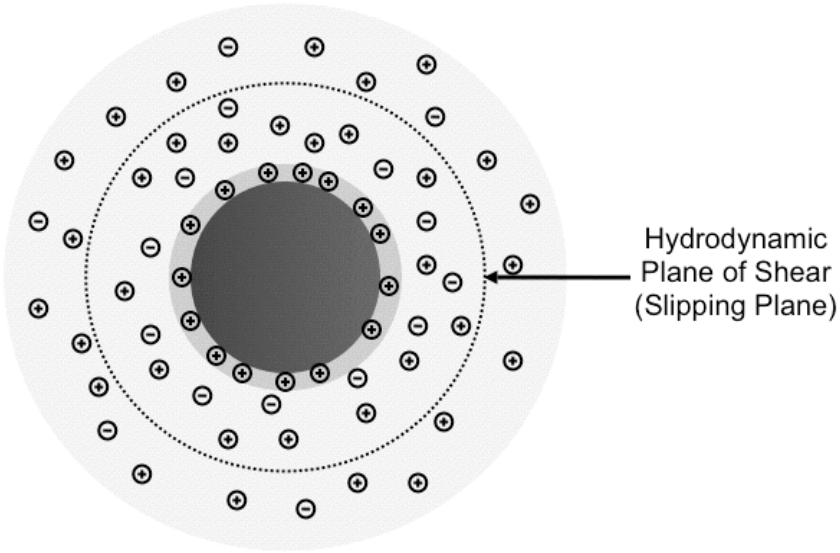

Figure 2.10: The Electric Double Layer

Zeta potentials are calculated using Henry's Law (Equation 2.8), shown below. Where U_E is the electrophoretic mobility, ε is the dielectric constant and f(ka) is a function known as Henry's function (where k is a constant and a is the particle radius). Henry's function is approximated to 1.5 in polar media, and 1.0 in non-polar media. η is the viscosity of the medium and z is the zeta potential.

$$U_E = \frac{2\varepsilon z f(ka)}{3\eta} \tag{2.8}$$

The experiment is carried out using a technique known as laser Doppler electrophoresis, which measures the movement of charged particles in a static medium. An electrophoresis cell is fitted with two laser sources, aligned to generate Young's interference fringes that are measured by a series of detectors. A known potential is applied over the cell, which causes the movement of charged particles relative to the medium, which in turn causes a Doppler shift in the laser beam. This Doppler shift is calculated from the movement of the interference fringes. The zeta potential (in mV) is then calculated from the measured U_E using the equation above.

2.7 Solid State NMR Spectroscopy

Solid state NMR experiments are more difficult than their solution state counterparts, due to line broadening and decreased signal to noise ratios. This is due to three effects, the first of which is the introduction of significant magnetic dipolar interactions in the solid state (dipolar coupling), which are averaged in solution by rapid molecular tumbling. The second effect is that the low isotopic abundance of important nuclei, including ^{13}C and ^{29}Si, results in low signals and long relaxation times, giving poor signal to noise ratios. The third effect is that the chemical shift of a nuclei is dependent upon the orientation of the surrounding atoms to the magnetic field, which in the solid state results in a broadening of the signal peak. There are methods to minimise the peak broadening and poor signal to noise ratios which are discussed below.

2.7.1 Dipolar Decoupling

Dipolar decoupling suppresses the magnetic dipolar interaction between localised nuclear spins. As the dipolar interactions between low abundance isotopes (such as ^{13}C) are not significant, due to the low probability of two such nuclei being located in close proximity, the most common dipolar interaction is between a proton and another atom, including ^{13}C - ^{1}H interactions and ^{1}H - ^{1}H interactions. When observing the signal of the heteronuclei (often ^{13}C), the sample is irradiated with a signal at the resonance frequency of the proton to suppress the dipolar interaction (heteronuclear decoupling).[11] It is more complex to decouple the dipolar interactions between two protons (homonuclear decoupling), and multiple pulse methods must be employed.[12, 13]

2.7.2 Cross-Polarisation

The low abundance of several suitable nuclei makes obtaining spectra difficult for two reasons, low signal intensity and long spin-lattice T_1 relaxation times.[14] Cross-polarisation is a method to reduce these problems by the transfer of polarisation from the abundant ^1H spins, which have short T_1 relaxation times, to the heteronuclei. A successful polarisation transfer will increase the signal intensity of the observed nuclei, and more significantly decrease the relaxation time T_1, which is now defined by the relaxation time of the proton. This allows a much shorter time between repeating the experiment, and a much quicker rate of data collection.

2.7.3 Magic Angle Spinning

The dipolar magnetic field between two different magnetic nuclei is described by the equation below (equation 2.9), where B is the magnetic field, μ is the magnetic moment, r is the distance and θ is the angle relative to the magnetic field.

$$B = \left(\frac{\mu}{r^3}\right)\left(3\cos^2\theta - 1\right) \tag{2.9}$$

When an angle of 54.74° is input into the equation above, the term on the right equals zero. As this term describes the anisotropy of the dipolar interaction, by spinning the sample at a sufficient rate at this angle, the average dipolar field will equal zero, and the signal obtained will not be broadened to the degree previously observed. This angle is known as the magic angle.

2.7.4 The CP-MAS Method

The cross-polarisation magic angle spinning (CP-MAS) method is a combination of the methods above to obtain high resolution spectra of solid-state systems.[15] It consists of a multiple pulse sequence, illustrated below (figure 2.11), while the sample is spun at the magic angle (54.74°) during the entire sequence.

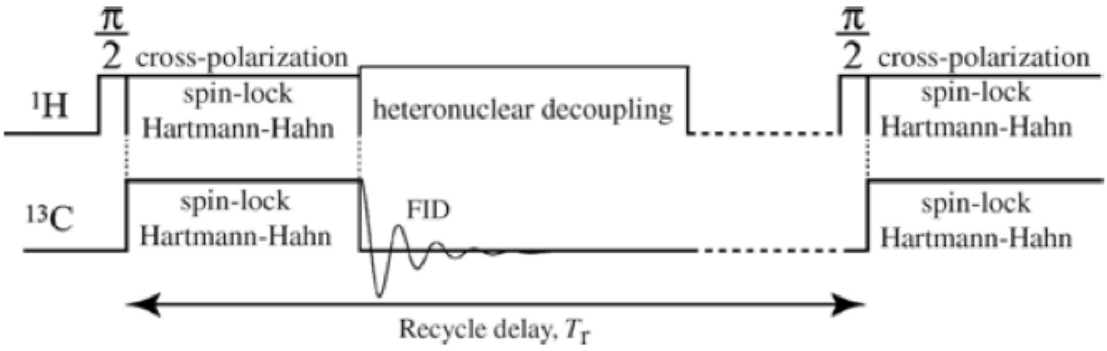

Figure 2.11: CP-MAS Pulse Sequence[16]

For mesoporous materials solid state NMR spectroscopy can provide information about the environment of proton and carbon atoms of the residual surfactant and of the organic functionality that has been incorporated into the material. Silicon (^{29}Si) NMR spectroscopy can provide information about the incorporation of organic groups via co-condensation and post-synthesis grafting, as well as the silicon oxide / silanol composition of the surface.

2.8 X-Ray Diffraction

To probe the atomic structure of a material we need radiation of comparable wavelength to the distances between atoms in the material. X-rays, with a wavelengths between 0.6 Å and 1.9 Å, are suitable for this purpose. When an incident X-ray interacts with an atom, it is scattered by the electron cloud of the atom. If the inter-atomic distance is comparable to the wavelength of the X-ray, then the scattered X-rays can cause interference. If the atoms are well ordered, the scattering will give rise to interference fringes, making it possible to detect a diffraction pattern. Analysis of this diffraction pattern can provide information about the long range order of the structure.

The X-rays are generated in an X-ray tube, illustrated below (figure 2.12). The electron beam is generated by thermionic emission from a tungsten filament, then accelerated through a vacuum toward a metal target. When a beam of electrons strikes the metal, electrons are ejected from an occupied orbital near the nucleus of the metal atom. This causes an electron from a higher energy orbital to drop into the vacancy created by

the ejected electron. The excess energy, the energy difference between the orbitals, is ejected as an X-ray of a quantum wavelength, described by Planck's law ($E = h\upsilon$), where E is the energy difference of the orbitals involved.

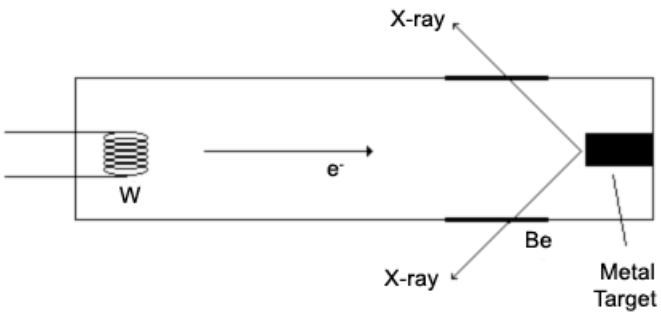

Figure 2.12: X-ray Tube Schematic

The output from an X-ray tube passes through a beryllium window, which is invisible to X-rays, as a mixture of background radiation (known as Bremstrahlung or braking radiation) and intense peaks, corresponding to the quantised transitions between the orbitals of the metal source. The labels describe the orbital from which the secondary electron is emitted, the orbital the primary electron decays from, and the spin state of this electron. K_α corresponds to the transition from 2p (L) to 1s (K), with K_β corresponding to the transition from 3p (M) to 1s (K). This is illustrated below (figure 2.13).

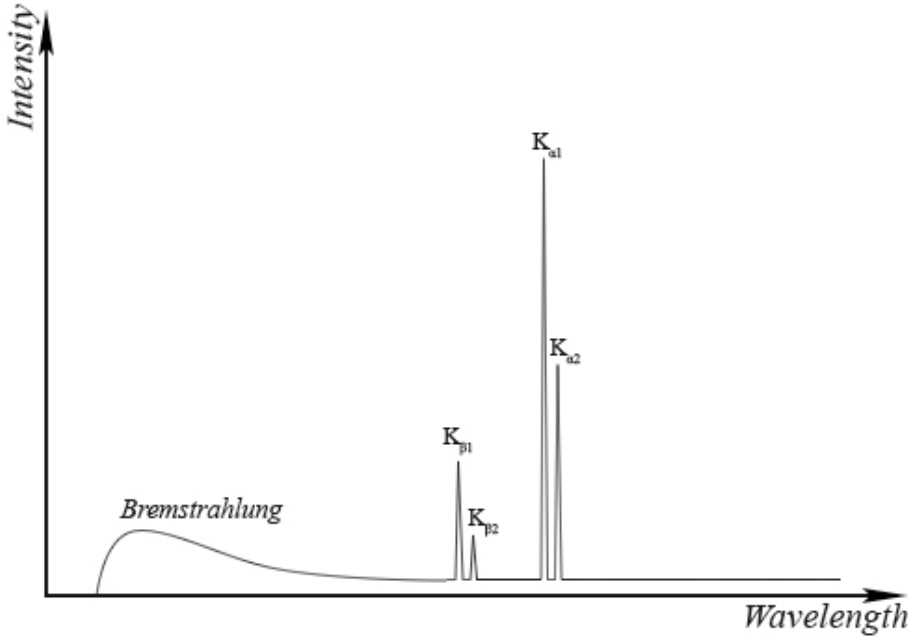

Figure 2.13: X-ray Tube Output

Typical metal sources used for the generation of X-rays are copper and molybdenum, which generate K_α lines at 1.54 Å and 0.71 Å respectively. It is preferable to use X-rays of a single wavelength for analysis, generally the $K_{\alpha 1}$ wavelength is selected as it has the greatest intensity.

The scattering of X-rays from parallel atomic planes is illustrated below (figure 2.14). To obtain useful data the scattered X-rays must be in phase. The resultant X-rays will be in phase if the extra distance travelled by more penetrating X-rays is an integral number of wavelengths. This is illustrated above as the distance from A to B plus the distance from B to C. The path length from A to C is dependent upon the incident angle of the X-ray beam and the distance between atomic planes (lattice spacing), given by the distance d_{hkl}.

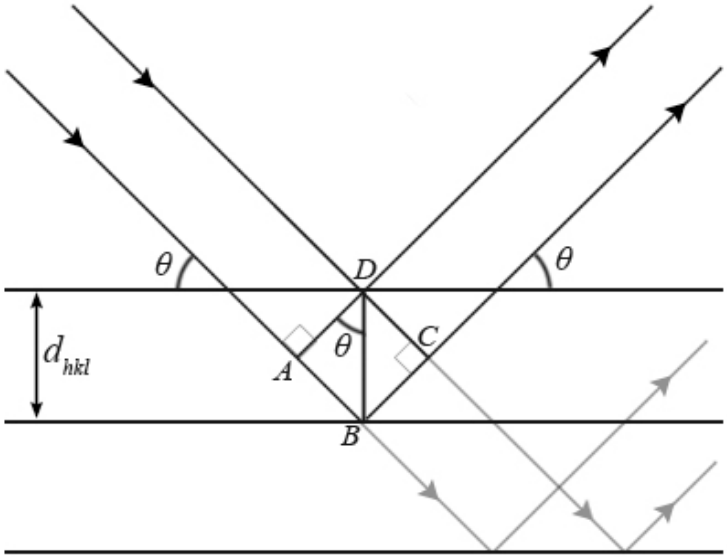

Figure 2.14: Bragg Diffraction

The relationship between the lattice spacing, the incident angle and the wavelength of the X-rays is described by Bragg's law (equation 2.10), where n is the scattering order.

$$n\lambda = 2d_{hkl}\sin\theta \tag{2.10}$$

Analysis of powder samples by X-ray diffraction is possible, as a powder sample will ideally contain an infinite number of crystalline domains, randomly orientated. A

monochromatic X-ray beam that is focused on a powder sample will diffract according to the 2θ value of the crystallite orientation, resulting in the diffraction of X-rays in cones (figure 2.15). The diffracted X-rays may be analysed in by a number of different methods.

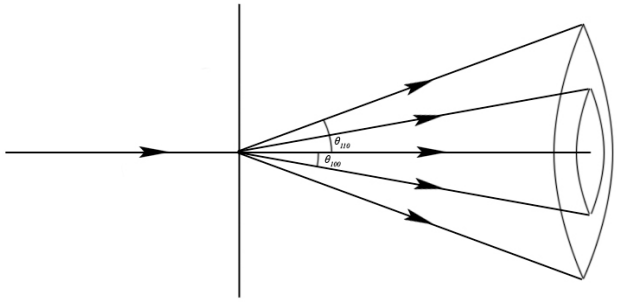

Figure 2.15: Powder Diffraction Scattering Cones

The X-ray diffraction of mesoporous materials is performed utilising a technique known as small angle X-ray scattering (SAXS). Typical diffraction angles are below two degrees (4θ), and care must be taken to avoid damaging the detector with non-diffracted X-rays. This is to measure scattering from inter-atomic planes with relatively large distances between the planes, as there is an inversely proportional relationship between the lattice spacing and the diffraction angle (from Bragg's law). SAXS can measure diffraction from ordered planes with inter-planar distances between 0.5 and 150 nm. In addition to mesoporous materials SAXS can be used to investigate nanoparticles, polymer films, micro-emulsions and liquid crystals. A typical SAXS diffraction pattern recorded for SBA-15 is plotted below (figure 2.16, see section 3.2.3 for more detail).

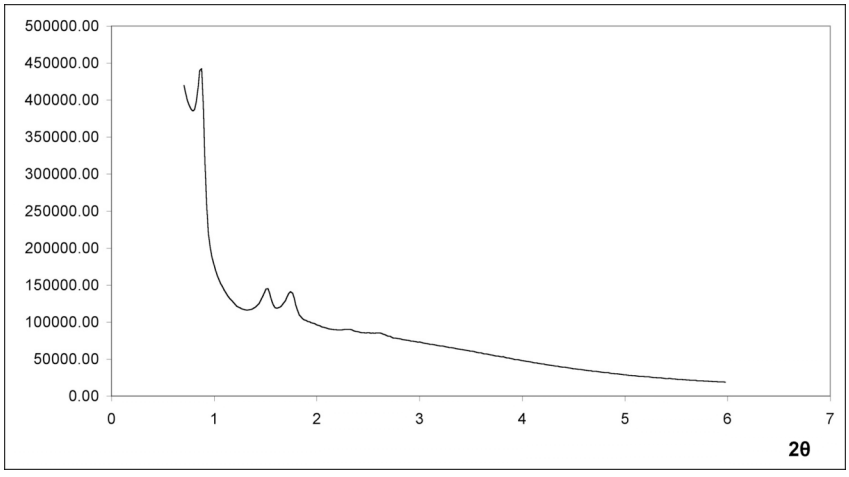

Figure 2.16: Small Angle X-ray Diffraction Pattern for SBA-15

2.9 Electron Microscopy

Electron microscopy is a technique that can be used to image the atomic structure of a material by its interaction with electrons. The electron beam is generated from a cathode filament, typically tungsten, by thermionic emission. The generated electron beam is then accelerated toward an anode through known potential E to give an electron beam of known wavelength υ, calculated by Planck's law E = hυ, where h is Planck's constant. The electron beam will then interact with the sample to produce diffracted and scattered electrons that , after manipulation by a series of lenses, can be captured on a film or a charge coupled device (CCD). The interaction of the electron beam with the sample is illustrated below (figure 2.17).

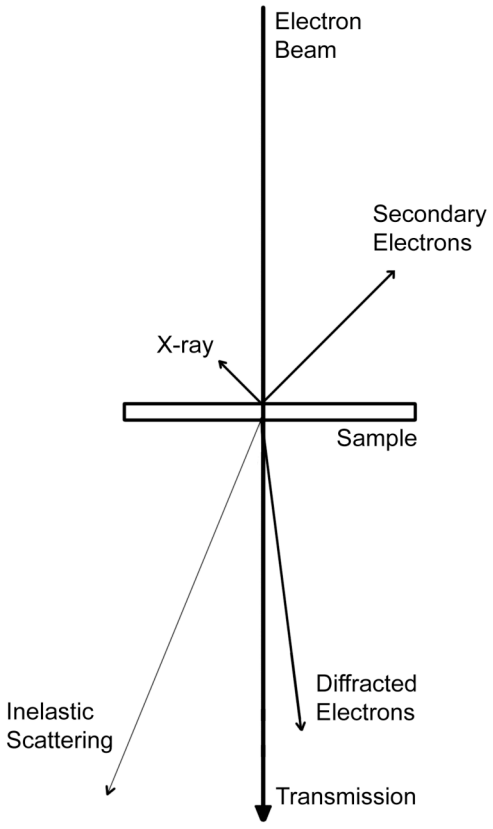

Figure 2.17: Electron Beam Sample Interaction

2.9.1 Scanning Electron Microscopy

Secondary electrons are electrons that are ejected from the sample as a result of a collision between the sample and the incident electron beam. Unlike backscattered electrons which are incident electrons that are scattered at much higher energy, secondary electrons are much lower in energy (< 50 eV). The electron beam is scanned across the surface of the sample, which emits secondary electrons, the intensities of which are governed by the angle of the sample relative to the incident beam. By detecting the secondary electrons and correlating the beam position and signal intensity, a three dimensional image can be generated. To prevent the build-up of surface charge in non-conducting samples the surface of the sample is typically coated with gold or a suitable metal. The magnification range of SEM is wide, with resolutions between 1 μm and 100 μm, allowing analysis of biological macromolecules, small particles, fibres and surfaces.

2.9.2 Transmission Electron Microscopy

Transmission electron microscopy (TEM) is the use of a transmitted electron beam, manipulated by magnetic lenses, to generate an image or a diffraction pattern for a sample. The image obtained from a TEM is a two dimensional image, as the electrons have passed through the sample, unlike SEM in which the detected intensity is relative to the surface. However, as the transmitted electron beam is of much higher energy than secondary electrons a much greater resolution can be achieved, with atomic resolution theoretically possible.

The beam path is shown below (figure 2.18). Firstly, the electron beam passes through the sample, where the scattering and diffraction are dependent upon the nature of the sample. After this the beam is focussed by the objective lens, and passes through the objective lens aperture, followed by a series of lenses until the image is detected by either film or a charge coupled device (CCD). By changing the focussing either an image or a diffraction pattern can be obtained.

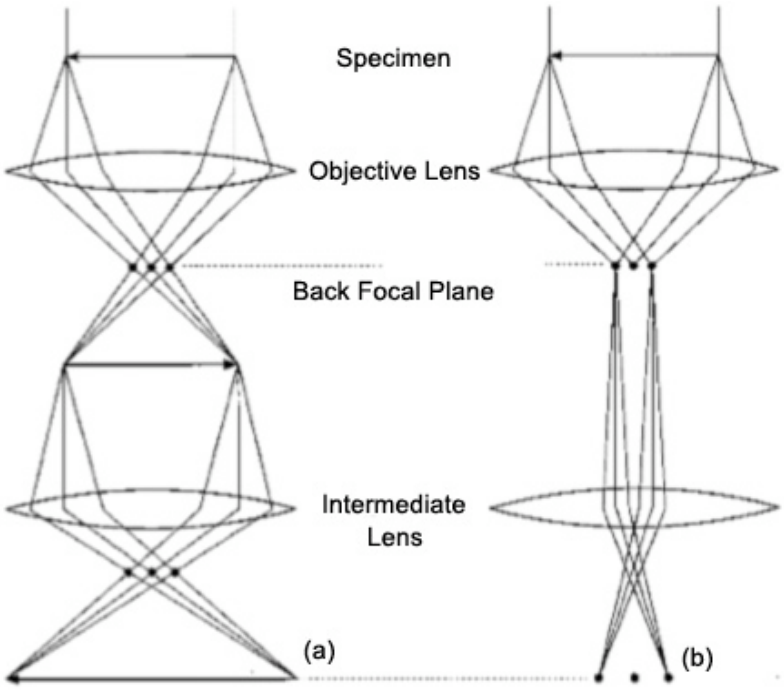

Figure 2.18: TEM Beam Diagram for Imaging (a) and Diffraction (b)[17]

The resolution of the final image is largely dependent upon the quality of the objective lens and the intensity of the incident electron beam. The objective lens must be very thin to minimise multiple scattering of the electron beam, with a typical thickness of 10 - 500 Å. The typical resolution of a TEM image is between 10 - 1000 Å. A TEM image of SBA-15 is shown below (figure 2.19).

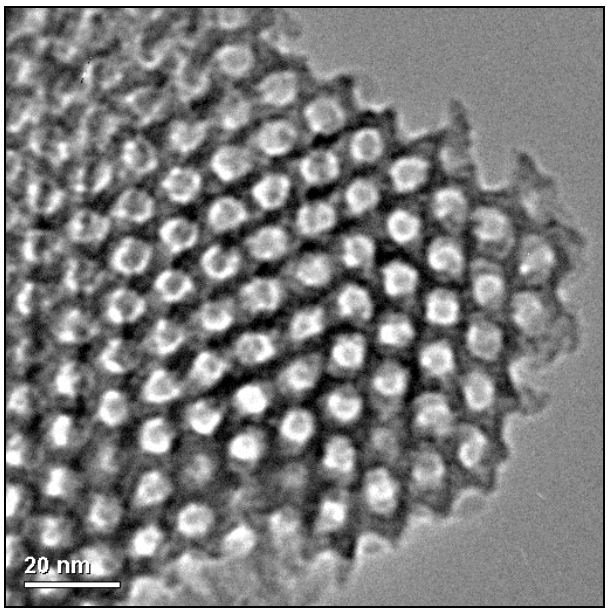

Figure 2.19: TEM Image of SBA-15

2.10 Conclusion

Using the methods described above it is possible to investigate many of the physical properties of bulk materials, and to gain information about the order and morphology of a material. The methods described are particularly applicable to mesoporous materials as they can be used to investigate the pore system and its properties. The application of these physical methods provides information about the nature of the materials, and by understanding this nature, useful applications and new materials can be developed.

References

[1] K. Sing, *Colloids Surf., A*, 2001, **187-188**, 3.
[2] S. Brunauer, L. S. Deming, W. E. Deming and E. Teller, *J. Am. Chem. Soc.*, 1940, **62**, 1723.
[3] S. Brunauer, P. H. Emmett and E. Teller, *J. Am. Chem. Soc.*, 1938, **60**, 309.
[4] J. H. DeBoer and C. Zwicker, *Z. Phys. Chem.*, 1929, **3**, 407.
[5] Bhambhan.Mr, D. H. Turk, K. S. W. Sing and P. A. Cutting, *J. Colloid Interface Sci.*, 1972, **38**, 109.
[6] J. M. Thomas and W. J. Thomas, *Principles and Practice of Heterogeneous Catalysis*, VCH, Weinheim, 1997.
[7] P. J. Branton, P. G. Hall, K. S. W. Sing, H. Reichert, F. Schuth and K. K. Unger, *J. Chem. Soc., Faraday Trans.*, 1994, **90**, 2965.
[8] P. I. Ravikovitch, S. C. Odomhnaill, A. V. Neimark, F. Schuth and K. K. Unger, *Langmuir*, 1995, **11**, 4765.
[9] J. Unterzaucher, *Analyst (Cambridge, U. K.)*, 1952, **77**, 584.
[10] G. L. Ellman, *Arch. Biochem. Biophys.*, 1959, **82**, 70.
[11] L. R. Sarles and R. M. Cotts, *Phys. Rev.*, 1958, **111**, 853.
[12] W. K. Rhim, D. D. Elleman and R. W. Vaughan, *J. Chem. Phys.*, 1973, **59**, 3740.
[13] M. Lee and W. I. Goldburg, *Phys. Rev.*, 1965, **140**, 1261.
[14] E. O. Stejskal and J. D. Memory, *High Resolution NMR in the Solid State: Fundamentals of CP/MAS*, Oxford University Press, Oxford, 1994.
[15] J. Schaefer and E. O. Stejskal, *J. Am. Chem. Soc.*, 1976, **98**, 1031.
[16] E. R. deAzevedo and T. J. Bonagamba, *Handbook of Applied Solid State Spectroscopy*, Springer, New York, 2006.
[17] P. J. Goodhew, J. Humphreys and R. Beanland, *Electron Microscopy and Analysis*, Taylor & Francis, London, 2001.

3. Mesoporous Silica Supports

3.1 Introduction

The synthesis of well ordered mesoporous silica supports is described in this section, as is the characterisation of these materials. A wide range of methods have been used for materials characterisation, including nitrogen adsorption, elemental analysis, thermal gravimetric analysis, scanning and transmission electron microscopy, small angle X-ray diffraction and solid state NMR spectroscopy. The materials are based on SBA-15, and include a range of organic functionalisation, incorporated into the materials by different methods.

The aim of this section is to describe the synthesis and characterisation of a series of well-ordered mesoporous support materials and the incorporation of organic functional groups into these materials for enzyme adsorption applications. The synthesis and characterisation of unfunctionalised SBA-15 materials is discussed, followed by the incorporation of organic groups by co-condensation and post-synthesis grafting. The expansion of the surfactant micelle by addition of trimethylbenzene and characterisation of the materials obtained is also described.

3.2 SBA-15

3.2.1 Synthesis of SBA-15

Mesoporous SBA-15 was prepared according to a previously reported literature procedure.[1] The surfactant P123 (4.0 g, 6.86 x 10^{-4} mol)($EO_{20}PO_{70}EO_{20}$, BASF) was dissolved in a solution of HCl (148 mL, 0.8 M) at 40 °C. Tetraethylorthosilicate (8.40 g, 0.04 mol) was added dropwise to the mixture, which was then stirred at 40 °C for 24 h. The mixture was then transferred to a thick walled Teflon flask and heated at 100 °C for 48 h. The white solid was then collected by filtration, washed with distilled water and dried in air. The surfactant was removed by calcination under flowing N_2 at 550 °C for 4 h, followed by calcination under flowing O_2 for 4 h. Alternatively, the surfactant was removed by solvent extraction, as described below.

3.2.2 Template Removal

The surfactant template was removed by one of two methods. The first method was calcination, which is expected to completely remove the surfactant template. This was achieved with a ceramic boat within a quartz tube furnace, with a two step calcination process. In the first step the material was placed in the furnace and heated to 550 °C under a nitrogen atmosphere, at a ramp rate of 5 °C min^{-1}. The furnace was held at 550 °C for 4 hours, then reduced to room temperature at 20 °C min^{-1}. This process yielded a light brown powder, the colour due to the presence of unoxidised breakdown products of the surfactant. The process was then repeated with an oxygen atmosphere and the same furnace conditions (figure 3.1). This yielded a pure white powder.

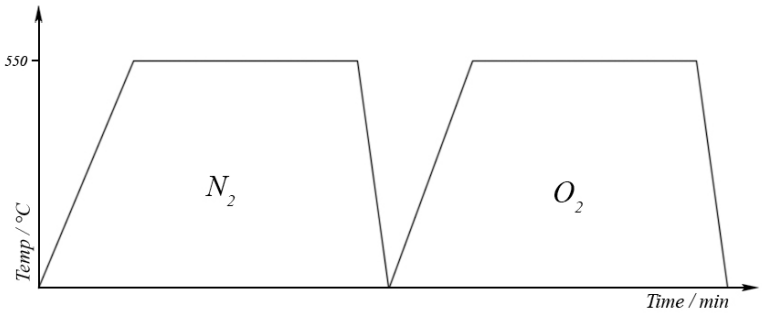

Figure 3.1: Furnace Conditions for SBA15 Calcination

The second method of surfactant extraction was by suspending the material in a suitable solvent, which was then heated to reflux. This method extracts the surfactant by dissolution into the solvent, from which the intact surfactant can be recovered for further templating. The effectiveness of this method of surfactant extraction with a range of different solvents was investigated. Each sample (1 g) was extracted three times with the appropriate solvent (50 mL), then recovered by filtration. After three consecutive washes the material was oven dried at 110 °C then analysed by TGA using a TA Instruments SDT 2960. The TGA analysis was run with a flow of O_2 gas, at a rate of 110 cm^3 min^{-1}.

Each TGA trace (figure 3.2, below), bar that from the calcined sample, shows an initial loss of weight between 25 - 165 °C due to the removal of residual solvent, followed by a marked drop in weight due to the decomposition of the surfactant at an onset temperature of 165 °C.

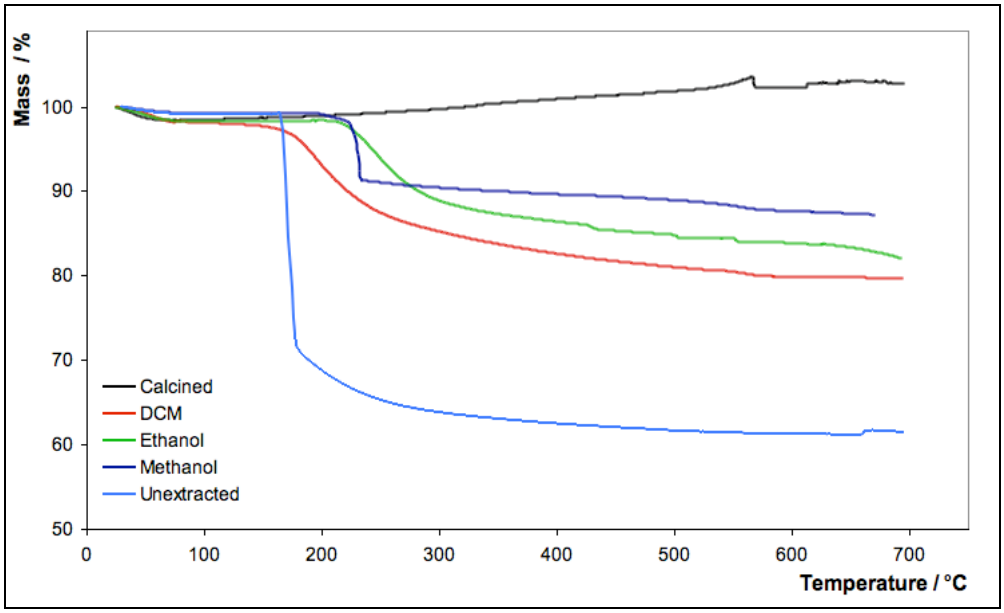

Figure 3.2: TGA Analysis of Surfactant Solvent Extraction from SBA-15

The total weight loss data, which reflects the amount of surfactant remaining in the support, are tabulated below (table 3.1). The table lists the weight loss for the first step between 25 - 165 °C, due to loss of solvent, and the second step between 165 - 700 °C, due to loss of surfactant. The number in brackets is the weight loss after correction for the loss in the previous step. The increase in weight for the calcined material is due to a decrease in the gas buoyancy at high temperatures, and is expected to increase the observed weight decrease for each sample by up to 4 %. It was also observed after measurement that the machine required calibration / maintenance, observable in the irregularity of the traces at high temperature, and may result in an additional uncertainly in the final weight loss of up to 2 %.

Table 3.1: Weight Loss of SBA-15 After Solvent Extraction

Sample	Step 1 Weight Loss / %	Step 2 Weight Loss / %	Surfactant / g g^{-1}
Calcined	1.2	-4.3 (-)	0
DCM Ext.	2.7	17.5 (18.0)	0.22
Ethanol Ext	1.7	16.3 (16.6)	0.20
Methanol Ext.	0.8	12.0 (12.1)	0.14
Unextracted	0.9	37.6 (37.9)	0.61

There is no weight loss observed for the calcined sample, indicating the surfactant was completely removed by the calcination process. During the synthesis 8.40 g TEOS is

added, which is a theoretical mass of 2.42 g SiO_2. A yield of 3.52 g was obtained after filtration and drying prior to extraction. The unextracted sample shows a weight loss of 37.9 % during the second step, indicating that not all of the P123 surfactant has been incorporated into the material, if 4.0 g surfactant was incorporated, the unextracted sample would show a weight loss of approximately 62%. A weight loss of 37.9% indicates that 1.48 g of the P123 surfactant is incorporated into the material during synthesis (0.61 g / g SiO_2). Partial extraction may be due to the formation of ethanol during synthesis (from hydrolysis of tetraethylorthosilicate).

The methanol, ethanol and DCM extracted samples show between 12 - 18% weight loss during the second stage. There is a considerable amount of surfactant remaining in each extracted material (~ 20% residual surfactant), partly due to incomplete extraction after three batches of solvent, but mainly due to the presence of surfactant in the solvent-inaccessible microporous corona of SBA-15.

3.2.3 X-Ray Diffraction

Low angle scattering X-ray diffraction (XRD) was used to investigate the degree of order inherent in the material, to identify the bulk phase of the material, and to obtain a characteristic fingerprint of each material. The XRD was obtained with a Panalytical X'Pert Pro model diffractometer, with 2θ values between 0.7 - 6. The X-rays used were the $K_{\alpha 1}$ line of Copper (λ = 1.5418 Å). The small angle X-ray diffraction pattern for SBA-15 is plotted below (figure 3.3).

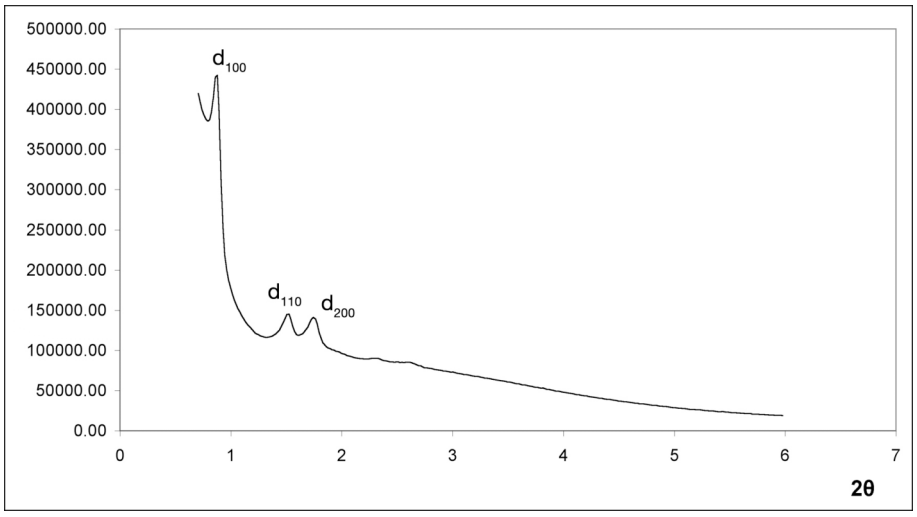

Figure 3.3: X-Ray Diffraction from Calcined SBA-15

The three peaks observed correspond to the 100, 110 and 200 reflections. The d_{100} and d_{110} planes are illustrated below (figure 3.4).

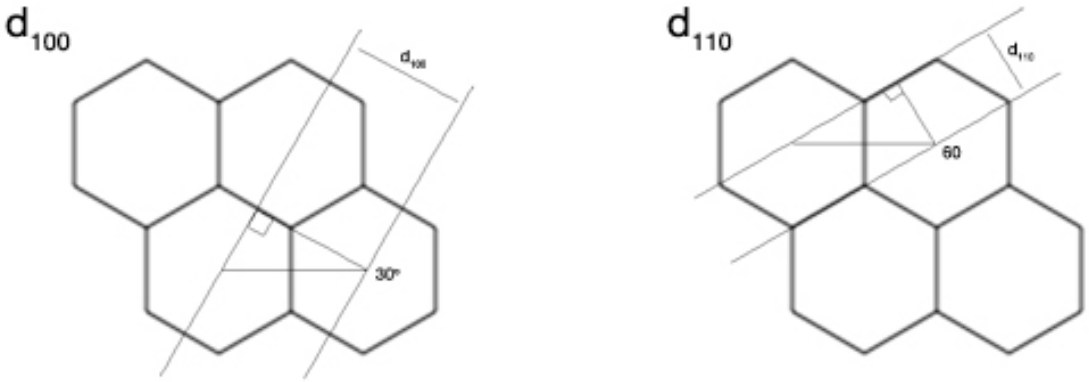

Figure 3.4: Hexagonal (*p6mm*) XRD Reflections

The distances between the Bragg diffraction planes (d values) were calculated from the 2θ angles using the Bragg equation. The unit cell parameter (a) was also calculated (table 3.2), and has an average value of 116.3 Å. Given that the average pore size diameter is 67.7 Å from nitrogen adsorption (see section 3.2.6), this indicates an average wall thickness of 48.6 Å.

Table 3.2: X-ray Diffraction Data for Calcined SBA-15

Reflection	2θ	d / Å	a / Å
100	0.878	100.61	116.17
110	1.524	57.97	115.94
200	1.745	50.63	116.92

3.2.4 Scanning Electron Microscopy

SEM images were obtained with a JEOL JSM-5600 scanning electron microscope. The image below (figure 3.5) was obtained for calcined SBA-15, and shows a rod-like particle shape, of width approximately 10 μm and of variable length between 20 - 100 μm.

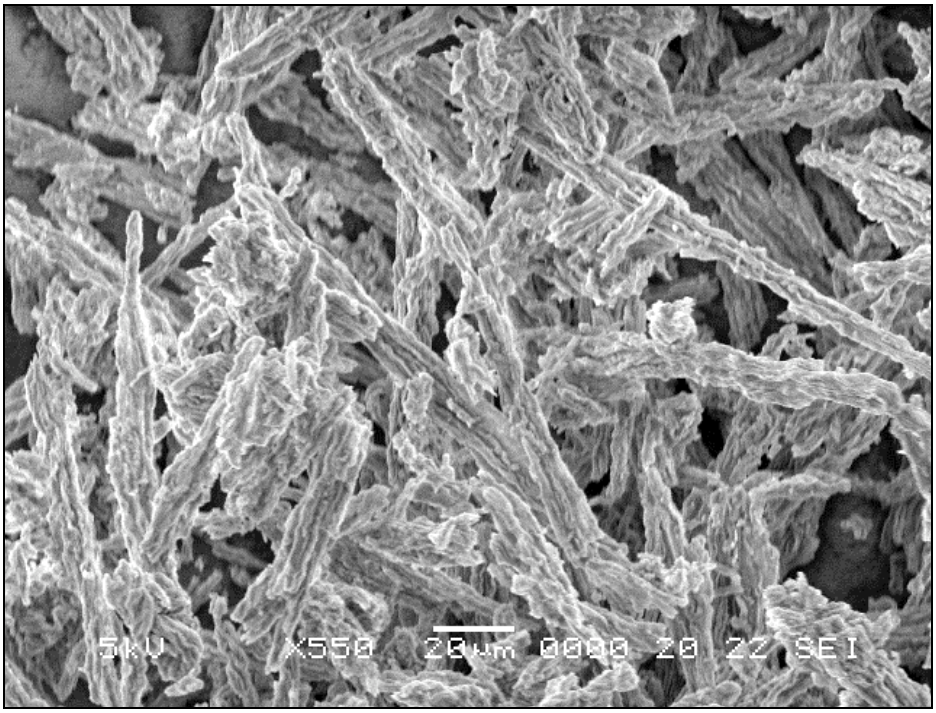

Figure 3.5: SEM Image of Calcined SBA-15

SEM analysis of ethanol extracted SBA-15 was also carried out, and two of the images obtained are shown below (figure 3.6). The rod-like structure has been disrupted, resulting in smaller particles, some of which are aggregated. This is due to grinding of the resultant material (using a pestle and mortar) after filtration and drying.

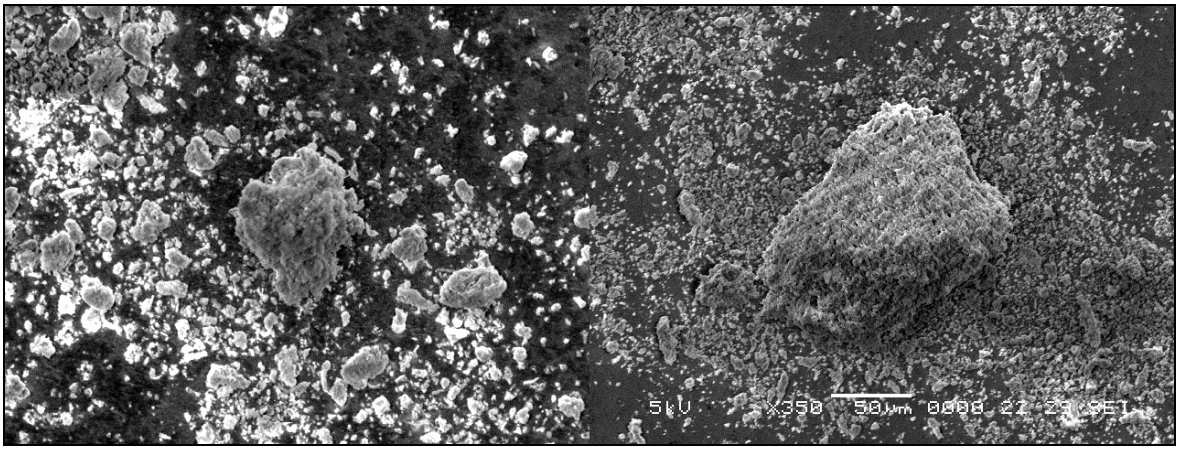

Figure 3.6: SEM Images of Ethanol Extracted SBA-15

3.2.5 Particle Size Analysis

The particle size of calcined SBA-15 was measured with a Beckman Coulter LS 230 particle size analyser. The LS 230 utilises laser diffraction to measure the size of particles, which are dispersed in distilled water, using the Fraunhofer approximation. Large particles diffract at small angles with high intensity and small particles diffract with large angles and lower intensity. A series of detectors at fixed angles relate the diffraction and intensity to the particle size, and the results for calcined SBA-15 are shown below (figure 3.7).

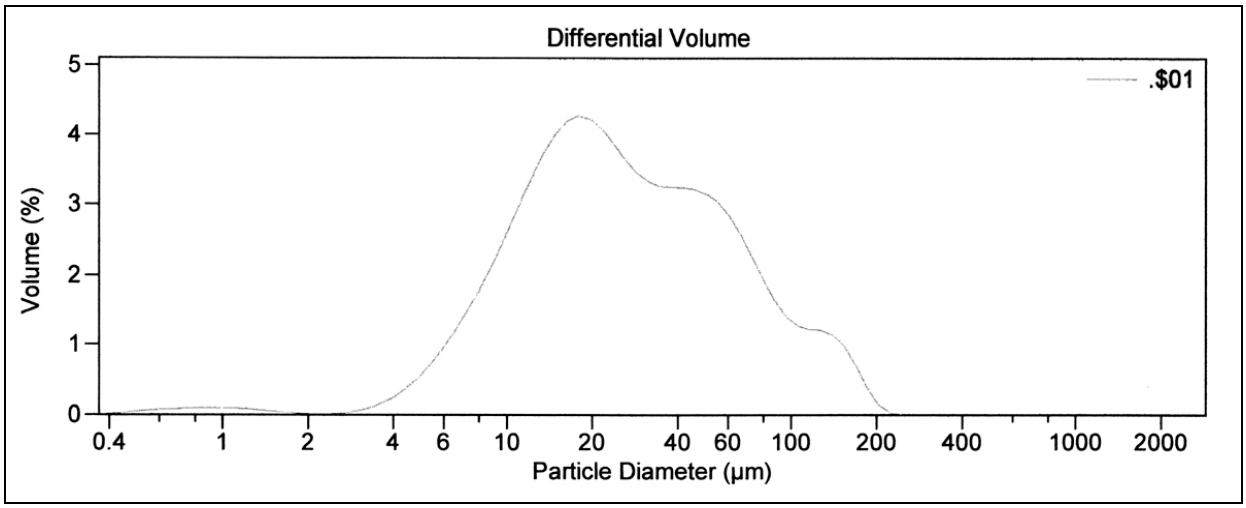

Figure 3.7: Calcined SBA-15 Pore Size

SBA-15 prepared by the method above has a broad range of particle sizes, with measured particle diameters between 5 - 200 µm, an average (mean) particle size of 38 µm, and an average (mode) particle size of 18 µm.

3.2.6 Nitrogen Adsorption

Nitrogen adsorption measurements were taken with a Hiden 002 Intelligent Gravimetric Analyser. The adsorption / desorption trace for calcined SBA-15 is shown below (figure 3.8).

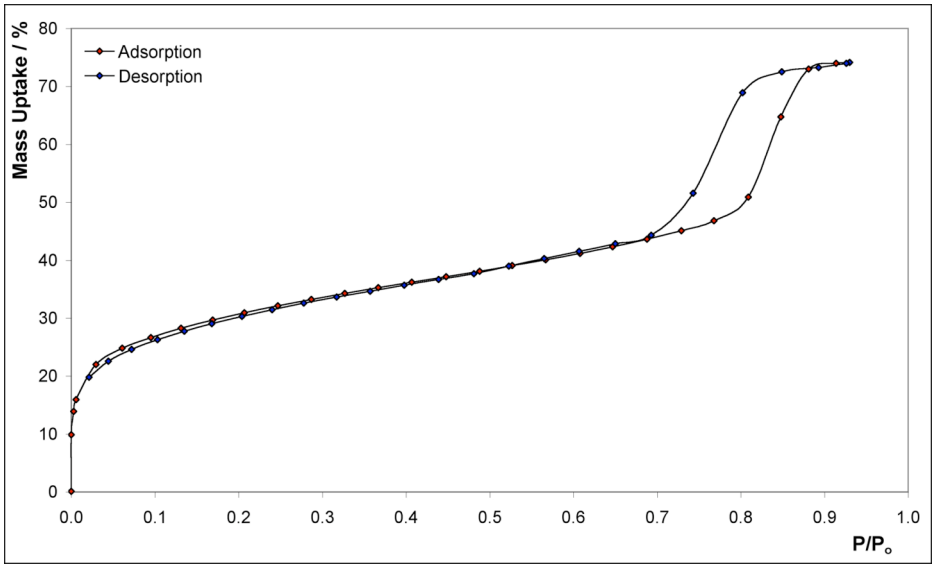

Figure 3.8: Calcined SBA-15 Nitrogen Adsorption

The adsorption shows a type IV isotherm typical of mesoporous materials. A type H1 hysteresis loop can be observed between the adsorption and desorption traces during the capillary condensation step, indicating capillary pores of uniform diameter throughout the length of the pore. Analysis of the size of these pores by the BJH method was carried out on the desorption branch of the isotherm, giving a lower limit to the average pore diameter, and is shown below (figure 3.9), indicating an average pore size diameter of 67.7 Å (weighted mean average between 23 - 50 Å).

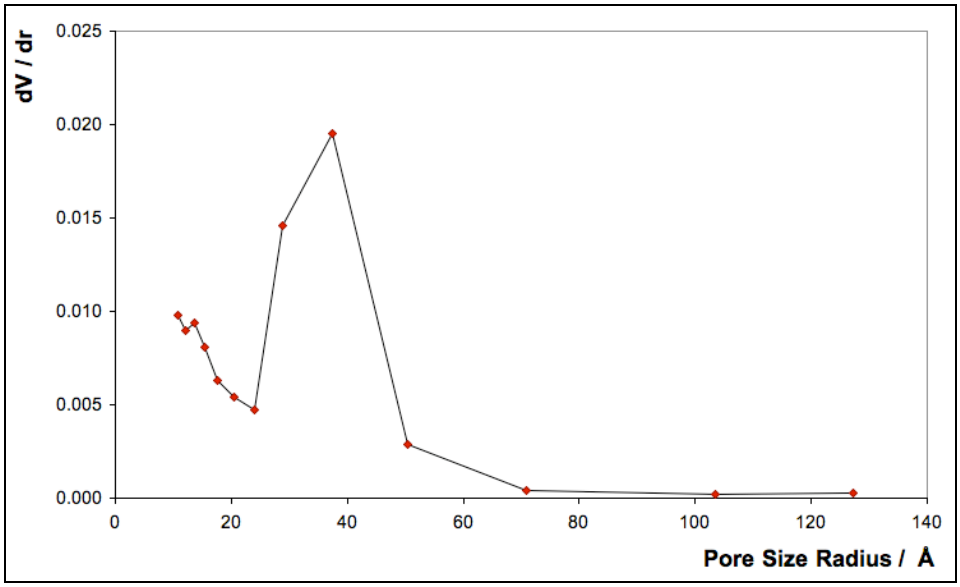

Figure 3.9: BJH Analysis of SBA-15 Pore Size

The surface area analysis by the BET method was carried out, using IGAswin v.2.25, and the graph is shown below (figure 3.10). The BET method is valid between partial pressures of 0.05 and 0.30, above which the deviation from the BET approximation can be observed. From the BET plot we obtain a surface area of 839 ± 15 $m^2 g^{-1}$.

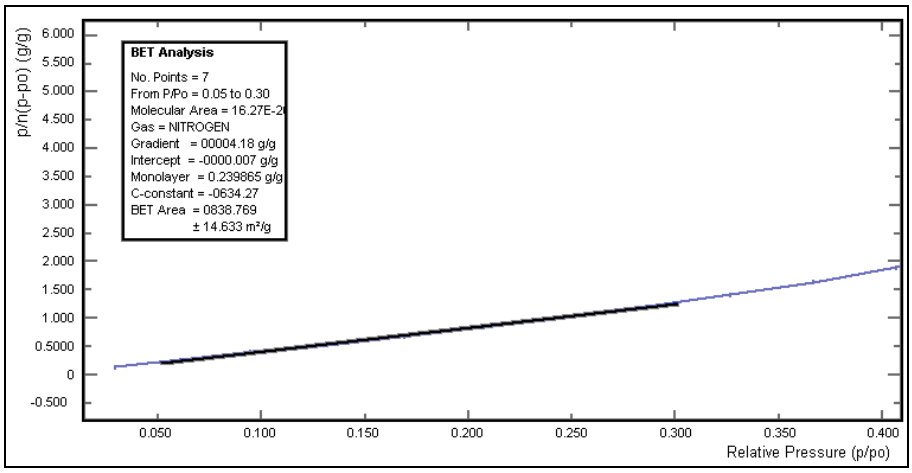

Figure 3.10: BET Analysis of SBA-15

3.2.7 Transmission Electron Microscopy

The morphology of the structure was investigated by transmission electron microscopy (TEM), to produce an image of the structure on the nanoscale. The X-ray analysis above shows us that the structure of SBA-15 has a hexagonal symmetry, with a *p6mm* space group. The porous channels are aligned, and can be observed in the images below (figure 3.11).

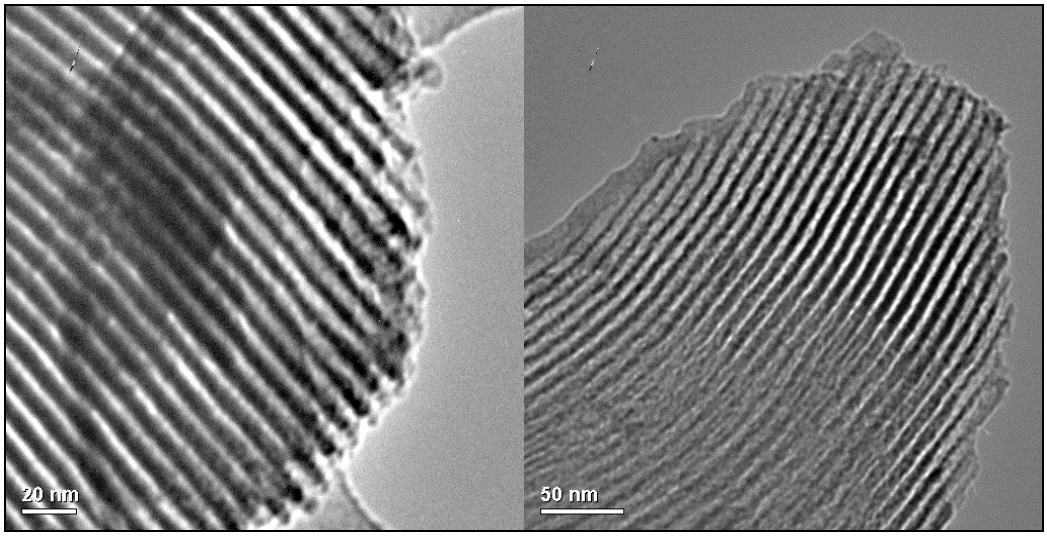

Figure 3.11: SBA-15 Pore Channels TEM Image

The images of the entrances to the pore system are shown in figure 3.12. Measurement of the pore diameter from the image shows that the average inter-pore distance is 107 Å, the measurement areas are annotated on the images below. This is smaller than the value of 116 Å obtained from x-ray diffraction, which is averaged all of the ordered regions. The average pore size by measurement is 64.0 ± 4.9Å. This agrees with the value of 68 Å obtained by nitrogen adsorption. This is of sufficient size to accommodate CALB, which has dimensions of 30 x 40 x 50 Å (see section 4.2).

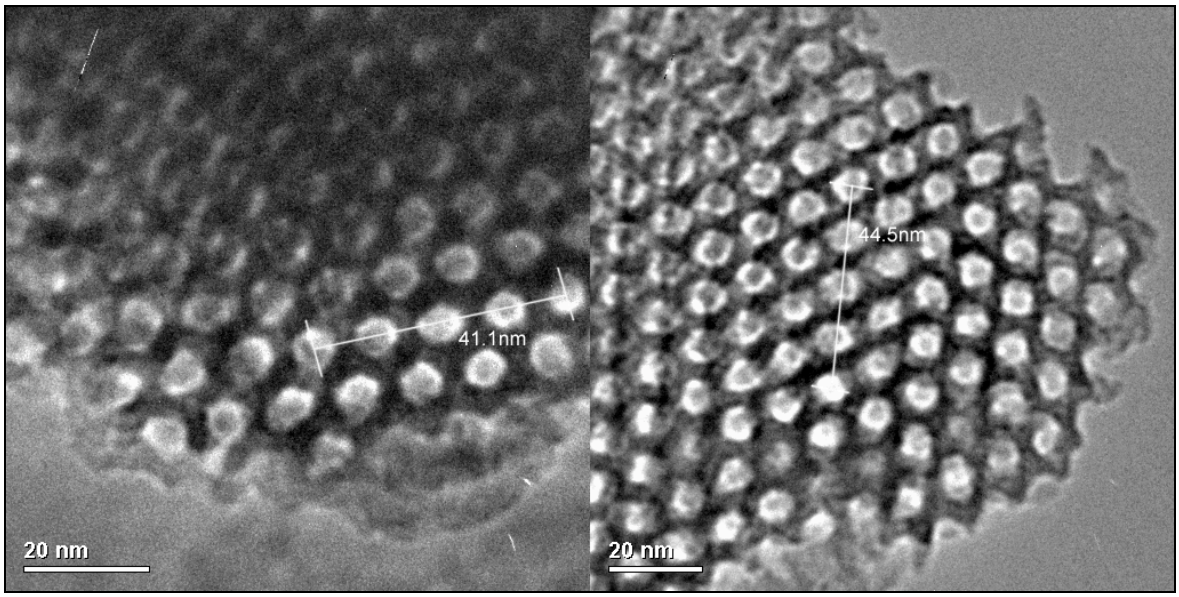

Figure 3.12: SBA-15 Pore Entrances TEM Image

3.2.8 Aqueous Stability and Silanol Regeneration

To test the stability of SBA-15 in aqueous systems, two 100 mg samples of calcined SBA-15 were suspended in 50 mL distilled H_2O. One of the samples was kept at room temperature and the other was heated to 50 °C and both were stirred for 12 hours with a magnetic follower. The samples were recovered by filtration, then oven dried at 110 °C.

3.2.8.1 Nitrogen Adsorption of Rehydrated SBA-15

To measure the stability of the pore system to the aqueous treatment, nitrogen adsorption measurements were taken. These adsorption traces are plotted below (figure 3.13). Each material exhibits a characteristic type IV isotherm, indicating the mesoporous

structure was retained. The mass uptake of the sample treated at room temperature is offset by 50%, and the mass uptake of the sample treated at 50 °C is offset by 100%.

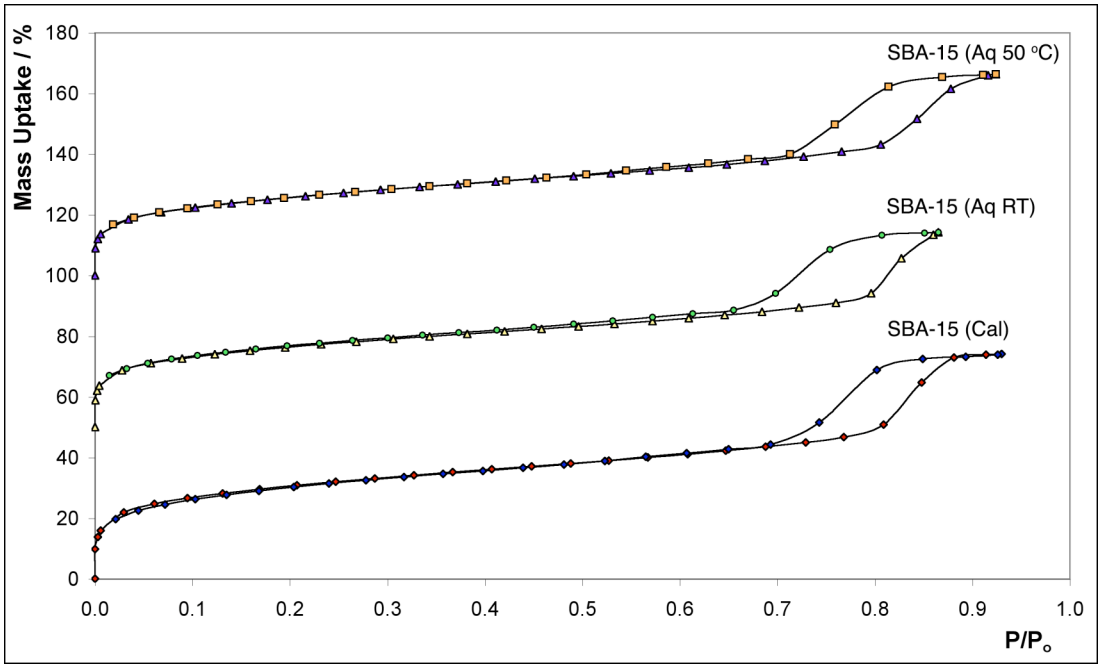

Figure 3.13: Nitrogen Adsorption of H_2O Treated SBA-15

The nitrogen adsorption data were analysed by using the BET and BJH models, and the results are tabulated below (table 3.3). The total uptake of nitrogen has decreased slightly in both treated samples, as has the surface area and average pore size distribution. This is almost certainly due to the hydrolysis of surface silicon oxygen bonds by addition of water. This results in a slightly smaller pore size, exhibited by a smaller surface area by BET analysis, and slightly lower uptake of nitrogen.

Table 3.3: Rehydration of Calcined SBA-15

Support	Total Uptake / %	Surface Area / $m^2 g^{-1}$	PSD / Å
SBA-15 (Cal)	74.1	805	68
SBA-15 (R.T.)	64.2	689	59
SBA-15 (50 °C)	66.4	680	62

3.2.8.2 Rehydrated SBA-15 ^{29}Si SSNMR Spectroscopy

To investigate the composition of the surface, ^{29}Si NMR spectroscopy was employed to probe the bonding of silicon within the material. The NMR results are shown below (figure 3.14). When compared to calcined SBA-15 which is mainly comprised of silicon bonded to four oxygen atoms bonded to another silica ($Si(OSi)_4$, denoted Q^4), the samples treated with water show the presence of a significant amount of silica bonded to three oxygen atoms bonded to silica with one oxygen bonded to hydrogen ($HOSi(OSi)_3$, denoted Q^3). This is due to hydrolysis of the silica surface, which is fully condensed after calcination, producing a surface comprised primarily of silanol groups.

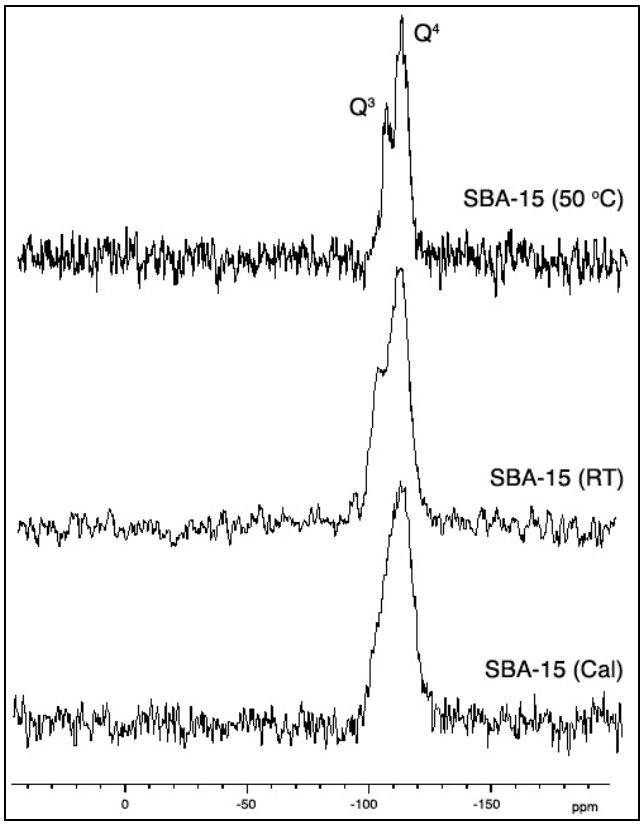

Figure 3.14: ^{29}Si NMR of H_20 Treated SBA-15

3.2.8.3 Small Angle X-ray Diffraction of Rehydrated SBA-15

To confirm that the order of the material is retained, the rehydrated SBA-15 (R.T.) was analysed by small angle X-ray diffraction, and the pattern obtained is plotted below (figure 3.15).

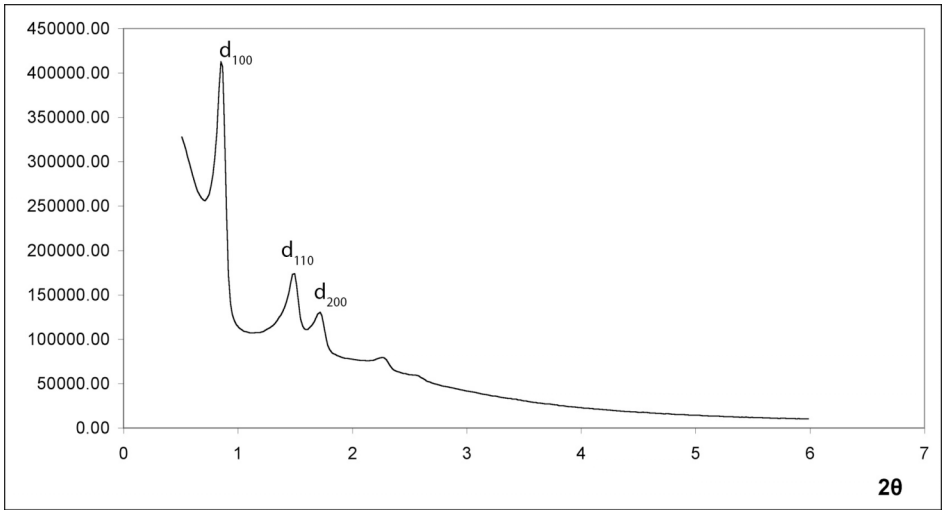

Figure 3.15: SAXS Diffraction Pattern for Rehydrated SBA-15

The Bragg diffraction plane spacing and the unit cell parameter have been calculated and are tabulated below (table 3.4). The unit cell distance calculated by this method is 119.0 Å, this is very close to the value for calcined SBA-15 of 116.3 Å. The slight expansion may be due to the hydrolysis of the surface layer of silicon oxygen bonds.

Table 3.4: X-ray Diffraction Data for R.T. Rehydrated SBA-15

Reflection	2θ	d / Å	a / Å
100	0.850	103.9	120.0
110	1.496	118.2	118.2
200	1.717	59.5	118.9

3.2.8.4 Water Adsorption with Calcined SBA-15

To investigate the hydrophilicity of calcined SBA-15, the adsorption of water was measured investigated by a gravimetric method using a Hiden IGA 002. The sample was degassed then the water was added as vapour, with a sample temperature of 20 °C. The adsorption / desorption isotherm, and a second adsorption / desorption isotherm are shown below (figure 3.16). The first desorption trace shows that not all of the water adsorbed is desorbed as the pressure is reduced. The subsequent adsorption / desorption is reversible. This is due to the irreversible adsorption of water during the first adsorption step, this water hydrolyses the surface silicon oxide bonds to silanol groups. This agrees with the

SSNMR spectroscopy results (section 3.2.8.2), which observe an increase in the Q^3 peak ($Si(OH)O_3$) after stirring in water.

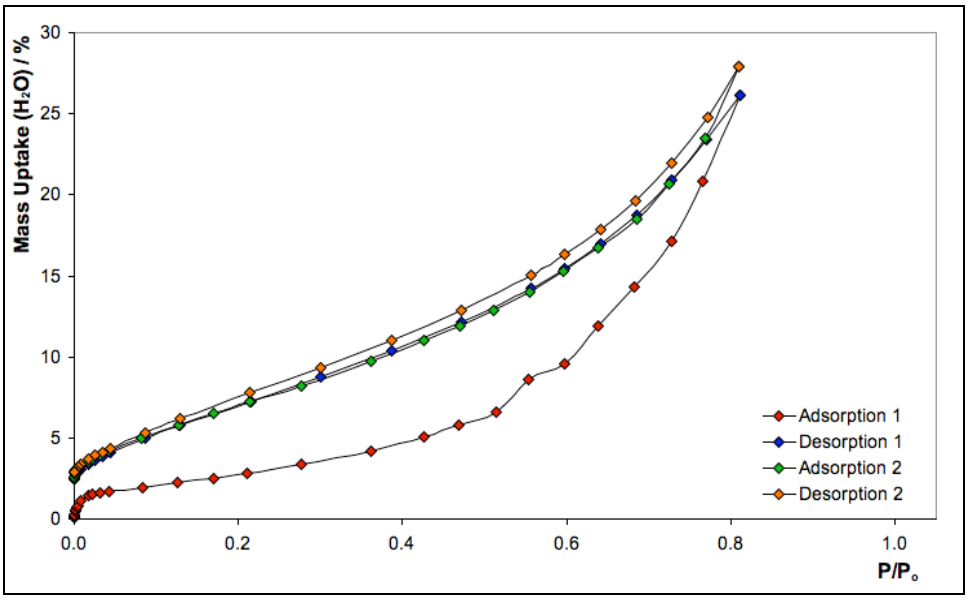

Figure 3.16: Adsorption of Water by Calcined SBA-15

3.3 Functionalised SBA-15

3.3.1 Introduction

The incorporation of functional groups is of interest for a few key reasons. The interaction between the support and the protein can be improved, resulting in improvements in stability and leaching properties. The diffusion properties of the material can be tailored to organic solvents for a particular application. With these ideas in mind, a range of functional groups were chosen to be incorporated into the material, to target specific amino acids, such as amine groups to target aspartic and glutamic acid residues, free thiols to target cysteine residues, carboxylic acid functionality to target basic residues, and phenyl groups to increase the hydrophobicity of the material. These groups were incorporated by co-condensation as a triethoxysilane (*in-situ*), and by grafting of a triethoxysilane post-synthesis. The functional groups, and the incorporation methods are illustrated below (figure 3.17). The surfactant was removed from the co-condensed samples by ethanol extraction, and removed by calcination for the post-synthesis samples prior to addition of triethoxysilane.

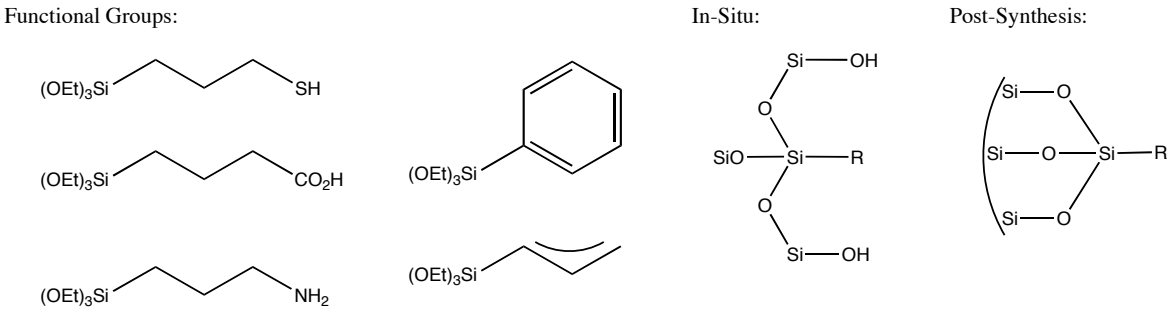

Figure 3.17: Incorporation of Organic Functional Groups

The sample names are obtained by taking the method of organic group incorporation, either *in-situ* (is) or post-synthesis (ps), followed by the organic group incorporated. This is then followed by the morphology of the material in question, and the molar percentage of the synthesis mixture. So the syntax is: (method)(group)-(material)(percentage). For example, the material obtained by co-condensation of $Si(OEt)_4$ with $(OEt)_3SiC_3H_6SH$ at five molar percent (by silica) is denoted isPrSH-SBA-15 (5%).

3.3.2 isPrSH-SBA-15

3.3.2.1 Synthesis

The surfactant P123 (4.0 g, 6.86 x 10^{-4} mol)($EO_{20}PO_{70}EO_{20}$, BASF) was dissolved in a solution of HCl (148 mL, 0.8 M) at 40 °C. Tetraethylorthosilicate and 3-mercaptopropyltriethoxysilane were mixed according to the table below (table 3.5), added drop-wise to the surfactant mixture and stirred at 40 °C for 24 h. The mixture was then transferred to a thick walled Teflon flask and heated at 100 °C for 48 h. The white solid was then collected by filtration, washed with distilled water and dried in air. The surfactant was removed by solvent extraction, using ethanol (100 mL, HPLC Grade), which was refluxed for 4 h before recovery of the solid by filtration. This was repeated three times for each sample. A third batch was extracted by Soxhlet extraction with ethanol (250 mL, HPLC Grade).

Table 3.5: isPrSH-SBA-15 Synthesis Composition

Loading	3-Mercaptopropyltriethoxysilane	Tetraethoxysilane
2%	0.192 g, 8.06 x 10^{-4} mol	8.232 g, 0.0395 mol
5%	0.482 g, 2.02 x 10^{-3} mol	7.979 g, 0.0383 mol
7%	0.672 g, 2.82 x 10^{-3} mol	7.812 g, 0.0375 mol

3.3.2.2 X-Ray Diffraction

The diffraction pattern for isPrSH-SBA-15 (5%) was recorded, and the results are plotted below (figure 3.18). The d_{100}, d_{110} and d_{200} peaks can be observed, and are typical for a hexagonally ordered material.

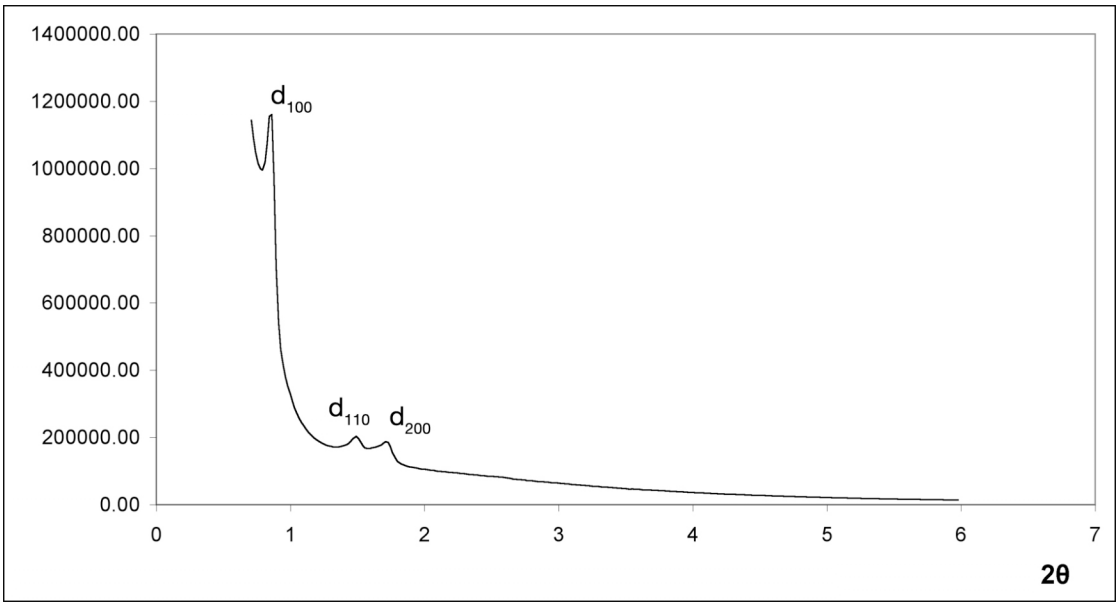

Figure 3.18: XRD Pattern for isPrSH-SBA-15 (5%)

The data is tabulated below (table 3.6), and the d-spacings and a values (inter-pore distance) have been calculated. From these peaks, the average value of a is 118.7 Å.

Table 3.6: X-ray Diffraction Data for isPrSH-SBA-15 (5%)

Reflection	2θ	d / Å	a / Å
100	0.861	102.60	118.47
110	1.490	59.26	118.52
200	1.711	51.63	119.23

3.3.2.3 Thermal Gravimetric Analysis

The weight loss upon heating of the ethanol extracted samples provides information about the residual surfactant in the material, as well as the incorporation of the organic functional group, which will decompose at high temperatures. The TGA traces for the thiol functionalised materials are plotted below (figure 3.19), measured on a Rheometric TG1000M with a maximum temperature of 600 °C. The onset temperature for

the decomposition of the surfactant increases with the concentration of thiol in the material, indicating that removal of the surfactant requires more energy in each case. This is most likely to be due to the changes in morphology across the series, as a change from p6mm symmetry to Ia3d symmetry is observed with increasing thiol content (see section 3.3.2.10).

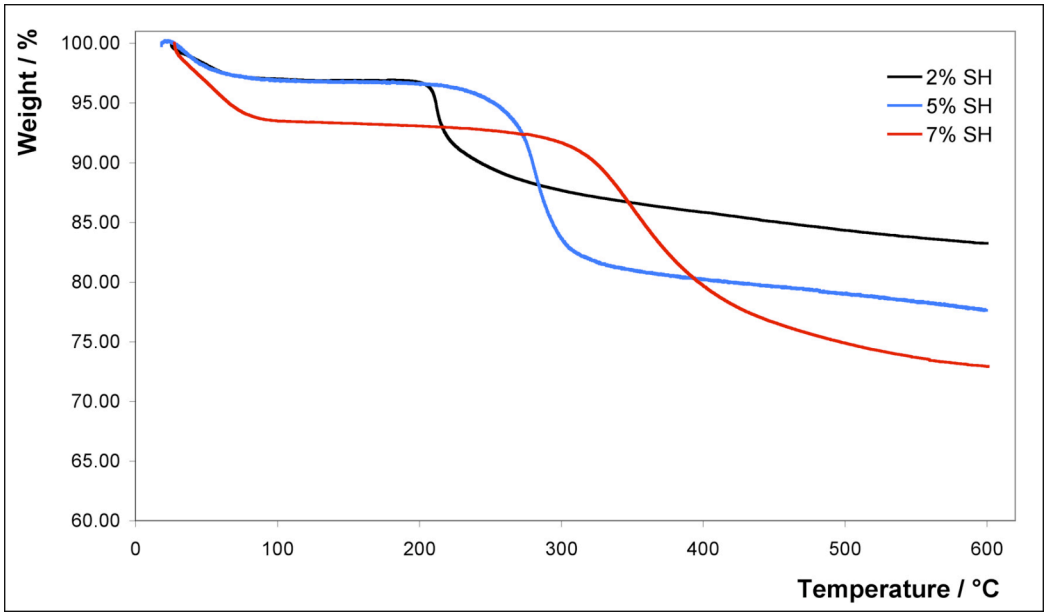

Figure 3.19: TGA Traces of isPrSH-SBA-15 Samples

The weight losses for each step are tabulated below (table 3.7). The numbers in brackets are the weight loss after correction for the loss of the previous step. The typical surfactant content of an unfunctionalised material is 0.61 g g^{-1}, indicating that as with the ethanol extracted samples discussed previously (section 3.2.2) approximately two thirds of the surfactant incorporated into the material is extracted.

Table 3.7: Weight Losses of isPrSH-SBA-15 Samples During TGA

Sample	Step 1 Weight Loss / %	Step 2 Weight Loss / %	Surfactant + PrSH / g g^{-1}
isPrSH-SBA-15 2%	3.1	13.7 (14.1)	0.16
isPrSH-SBA-15 5%	3.3	19.1 (19.7)	0.25
isPrSH-SBA-15 7%	6.8	20.3 (21.8)	0.28

3.3.2.4 Elemental Analysis

The incorporation of 3-mercaptopropyltriethoxysilane into the structure of SBA-15 was investigated by elemental analysis. The results are tabulated below (table 3.8). isPrSH-SBA-15 (5%) batch 3 was extracted by Soxhlet extraction. The carbon and hydrogen content of this sample is greatly reduced relative to the ethanol extracted samples, indicating that there is less residual surfactant in this material due to a more efficient extraction process. This efficient extraction is due to continuous extraction by pure solvent rather than a solvent with a high concentration of dissolved surfactant, despite a lower temperature of the extracting solvent during Soxhlet extraction (as the ethanol is condensed rather than refluxing). The elemental analysis shows that the thiol has been incorporated into the structure, and the accessibility of these thiol groups was measured by Ellman's analysis (see 3.3.2.5).

Table 3.8: isPrSH-SBA-15 Elemental Analysis

Sample	C	H	S
isPrSH-SBA-15 (2%)	8.41	2.00	0.79
isPrSH-SBA-15 (5%)	12.70	3.17	1.72
isPrSH-SBA-15 (5%) Batch 2	12.86	2.45	1.91
isPrSH-SBA-15 (5%) Batch 3	4.77	1.09	1.88
isPrSH-SBA-15 (7%)	17.34	3.52	2.33

3.3.2.5 Ellman's Analysis

The incorporation of the thiol functional group into the material was measured by elemental analysis, but to investigate the accessibility of the free thiols incorporated into the material Ellman's assay was used. The concentration of free thiol in each material was related to the cleavage of 5,5'-dithiobis(2-nitrobenzoic acid) (DNTB), calibrated with known concentrations of cysteine (see section 2.5). To measure the free thiol content of each sample the material (25 mg) was dissolved in distilled H_2O (9.5 mL) and diisopropylethylamine (DIPEA, 500 μL) was added. To this DTNB (0.5 mL, 0.1 M, 0.05 mol) was added and the mixture was stirred at room temperature for two hours using a roller mixer (Spiromix 5). The sample was diluted if required to obtain an absorbance between 0.2 - 1.0, measured using a UVIKON 930 UV-Visible spectrometer at 412 nm.

From this absorbance, the percentage of accessible thiol was calculated, and is plotted below (table 3.9).

Table 3.9: Investigating Accessible Thiol Groups by Ellman's Assay

Sample	Measured Thiol / $mmolg^{-1}$	Total Thiol (CHNS) / $mmolg^{-1}$	Accessible Thiol
SBA-15 (Calcined)	0.00	-	-
isPrSH-SBA-15 (2%)	0.13	0.25	52%
isPrSH-SBA-15 (5%)	0.39	0.54	72%
isPrSH-SBA-15 (7%)	0. 55	0.73	75%

The measured accessible thiol concentration corresponds well to the values obtained by CHNS analysis. In all samples a large proportion of the thiol is available on the internal surface of the material, with the remaining thiol either present in surface regions inaccessible to Ellman's reagent or impregnated within the silica matrix. The lower accessibility of the 2% sample when compared to the 5% and 7% samples may be due to differences in wall thickness between the samples (see section 3.3.2.11).

3.3.2.6 Solid State NMR Spectroscopy

A sample of isPrSH-SBA-15 (5%) was investigated by solid state NMR spectroscopy, observing ^{1}H, ^{13}C and ^{29}Si. A CP-MAS experimental setup was used for the carbon and silicon spectra. The ^{29}Si spectrum for isPrSH-SBA-15 (5%) is shown below (figure 3.20). The three peaks between -90 and -115 are from silicon atoms bound only to oxygen, the peaks at -58 and -66 are silicon that is bound to one carbon. The three oxygen bound Si peaks are Q^4 (-110.7 ppm, SiO_4), Q^3 (-101.1 ppm, $HOSiO_3$) and Q^2 (-91.3 ppm, $(HO)_2SiO_2$). The carbon bound Si peaks are T^2 (-58.4 ppm, $RSi(OR')O_2$) and T^3 (-66.4, $RSiO_3$).

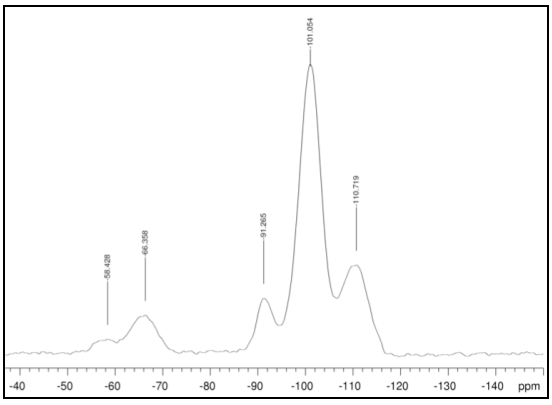

Figure 3.20: ^{29}Si SSNMR Spectrum of isPrSH-SBA-15 (5%)

The ^{1}H spectrum for isPrSH-SBA-15 (5%) is shown below (figure 3.21). There are five proton environments in isPrSH-SBA-15, the surface silanols, three sets of two protons on the propyl chain and the thiol proton. Unlike a solution phase NMR spectrum, the CP-MAS NMR spectra do not show a quantitative relationship between number of protons in an environment and the peak intensity, due to the cross polarisation. In the spectrum below, there are three resolved peaks, the 4.84 ppm peak is from the surface silanol protons, the peak at 2.28 ppm from protons on the alkyl chain, and the peak at 5.81 ppm from the proton of the thiol group.

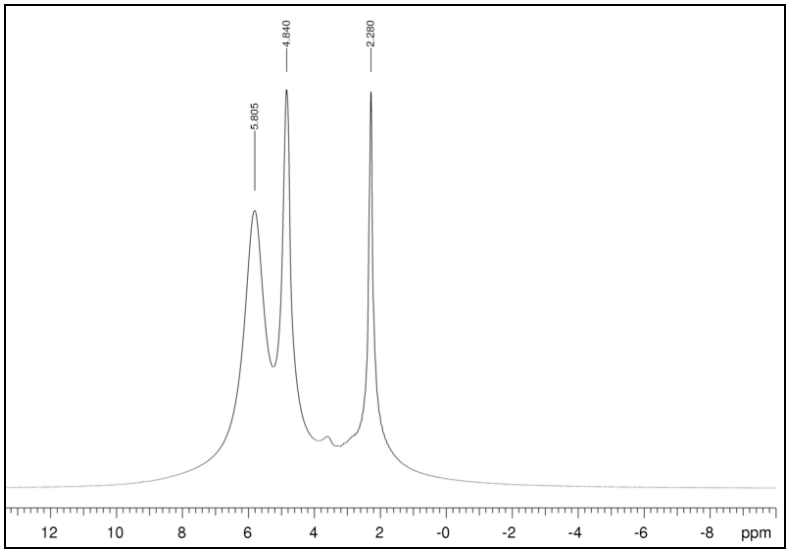

Figure 3.21: ^{1}H SSNMR Spectra of isPrSH-SBA-15 (5%)

The ^{13}C spectrum for isPrSH-SBA-15 (5%) is shown below (figure 3.22). Three peaks for the propyl chain can be observed at 10.8 ppm, 16.1 ppm and 27.4 ppm, in order of distance from silica. The remaining peaks are due to residual P123 surfactant, which is a block copolymer of structure $(CH_2CH_2O)_{20}(CH_2CH_2CH_2O)_{70}(CH_2CH_2O)_{20}$. The peaks at 70.4 ppm, 73.1 ppm and 76.0 ppm are due to CH_2 carbon atoms which are adjacent to oxygen, the peak at 22.7 ppm due to the central carbon atom of the propyl chain. the peak at 59.2 ppm is due to an OCH_2 carbon atom, from the ethanol used during extraction. The other carbon peak from the ethanol is not resolved, and is expected to have a chemical shift of 15 - 20 ppm.

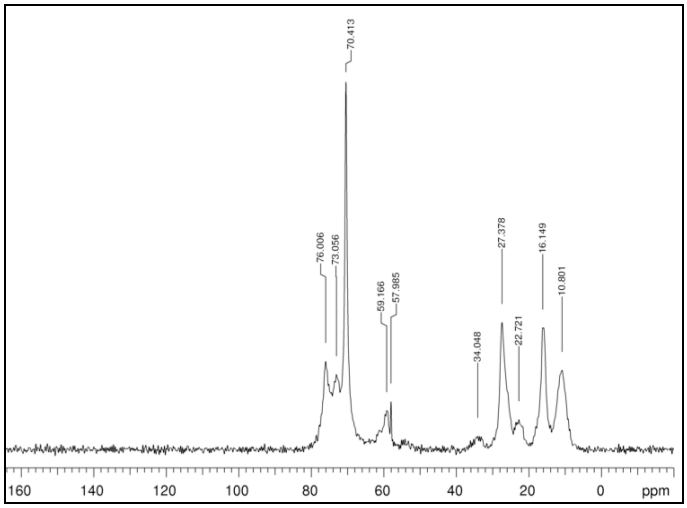

Figure 3.22: ^{13}C SSNMR Spectra of isPrSH-SBA-15 (5%)

3.3.2.7 Scanning Electron Microscopy

The particle size was analysed by SEM, using a JEOL 5600. The material shows a broad distribution of particle sizes, as can be observed in the image below (figure 3.23). As with the extracted SBA-15 the rod-like particle structure of calcined SBA-15 is disrupted during the extraction procedure and the resulting material has a very similar morphology to the extracted SBA-15 SEM images above (section 3.2.4).

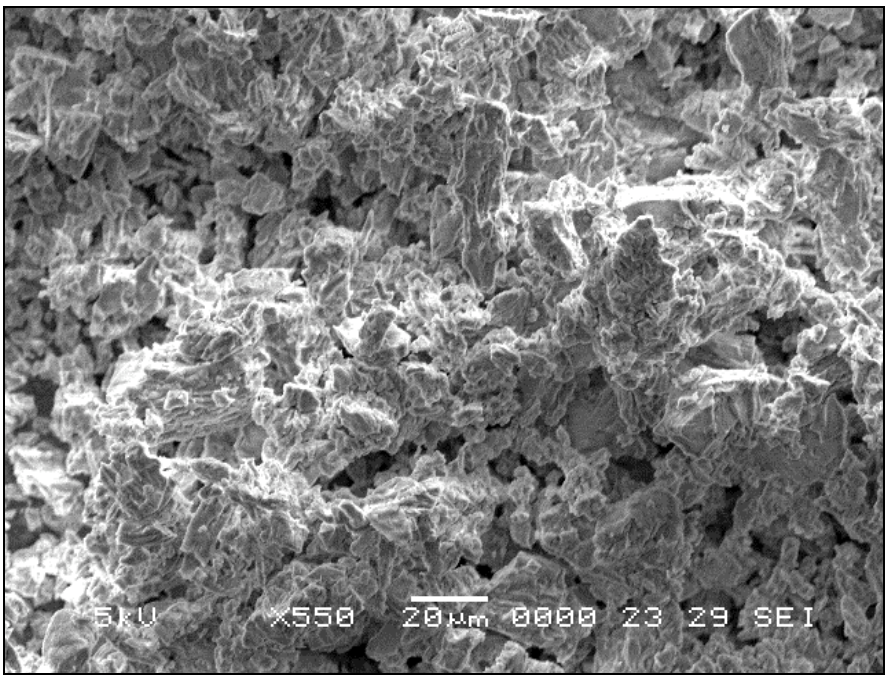

Figure 3.23: SEM Image of isPrSH-SBA-15 5%

3.3.2.8 Zeta Potential

The zeta potential was measured by suspending isPrSH-SBA-15 (5%) in distilled water, taking 16 portions of this mixture and adjusting the pH of each with sodium hydroxide / hydrochloric acid to reach the desired pH. The zeta potential was then measured with a Malvern Zetasizer. The pH is plotted versus zeta potential below (figure 3.24). The isoelectric point is the point at which the net charge on the particles is zero, when the plot crosses the x-axis. This is at pH 4.1 for isPrSH-SBA-15 (5%). The decrease in zeta potential at low pH is due to decomposition of the silica particles under strongly acidic conditions.

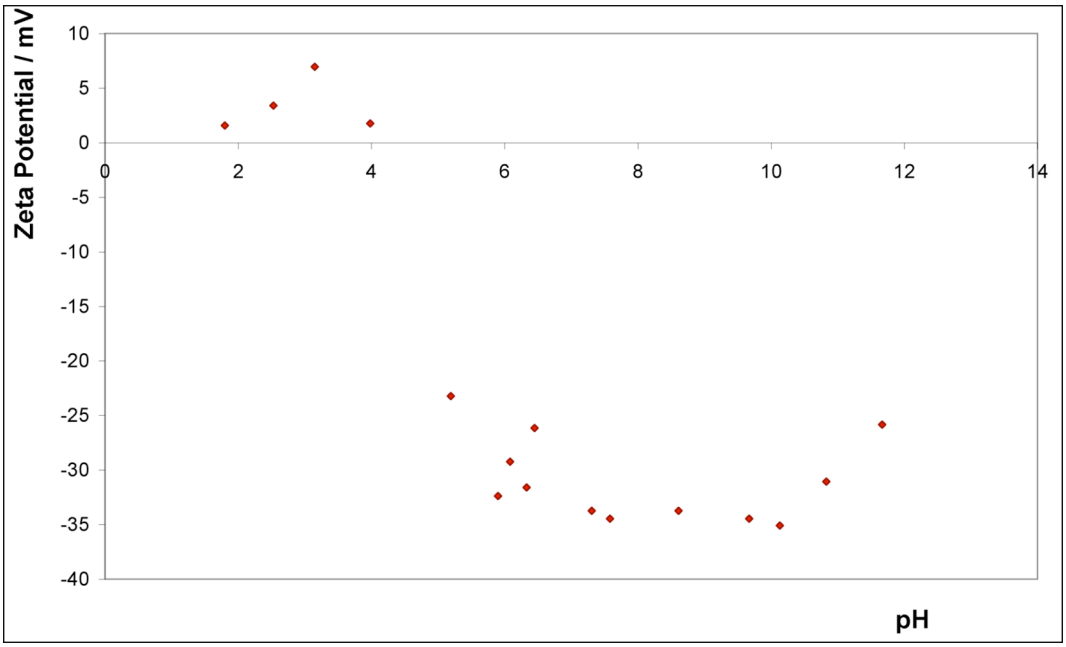

Figure 3.24: Zeta Potential Measurement of isPrSH-SBA-15 (5%)

3.3.2.9 Nitrogen Adsorption

The nitrogen adsorption was measured for each thiol sample, and the results are plotted below (figure 3.25). Each sample shows a type IV isotherm and type A hysteresis during the capillary condensation step.

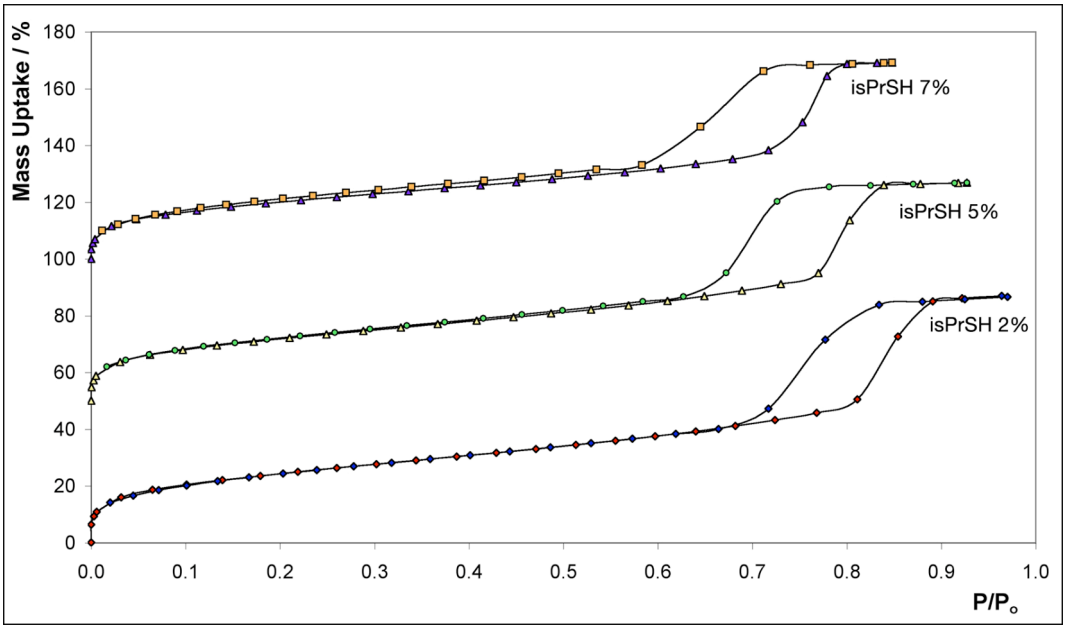

Figure 3.25: Nitrogen Adsorption Traces for Thiol Functionalised SBA-15

The pore size and surface area were calculated for each material and the results are tabulated below (table 3.10). The uptake remains high for each sample, as well as high surface areas across the three samples. There is a trend that as the incorporation of thiol increases, the uptake, surface area and pore size of the material decreases, due to the change in pore structure from p6mm to Ia3d (see section 3.3.2.10).

Table 3.10: isPrSH-SBA-15 Nitrogen Adsorption Results

Sample	BET / $m^2 g^{-1}$	BJH / Å	PSD / Å	Uptake / %
isPrSH-SBA15 (2%)	667 ± 12	32.3	64.6	87.0
isPrSH-SBA15 (5%)	627 ± 7	25.1	50.2	76.9
isPrSH-SBA15 (7%)	572 ± 8	21.7	43.4	69.2

3.3.2.10 Transmission Electron Microscopy

The pore structure of isPrSH-SBA-15 has been reported to change as the relative composition of thiol increases.[2] As the ratio of 3-mercaptopropyltriethoxysilane to tetraethoxysilane increases, a structural change is observed from hexagonal (p6mm) to cubic (Ia3d) symmetry. The TEM images obtained for isPrSH-SBA-15 (2%) are shown below (figure 3.26), in which the hexagonal symmetry of the material can be clearly

observed. The first image shows the pore channel openings, and the second the aligned porous channels.

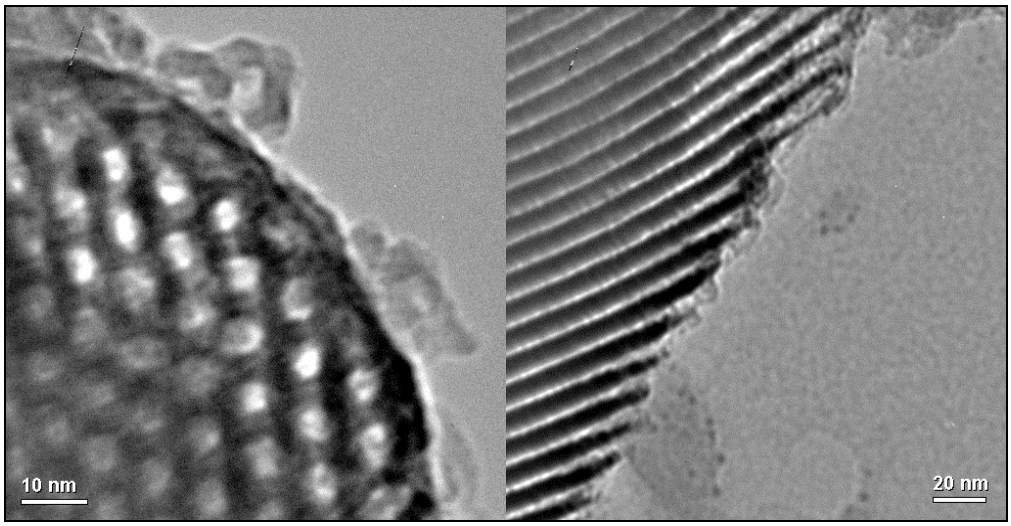

Figure 3.26: isPrSH-SBA-15 (2%) Hexagonal Morphology

This hexagonal symmetry is also observed for the isPrSH-SBA-15 (5%) sample, and the images are shown below (figure 3.27).

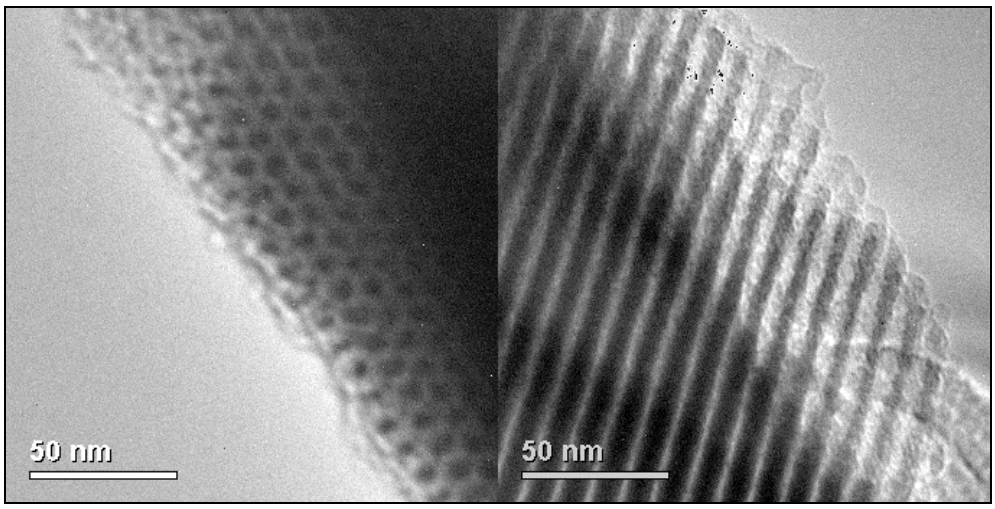

Figure 3.27: isPrSH-SBA-15 (5%) Hexagonal Phases

However, in the 5% sample, a significant amount of the material is observed to have a cubic symmetry, and these images are shown below (figure 3.28). This is indirect evidence for the mechanism of formation being silicate anion initiated, rather than condensation around pre-formed micellar arrays (see section 1.2.2), as it is unlikely that two different micellar packing methods will be found in solution. Instead it is probable that the silicate anion initiates the precipitation of the surfactant templated material with little

difference between the energy of the two stable states, resulting in the formation of more than one morphology in the final material. However, the X-ray diffraction (section 3.3.2.2) pattern is typical of a hexagonally ordered material.

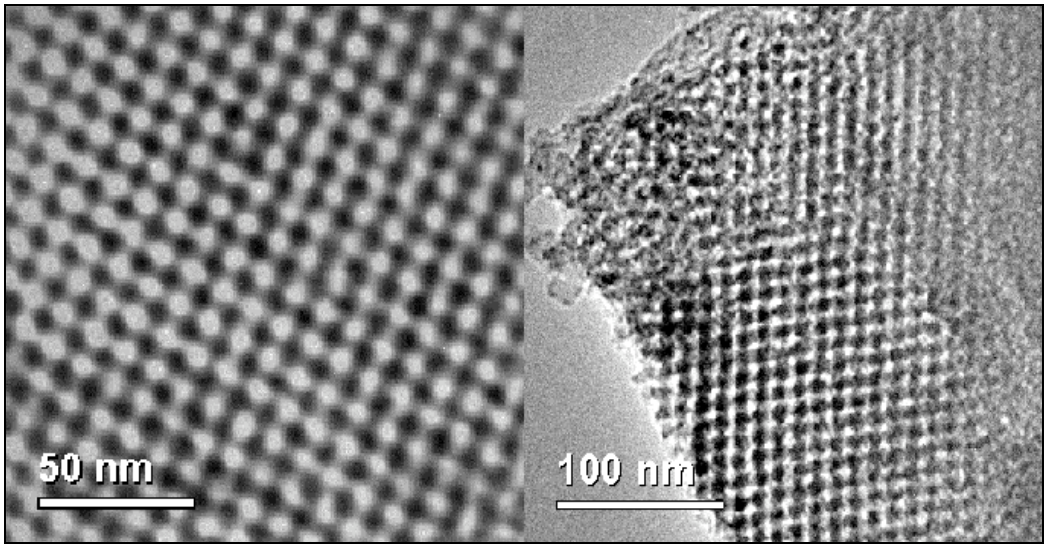

Figure 3.28: isPrSH-SBA-15 (5%) Cubic Phases

As the relative concentration of the 3-mercaptopropyltriethoxysilane increases to 7%, the material obtained has a cubic order, with no hexagonal ordering observed at all. The TEM images obtained for this material are shown below (figure 3.29).

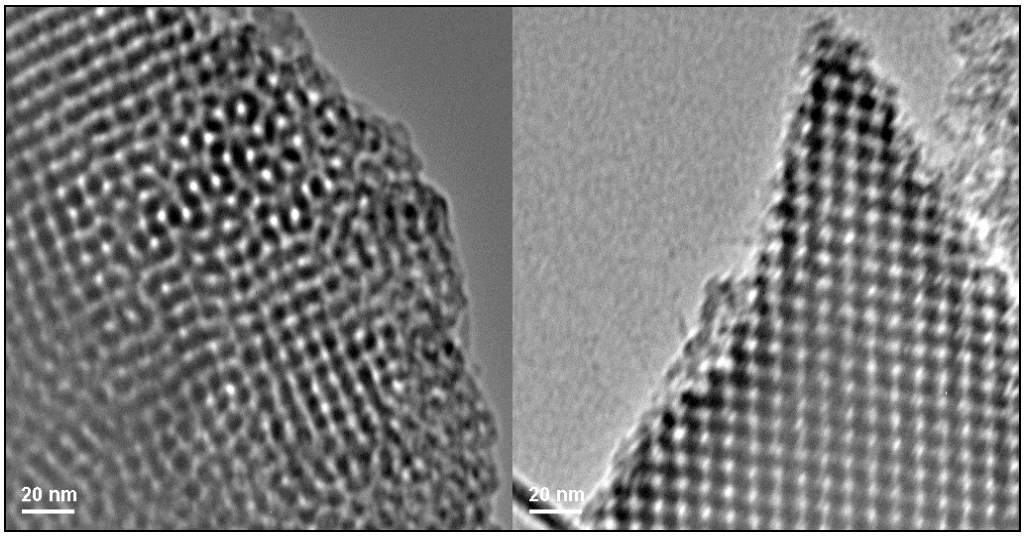

Figure 3.29: isPrSH-SBA-15 (7%) Cubic Morphology

3.3.3 psPrSH-SBA-15

The incorporation of propylthiol groups into the material as described above is a method of obtaining a material with well integrated organic functionality. However, as observed in section 3.3.2.11 the morphology of the material can change at high levels of organic incorporation. The material also contains residual surfactant within the micropores perpendicular to the mesopore. The method described below, post-synthesis grafting, involves modification of calcined SBA-15, there is no residual surfactant in the material, and little possibility of structural change. However, it is possible the organic functionality is not as well integrated into the material as by a co-condensed method as partial binding to the surface is possible, as illustrated below (figure 3.30).

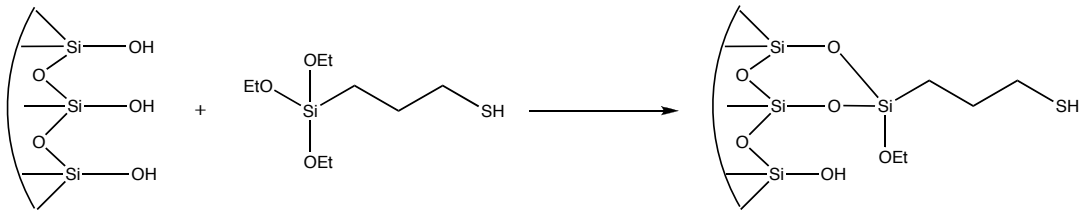

Figure 3.30: Potential Incomplete Condensation of Triethoxysilane During Post-Synthesis Modification

3.3.3.1 Synthesis

Calcined SBA-15 (0.25 g) was rehydrated by stirring at room temperature for 12h, then collected by filtration, and dried in an oven at 110 °C. To investigate the incorporation of thiol into the material the rehydrated SBA-15 was suspended in toluene (25 mL), to which 3-mercaptopropyltriethoxysilane (0.05 g, 2.08 x 10^{-4} mol) was added. This mixture was heated to reflux for 24 hours, and the sample recovered by filtration (toluene wash, 10 mL x 3). This process was repeated with another sample, which was stirred at room temperature for 72 hours, rather than heated to reflux. A third sample was prepared by using a large excess of 3-mercaptopropyltriethoxysilane (0.5 g, 2.10 x 10^{-3} mol), and heating at reflux for 24 hours.

3.3.3.2 Elemental Analysis

The composition of each material was investigated by elemental analysis, and the results are tabulated below (table 3.11). The first two samples show relatively low

incorporation of the 3-mercaptopropyltriethoxysilane, with 0.3 and 0.4% thiol content, corresponding to a 0.6% and 0.9% molar incorporation (compared to 5% for isPrSH-SBA-15 (5%)). The sample which was treated with an excess of triethoxysilane has a high thiol content of 2.1%, which is equal to a 4.0% (molar) incorporation of the organic group (denoted HL below).

Table 3.11: Elemental Analysis of psPrSH-SBA-15 Materials

Sample	C	H	S
psPrSH-SBA-15 (R.T.)	1.97	0.80	0.32
psPrSH-SBA-15 (Reflux)	1.93	0.78	0.43
psPrSH-SBA-15 (HL)	3.87	0.97	2.12

3.3.3.3 Thermal Gravimetric Analysis

The lack of residual surfactant in psPrSH-SBA-15 makes the weight loss due to decomposition of the organic functionality clearly visible by TGA (figure 3.31). Due to a problem with the TA Instruments machine, the weight loss for the high incorporation sample was measured on a Rheometric TG1000M, using air as the carrier gas. There is a pronounced step at 500 °C for the samples measured on the TA instrument, with a greater weight loss for the for the sample that was heated at reflux. The same step has an lower onset temperature when measured on the TG1000M instrument, which may be due to the faster temperature ramp rate used with this machine. This indicates that a larger amount of thiol was incorporated into the material with the higher temperature treatment, this is in agreement with the elemental analysis results.

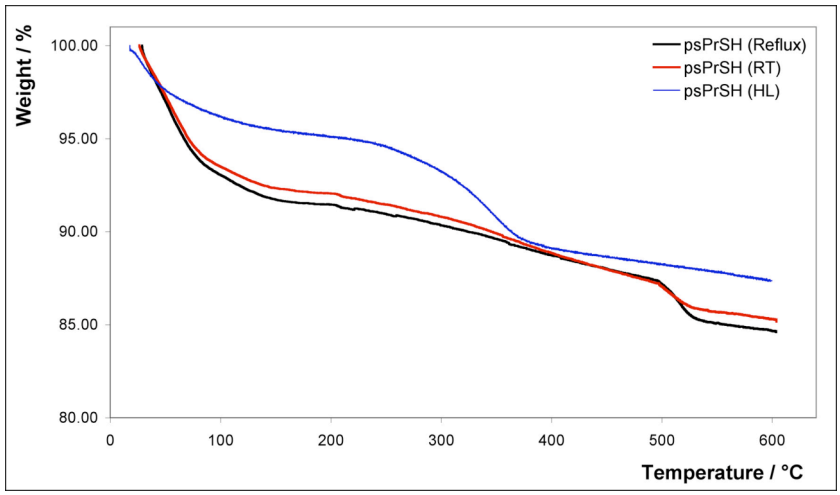

Figure 3.31: Thermal Gravimetric Analysis of psPrSH-SBA-15

The weight loss associated with each step is tabulated below (table 3.12). The values in brackets are after accounting for the loss of solvent from 0 - 165 °C. The weight losses agree with the results from the elemental analysis, indicating that the sample treated at room temperature has the lowest incorporation of the triethoxysilane, with a 1.4% weight loss due to the organic group. The other samples show higher incorporation with the refluxed samples, with 2.1% and 6.3% weight loss due to the organic group in these samples.

Table 3.12: TGA Weight Loss of psPrSH-SBA-15 Samples (TA Instruments)

Sample	0 - 165 °C / %	165 - 500 °C / %	500 - 535 °C / %
psPrSH (RT)	7.8	5.2 (5.6)	1.3 (1.4)
psPrSH (Reflux)	8.4	4.5 (4.9)	1.9 (2.1)

Sample	0 - 200 °C / %	200 - 400 °C / %	400 - 600 °C / %
psPrSH (HL)	4.9	6.0 (6.3)	1.8 (1.9)

3.3.3.4 Ellman's Analysis

The accessible thiol content of the post-synthesis grafted materials was measured using Ellman's assay as described previously (section 3.3.2.5). The results of this analysis are tabulated below (table 3.13).

Table 3.13: Ellman's Assay Results for psPrSH-SBA-15 Samples

Sample	Measured Thiol / $mmolg^{-1}$	Total Thiol (CHNS) / $mmolg^{-1}$	Accessible Thiol
psPrSH-SBA-15 (RT)	0.10	0.10	94%
psPrSH-SBA-15 (Rf)	0.12	0.13	96%
psPrSH-SBA-15 (HL)	0.58	0.66	88%

Unlike the co-condensed samples, which can incorporate the organic functionality within the silica wall, functionality that is attached by post-synthesis grafting is localised on the surface of the material. This is confirmed by measurement of the accessible thiol, in which the majority of the thiol is accessible to DNTB. The accessible thiol is much higher than with the co-condensed materials, which show between 52 - 75% accessibility.

3.3.3.5 Solid State NMR Spectroscopy

The incorporation of the 3-mercaptopropyltriethoxysilane was investigated by solid state NMR spectroscopy, observing ^{13}C and ^{29}Si of psPrSH-SBA-15 (Rf) by a CP-MAS method. The low concentration of the organic group in this sample makes obtaining a well resolved spectrum difficult. The ^{29}Si spectrum is shown below (figure 3.32), and shows a very similar pattern to that of isPrSH-SBA-15. The ^{29}Si peaks observed are Q^4 (-109.6 ppm, SiO_4), Q^3 (-100.7 ppm, $HOSiO_3$), Q^2 (-91.3 ppm, $(HO)_2SiO_2$), T^3 (-66.7 ppm, $RSiO_3$) and T^2 (-57.5 ppm, $RSi(OR')O_2$). The greater intensity of the T^2 peak relative to the T^3 peak indicates that the 3-mercaptopropyltriethoxysilane is not fully condensed during synthesis.

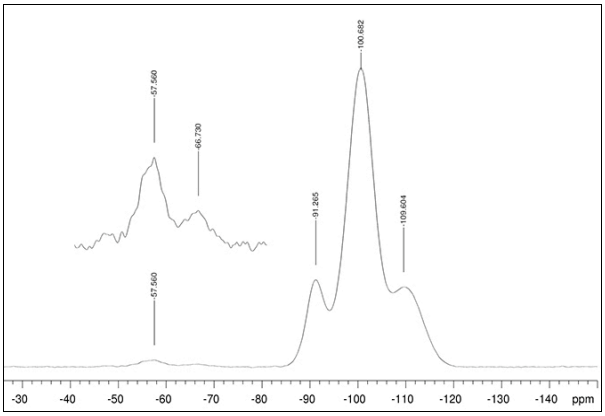

Figure 3.32: ^{29}Si SSNMR Spectra of psPrSH-SBA-15

The solid-state ^{1}H spectrum is shown below (figure 3.33), with two resolved peaks, from silanol protons (4.87 ppm, SiOH) and from the propyl hydrogen atoms (2.36 ppm, CH_2). The proton from the free thiol is not observed (~ 6 ppm), and is obscured by the silanol peak.

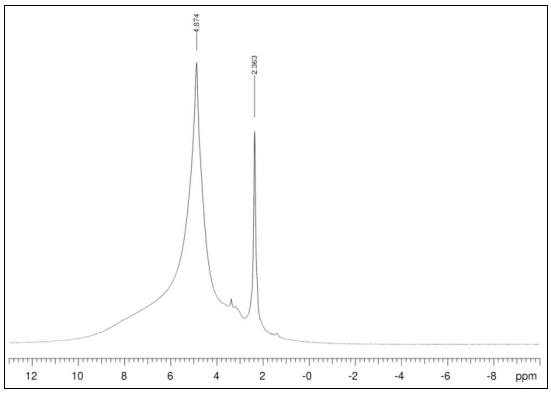

Figure 3.33: ^{1}H SSNMR Spectra of psPrSH-SBA-15

The ^{13}C spectrum is shown below (figure 3.34), the spectrum is not particularly well resolved due to the low incorporation of 3-mercaptopropyltriethoxysilane. The three peaks due to ^{13}C atoms in the carbon chain can be observed at 11.0, 16.1 and 27.4 ppm. The peak at 59.1 ppm is due to OCH_2, indicating that not all of the ethoxysilane groups are condensed during synthesis. There is no peak observed at 70 ppm indicating complete removal of the surfactant during calcination.

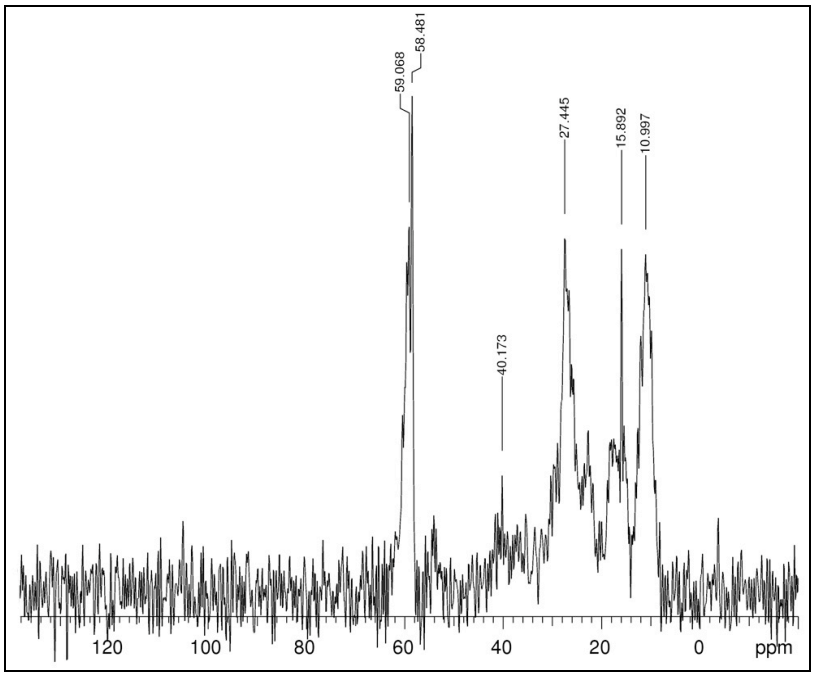

Figure 3.34: ^{13}C SSNMR Spectra of psPrSH-SBA-15

3.3.3.6 Scanning Electron Microscopy

Investigation of psPrSH-SBA-15 (HL) by SEM (figure 3.35) shows very similar results to SBA-15 (section 3.2.4). As with SBA-15, the particles are rod-like, and the treatment in toluene at reflux has not broken up these rods as the ethanol does during extraction of SBA-15.

As with SBA-15 the length of the rods is variable, generally between 20 - 100 μm, and of width 5 - 10 μm. There are reports in literature that the length of these rods, and thus the total number of pore entrances available, has an effect on the uptake of lysozyme, with a shorter rod length (1 - 2 μm) resulting in rapid adsorption of enzyme.[3]

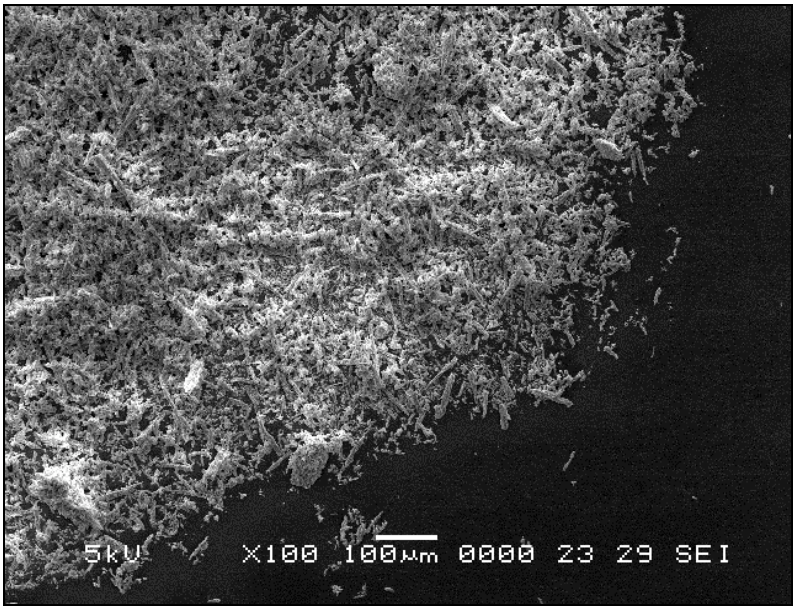

Figure 3.35: SEM Image of psPrSH-SBA-15

3.3.3.7 Zeta Potential

The zeta potential was measured by suspending psPrSH-SBA-15 (HL) in distilled water, taking 16 portions of this mixture and adjusting the pH of each with sodium hydroxide / hydrochloric acid to reach the desired pH. The zeta potential was then measured with a Malvern Zetasizer, and the results plotted as pH versus zeta potential (figure 3.36). The isoelectric point, the point at which the net charge on the particles is zero, is measured as pH 2.0 from the plot below.

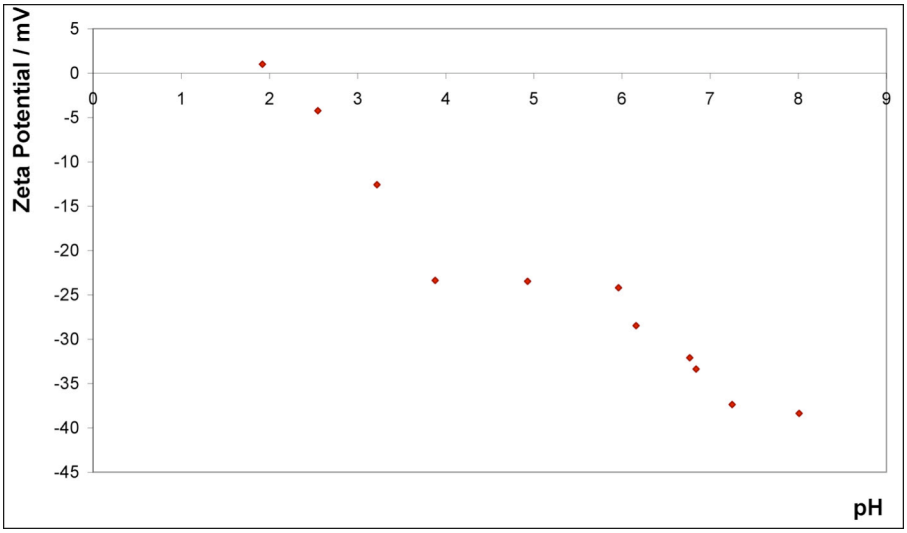

Figure 3.36: Zeta Potential Plot for psPrSH-SBA-15

3.3.3.8 Transmission Electron Microscopy

To make sure the mesostructure is retained during the post-synthesis treatment a sample of psPrSH-SBA-15 (HL) was investigated by TEM. Two images are shown below (figure 3.37), in which the aligned porous channels and the entrances to the pore system can be clearly observed.

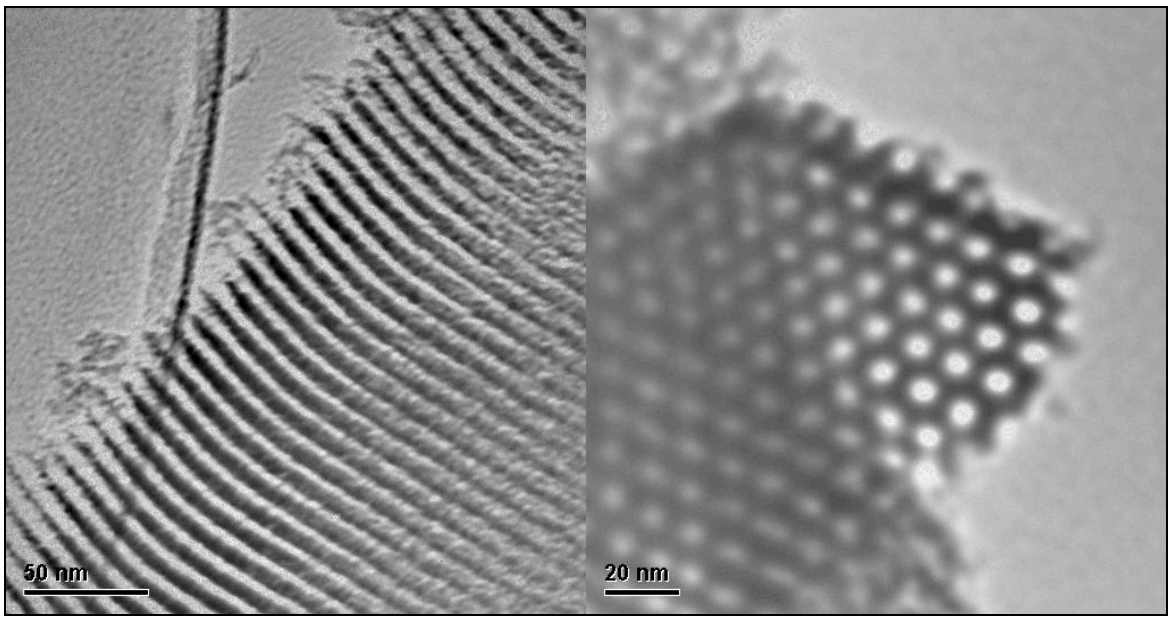

Figure 3.37: Transmission Electron Microscopy Images of psPrSH-SBA-15

3.3.4 isPrSMe-SBA-15

The preparation of isPrSMe-SBA-15 was required to investigate the interaction between free thiol groups on the surface of a material and CALB (see section 5.5.3). The methylated thiol precursor, 3-(methylthio)propyltriethoxysilane, is not commercially available and was prepared as described below.

3.3.4.1 $(OEt)_3SiPrSMe$ Synthesis

3-(Methylthio)propyltriethoxysilane was prepared by the methylation of 3-mercaptopropyltriethoxysilane, as per the scheme below (figure 3.38). Several attempts were required to optimise the yield and care had to be taken to prevent the hydrolysis of the silicon oxygen bonds of the starting material and product.

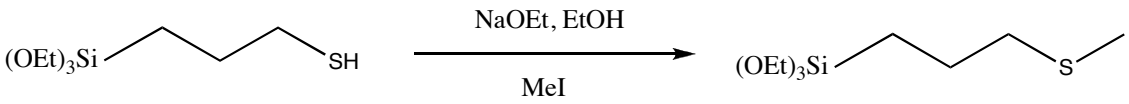

Figure 3.38: Methylation of 3-Mercaptopropyltriethoxysilane

'Super-dry' ethanol was prepared as per Vogel.[4] Magnesium turnings (2.5 g, 0.103 mol) and iodine (0.25 g, 9.85 x 10^{-4} mol) were added to ethanol (50 mL, HPLC grade) and mixed with heating at 45 °C for 1 hour. More ethanol (450 mL, HPLC grade) was added, and the mixture was heated to reflux for 1 hour. The ethanol was distilled and collected in a dry flask containing oven-dried 4Å molecular sieves (25 g).

In an inert atmosphere, dry ethanol (20 mL) was added to sodium (0.115 g, 5.0 x 10-3 mol), and stirred until the evolution of hydrogen could no longer be observed. To this solution, 3-mercaptopropyltriethoxysilane (1 g, 4.2 x 10^{-3} mol) was added and the mixture was stirred for 30 minutes. Methyl iodide (0.71 g, 5.0 x 10^{-3} mol) was then added and the mixture stirred for 12 hours at room temperature. Diethyl ether (100 mL) was added to the reaction mixture, which was then washed with pH 6 phosphate buffer (3 x 50 mL, 50 mM). The organic layer was dried with magnesium sulfate (10 g, 0.069 mol) and the product (0.72 g, 2.85 x 10^{-3} mol, 68% yield) collected by rotary evaporation after filtration. δ_H (300 MHz, $CDCl_3$, TMS), 0.68 (2H, t, CH_2), 1.15 (9H, t, CH_3), 1.58-1.75 (2H, m, CH_2), 2.01 (3H, s, CH_3), 2.48 (2H, t, CH_2), 3.75 (6H, q, CH_2). δ_c (75.48 MHz, $CDCl_3$) 15.3 (SCH_3), 16.4 (CH_2), 18.3 (CH_3), 22.7 (CH_2), 37.2 (CH_2S), 58.3 (OCH_2).

3.3.4.2 isPrSMe-SBA-15 Synthesis

The synthesis of isPrSMe-SBA-15 (5%) was as previously described (section 3.3.2.1). The silica source mixture was 3-(methylthio)propyltriethoxysilane (0.51 g, 2.02 x 10^{-3} mol) and tetraethylorthosilicate (7.98 g, 0.03838 mol). The surfactant was removed by Soxhlet extraction.

3.3.4.3 Elemental Analysis

The incorporation of the methylated thiol into the structure of ethanol extracted isPrSMe-SBA-15 (5%) was investigated by elemental analysis. The results are tabulated below (table 3.14), with the values from section 3.3.2.4 for comparison. From the carbon and hydrogen values there is a greater degree of residual surfactant present in the isPrSMe-

SBA-15 sample, indicating a less efficient extraction process. The incorporation of the organic group, as indicated by the sulfur content, is very similar to the incorporation with the free thiol.

Table 3.14: isPrSMe-SBA-15 Elemental Analysis

Sample	C	H	S
isPrSMe-SBA-15 (5%)	9.78	2.24	1.63
isPrSH-SBA-15 (5%) Batch 3	4.77	1.09	1.88

3.3.4.4 Ellman's Analysis

To make sure that the methylation was successful, the isPrSMe-SBA-15 (5%) sample was analysed by Ellman's analysis. The results are tabulated below (table 3.15), with the results obtained for isPrSH-SBA-15 (5%) for comparison. As the Ellman assay is highly selective for free thiols there is very little response for the isPrSMe-SBA-15 sample, indicating the methylation was successful.

Table 3.15: Ellman's Analysis of isPrSMe-SBA-15

Sample	Measured Thiol / $mmolg^{-1}$	Total Thiol (CHNS) / $mmolg^{-1}$	Accessible Thiol
SBA-15 (Calcined)	0	-	0%
isPrSMe-SBA-15 (5%)	0.67×10^{-3}	0.51	0.1%
isPrSH-SBA-15 (5%)	0.39	0.54	72.2%

3.3.4.5 Solid State NMR Spectroscopy

isPrSMe-SBA-15 was investigated by solid state NMR spectroscopy, using a CP-MAS experiment, to observe ^{29}Si and ^{13}C. The ^{29}Si spectrum is shown below (figure 3.39). The peak assignments are Q^4 (-110.3 ppm, SiO_4), Q^3 (-101.2 ppm, $HOSiO_3$), Q^2 (-92.4 ppm, $(HO)_2SiO_2$), T^3 (-66.1 ppm, $RSiO_3$) and T^2 (-57.5 ppm, $RSi(OR')O_2$). The alkyl triethoxysilane is well integrated into the silica matrix, as shown by the predominance of T^3 peak rather than the T^2 peak, as is seen with psPrSH-SBA-15.

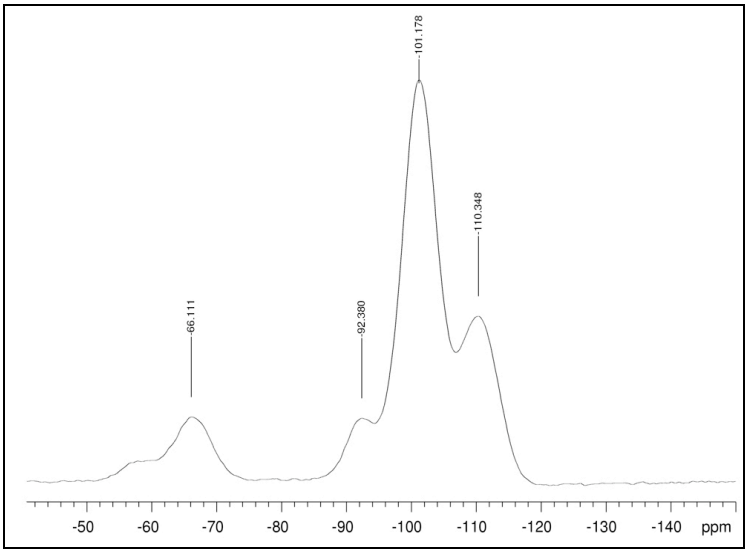

Figure 3.39: ^{29}Si SSNMR Spectra of isPrSMe-SBA-15 (5%)

The solid state ^{1}H spectrum for isPrSMe-SBA-15 is shown below (figure 3.40). The peak at 4.6. ppm is due to the silanol protons, the peak at 2.0 ppm is due to the propyl chain protons can be observed, as well as a peak at 2.8 ppm due to the protons on the methyl group of the thioether.

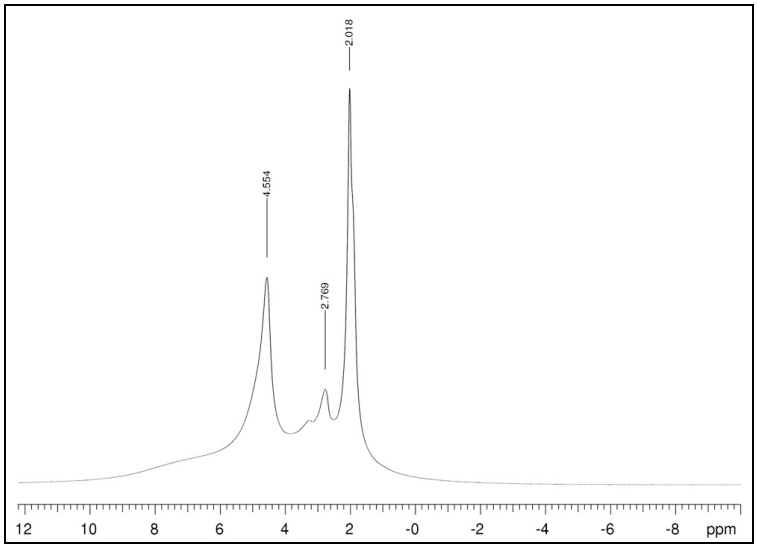

Figure 3.40: ^{1}H SSNMR Spectra of isPrSMe-SBA-15 (5%)

The ^{13}C spectrum for isPrSMe-SBA-15 (5%) is shown below (figure 3.41). The peaks at 10.9, 22.4 and 36.5 ppm correspond to the CH_2 carbon atoms of the propyl chain. The peak at 15.9 ppm is from the thioether carbon. The peak at 59.1 ppm is from the ethanol used to extract the material and any uncondensed ethoxide groups, the peak from the ethoxide CH_3 is not resolved, and is expected at 18 ppm from the solution state NMR.

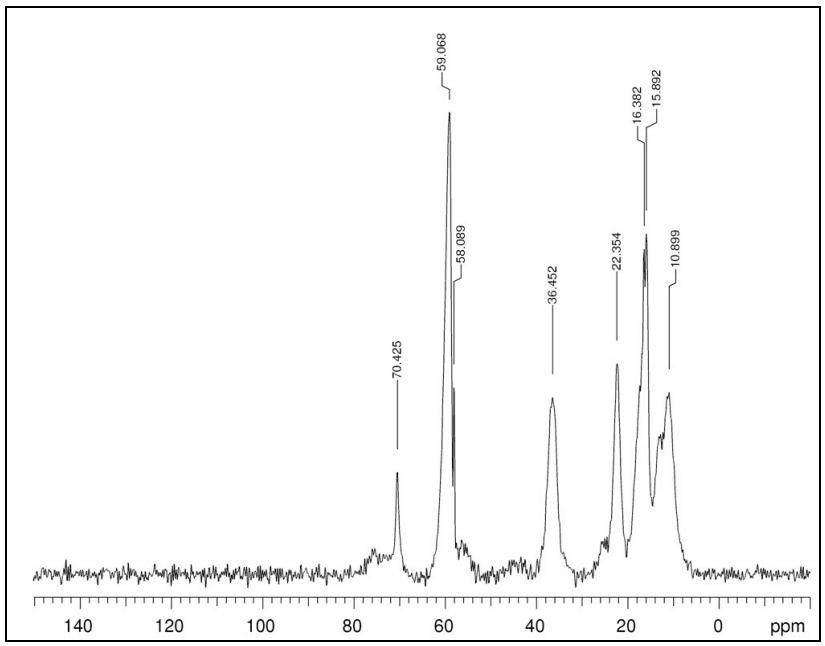

Figure 3.41: ^{13}C SSNMR Spectra of isPrSMe-SBA-15 (5%)

3.3.4.6 Nitrogen Adsorption

The nitrogen adsorption trace for isPrSMe-SBA-15 is shown below (figure 3.42). It shows a type IV isotherm with a type I hysteresis during the capillary condensation step, indicating a mesoporous structure with a uniform pore entrance and cavity diameter.

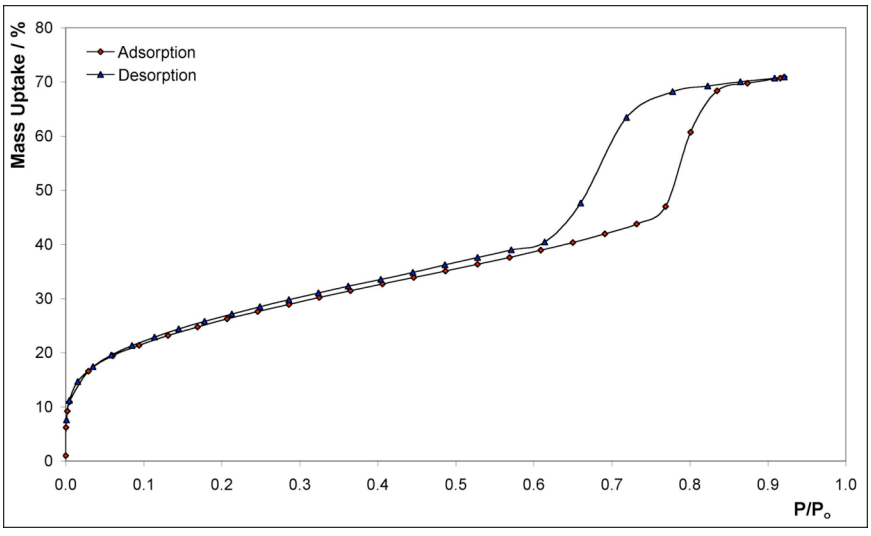

Figure 3.42: Nitrogen Adsorption Trace for isPrSMe-SBA-15 (5%)

The results from the analysis of the nitrogen trace by the BET and BJH methods are shown below (table 3.16). The material has a very high surface area of 734 m^2 g^{-1} and a large pore diameter of 47.6 Å, very similar to the properties of isPrSH-SBA-15 (5%).

Table 3.16: Nitrogen Adsorption Data for isPrSMe-SBA-15

Sample	BET / $m^2 g^{-1}$	BJH / Å	PSD / Å	Uptake / %
isPrSMe-SBA15 (5%)	734 ± 10	23.8	47.6	71
isPrSH-SBA-15 (5%)	627 ± 7	25.1	50.2	77

3.3.4.7 Thioether Synthesis Conclusion

The synthesis of 3-(thiomethyl)propyltriethoxysilane was successful, and this compound was used to prepare mesoporous isPrSMe-SBA-15 (5%). The properties of this material are very similar to that of isPrSH-SBA-15 (5%), with the exception that there is no free thiol on the surface, this material was used to investigate the effect of free thiol groups on the CALB support properties (section 5.5.2).

3.3.5 isPrCN/CO_2H-SBA-15

3.3.5.1 Synthesis

Carboxylic acid functionalised SBA-15 was synthesised by the same method as described previously for thiol functionalised SBA-15, with the replacement of 3-mercaptopropyltriethoxysilane by 3-cyanopropyltriethoxysilane (section 3.3.2.1). Tetraethylorthosilicate and 3-cyanopropyltriethoxysilane were mixed according to the table below (table 3.17). The surfactant was removed by solvent extraction, using ethanol (50 mL, HPLC Grade) with sulfuric acid (2 mL, 1M), which was refluxed for 4 h before recovery of the solid by filtration. This extraction was repeated three times for each sample.

Table 3.17: isPrCO_2H-SBA-15 Synthesis

Loading	3-Cyanopropyltriethoxysilane	Tetraethoxysilane
2%	0.187 g, 8.06 x 10^{-4} mol	8.232 g, 0.0395 mol
5%	0.466 g, 2.02 x 10^{-3} mol	7.979 g, 0.0383 mol
7%	0.653 g, 2.82 x 10^{-3} mol	7.812 g, 0.0375 mol

3.3.5.2 X-Ray Diffraction

The small angle X-ray diffraction pattern for isPrCO_2H-SBA-15 (5%) is shown below (figure 3.43). The pattern is characteristic of a hexagonally ordered material, with three peaks corresponding to d_{100}, d_{110} and d_{200}.

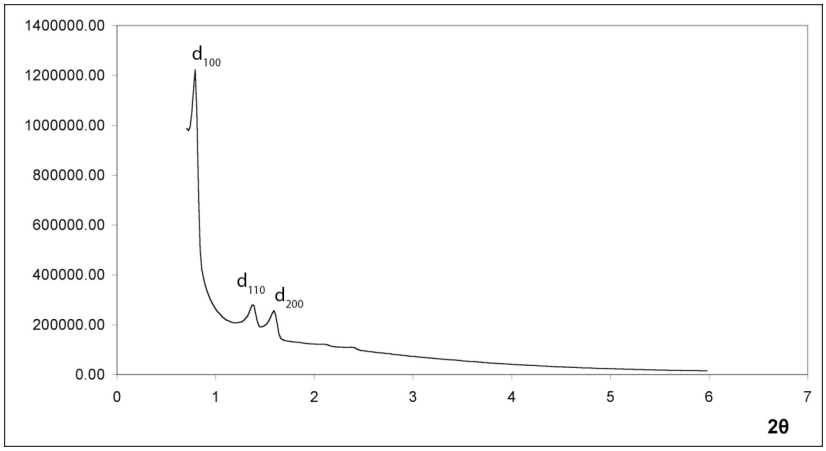

Figure 3.43: Small Angle XRD of isPrCO$_2$H-SBA-15 (5%)

The 2θ values from the pot above, and the calculated d spacing and the length of a are tabulated below (figure 3.18). The average inter-pore distance is 128.5 Å.

Table 3.18: X-ray Diffraction Data for isPrCO$_2$H-SBA-15 (5%)

Reflection	2θ	d / Å	a / Å
100	0.793	111.4	128.6
110	1.371	64.4	128.8
200	1.592	55.5	128.2

3.3.5.3 Thermal Gravimetric Analysis

The weight losses upon heating were measured and the results are plotted below (figure 3.44). The 2% and 7% samples were measured with a TA SDT 2960, and the 5% sample with a Rheometric TG1000M.

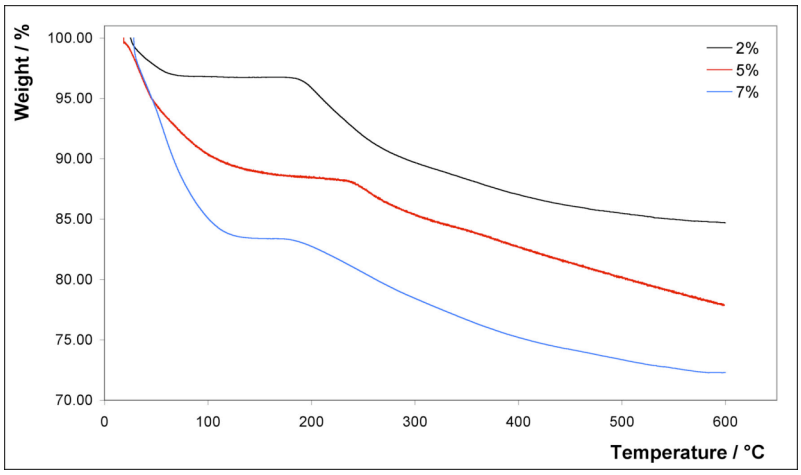

Figure 3.44: isPrCO$_2$H-SBA-15 Thermal Gravimetric Analysis

There are two weight loss steps observed, the first due to solvent, the second due to surfactant, organic groups and silanol condensation. These weight losses are tabulated below (tables 3.19). The numbers in brackets are corrected for the weight loss due to solvent.

Table 3.19: Weight Losses of isPrCO$_2$H-SBA-15 Samples During TGA (TA 2960)

Sample	0 - 165 °C Weight Loss / %	165 - 600 °C Weight Loss / %	Surfactant + PrCO$_2$H / g g^{-1}
isPrCO$_2$H-SBA-15 (2%)	3.3	12.0 (12.4)	0.14
isPrCO$_2$H-SBA-15 (7%)	16.6	11.1 (13.3)	0.15

Sample	0 - 200 °C Weight Loss / %	200 - 600 °C Weight Loss / %	Surfactant + PrCO$_2$H / g g^{-1}
isPrCO$_2$H-SBA-15 (5%)	11.6	10.5 (11.9)	0.14

3.3.5.4 Elemental Analysis

The addition of the sulfuric acid during the extraction step is to convert any nitrile groups that are not hydrolysed during synthesis to carboxylic acid groups. This conversion was measured by elemental analysis, which shows how much nitrogen (and therefore nitrile) remains within the material. The theoretical values for the nitrogen content based upon the synthesis mixture are shown below (table 3.20), and have been adjusted by 20% (in brackets) for the residual surfactant. The measured nitrogen content is approximately half that of the expected nitrogen content in all samples, indicating that there is a significant degree of unhydrolysed nitrile groups remaining within the material. These groups are probably located within the silica wall, and are not hydrolysed during synthesis.

Table 3.20: CHN Elemental Analysis of isPrCO$_2$H-SBA-15 Samples

Sample	C / %	H / %	N / %	Calc. N / %
isPrCO$_2$H-SBA15 (2%)	7.49	1.65	0.14	0.46 (0.37)
isPrCO$_2$H-SBA15 (5%)	9.00	1.73	0.52	1.12 (0.90)
isPrCO$_2$H-SBA15 (7%)	9.39	1.59	0.65	1.54 (1.23)

3.3.5.5 Nitrogen Adsorption

The nitrogen adsorption traces were measured for all three samples, and are plotted below (figure 3.45). The 5% and 7% samples have been offset by 50% and 100% uptake respectively.

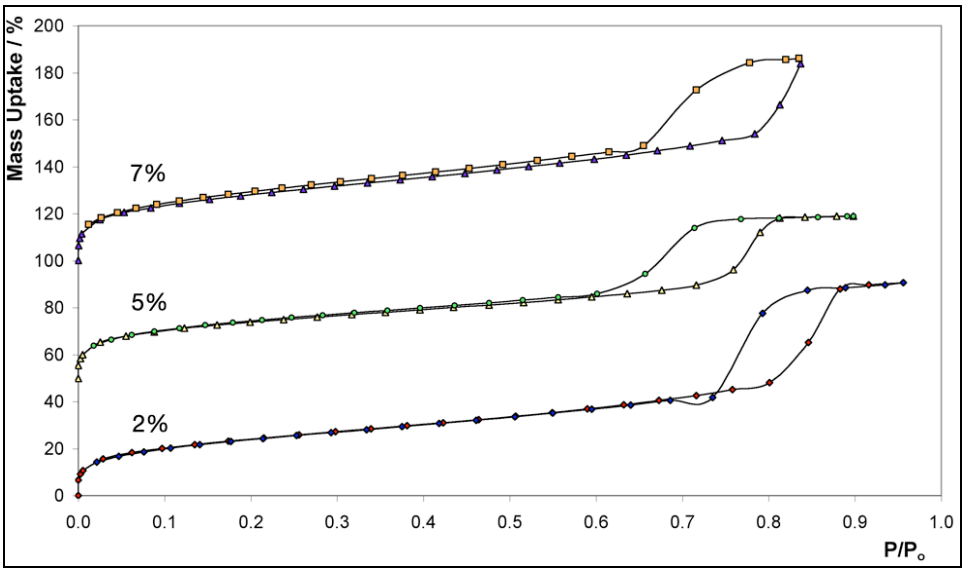

Figure 3.45: Nitrogen Adsorption by isPrCO$_2$H-SBA-15 Materials

The pore size and surface areas were measured as above, using the BJH and BET models, and are tabulated below (table 3.21). The materials all have high uptakes and large pore size diameters, with very high surface areas calculated with the BET method. The surface area measured for isPrCO$_2$H-SBA-15 (7%) is much higher than for the other materials, which may indicate a change in morphology as observed with isPrSH-SBA-15 (see section 3.3.2.10).

Table 3.21: Nitrogen Adsorption Analysis of isPrCO$_2$H-SBA-15 Samples

Sample	BET / m^2 g^{-1}	BJH / Å	PSD / Å	Uptake %
isPrCO$_2$H-SBA15 (2%)	659 ± 12	37.8	75.6	90.7
isPrCO$_2$H-SBA15 (5%)	630 ± 14	23.5	47.0	69.0
isPrCO$_2$H-SBA15 (7%)	803 ± 7	25.9	51.8	86.2

3.3.5.6 Zeta Potential

The zeta potential for isPrCO$_2$H-SBA-15 (5%) was measured as described above, using a Malvern Zetasizer. The zeta potential versus pH is plotted below (figure 3.46). The

isoelectric point of the material surface measured by this method is at pH 2.45, lower than observed for calcined SBA-15 (pH 3.25). This decrease in the isoelectric point is due to the acidic groups on the surface of the material, and is further evidence that the surface nitrile groups are converted during synthesis.

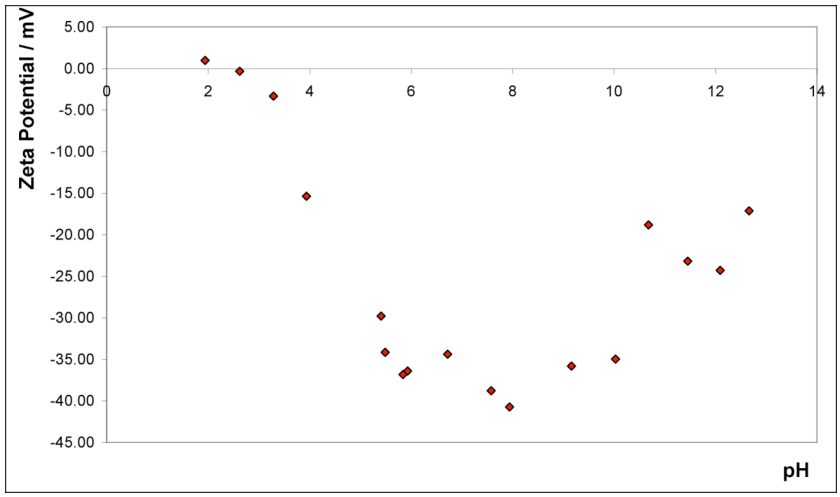

Figure 3.46: isPrCO$_2$H-SBA-15 Zeta Potential

3.3.6 Other Materials for Enzyme Immobilisation

The following materials were synthesised and characterised by the same methods as described above. Materials incorporating phenyl, allyl and amine groups are described below, in addition to the synthesis of a material incorporating two different functional groups, isPrSH/isPh-SBA-15 (2% / 4%).

3.3.6.1 Synthesis

The surfactant P123 (4.0 g, 6.86 x 10^{-4} mol)($EO_{20}PO_{70}EO_{20}$, BASF) was dissolved in a solution of HCl (148 mL, 0.8 M) at 40 °C. The silica sources were mixed according to the table below (table 3.22), then added drop-wise to the surfactant mixture and stirred at 40 °C for 24 h. The mixture was then transferred to a thick walled Teflon flask and heated at 100 °C for 48 h. The white solid was then collected by filtration, washed with distilled water and dried in air. The surfactant was removed by three successive solvent extractions, using ethanol (3 x 100 mL, 4 h), before recovery by filtration.

To synthesise psPrNH$_2$-SBA-15, a sample of calcined SBA-15 (0.25 g) was rehydrated by stirring at room temperature for 12h, the sample was collected by filtration

then dried at 110 °C for 12 h. Rehydrated SBA-15 was suspended in toluene (25 mL), to which 3-aminopropyltriethoxysilane (0.139 mg, 6.3 x 10^{-4} mol) was added (15% molar percent). This mixture was heated to reflux for 24 hours, and the sample recovered by filtration and washed with toluene (3 x 25 mL).

Table 3.22: Synthesis Silica Sources

Material	Triethoxysilane	Tetraethoxysilane
isPh-SBA-15 (5%)	$(OEt)_3SiPh$ (0.48 g, 2.02 x 10^{-3} mol)	7.979 g, 0.0383 mol
isC_3H_5-SBA-15 (2%)	$(OEt)_3SiC_3H_5$ (0.16 g, 8.06 x 10^{-4} mol)	8.232 g, 0.0395 mol
isC_3H_5-SBA-15 (5%)	$(OEt)_3SiC_3H_5$ (0.41 g, 2.02 x 10^{-3} mol)	7.979 g, 0.0383 mol
isC_3H_5-SBA-15 (7%)	$(OEt)_3SiC_3H_5$ (0.58 g, 2.82 x 10^{-3} mol)	7.812 g, 0.0375 mol
is$PrNH_2$-SBA-15 (2%)	$(OEt)_3SiPrNH_2$ (0.178 g, 8.06 x 10^{-4} mol)	8.232 g, 0.0395 mol
is$PrNH_2$-SBA-15 (5%)	$(OEt)_3SiPrNH_2$ (0.447 g, 2.02 x 10^{-3} mol)	7.979 g, 0.0383 mol
is$PrNH_2$-SBA-15 (7%)	$(OEt)_3SiPrNH_2$ (0.624 g, 2.82 x 10^{-3} mol)	7.812 g, 0.0375 mol
isPrSH-isPh-SBA-15 (2 / 4%)	$(OEt)_3SiPrSH$ (0.192 g, 8.060 x 10^{-4} mol) $(OEt)_3SiPh$ (0.387 g, 1.612 x 10^{-3} mol)	(7.896 g, 0.0379 mol)

3.3.6.2 X-Ray Diffraction

The X-ray diffraction patterns for the functionalised SBA-15 materials are shown below (table 3.47). The pattern for is$PrNH_2$-SBA-15 (5%) was also measured, but no peaks were observed, indicating no long range ordering in this material. The is$PrNH_2$-SBA-15 (2%) shows particularly intense diffraction peaks, indicating a well ordered, homogenous material.

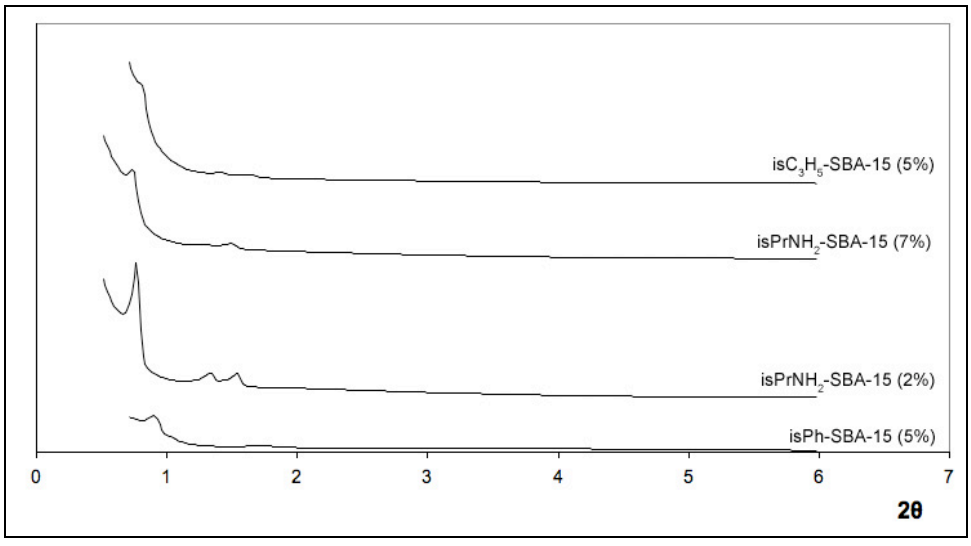

Figure 3.47: Small Angle X-ray Diffraction Patterns of Functionalised SBA-15 Materials

The peak positions and the average inter-pore distance a are tabulated below (table 3.23). The d_{100} peak for isC_3H_5-SBA-15 (5%) was calculated at a 2θ value of 0.813 by doubling the d_{200} inter-planar distance and calculating the angle from this value as the peak was not sufficiently resolved. Only two peaks are observed for isPh-SBA-15 (5%), this may be due a cubic morphology, and a_{cubic} is calculated from the first peak.

Table 3.23: X-ray Diffraction Data for Functionalised SBA-15 Materials

Sample	d_{100} / 2θ	d_{110} / 2θ	d_{200} / 2θ	a / Å
isPh-SBA-15 (5%)	0.895	-	-	114.0
is$PrNH_2$-SBA-15 (2%)	0.765	1.326	1.530	133.3
is$PrNH_2$-SBA-15 (7%)	0.731	1.292	1.479	138.1
isC_3H_5-SBA-15 (5%)	0.813	1.405	1.626	125.6

3.3.6.3 Thermal Gravimetric Analysis

The weight losses during TGA are tabulated below (table 3.24). The samples show weight losses between 14 - 17% due to surfactant and organic group decomposition.

Table 3.24: Weight Losses of Functionalised SBA-15 During TGA

Sample	0 - 165 °C Weight Loss / %	165 - 700 °C Weight Loss / %	Surfactant + Organic / g g^{-1}
isPh-SBA-15 (5%)	7.8	13.5 (14.6)	0.17
isC_3H_5-SBA-15 (2%)	2.3	15 (15.4)	0.18
isC_3H_5-SBA-15 (7%)	1.9	16.7 (17.0)	0.20
is$PrNH_2$-SBA-15 (2%)	9.9	12.8 (14.2)	0.17

3.3.6.4 Elemental Analysis

The elemental analysis results for the functionalised SBA-15 materials are shown below. The post-synthesis amine functionalised material shows a very high nitrogen content, indicating very high uptake of 3-aminopropyltriethoxysilane (table 3.25). It is likely that the amine functional group binds strongly to the surface during grafting, resulting in an intra-molecular type condensation between the silica surface and the ethoxysilane groups. The elemental analysis results for isPrSH-SBA-15 (2%) are shown for comparison with the isPrSH/isPh-SBA-15 (2% / 4%) results. The sulfur content of each

material is very similar, with a greater carbon composition in the mixed functionality material from the phenyl groups.

Table 3.25: Functionalised SBA-15 Elemental Analysis

Sample	C	H	N	S
isPh-SBA15 (5%)	12.67	2.36	-	-
isPrNH$_2$-SBA-15 (2%)	7.41	1.63	0.14	-
isPrNH$_2$-SBA-15 (5%)	7.14	1.74	0.89	-
isPrNH$_2$-SBA-15 (7%)	12.33	2.81	0.54	-
psPrNH$_2$-SBA-15	9.52	1.82	3.41	-
isPrSH-SBA-15 (2%)	8.41	2.00	-	0.79
isPrSH/isPh-SBA-15 (2% / 4%)	12.34	1.81	-	0.75

3.3.6.5 Zeta Potential Measurement

The zeta potential versus pH for isPrNH$_2$-SBA-15 (2%) is plotted below (figure 3.48). The isoelectric point of the material is much higher than other functionalised silica materials due to the basic groups on the surface of the material. The isoelectric point of isPrNH$_2$-SBA-15 (2%) measured by this method is pH 6.1.

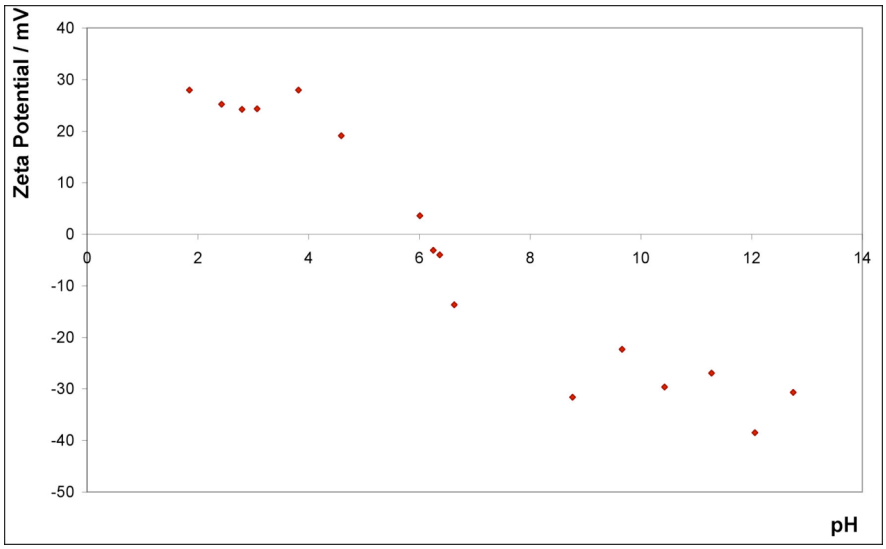

Figure 3.48: isPrNH$_2$-SBA-15 Zeta Potential

The zeta potentials for the other materials was measured, with isoelectric points of pH 3.3 for isC$_3$H$_5$-SBA-15 (5%), pH 8.1 for psPrNH$_2$-SBA-15 and pH 2.8 for isPh-SBA-15 (5%).

3.3.6.6 Nitrogen Adsorption

The nitrogen adsorption traces for the isC_3H_5-SBA-15 materials are plotted below (figure 3.49). The 5 and 7% samples are offset by 50 and 100% respectively. Each material has an type IV adsorption trace with a hysteresis of the capillary condensation during the adsorption and desorption.

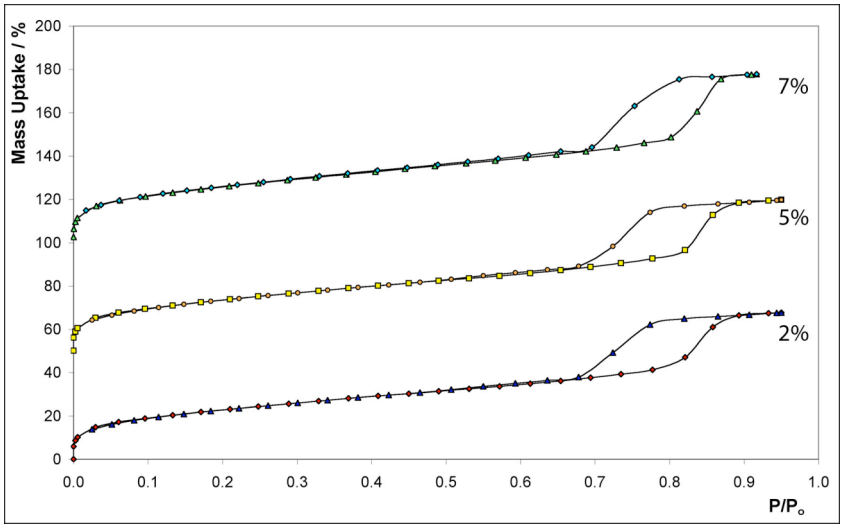

Figure 3.49: Nitrogen Adsorption Traces for isC_3H_5-SBA-15

The results of the analysis by the BET method to obtain the surface area, and the BJH method to obtain the pore size radius are tabulated below (table 3.26), along with the total mass uptake for each sample. The materials all exhibit high surface areas and all have large pore size diameters, indicating that the order of the material is not disrupted by the introduction of the allyl functionality.

Table 3.26: Nitrogen Adsorption Data for isC_3H_5-SBA-15 Samples

Support	Surface Area / $m^2\ g^{-1}$	BJH Radius / Å	PSD / Å	Mass Uptake / %
isC_3H_5-SBA-15 (2%)	637 ± 10	29.7	59.4	67.7
isC_3H_5-SBA-15 (5%)	652 ± 10	29.9	59.8	69.7
isC_3H_5-SBA-15 (7%)	730 ± 8	31.8	63.6	77.8

The nitrogen adsorption traces for the is$PrNH_2$-SBA-15 materials are shown below (figure 3.50). The 5% sample does not have a typical type IV isotherm, indicating the material has not been templated uniformly by the surfactant.

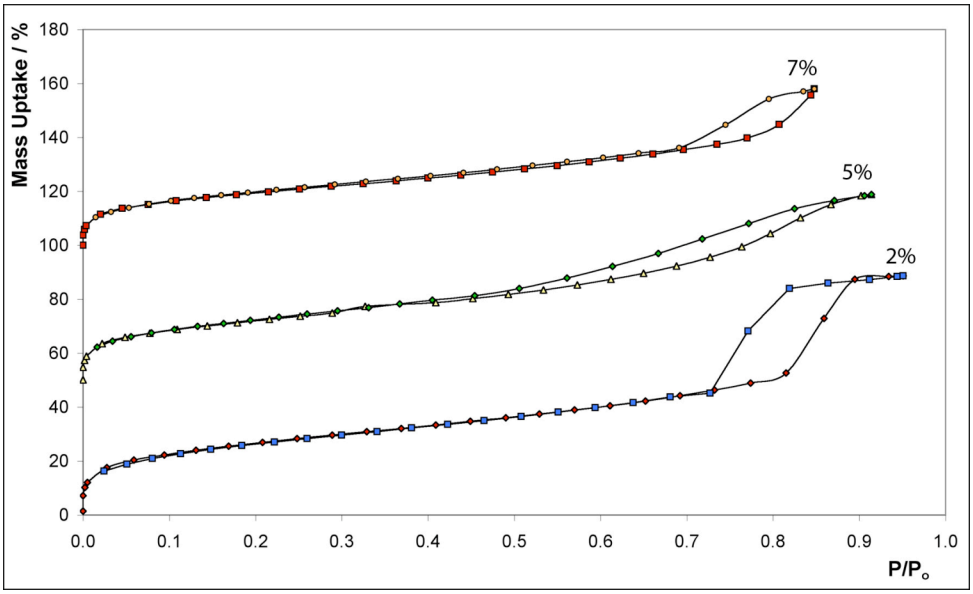

Figure 3.50: Nitrogen Adsorption of isPrNH$_2$-SBA-15 Materials

The results of the analysis of the nitrogen adsorption traces are shown below (table 3.27). The 2% and 7% samples show good pore size distributions from BJH analysis, but the average pore size is much lower for the 5% sample. This, in addition to the lack of peaks observed during X-ray diffraction, indicates the pore system of this sample is not well ordered. The material is still mesoporous, as it exhibits a type IV isotherm and a high surface area, but is unlikely to have either a narrow pore size distribution or a homogenous morphology.

Table 3.27: Functionalised SBA-15 Nitrogen Adsorption Results

Sample	BET / $m^2 g^{-1}$	BJH / Å	PSD / Å	Uptake %
isPrNH$_2$-SBA15 (2%)	734 ± 13	35.8	71.6	88.7
isPrNH$_2$-SBA15 (5%)	650 ± 9	14.9	28.9	68.8
isPrNH$_2$-SBA15 (7%)	555 ± 5	31.9	63.8	58.1

The nitrogen adsorption / desorption trace for isPrSH/isPh-SBA-15 (2% / 4%) is shown below (figure 3.51). The material does not exhibit a sharp type A capillary condensation step typical of many of the well ordered materials, indicating a non-homogenous pore system. The surface area by BET is calculated at 723 $m^2 g^{-1}$, and the average pore size as 35.4 Å, smaller than for the other functionalised SBA-15 materials. As above, with isPrNH$_2$-SBA-15 (5%) this material is likely to be composed of a fairly disordered mesoporous pore system.

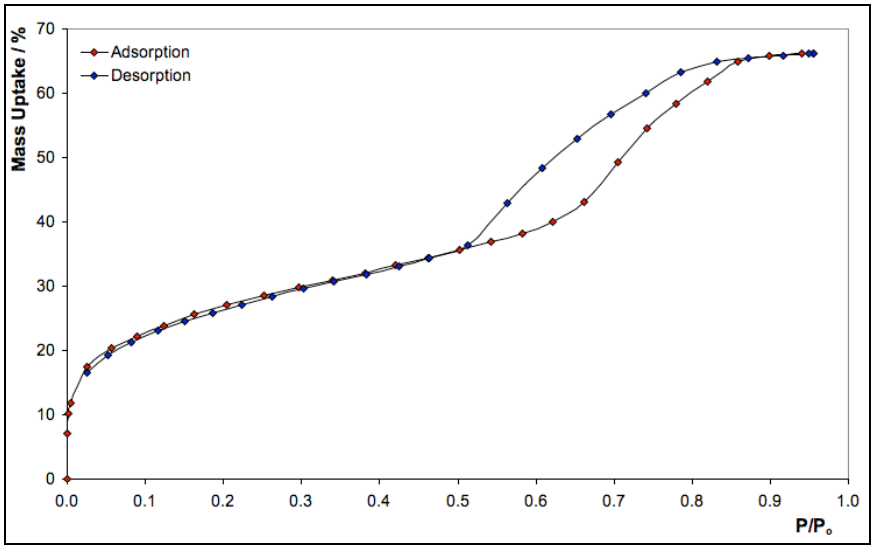

Figure 3.51: Nitrogen Adsorption by isPrSH/isPh-SBA-15 (2% / 4%)

3.3.6.7 Transmission Electron Microscopy

The mesostructure of isPrNH$_2$-SBA-15 (2%) was investigated by transmission electron microscopy, and the images obtained are shown below (figure 3.52). The material has a clear hexagonal order, with both orientations of the p6mm structure displayed below.

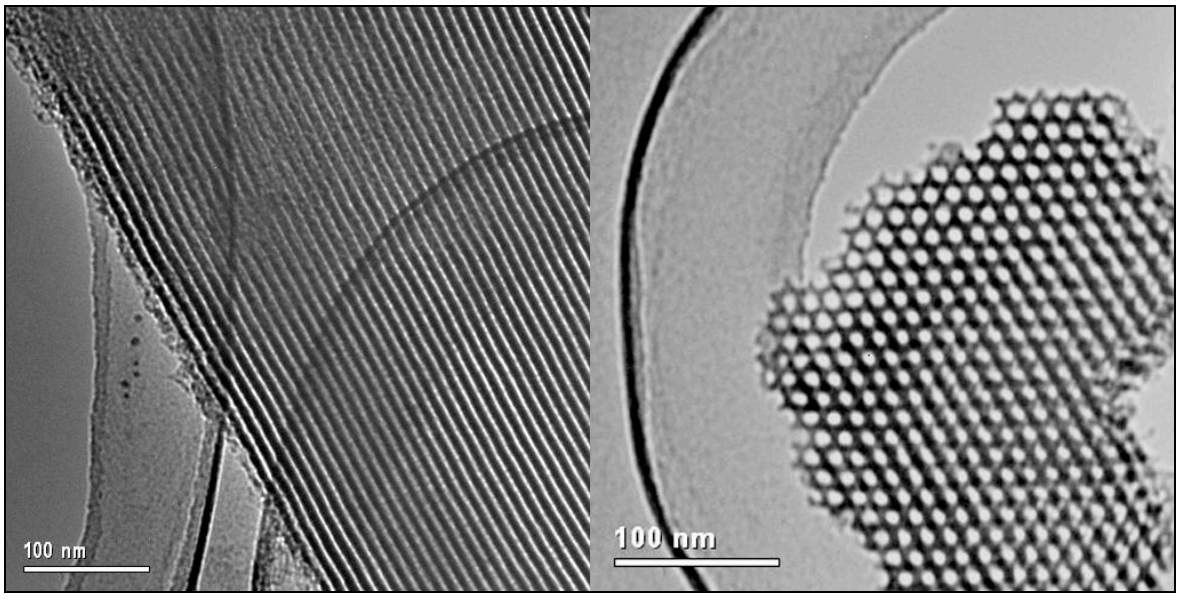

Figure 3.52: TEM Images of isPrNH$_2$-SBA-15 (2%)

The inter-pore distance was measured, and the TEM image is annotated below (figure 3.53). The distance between 4 adjacent pores is measured at 560 Å, which is an

inter pore distance of 140 Å. From X-ray diffraction (section 3.3.6.2) we calculate an inter-pore distance of 133.3 Å. The average pore size distribution for isPrNH$_2$-SBA-15 (2%) by BJH analysis is 71.6, which when subtracted from the average inter-pore distance gives a wall thickness of 65 Å.

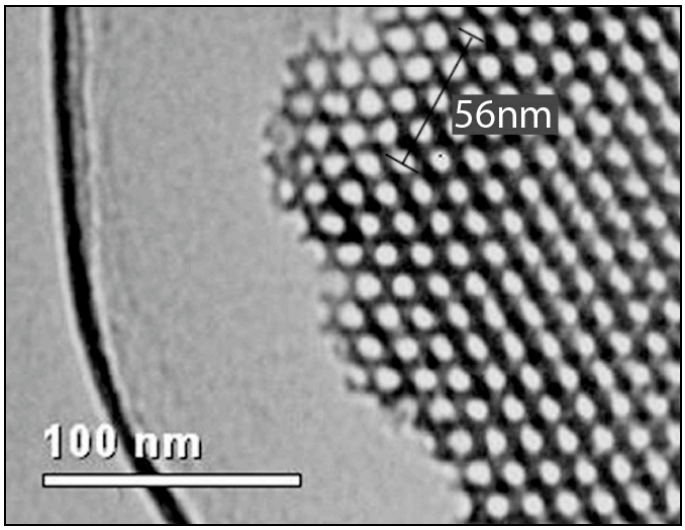

Figure 3.53: Inter-pore Distance Measured By TEM

The morphology of mixed functionality isPrSH/isPh-SBA-15 (2% / 4%) was investigated by TEM. The material, which shows some disorder during nitrogen adsorption, is comprised of regions of hexagonal symmetry (figure 3.54).

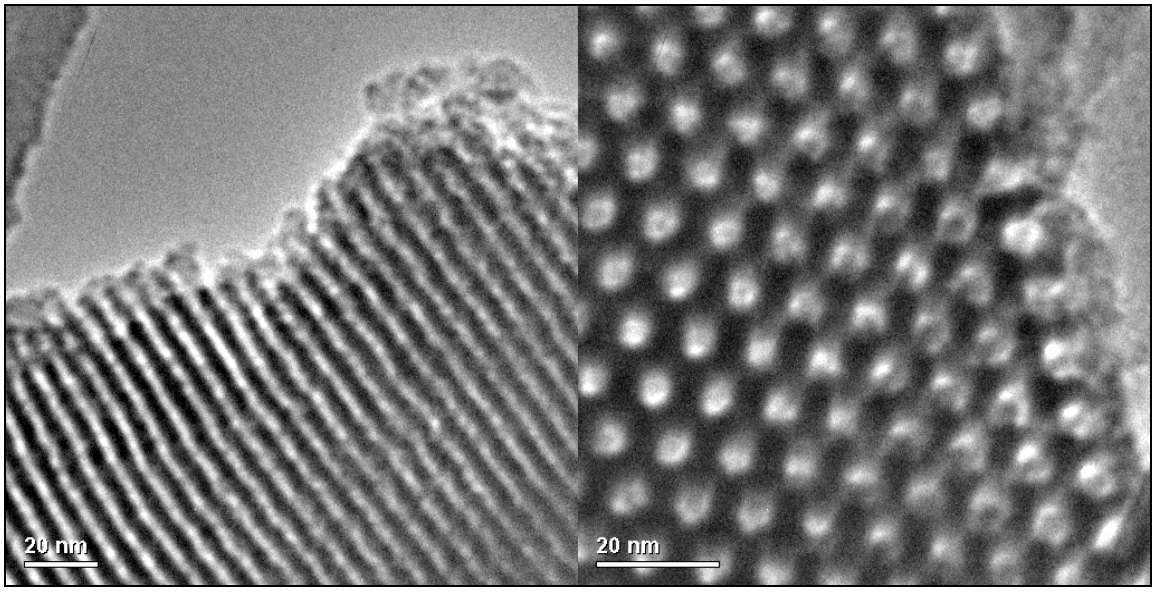

Figure 3.54: TEM Images of isPrSH/isPh-SBA-15 (2% / 4%)

The material also contains regions in which the structure is disordered (figure 3.55). It is not known if the organic functionality is distributed throughout the material, or is localised within different regions of the material.

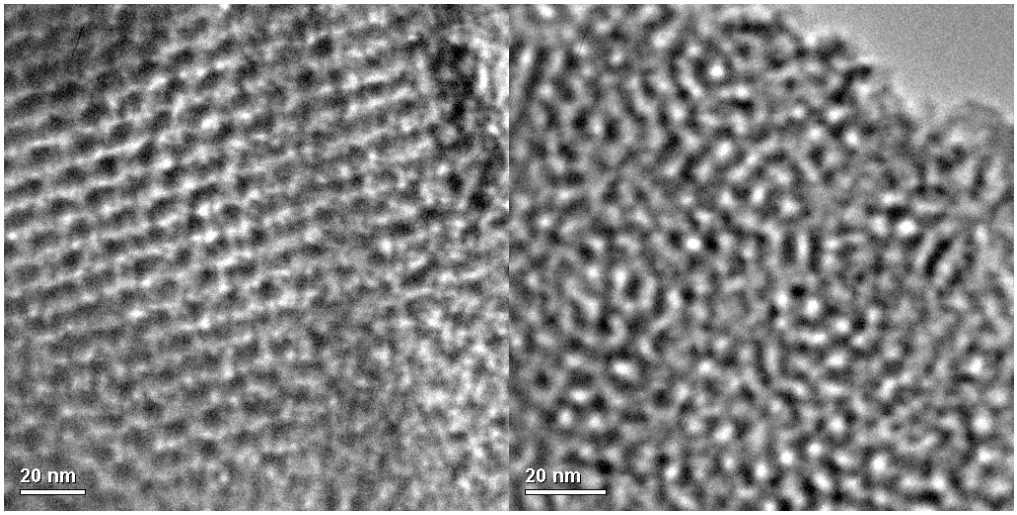

Figure 3.55: Disordered Regions of isPrSH/isPh-SBA-15 (2% / 4%)

3.4 Expanded Pore SBA-15 Materials

3.4.1 Ratio of Surfactant to Trimethylbenzene

To prepare the expanded pore materials, the surfactant micelle is swollen by the addition of trimethylbenzene (TMB) during synthesis. The weight ratio of the swelling agent to the surfactant defines the degree to which the material is altered, with low ratios of 0.2 - 0.4 increasing the pore size of the resultant material while retaining the structure, and with higher ratios disrupting the structure more significantly, resulting in foam like materials. Described below is the synthesis and characterisation of a range of swollen SBA-15 and isPrSH-SBA-15 materials, which are of interest as they potentially can accommodate larger enzymes and higher loadings with improved diffusion properties.

3.4.2 Synthesis

To a solution of hydrochloric acid (148 mL, 0.8 M) the surfactant P123 (4.0 g, 6.86 x 10^{-4} mol) was added, and stirred at 40 °C until the surfactant was completely dissolved (~ 1 hour). The trimethylbenzene was added according to the table below (table 3.28) to achieve the desired ratio. This mixture was stirred at 40 °C for 12 hours, after which the

silica source, prepared according to the table below, was added dropwise. The mixture was stirred for 24 hours, then transferred to a thick walled sealed Teflon flask, and heated at 100 °C for 48 hours. The material was recovered by filtration and the surfactant was removed by calcination for the unfunctionalised materials, and by solvent extraction (3 x 100 mL) for the functionalised materials.

Table 3.28: Synthesis of Expanded Pore Materials

Sample	TMB	TEOS	3-MPTES
0.2TMB-SBA-15	0.8 g, 6.7 x 10^{-4} mol	8.40g, 0.0403 mol	-
0.4TMB-SBA-15	1.6 g, 0.013 mol	8.40g, 0.0403 mol	-
1.0TMB-SBA-15	4.0 g, 0.033 mol	8.40g, 0.0403 mol	-
0.2TMB-isPrSH-SBA-15 (5%)	0.8 g, 6.7 x 10^{-4} mol	7.979 g, 0.0383 mol	0.482 g, 2.02 x 10^{-3} mol
0.4TMB-isPrSH-SBA-15 (5%)	1.6 g, 0.013 mol	7.979 g, 0.0383 mol	0.482 g, 2.02 x 10^{-3} mol
1.0TMB-isPrSH-SBA-15 (5%)	4.0 g, 0.033 mol	7.979 g, 0.0383 mol	0.482 g, 2.02 x 10^{-3} mol

3.4.3 Nitrogen Adsorption

The nitrogen adsorption isotherms for the expanded pore materials are shown below. The 0.2TMB and 0.4TMB samples were measured using a Micromeritics ASAP 2020 machine. The 1.0TMB samples was measured with a Hiden Intelligent Gravimetric Analyser 002. The adsorption / desorption traces for the 0.2TMB samples are shown below (figure 3.56). The mass uptake for the 0.2TMB-isPrSH (5%) sample is offset by 100%.

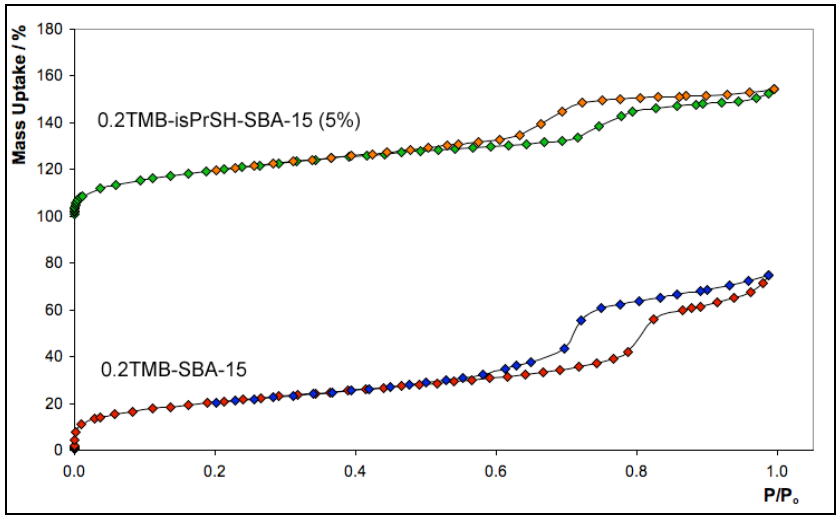

Figure 3.56: Nitrogen Adsorption by 0.2TMB Samples

The nitrogen adsorption results for the 0.4TMB Samples, measured using an ASAP 2020 machine, are plotted below (figure 3.57). The materials show type IV adsorption isotherms, indicating mesoporosity, with very high uptake of nitrogen during the capillary condensation step. The mass uptake for the 0.4TMB-SBA-15 (5%) sample is offset by 100%.

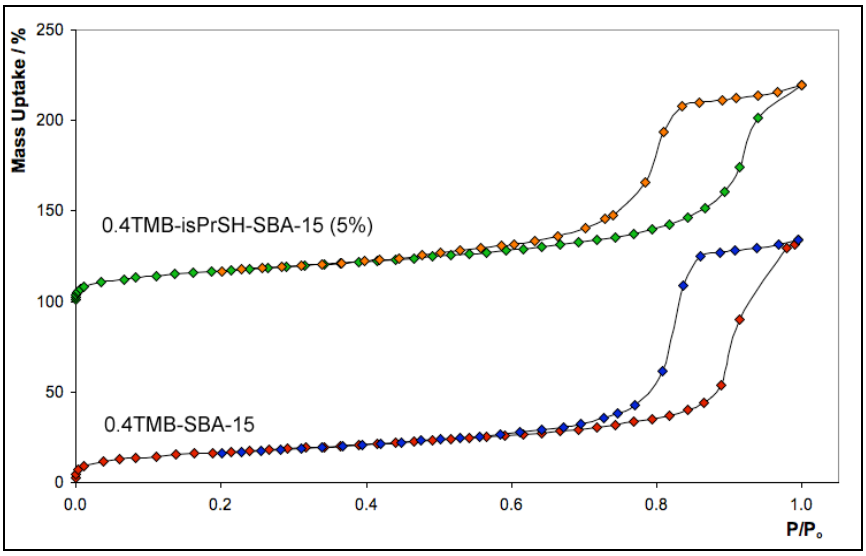

Figure 3.57: Nitrogen Adsorption by 0.4TMB Samples

The nitrogen adsorption results for the 1.0TMB Samples are shown below (figure 3.58). The maximum saturation pressure (P_o) of the Hiden IGA was not sufficient to measure the capillary condensation step within these materials, and only the multilayer adsorption and onset of condensation was observed.

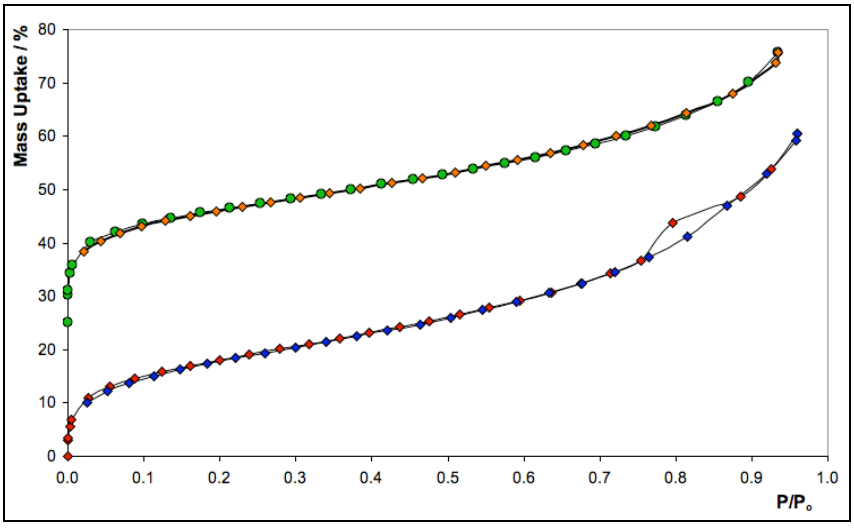

Figure 3.58: Nitrogen Adsorption by 1.0TMB Samples

The nitrogen adsorption analysis results for the expanded pore solids are tabulated below (table 3.29). The addition of 0.2TMB during synthesis has not significantly increased the pore size relative to conventional SBA-15 (68 Å) and isPrSH-SBA-15 (5%) (50.2 Å). The addition of 0.4TMB during synthesis increases the pore size significantly, with much larger pore sizes calculated by BJH analysis. The mass uptake of these materials is very high, with more than the weight of the material adsorbed. The 1.0TMB samples were not analysed by the BJH method, as the capillary condensation step was not measured (figure 3.58).

Table 3.29: Expanded Pore Nitrogen Adsorption Data Analysis

Sample	BET / $m^2 g^{-1}$	PSD / Å	Uptake %
0.2TMB-SBA-15	507 ± 5	65.6	74.8
0.2TMB-isPrSH-SBA-15 (5%)	560 ± 5	50.9	54.5
0.4TMB-SBA-15	481 ± 4	109.7	133.8
0.4TMB-isPrSH-SBA-15 (5%)	508 ± 5	88.5	119.6
1.0TMB-SBA-15	564 ± 12	-	50.7*
1.0TMB-isPrSH-SBA-15 (5%)	509 ± 8	-	60.4*

* Possible incomplete capillary condensation

3.4.4 Elemental Analysis

The elemental analysis results for the functionalised expanded pore materials are tabulated below (table 3.30). The unfunctionalised materials were extracted by calcination and were not measured.

Table 3.30: Expanded Pore SBA-15 Elemental Analysis

Sample	C	H	N	S
0.2TMB-isPrSH-SBA-15 (5%)	11.65	2.00	-	1.79
0.4TMB-isPrSH-SBA-15 (5%)	8.61	1.69	-	1.92
1.0TMB-isPrSH-SBA-15 (5%)	9.45	1.69	-	1.95

3.4.5 Transmission Electron Microscopy

The TEM images obtained for 0.4TMB-SBA-15 are shown below (figure 3.59). The array of aligned pores previously observed for SBA-15 have been swollen due to the

intercalation of the TMB within the surfactant micelle, and the material appears to be comprised of a swollen hexagonal (*p6mm*) morphology.

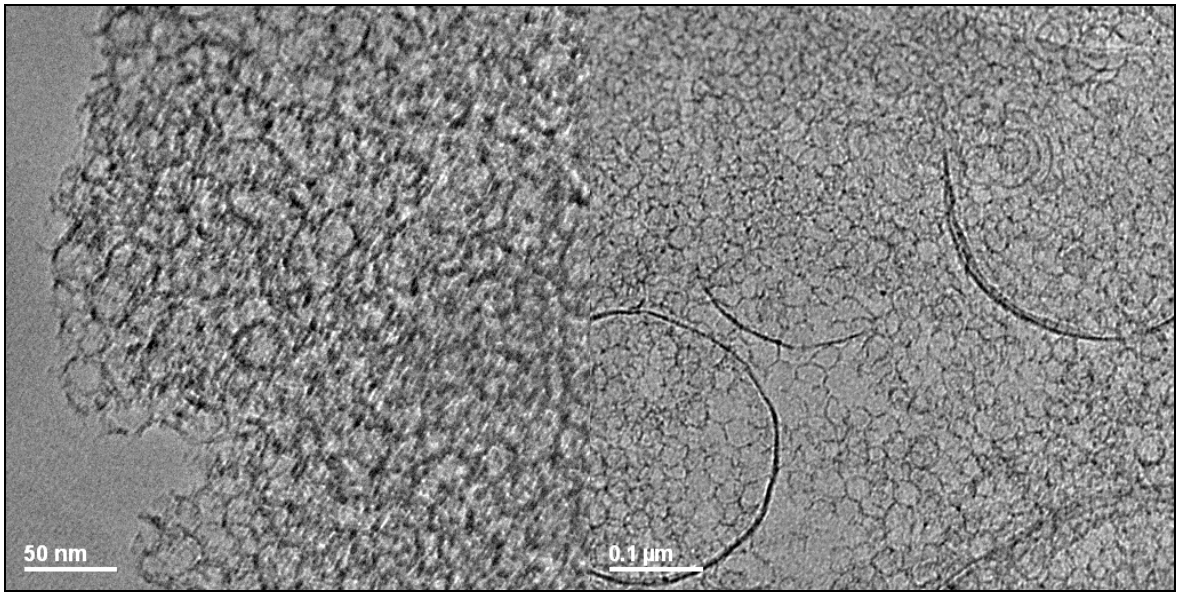

Figure 3.59: TEM Images of 0.4TMB-SBA-15

The TEM images obtained for 0.4TMB-isPrSH-SBA-15 (5%) are shown below (figure 3.60). The material is comprised of a foam-like morphology, with no evidence observed of structural similarity to SBA-15. From nitrogen adsorption, the material is comprised of mesopores, which must be inter-connected spheres of a foam.

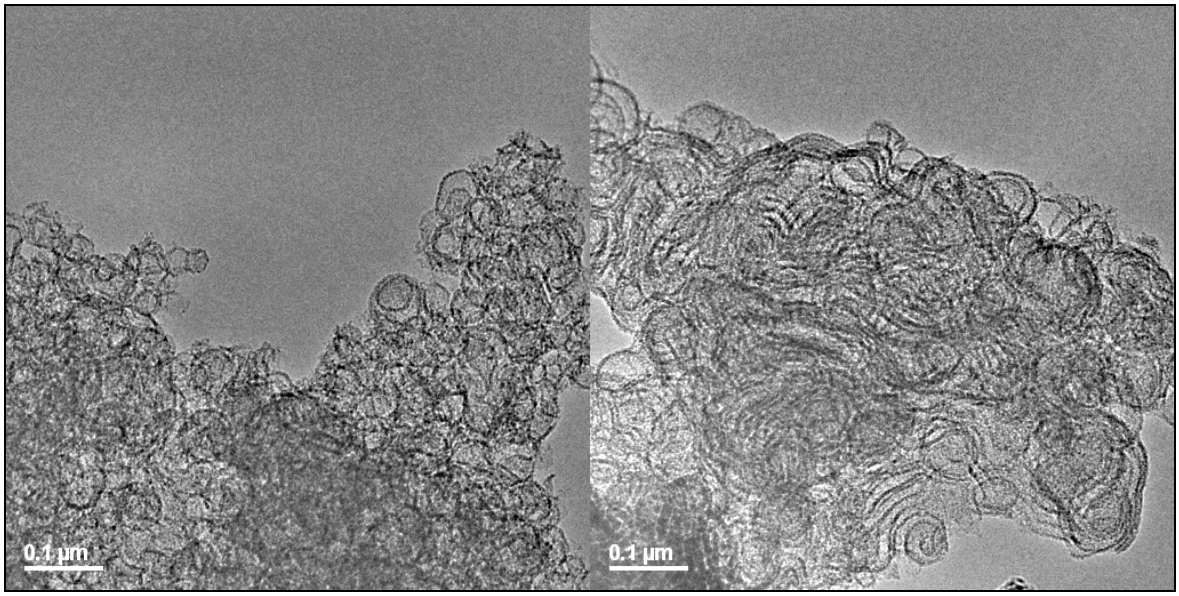

Figure 3.60: TEM Images of 0.4TMB-isPrSH-SBA-15 (5%)

3.5 Supports for Enzyme Immobilisation

3.5.1 Comparison of Support Materials

The materials used to study the support properties of mesoporous materials for enzyme immobilisation, together with the physical properties that are important for supporting enzymes are given below (table 3.31). The materials prepared by calcination have a microporous network parallel to the mesopores. With the solvent extracted materials, this microporous network remains blocked by residual surfactant, and there may also be some ethoxy groups incorporated into the surface. The pore size of the materials is greater than 40 Å by BJH analysis, large enough for CALB and smaller enzymes such as cytochrome c (the pore sizes below were measured using the desorption branch of the isotherm, which produces values lower than by analysis of the adsorption isotherm). The isoelectric point of each material, excluding the amines, is lower than pH 6, the isoelectric point of CALB, and the surface of each material during adsorption of enzyme has an net negative charge. The amine functionalised materials will have localised positive charges resulting from proton exchange between the amine groups and the surface, and these materials have a net positive charge at pH 6.

Table 3.31: Summary of Support Properties

Material	Pore Size / Å	Zeta Potential / pH	Symmetry	Extraction Method
SBA-15 (Cal)	67.7	3.3 (2.0 Rehyd)	*p6mm*	Calcination
SBA-15 (Ext)	72.0	2.4	*p6mm*	Ethanol Ext.
isPrSH-SBA-15 (2%)	64.6	-	*p6mm*	Ethanol Ext.
isPrSH-SBA-15 (5%)	50.2	4.1	*p6mm*	Ethanol Ext.
isPrSH-SBA-15 (7%)	43.4	-	*Ia3d*	Ethanol Ext.
psPrSH-SBA-15	-	2.0	*p6mm*	Calcination
isPrSMe-SBA-15 (5%)	47.6	-	*p6mm*	Ethanol Ext.
isPrCO_2H-SBA-15 (5%)	47.0	2.5	*p6mm*	Ethanol Ext.
isPh-SBA-15 (5%)	57.0	2.8	*Ia3d*	Ethanol Ext.
isPrNH_2-SBA-15 (2%)	71.6	6.1	*p6mm*	Ethanol Ext.
psPrNH_2-SBA-15	-	8.1	*p6mm*	Calcination
isC_3H_5-SBA-15 (5%)	59.8	3.3	*p6mm*	Ethanol Ext.
0.4TMB-SBA-15	109.7	-	foam	Calcination
0.4TMB-isPrSH (5%)	88.5	-	foam	Ethanol Ext.

3.5.2 Affinity of Supports for H_2O

To understand the surface properties of the functionalised materials, the adsorption of water at 10 °C was investigated by gravimetric analysis using a Hiden IGA 002 (figure 3.61). Each sample is offset from the previous sample by 10% mass uptake. The adsorption of water on calcined SBA-15 results in irreversible adsorption for the initial adsorption / desorption run, followed by reversible adsorption / desorption for subsequent runs (see section 3.2.8.4). Adsorption / desorption by propylthiol functionalised silica is fully reversible, with identical adsorption / desorption isotherms. The uptake by phenyl functionalised SBA-15 is slightly lower than the other samples, due to the hydrophobicity of the surface. The amine functionalised material has a high uptake of water, with some hysteresis. There may be some proton exchange between water and the amine groups on the surface (resulting in $PrNH_3^+OH^-$), which may account for the hysteresis observed.

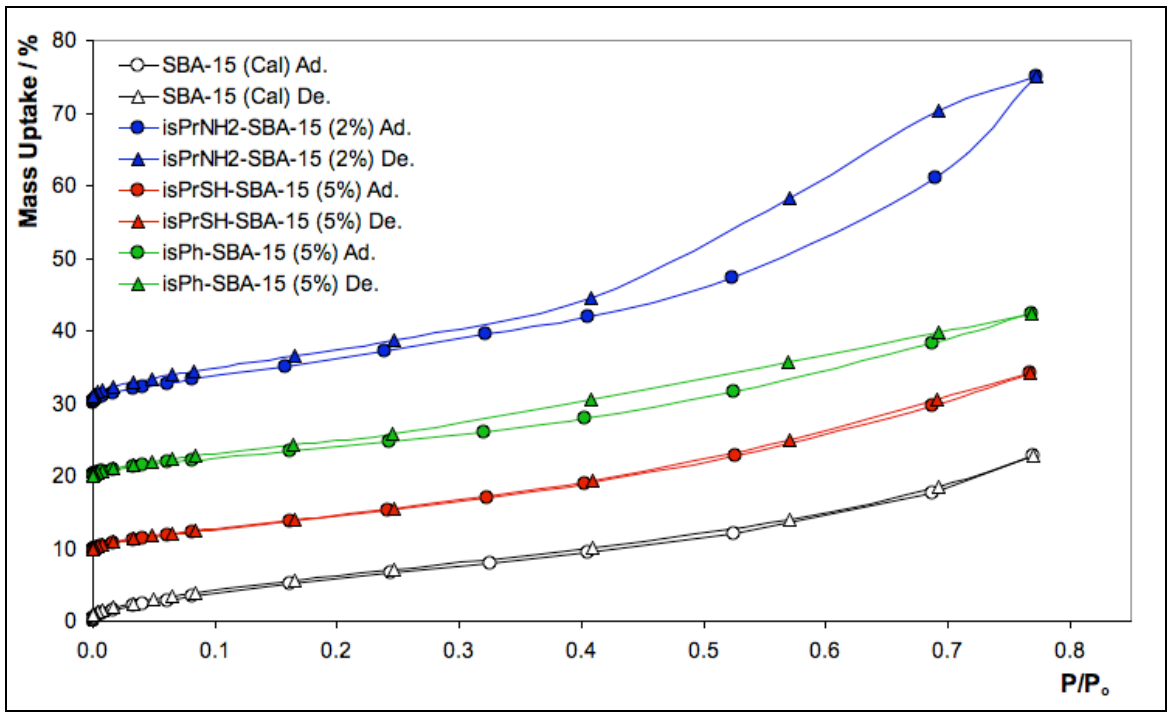

Figure 3.61: Adsorption of Water at 30 °C

3.6 Conclusion

The synthesis of a series of functionalised SBA-15 materials has been achieved, and the material characterised by a range of methods. The surfactant can be removed by calcination or extraction, although with extraction methods there is incomplete removal of the surfactant template. The use of extraction is unavoidable when organic functionality has been introduced into the material, as calcination cannot be used in this case, although Soxhlet extraction is an efficient method to remove the surfactant. The ordered mesoporous material shows good stability to aqueous conditions, with the mesostructure retained even after 12 hours with heating at 50 °C.

The incorporation of organic functional groups into the materials has been achieved by co-condensation of suitable alkyltriethoxysilanes, or by post synthesis grafting of triethoxysilanes. For the co-condensation route, the incorporation of organic material into the structure depends upon the synthesis mixture, although this can have an effect upon the ordering and morphology of the structure obtained. The grafting method can incorporate the functional groups without a loss of order, and into a material with an open microporous network, although the organic group is not as well integrated into the material as by co-condensation.

References

[1] D. Y. Zhao, Q. S. Huo, J. L. Feng, B. F. Chmelka and G. D. Stucky, *J. Am. Chem. Soc.*, 1998, **120**, 6024.
[2] R. P. Hodgkins, A. E. Garcia-Bennett and P. A. Wright, *Microporous Mesoporous Mater.*, 2005, **79**, 241.
[3] J. Lei, J. Fan, C. Z. Yu, L. Y. Zhang, S. Y. Jiang, B. Tu and D. Y. Zhao, *Microporous Mesoporous Mater.*, 2004, **73**, 121.
[4] B. S. Furniss, A. J. Hannaford, P. W. G. Smith and A. R. Tatchell, *Vogel's Textbook of Practical Organic Chemistry*, Longman Scientific & Technical, Harlow, 1989.

4. Enzyme Assays

4.1 Introduction

Described below are the methods used to measure enzyme concentration and activity during the immobilisation studies, as well as a description of the enzyme used as a model protein for study of the support properties. These assays were chosen because they are reliable and well established in literature, and they provide good model systems for catalysis in aqueous media and enantioselective catalysis in organic media.

4.2 Candida Antarctica Lipase B

Candida Antarctica Lipase B (CALB) was chosen as a model enzyme for the immobilisation experiments with mesoporous silica supports. CALB is a triacylglycerol hydrolase (E.C. 3.1.1.3) composed of 317 amino acid residues with a molecular weight of 33 kDa.[1] It is a small protein of approximate dimensions 30 x 40 x 50 Å.[2] As with all lipases, CALB catalyses the hydrolysis of triacylglycerols in aqueous conditions, and the transesterification of secondary alcohols in organic media.[3, 4] The tertiary structure of CALB is shown below (figure 4.1, image generated with PYMOL v1.0edu1).

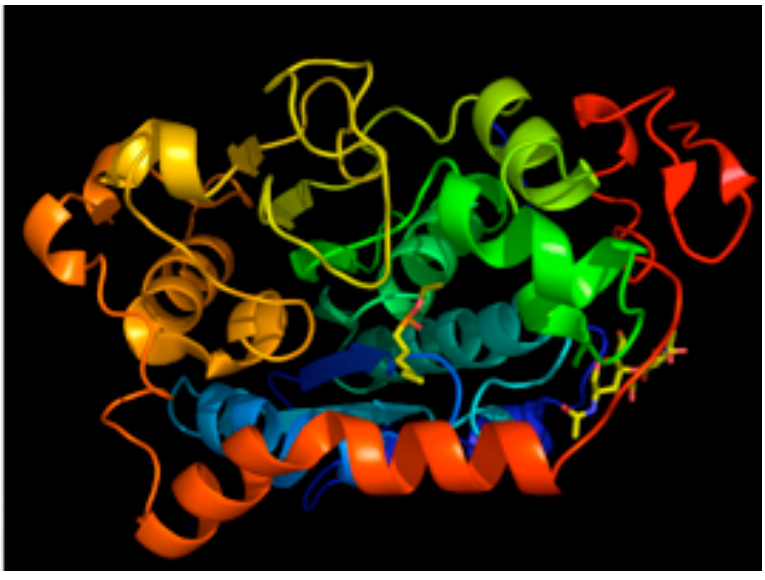

Figure 4.1: Candida Antarctica Lipase B

The active site of CALB contains a catalytic triad, composed of serine (105), aspartic acid (187) and histidine (224), this is illustrated below (figure 4.2). The active site is very similar to other lipases including *rhizomucor miehei* and human pancreatic lipase.[5, 6] These enzymes incorporate a helical lid which blocks access to the serine of the active site. At the interface between an oil and water this lid opens, dramatically increasing the catalytic rate (interfacial activation). This behaviour is also observed for *candida rugosa*, in which the *cis-trans* isomerisation of a proline reside results in the opening of the lid.[7] An alpha helix containing a proline residue has been identified in CALB, that may prevent access to the active site in a similar way to that of *candida rugosa,* although this has not been proven.[2] If there is a lid present in CALB, it is open in most conformations, and CALB does not exhibit interfacial activity increases as with similar enzymes.[8] In CALB the active site is accessible to solvent via a hydrophobic channel comprised of aliphatic amino acid residues. There are six cysteine residues on the surface of CALB, all bound as disulfides. There is also a large hydrophobic region on the surface surrounding the active site, which is responsible for the interfacial activation observed with CALB.[2]

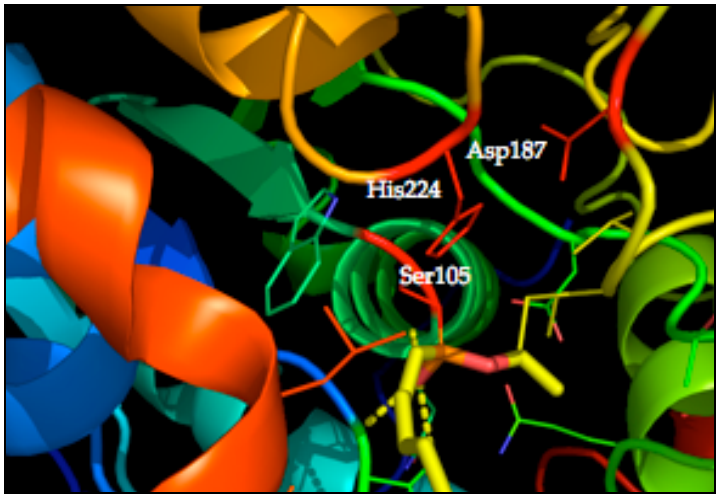

Figure 4.2: CALB Active Site

4.3 Bradford's Assay

For accurate measurement of protein concentration in solution the Bradford assay[9] is well established as an easy and reliable method.[10, 11] The assay is measured by UV, and

monitors the shift in maximum UV adsorption of a dye molecule, Coomassie Brilliant Blue G-250 (figure 4.3).

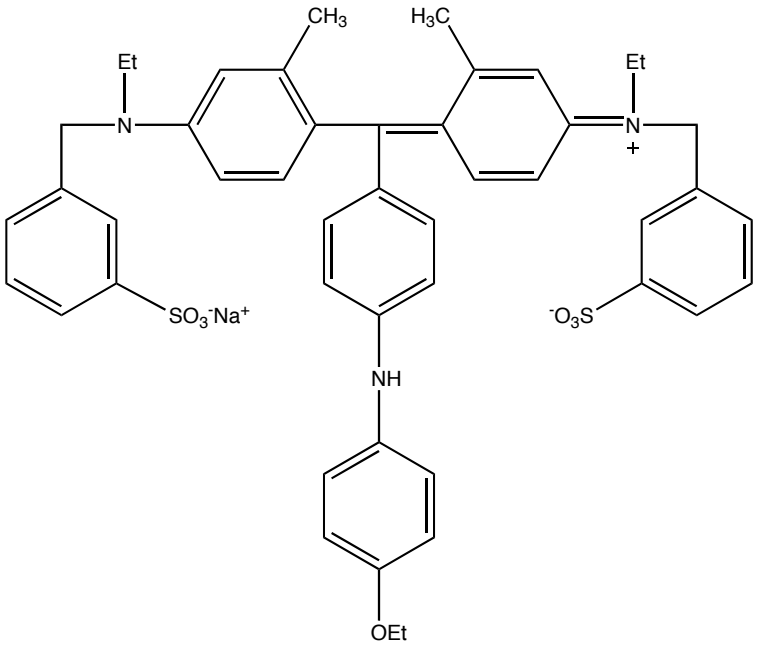

Figure 4.3: Coomassie Brilliant Blue G-250

In the unbound cationic form, the dye molecule adsorbs at 465 nm, and when in the presence of protein, the dye binds to arginine, tryptophan, tyrosine, histidine and phenylalanine residues, with the primary response from arginine binding. The dye binds in the anionic form, which has an absorbance maximum at 595 nm.[12]

The binding of the dye is rapid upon addition to the protein sample, with development of the blue colour occurring within 2 minutes at room temperature, and persisting for up to an hour. For the measurements in this study, the samples were incubated for 15 minutes at room temperature, then measured with a UVIKON 930 spectrophotometer. The dye is known to bind strongly to quartz cuvettes, plastic cuvettes were used for all measurements. The absorbance is measured relative to a standard of known protein concentration, for this a sample of 1 mg mL^{-1} bovine serum albumin (BSA) standard (Fluka, 0.15 M NaCl) was used. This calibration curve is plotted below (figure 4.4), and from this the concentration of protein in a given sample can be calculated by measuring the dye response.

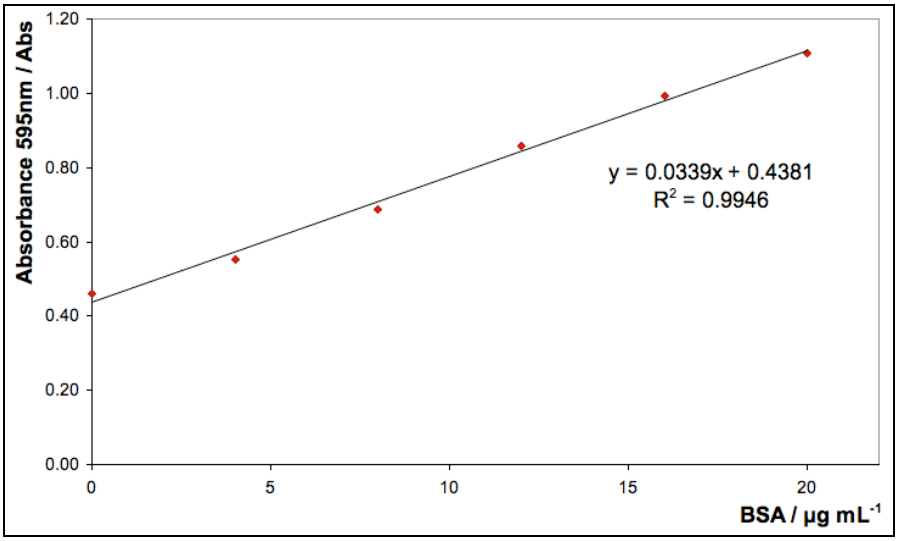

Figure 4.4: Bradford's Protein Assay BSA Calibration

4.4 Hydrolysis of 4-Nitrophenyl Butyrate

To measure the activity of CALB the hydrolysis of *para*-nitrophenyl butyrate (*p*-NPB) is a facile and reliable method that can be monitored by UV-Visible spectroscopy.[13] The cleavage of *p*-NPB is illustrated in the scheme below (figure 4.5). The hydrolysis products are butyric acid and para-nitrophenol, of which the production of para-nitrophenol can be monitored by UV-Vis spectroscopy at 340 - 400nm, due to its intense yellow colour. The length of the carbon chain of the carboxylic acid produced is not critical, and *para*-nitrophenyl acetate is also commonly used.[14]

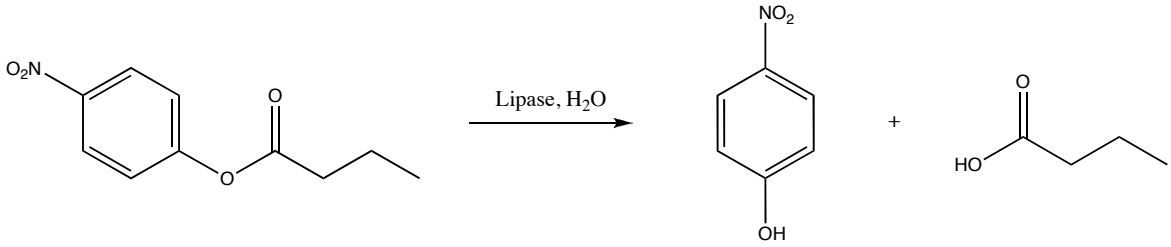

Figure 4.5: Lipase Catalysed Hydrolysis of *p*-NPB

The pKa of *p*-nitrophenol is 7.15, with different extinction coefficients for the protonated and deprotonated forms.[15] To obtain accurate results the assay must be run at a pH sufficiently removed from 7.15, making sure the para-nitrophenyl is fully deprotonated. The extinction coefficients were calculated at pH 7.2 and 8.0 by taking a

known concentration of *p*-nitrophenol (Aldrich, > 99%) using the Beer-Lambert Law (equation 4.1), where A is adsorption, ε is the extinction coefficient, C is concentration and L is the path length through the sample.

$$A = \varepsilon CL \tag{4.1}$$

The data are plotted as concentration versus absorbance (figure 4.6), which gives the gradient for a straight line graph as the extinction coefficient versus the path length. As the path length is 1 cm the extinction coefficient at pH 7 and 8 for p-nitrophenol can be calculated from the graphs below. For the data below, the absorbance was measured at 400 nm using a Kontron UVIKON 930 UV-Vis spectrometer.

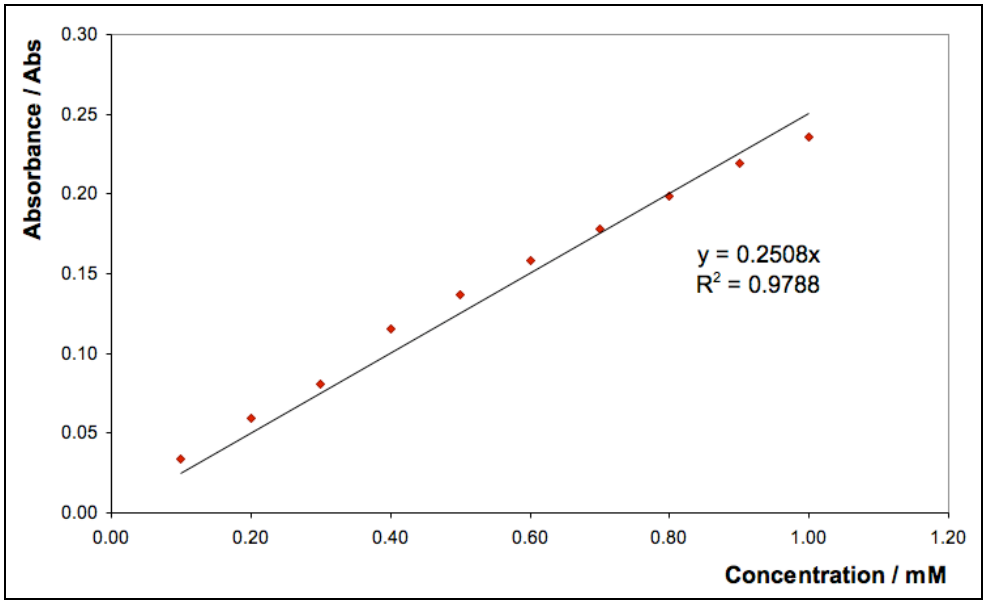

Figure 4.6: *p*-Nitrophenol Extinction Coefficient at pH 7.0

The absorbance was measured for a known concentration of 4-nitrophenol at pH 8.0, and the data are plotted below (figure 4.7). The extinction coefficient for p-nitrophenol at pH 7 is measured at 250.8 cm^{-1}, and at pH 8 is measured at 17052 cm^{-1}, with 50 mM potassium hydrogen phosphate buffer ($K_xH_yPO_4$, where x + y is 3) at room temperature. For elevated temperatures this value would need to be recalculated, as there is a significant shift in the UV-Vis spectra for *p*-nitrophenol.[16] These values correspond quite closely to values given in literature of 16808 cm^{-1} (pH 8)[15] and 12000 cm^{-1} (pH 7.2).[13]

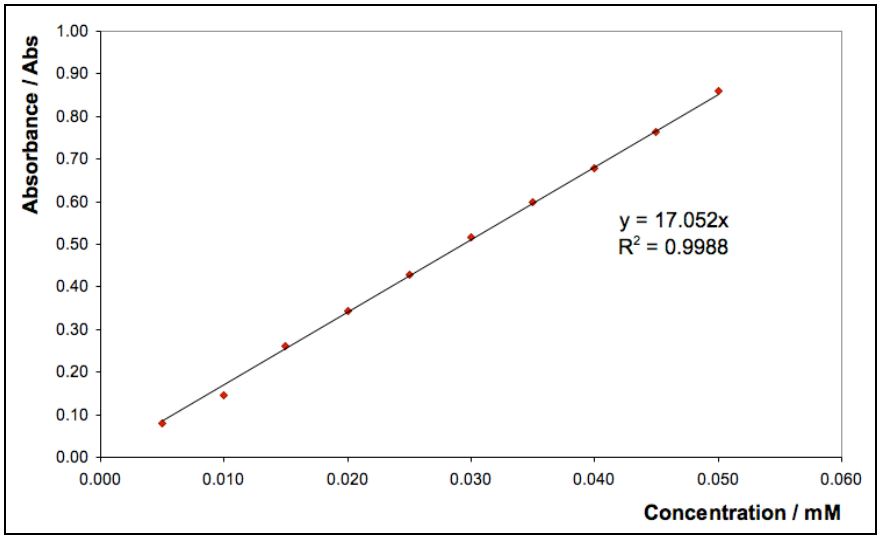

Figure 4.7: *p*-Nitrophenol Extinction Coefficient at pH 8.0

The rate of hydrolysis of *p*-NPB by CALB was measured at a range of pH values and the results are shown below (figure 4.8). The enzyme concentration was kept constant, and the graph shows that the highest absorbance per enzyme unit is between pH 8.0 and 8.5. This is due to both the enzyme activity difference across the pH range (optimum at pH 7),[17] and to the intensity of *p*-nitrophenol at pH 8. The *p*-NPB hydrolysis experiments described in this thesis were carried out at pH 8 (50 mM phosphate buffer) at room temperature, with the measured extinction coefficient used for all rate calculations.

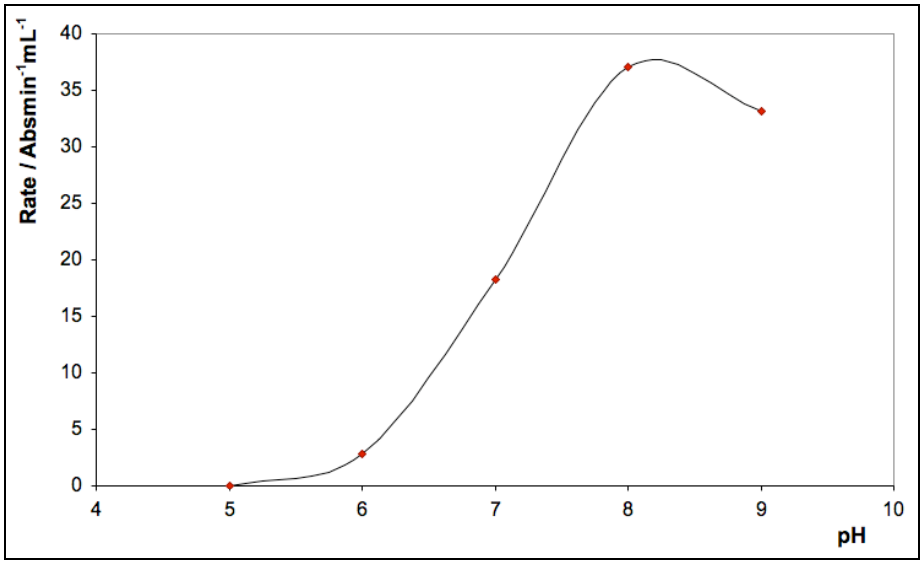

Figure 4.8: Hydrolysis of *p*-NPB by CALB

4.5 Hydrolysis of Tributyrin

In biological systems lipases catalyse the hydrolysis of esters of glycerol, typically long chain fatty acids. The lipase operates at the interface between the hydrophobic ester and water, as described above. To measure the activity of CALB both in solution and immobilised, the rate of the hydrolysis of tributyrin was measured. The reaction scheme for the hydrolysis of tributyrin to glycerol and butyric acid is shown below (figure 4.9).

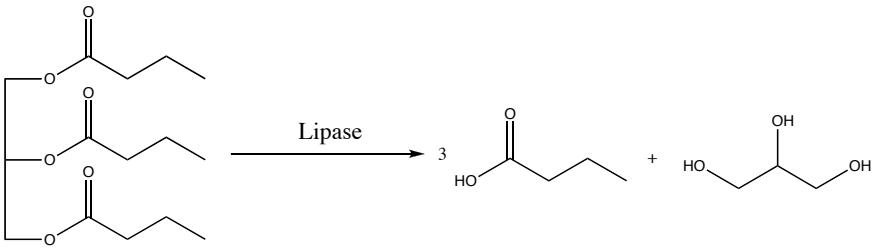

Figure 4.9: Tributyrin Hydrolysis

The rate of tributyrin hydrolysis was measured by following the production of butyric acid by autotitration. The autotitrator, working in pH stat mode, will maintain the pH of a solution, in this case an emulsion of tributyrin and buffer, by measuring the pH of the solution and titrating a known amount of sodium hydroxide. As the rate of sodium hydroxide addition, after accounting for concentration, must equal the rate of production of butyric acid, the rate of the reaction can be followed. The experiments in this thesis were measured initially with a Mettler Toledo DL21 autotitrator, and subsequently with a Metrohm 751 Titrino autotitrator (figure 4.10).

The reaction was carried out with a jacketed flask attached to a water bath at a temperature of 25 °C. To the sample (100 mg immobilised CALB catalyst) 25 mL phosphate buffer (10 mM) was added, at a pH 0.5 below that of the operation pH, which was between pH 6.0 - 8.0 depending on the experiment. The mixture was stirred using a magnetic follower, and the pH probe and sodium hydroxide tube attached. The mixture was pre-titrated to the operating pH with 0.5 M sodium hydroxide, after which 5 mL tributyrin was added to initiate the reaction. The autotitrator was set to operate in static pH mode (pH STAT), and the production of butyric acid was compensated for automatically by the addition of 0.5 M sodium hydroxide. The sodium hydroxide solution was protected with a soda lime trap to prevent the adsorption of carbon dioxide, and subsequent neutralisation by carbonic acid.

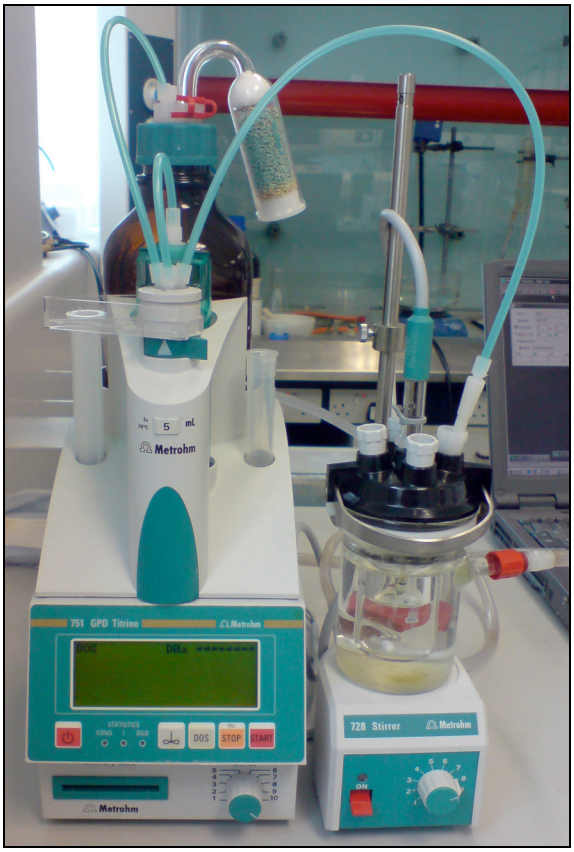

Figure 4.10: Metrohm 751 Autotitrator

The results are plotted as the concentration of sodium hydroxide against time, and the initial rate of reaction is calculated from this. There is an initial lag phase, due to the emulsion formation after the addition of tributyrin which is accounted for by calculating the rate from two later timepoints. The autotitration trace for a sample of CALB immobilised within psPrSH-SBA-15 at a loading of 10 mg g^{-1} is shown below (figure 4.11).

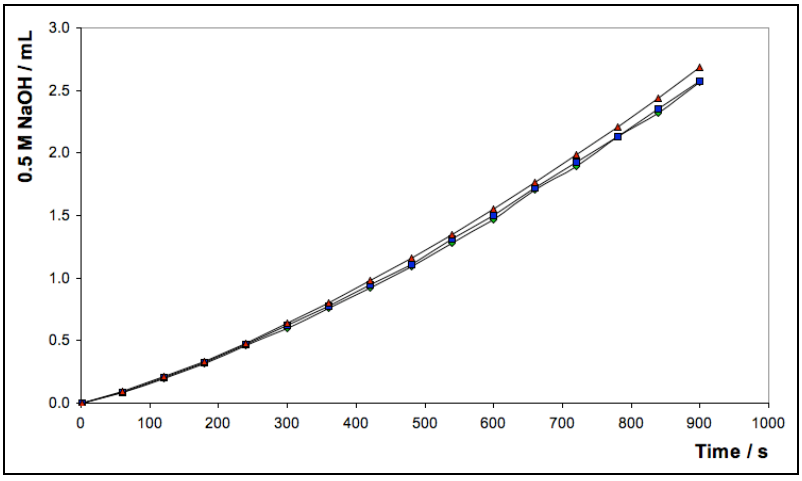

Figure 4.11: Addition of Sodium Hydroxide During Tributyrin Hydrolysis

4.6 Transesterification of 1-Phenylethanol

4.6.1 Introduction

To measure the activity of CALB in organic solvents, the acylation of 1-phenylethanol (figure 4.12) was followed by gas chromatography. The transesterification is selective for the production of (R)-1-phenylethyl acetate. The acyl source (isopropenyl acetate) is present in excess, and tautomerism of the propen-2-ol by-product to acetone drives the reaction to completion.

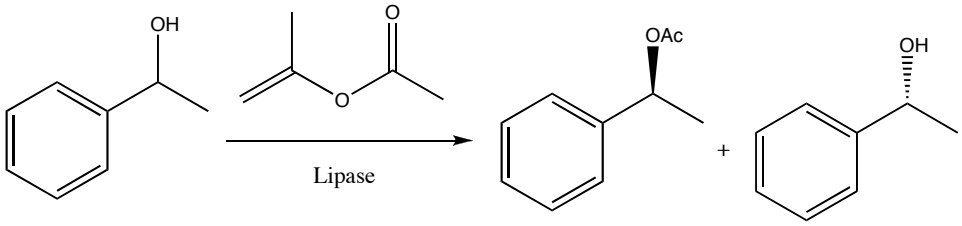

Figure 4.12: Transesterification of (R)-1-Phenylethanol

4.6.2 Equipment

The reaction was followed by gas chromatography (GC), using a CE Instruments GC 8000Top (figure 4.13) with a Chirasil-DEX CB WCOT 25m fused silica chiral column. A flame ionisation detector (FID) was used for detection, output to a Fisons DP700 integrator. Helium was used as the carrier gas, with a split ratio of 100:1 for a 1 μL injection (positive displacement syringe). The oven temperature was isothermal, at 130 °C, with an injection chamber and FID temperature of 200 °C.

Figure 4.13: CE Instruments GC 8000Top

4.6.3 Transesterification with Immobilised CALB

The GC substrate mixture was prepared by adding 1-phenylethanol (15.25 g, 0.125 mol) and isopropenyl acetate (25.00 g, 0.250 mol) in methyl tert-butyl ester (MTBE, HPLC Grade) to a total volume of 250 mL. Oven dried (120 °C) 4A molecular sieves (50 g) were added to this mixture, which was stirred overnight before use. In a typical transesterification experiment 5 mL of this substrate mixture was added to 100 mg immobilised CALB, followed by stirring at room temperature (Spiramix 5). The sample was separated by centrifugation at each time point and the conversion of 1-phenylethanol measured by the injection of 1 μL sample with a split ratio of 1:100.

As the reaction progresses the conversion is followed by measuring the disappearance of the (R)-1-phenylethanol peak (~6.95 min), and by measuring the appearance of the (R)-1-phenylethyl acetate peak (~ 5.40 min). The integrator readouts are shown below (figure 4.14). After 30 minutes, the area of the (R)-1-phenylethanol peak (6.97 min) has decreased, and the product peak can be observed (5.51 min). After 48 hours, the (R)-1-phenylethanol peak can no longer be observed.

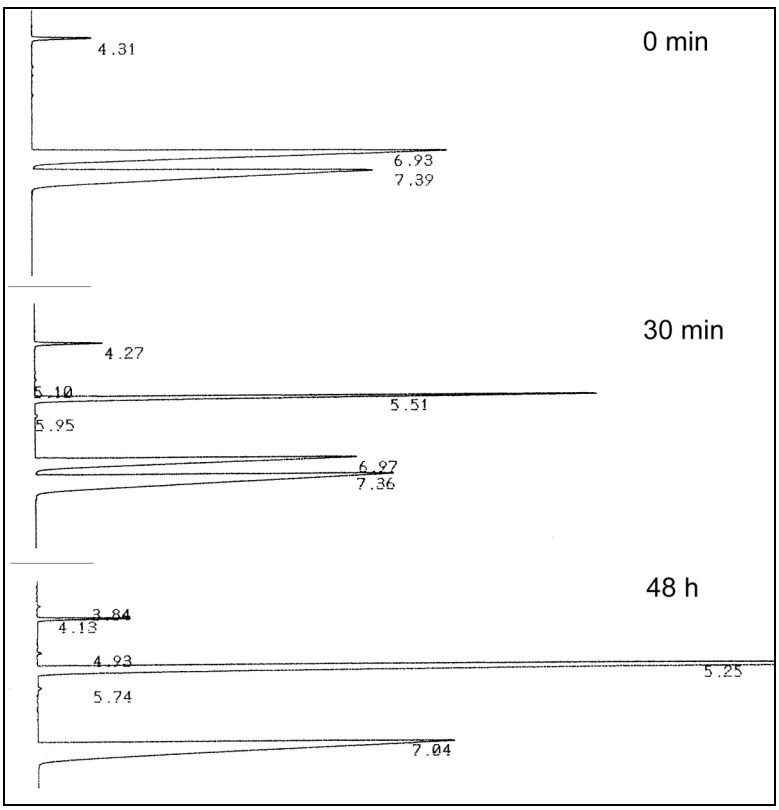

Figure 4.14: Typical GC Trace for the Acylation of 1-Phenylethanol with Immobilised CALB

From the peak integrals we can measure the concentration of starting material and product relative to time. This is plotted below (figure 4.15) for the conversion by CALB immobilised within isPrSH-SBA-15 (2%). The disappearance of the starting material and the formation of the product can be clearly observed. The reaction is highly enantioselective, with greater than 99.9% e.e. at complete conversion after 48 hours.

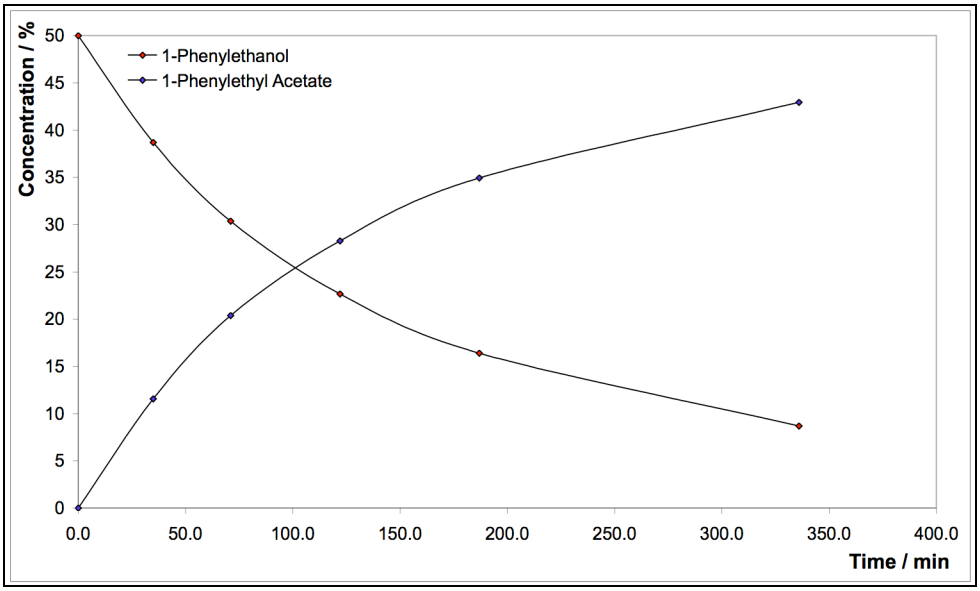

Figure 4.15: Conversion of (R)-1-Phenylethanol by Immobilised CALB

4.7 Conclusion

The methods described above provide a reliable set of tests to measure the concentration and activity of CALB for the purposes of this study. The concentration of protein can accurately be measured in solution to investigate the support properties of mesoporous silica using *p*-NPB hydrolysis and Bradford's assay. The activity of the bound protein can then be measured in both aqueous and organic environments by tributyrin hydrolysis and enantioselective (R)-1-phenylethanol transesterification.

References

[1] J. Uppenberg, N. Ohrner, M. Norin, K. Hult, G. J. Kleywegt, S. Patkar, V. Waagen, T. Anthonsen and T. A. Jones, *Biochemistry*, 1995, **34**, 16838.
[2] J. Uppenberg, M. T. Hansen, S. Patkar and T. A. Jones, *Structure*, 1994, **2**, 293.
[3] H. Frykman, N. Ohrner, T. Norin and K. Hult, *Tetrahedron Lett.*, 1993, **34**, 1367.
[4] V. Waagen, I. Hollingsaeter, V. Partali, O. Thorstad and T. Anthonsen, *Tetrahedron-Asymmetry*, 1993, **4**, 2265.
[5] L. Brady, A. M. Brzozowski, Z. S. Derewenda, E. Dodson, G. Dodson, S. Tolley, J. P. Turkenburg, L. Christiansen, B. Hugejensen, L. Norskov, L. Thim and U. Menge, *Nature*, 1990, **343**, 767.
[6] F. K. Winkler, A. Darcy and W. Hunziker, *Nature*, 1990, **343**, 771.
[7] P. Grochulski, Y. G. Li, J. D. Schrag, F. Bouthillier, P. Smith, D. Harrison, B. Rubin and M. Cygler, *J. Biol. Chem.*, 1993, **268**, 12843.
[8] O. Kirk and M. W. Christensen, *Org. Process Res. Dev.*, 2002, **6**, 446.
[9] M. M. Bradford, *Anal. Biochem.*, 1976, **72**, 248.
[10] C. V. Sapan, R. L. Lundblad and N. C. Price, *Biotechnol. Appl. Biochem.*, 1999, **29**, 99.
[11] C. G. Jones, J. D. Hare and S. J. Compton, *J. Chem. Ecol.*, 1989, **15**, 979.
[12] S. J. Compton and C. G. Jones, *Anal. Biochem.*, 1985, **151**, 369.
[13] K. Shirai and R. L. Jackson, *J. Biol. Chem.*, 1982, **257**, 1253.
[14] T. Kudanga, E. Mwenje, F. Mandivenga and J. S. Read, *J. Basic Microbiol.*, 2007, **47**, 138.
[15] A. E. Beg, *J. Chem. Soc. Pak.*, 1984, **6**, 55.
[16] L. Fourage, M. Helbert, P. Nicolet and B. Colas, *Anal. Biochem.*, 1999, **270**, 184.
[17] A. R. McCrae, E. L. Roehl and H. M. Brand, *SOeFW-Journal*, 1990, **116**, 201.

5. Immobilisation Within Mesoporous Supports

5.1 Introduction

The aim of the studies described below are to investigate a model system that may be used with a variety of different proteins and to investigate the properties of mesoporous support materials for enzyme immobilisation. As enzyme leaching from the support can be a considerable problem in enzyme adsorption systems, CALB leaching from mesoporous supports was investigated using a one pot washing process and washing of an immobilised enzyme packed column system.

A typical protein has hydrophobic and hydrophilic surface regions, defined by the composition of the amino acids that make up the surface. Many proteins have hydrophobic core regions that are integral to the protein folding and stability in aqueous systems. The surface of a typical silica mesoporous material is comprised of silanol groups, and is reasonably hydrophilic, yet less so than aqueous media. For the enzyme to be adsorbed by the support there must be a driving force for this adsorption. As the enzyme is bound to the surface there is increased van der Waals bonding within the confined environment of the pore, and the solvation shell of water surrounding the protein is released for the areas of contact between the protein and the support. This results in reduced hydrogen bonding by water molecules that were associated with the hydrophobic regions of the protein surface and a positive entropic effect as these water molecules are released.[1] For supports that have organic functional groups on the surface of the support, there are positive coulombic and dipole-dipole interactions, depending on the composition of the functional groups and the protein.

5.2 CALB Adsorption by Mesoporous Silica Supports

5.2.1 Conditions

The enzyme was immobilised by mixing the support and the enzyme solution, typically at a concentration of 0.25 mg mL^{-1} CALB. The amount of enzyme bound to the support was calculated by measuring the *p*-NPB hydrolysis activity of the enzyme solution before immobilisation, followed by measurement of activity of the supernatant solution

obtained after separation of the support by centrifugation. This method assumes that no enzyme aggregation or deactivation occurs during the course of the reaction. This is a reasonable assumption, as the half life of a CALB enzyme solution at room temperature is over one week, while the majority of the immobilisations took place at 4 °C. For immobilisations performed over longer times and at high temperatures, when deactivation and aggregation of enzyme could result in a significant error, the supernatant enzyme concentration was measured by Bradford's assay as well as *p*-NPB hydrolysis.

In a typical immobilisation 100 mg of solid support was mixed with a solution of CALB buffered at pH 6. The enzyme solution was prepared by diluting a Novozyme Chirazyme L2 stabilised liquid preparation of CALB from a concentration of 10 mg mL^{-1} to a final concentration of 0.25 mg mL^{-1}. The buffer was a mixture of KH_2PO_4 and K_2HPO_4 at a concentration of 50 mM, prepared and adjusted to pH 6 by dropwise addition of the appropriate $K_xH_yPO_4$ stock solution (referred to as phosphate buffer below). The support and enzyme solution were mixed at 4°C by a Spiramix 5 roller, typically for 5 or 12 hours, after which time the solid was recovered by centrifugation (Beckman fixed-angle JA-25.50 rotor at 10000 rpm (*k*-factor 2613)). For higher concentration samples, the protein content of the supernatant and free enzyme solutions were measured by Bradford's assay and used to calculate the degree of immobilisation. For activity analysis by *p*-NPB hydrolysis 10 μL sample was added to 1 mL of a *p*-NPB solution (25 μM) at pH 8 (50 mM, phosphate), and the activity was averaged over three assays. The sample was then washed with pH 7.2 buffer (4 x 5 mL, phosphate, 50 mM), and the activity of the second wash is quoted in the sections below, as the activity of the first wash was contaminated by unbound enzyme.

5.2.2 Immobilisation of CALB within Calcined SBA-15

The immobilisation of CALB within SBA-15 at a loading of 10 mg g^{-1} was carried out as described above, and activity of the supernatant liquid was measured, the results are plotted below (figure 5.1). The amount of enzyme adsorbed is taken as the difference between the activity of the supernatant and the activity of the free enzyme. It can be observed that the enzyme activity of the supernatant is greatly reduced, with Bradford's assay confirming that the protein is no longer present in solution. By working out the difference between the activities, the amount of enzyme immobilised was calculated.

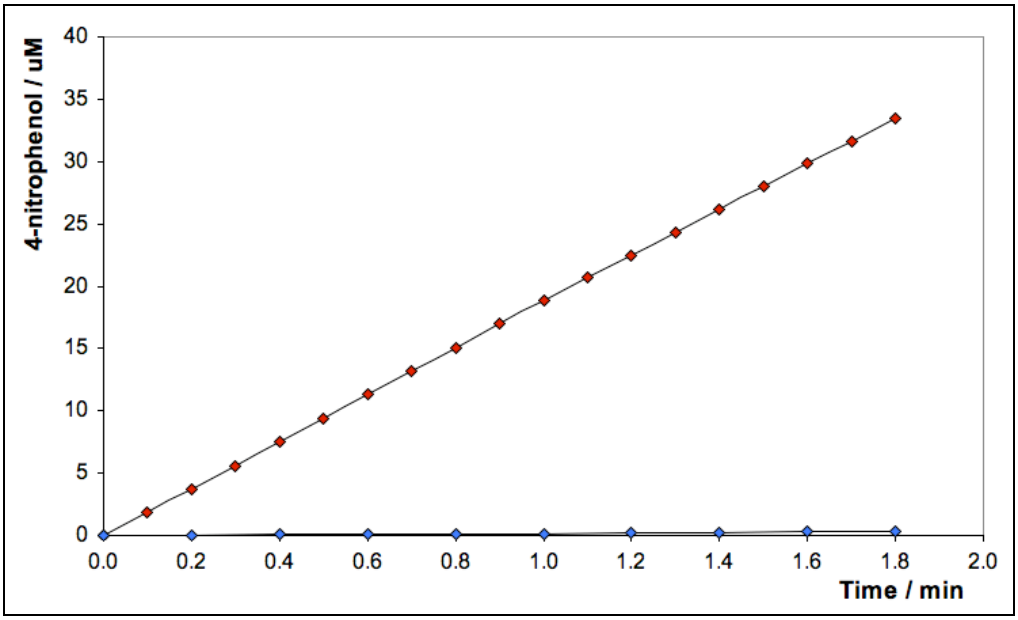

Figure 5.1: Supernatant CALB Activity After Adsorption by SBA-15

The uptake with time is tabulated below (table 5.1). The enzyme was nearly completely adsorbed after 5 hours mixing and was completely adsorbed after 12 hours. The supernatant activity of the second 5 mL pH 7.2 wash was measured, with an activity of 0.01 mg mL^{-1}, which is 0.1% of the loaded enzyme washed from the support per millilitre at pH 7.2. The enzyme is thus taken up rapidly by the support, and the leaching of enzyme at pH 7.2 is relatively low.

Table 5.1: CALB Immobilisation on SBA-15

	Temp. / °C	Time / h	Immobilised / %	Loading / mg g^{-1}	Wash Act. / mg mL^{-1} (%)
SBA-15 (Cal)	4	0	0	0	-
SBA-15 (Cal)	4	5	99.5	10	-
SBA-15 (Cal)	4	12	100	10	0.010 (0.1%)

5.2.3 Effect of Extraction Procedure on Support Properties

An important control reaction is a comparison of immobilisation on SBA-15 in which the surfactant has been removed by different methods, or not removed after synthesis. This is of use when comparing immobilisation on calcined materials to immobilisation on organo-functionalised silicas, which cannot be calcined without removal

of the organic functionality. There is also an appreciable structural shrinkage upon calcination which may affect the support properties. The uptake of enzyme by calcined SBA-15, ethanol extracted SBA-15, unextracted SBA-15 and rehydrated calcined SBA-15 was investigated, and the residual supernatant activities are plotted below (figure 6.2). The rehydrated sample was prepared by the removal of surfactant by calcination, followed by suspension and mixing in pH 6 buffer overnight, which has the effect of regenerating the silanol groups on the silica surface (see section 3.2.8).

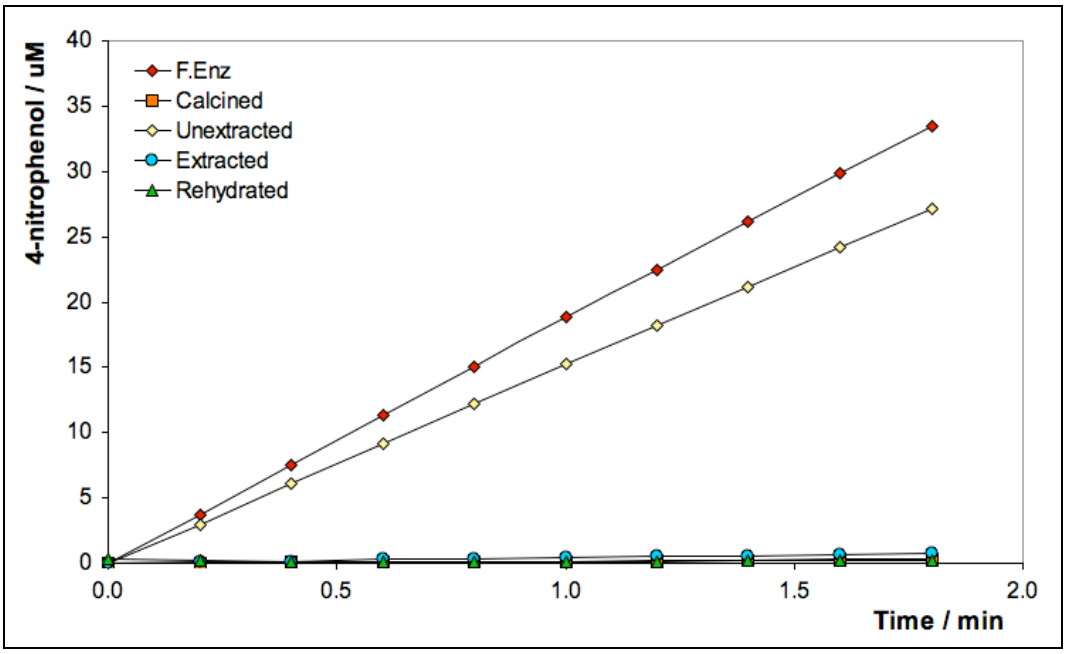

Figure 5.2: Supernatant CALB Activity After Immobilisation

The uptake and loading are tabulated below (table 5.2). From the table below it can be seen that there is very little difference between the fully extracted samples, with near-complete immobilisation after five hours.

Table 5.2: Immobilisation Within Extracted SBA-15 Materials

Support	Temp. / °C	Time / h	Immobilised / %	Loading / mg g^{-1}	Wash Act. / mg mL^{-1} (%)
SBA-15 (Cal.)	4	5	99.5	10	-
SBA-15 (Ext.)	4	5	98.8	9.9	0.010 (0.1%)
SBA-15 (Unex.)	4	5	19.0	1.9	0.018 (0.9%)
SBA-15 (Rehd.)	4	5	100.0	10	0.008 (0.1%)

The unextracted sample shows poor uptake of protein, with 81% of available CALB remaining in solution. This indicates that although there is some surface adsorption, the majority of the immobilised enzyme that is adsorbed by an extracted material is localised within the pore system. However, this does not necessarily mean that up to 19% of enzyme is localised on the surface after immobilisation with extracted materials, as there is preferential binding within the pore system, due to the reasons discussed above (section 5.1.2). There is also likely to be partial extraction of the surfactant at the pore entrances during the filtration after synthesis and during the immobilisation process, which may account for some of the uptake.

5.2.4 High Loading of CALB on SBA-15

The uptake of CALB by SBA-15 at higher loadings enzyme loading of up to 500 mg g^{-1} is shown below (table 5.3). The conditions for the immobilisations are described above (section 5.2.1), only the concentration of the free enzyme solution was increased. The capacity of the support for CALB is high, with up to 450 mg g^{-1} maximum loading. The adsorption of CALB by extracted SBA-15 is slightly slower than calcined SBA-15 with lower uptake at high loadings of 25 and 50 mg g^{-1}. This may be due to different surface properties of the ethanol extracted sample, which may incorporate ethoxide groups on the surface during extraction.

Table 5.3: High Loading with Calcined SBA-15

Support	Temp. / °C	Mixing / h	Enz. Available / mg g^{-1}	Immobilised / %	Loading / mg g^{-1}
SBA-15 (Cal)	4	12	10	100.0	10.0
SBA-15 (Cal)	4	72	25	98.7	24.7
SBA-15 (Cal)	4	72	50	97.3	48.7
SBA-15 (Cal)	4	168	50	99.2	49.6
SBA-15 (Cal)	4	24	100	59.3	59.3
SBA-15 (Cal)	37	48	100	80.7	80.7
SBA-15 (Cal)	37	168	100	94.9	94.9
SBA-15 (Cal)	37	24	500	17.7	88.4
SBA-15 (Cal)	37	168	500	90.1	450.7
SBA-15 (Ext)	4	72	10	98.8	9.9
SBA-15 (Ext)	4	72	25	91.3	22.8
SBA-15 (Ext)	4	72	50	84.0	42.0

As the loading increases, the time required for uptake increases significantly, with up to seven days required for maximum uptake. No further uptake was observed for the immobilisation with a maximum enzyme available of 500 mg g^{-1}. To reach high levels of immobilisation within reasonable timescales the immobilisation temperature was increased to 37 °C. Bradford's assay was used to measure the enzyme content of the supernatant to prevent any errors due to denatured enzyme. The uptake versus enzyme available is plotted below (figure 5.3).

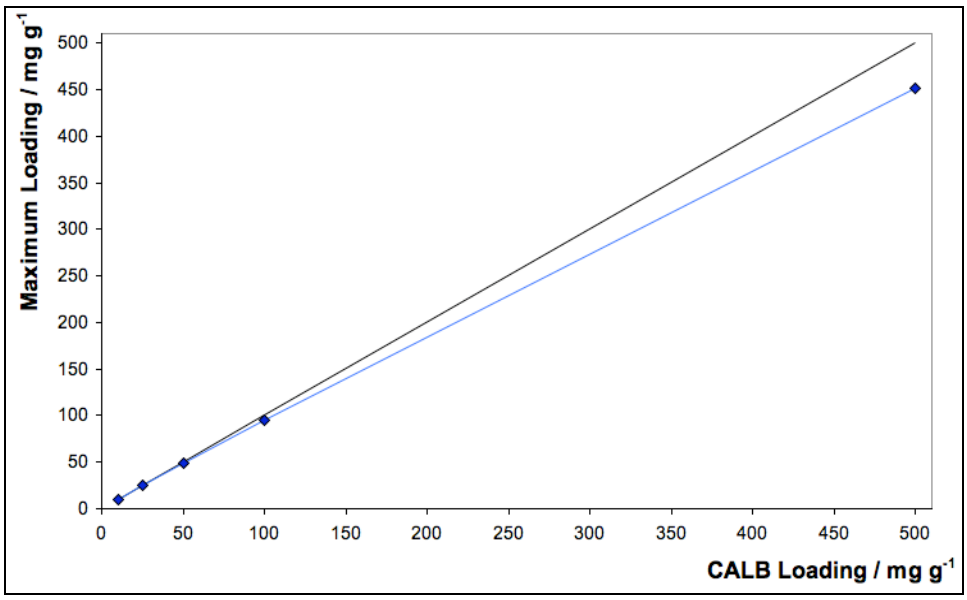

Figure 5.3: CALB Uptake by Calcined SBA-15

As the concentration of available enzyme increases, the time for complete immobilisation increases significantly. This is most likely to be due to fast binding at the entrances to the pore system, followed by slower diffusion of protein within the pore system. The rate of adsorption is faster at higher temperatures, due to an increased mobility of species and a faster rate of diffusion of the protein through the pore system. A very high capacity for loading is possible, and was useful to investigate the degree to which the enzyme is located in the support (see section 5.2.5 below). For catalysis, the specific activity of samples with very high loading is expected to be significantly reduced, due to inaccessibility of some of the enzyme active sites to the substrate and reduced substrate diffusion rates.

5.2.5 Nitrogen Adsorption on Immobilised CALB Samples

With a porous support material it is important to know whether the enzyme is localised within the pore system or adsorbed onto the surface. There are two methods that have been used to investigate this, immobilisation with unextracted mesoporous material and nitrogen adsorption experiments on immobilised samples (see 5.2.3).

The enzyme was immobilised by mixing as described above, and collected by centrifugation. The solid was then dried on a vacuum line prior to adsorption. The adsorption / desorption traces are shown below (figure 5.4), with the CALB loading shown as a percentage, as well as the adsorption / desorption traces for calcined SBA-15 (denoted 0%). As the concentration of CALB within the pores is increased, we see a decrease in overall nitrogen uptake, as well as an increased hysteresis for the capillary condensation. This indicates that the diameter of the pore entrances have been reduced relative to the diameter of the internal pore. As the concentration of CALB is increased to the maximum loading, we see very little nitrogen adsorption by the material, indicating the pore system is completely filled by protein.

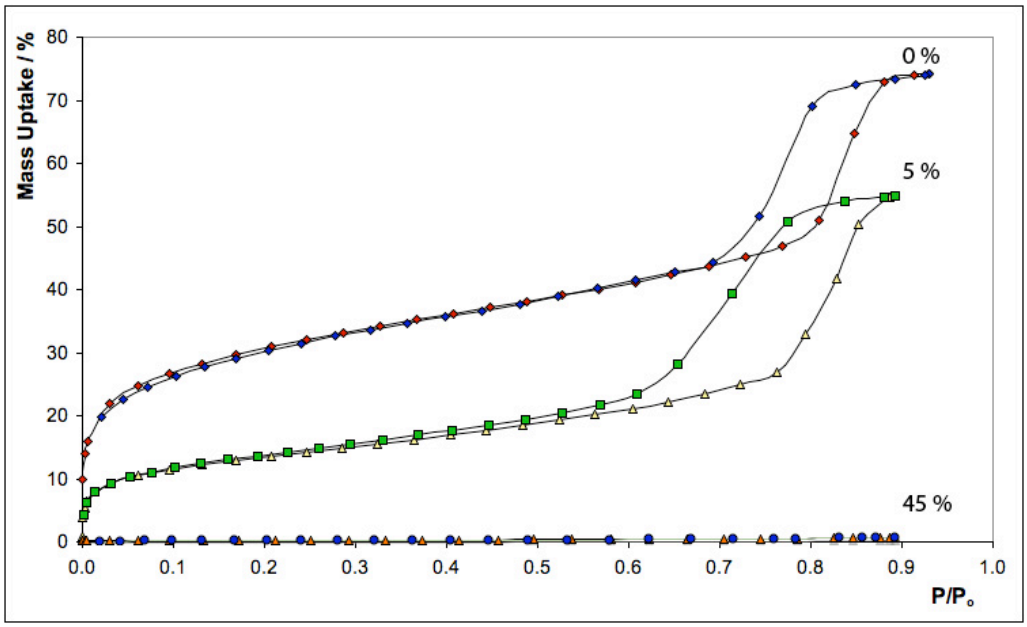

Figure 5.4: Nitrogen Adsorption Isotherms for Immobilised CALB Samples

The data from the nitrogen adsorptions, as well as the BJH analysis of the desorption branch, are shown below (table 5.3). As the enzyme content of the material

increases, the total uptake decreases, with no significant uptake for the 45% sample, indicating complete occlusion of the pore system. The surface areas and pore size diameters also decrease as the enzyme content increases, indicating that the pore system is increasingly inaccessible to nitrogen.

Table 5.3: Nitrogen Adsorption with Immobilised CALB Samples

Enzyme Loading	BET / $m^2 g^{-1}$	BJH / Å	PSD / Å	Uptake / %
0%	805 ± 19	33.8	67.6	74.2
5%	381 ± 4	25.1	50.2	54.7
45%	7 ± 0.2	-	-	0.6

5.3 Functionalised Mesoporous Silica Supports

5.3.1 Why Functionalise The Surface?

There are several reasons to functionalise the surface of an inorganic material for support properties. The primary reason is to improve the binding of the protein to the surface, either through direct covalent attachment, or electrostatic effects. Improved binding properties will result in a bound protein that is less likely to leach, and is stabilised against deactivation by unfolding.[2-4] Another reason to incorporate functional groups into a material is to change the interface and wetting properties for a particular solvent or substrate, potentially increasing diffusion through the pore system. The sections below describe the adsorption of the protein by functionalised materials. For the catalytic properties of the adsorbed enzyme see chapter 6.

5.3.2 isPrCO_2H-SBA-15

The immobilisation of CALB on isPrCO_2H-SBA-15 at a maximum loading of 10 mg g^{-1} was carried out and the results are tabulated below (table 5.4). The conditions were identical to previously described (section 5.2.1). The uptake of enzyme by each carboxy-functionalised material is very fast, with near complete uptake of available enzyme after five hours, and complete uptake for the isPrCO_2H-SBA-15 (5%) repeat which was measured after 12 hours. There is no difference observed between the uptake of CALB by calcined SBA-15 and carboxy-functionalised SBA-15. The amount of enzyme washed from the material (0.1% per millilitre) is identical to that of unfunctionalised SBA-15.

Table 5.4: Adsorption of CALB by isPrCO2H-SBA-15

Support	Temp. / °C	Time / h	Immobilised / %	Loading / mg g^{-1}	Wash Act. / mg mL^{-1} (%)
isPrCO2H-SBA-15 (2%)	4	5	98.2	9.8	0.009 (0.1%)
isPrCO2H-SBA-15 (5%)	4	5	96.7	9.7	0.010 (0.1%)
isPrCO2H-SBA-15 (5%)	4	12	100	10	0.009 (0.1%)
isPrCO2H-SBA-15 (7%)	4	5	97.1	9.7	0.010 (0.1%)

5.3.3 isPh-SBA-15

The immobilisation of CALB within isPh-SBA-15 (5%) was carried out as described above (section 5.3.2), and the results are tabulated below (table 5.5). The sample shows high uptake of enzyme after five hours, indicating that the incorporation of the hydrophobic phenyl rings does not reduce the uptake of enzyme relative to SBA-15.

Table 5.5: Adsorption of CALB by isPh-SBA-15

Support	Temp. / °C	Time / h	Immobilised / %	Loading / mg g^{-1}	Wash Act. / mg mL^{-1} (%)
isPh-SBA-15 (5%)	4	5	97.9	9.8	0.012 (0.1%)
isPh-SBA-15 (5%) Repeat	4	5	99.3	9.9	0.011 (0.1%)

5.3.4 isPrNH_2-SBA-15

The immobilisation with the co-condensed amine functionalised materials was carried out as previously described (section 5.3.2), and the data obtained are tabulated below (table 5.6). Non-intuitively, the highest uptake of CALB is with the least ordered of the materials, the isPrNH_2-SBA-15 (5%) sample. The leaching from all three materials is higher than observed for the other functionalised materials (0.029 - 0.043 mg mL^{-1}), with up to 1.8% of the enzyme leached from the material per mL of pH 7.2 buffer (~ 36% removed during washing with 20 mL).

Table 5.6: Adsorption of CALB by isPrNH_2-SBA-15

Support	Temp. / °C	Time / h	Immobilised / %	Loading / mg g^{-1}	Wash Act. / mg mL^{-1} (%)
isPrNH2-SBA-15 (2%)	4	5	16.1	1.6	0.029 (1.8%)
isPrNH2-SBA-15 (5%)	4	5	48.6	4.9	0.043 (0.9%)
isPrNH2-SBA-15 (7%)	4	5	32.1	3.2	0.035 (1.1%)

5.3.5 psPrNH$_2$-SBA-15

The support properties of psPrNH$_2$-SBA-15 were measured as described above (section 5.3.2), and the data are tabulated below (table 5.7). The uptake of CALB is very similar to the uptake observed for the amine functionalised co-condensed samples (section 5.3.4), indicating that it is the functional group, rather than the morphology of the material, that is responsible for the poor uptake.

Table 5.7: Adsorption of CALB by psPrNH$_2$-SBA-15

Support	Temp. / °C	Time / h	Immobilised / %	Loading / mg g^{-1}	Wash Act. / mg mL^{-1} (%)
psPrNH2-SBA-15	4	5	40.5	4.1	0.076 (1.9%)

5.3.6 isC$_3$H$_5$-SBA-15

The immobilisation of CALB within allyl-functionalised SBA-15 was carried out as described above (section 5.3.2) and the results are tabulated below (table 5.8). The uptake of protein is rapid, with high uptake after 5 hours and near complete uptake after 12 hours for the isC$_3$H$_5$-SBA-15 (5%) sample. The leaching at pH 7 is slightly higher for these material at pH 7 than for unfunctionalised SBA-15.

Table 5.8: Adsorption of CALB by isC$_3$H$_5$-SBA-15

Support	Temp. / °C	Time / h	Immobilised / %	Loading / mg g^{-1}	Wash Act. / mg mL^{-1} (%)
isC$_3$H$_5$-SBA-15 (2%)	4	5	92.3	9.2	0.011 (0.1%)
isC$_3$H$_5$-SBA-15 (5%)	4	5	84.8	8.5	0.018 (0.2%)
isC$_3$H$_5$-SBA-15 (5%)	4	12	98.3	9.8	-
isC$_3$H$_5$-SBA-15 (7%)	4	5	85.6	8.6	0.015 (0.2%)

5.3.7 isPrSH-SBA-15

5.3.7.1 Adsorption at 10 mg g^{-1}

The enzyme uptake of the thiol functionalised materials, at a maximum loading of 10 mg g^{-1} was investigated, with the uptake tabulated below (figure 5.9). All three materials show rapid uptake after five hours, and complete uptake after 12 hours. No enzyme was observed to leach at pH 7 during washing.

Table 5.9: Adsorption of CALB by isPrSH-SBA-15

Support	Temp. / °C	Time / h	Immobilised / %	Loading / mg g^{-1}	Wash Act. / mg mL^{-1} (%)
isPrSH-SBA-15 (2%)	4	5	97.8	9.8	-
isPrSH-SBA-15 (2%)	4	12	99.2	9.9	0 (0%)
isPrSH-SBA-15 (5%)	4	5	94.4	9.4	-
isPrSH-SBA-15 (5%)	4	12	100	10	0 (0%)
isPrSH-SBA-15 (7%)	4	5	98.8	9.9	-
isPrSH-SBA-15 (7%)	4	12	100	10	0 (0%)

5.3.7.2 Rate of Adsorption

The uptake of CALB by isPrSH-SBA-15 (5%) at various time points was measured by preparing the immobilisation mixture as described above. The support (100 mg) was suspended in pH 6 buffer (phosphate, 3.9 mL, 50 mM) and the enzyme source was added (100 μL, 10 $mgmL^{-1}$). The mixture was stirred at 4 °C, at each time point the sample was separated by centrifugation, the enzyme content measured by p-NPB hydrolysis as described above, and the support re-suspended and mixed at 4 °C. The uptake with time is plotted below (figure 5.5). The uptake is rapid, with 67% uptake after 30 minutes, and 96.1% uptake after five hours, which agrees well with the measured value in section 5.3.7.1 (94.4%). The uptake is complete after 24 hours.

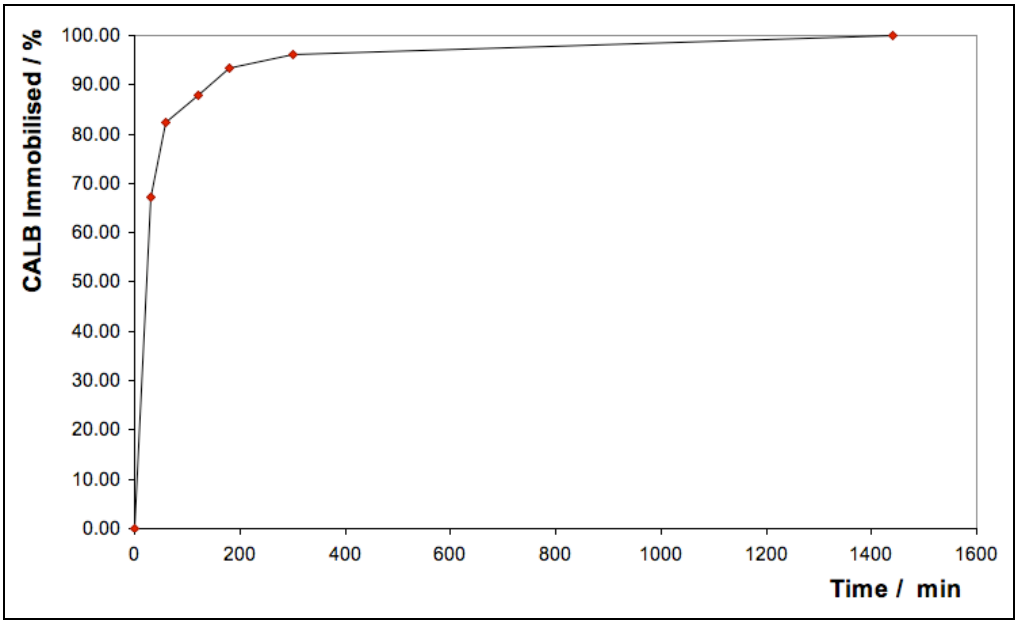

Figure 5.5: Uptake of CALB by isPrSH-SBA-15 (5%)

5.3.7.3 Unextracted isPrSH-SBA-15 (5%)

To make sure the enzyme is located within the pore system of isPrSH-SBA-15 the adsorption properties of an unextracted sample of isPrSH-SBA-15 (5%) were measured. The uptake by this sample compared to extracted isPrSH-SBA-15 (5%) is tabulated below (table 5.10). The uptake after 12 hours is 24.2%, which is reasonably high, but far lower than for the extracted sample. The enzyme is also washed more readily from the material, with 0.8% of the bound enzyme removed per mL.

Table 5.10: Adsorption of CALB by Unextracted isPrSH-SBA-15

Support	Temp. / °C	Time / h	Immobilised / %	Loading / mg g^{-1}	Wash Act. / mg mL^{-1} (%)
isPrSH-SBA-15 (Unextracted)	4	12	24.2	2.4	0.019 (0.8%)
isPrSH-SBA-15 (Extracted)	4	12	100	10.0	0 (0%)

5.3.7.4 High Loading

To investigate the higher loading of CALB on isPrSH-SBA-15 (5%) the conditions from the previous experiments were retained, with the exception that the enzyme concentration of the initial solution was increased. The results of these experiments are tabulated below (table 5.11).

Table 5.11: Adsorption of CALB by isPrSH-SBA-15

Support	Temp. / °C	Time / h	Enz. Available / mg g^{-1}	Immob. / %	Loading / mg g^{-1}
isPrSH-SBA-15 (2%)	4	24	100	30.5	30.5
isPrSH-SBA-15 (2%)	4	48	100	56.7	56.7
isPrSH-SBA-15 (5%)	4	24	100	29.5	29.5
isPrSH-SBA-15 (5%)	4	48	100	46.3	46.3
isPrSH-SBA-15 (7%)	4	24	100	30.5	30.5
isPrSH-SBA-15 (7%)	4	48	100	34.1	34.1

Each sample shows fairly similar rapid uptake of enzyme over 24 hours, with the uptake over the subsequent 24 hours showing some marked differences, this is plotted below (figure 5.6). The 2% sample continues to take up the enzyme at a similar rate, with

56.7 mg enzyme adsorbed after 48 hours, the uptake from the other two samples decreases significantly as the thiol concentration is increased. This is constant with a model that consists of a fast initial binding to the surface / entrances to the pore system, followed by slower diffusion of the protein through the material. The thiol concentration reduces the rate of this diffusion step through increased van der Waals bonding between the support and the enzyme, and as the thiol concentration is increased, this effect is more pronounced. The uptake is also much slower than previously observed with calcined SBA-15 (section 5.2.4) at the same temperature and loading, which adsorbs 59.3 mgg^{-1} after 24 hours, nearly twice the rate of all the *in-situ* thiol samples.

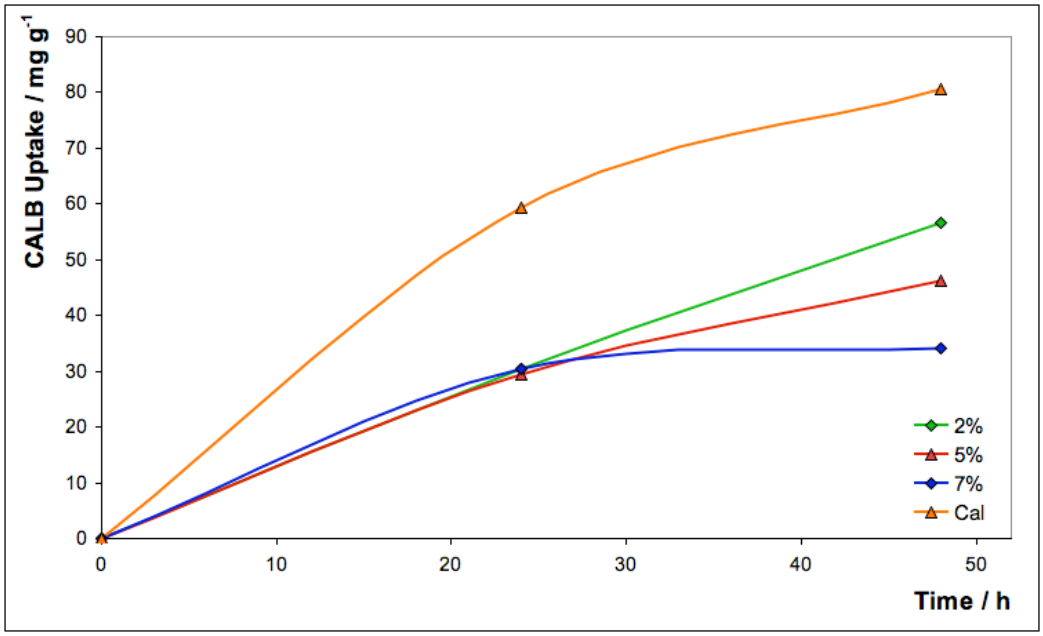

Figure 5.6: Uptake of CALB at a Maximum Loading of 100 mg g^{-1}

A range of loadings were investigated for isPrSH-SBA-15 (5%), and the results are tabulated below (table 5.12). The rate of uptake is related to the concentration of the enzyme solution, with higher concentration solutions resulting in higher uptake for the same time period and temperature. Higher uptake is also obtained by increasing the temperature of immobilisation from 4 °C to 37 °C, due to increased mobility of the species and faster diffusion of protein through the support. The amount of enzyme incorporated into the material is lower than for unfunctionalised SBA-15 due to the slower rate of adsorption.

Table 5.12: Adsorption of CALB by isPrSH-SBA-15

Support	Temp. / °C	Time / h	Enz. Available / mg g^{-1}	Immobilised / %	Loading / mg g^{-1}
isPrSH-SBA-15 (5%)	4	24	10	100	10
isPrSH-SBA-15 (5%)	4	12	25	66.1	16.5
isPrSH-SBA-15 (5%)	4	72	25	98.4	24.6
isPrSH-SBA-15 (5%)	37	24	25	99.2	24.8
isPrSH-SBA-15 (5%)	4	12	50	53.7	26.9
isPrSH-SBA-15 (5%)	4	72	50	64.5	32.3
isPrSH-SBA-15 (5%)	37	24	50	68.7	34.4
isPrSH-SBA-15 (5%)	37	48	50	73.1	36.6
isPrSH-SBA-15 (5%)	4	24	100	29.5	29.5
isPrSH-SBA-15 (5%)	4	48	100	46.3	46.3

5.3.8 psPrSH-SBA-15

The support properties of the post-synthesis thiol are potentially different to the properties for the isPrSH-SBA-15 materials, due to the accessibility of the microporous regions of the support, and the lack of residual surfactant within the material. The residual surfactant does not interfere with the adsorption process, as shown above with extracted SBA-15 samples perform similarly to the calcined SBA-15 materials (section 5.2.3), and the immobilisation properties with several functionalised extracted samples is not diminished.

The immobilisation procedure was identical to the previously described method (section 5.3.2). The uptake is excellent (table 5.13), with near complete loading after five hours, and complete loading at 10 mg g^{-1} after twelve hours. Any leaching during the pH 7.2 wash was below the detection limit of the assay.

Table 5.13: Adsorption of CALB by psPrSH-SBA-15

Support	Temp. / °C	Time / h	Immobilised / %	Loading / mg g^{-1}	Wash Act. / mg mL^{-1} (%)
psPrSH-SBA-15 (HL)	4	5	99.1	9.9	-
psPrSH-SBA-15 (HL)	4	12	100	10	0 (0%)

5.3.9 isPrSH / isPh-SBA-15

The mixed functionality of isPrSH / isPh-SBA-15 (2% / 4%) is of interest as it could potentially combine the binding properties of thiol functionalised materials (see section 5.4.2 below), and increase the affinity for the material in organic solvents, resulting in faster diffusion and improved wetting properties. The adsorption of the enzyme is good (table 5.14), with 97.1% immobilised after 12 hours mixing.

Table 5.14: Adsorption of CALB by isPh/isPrSH-SBA-15

Support	Temp. / °C	Time / h	Immobilised / %	Loading / mg g^{-1}	Wash Act. / mg mL^{-1} (%)
isPh/isPrSH-SBA-15 (2/4%)	4	12	97.1	9.7	0.002 (0.02%)

5.4 Mesoporous Silica Packed Columns

5.4.1 Immobilisation of CALB Within Column Packed SBA-15

Mesoporous silica can be readily packed in a column system, as is often done with chromatography supports. To investigate the immobilisation properties of CALB on column packed mesoporous silica, calcined SBA-15 (0.25 g) as a slurry in pH 6 buffer (phosphate, 50 mM) was packed within an Omnifit adjustable chromatography column (bed volume 1.3 cm^3), pictured below (figure 5.7).

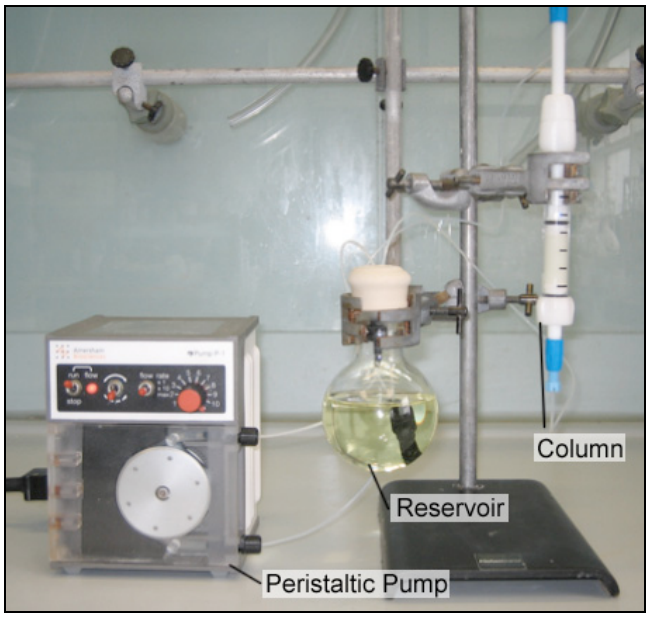

Figure 5.7: Column Packed Immobilised CALB

To immobilise the enzyme, a solution of CALB (10 mL, 0.25 mg mL^{-1}, pH 6) was cycled through the packed column for 12 hours. The residual enzyme content of the stock solution was measured by *p*-NPB hydrolysis. The enzyme was completely adsorbed after 12 hours, after which time the activity was tested by cycling a stock solution of *p*-NPB (10 μM, 60 mL), which was completely hydrolysed after ten minutes. The yellow colour of the solution observed in the image above is due to the 4-nitrophenol produced during the hydrolysis. This method is likely to produce a uneven distribution of enzyme throughout the column, when compared with the mixing method used previously.

5.4.2 Column Packed Immobilised CALB Leaching

To investigate the leaching of bound protein from several supports the immobilised enzyme (0.25 g, 10 mg g^{-1} CALB) was packed onto an adjustable Omnifit column, the support was washed with buffer, and then the protein concentration of each wash was measured by *p*-NPB hydrolysis. For these leaching studies CALB was immobilised within the support by mixing at 4 °C rather than by cycling through a pre-packed column as above (section 5.4.1).

The initial wash was with pH 6 buffer (0 - 10 mL, phosphate, 50 mM), followed by pH 8 buffer (10 - 60 mL, phosphate, 50 mM). The activity of each aliquot was then measured for *p*-NPB hydrolysis activity. These activities are plotted below as activity versus volume (figure 5.8). It can be seen from the graph that there is a dramatic effect with the change in buffer pH, with very high amounts of enzyme leached during the pH 8 wash. There is little difference between SBA-15 in which the surfactant has been extracted by solvent rather than calcined, showing that there is no effect from the residual surfactant localised in the mesoporous regions of the extracted sample. The leaching from the carboxylic acid functionalised support shows no positive effect upon the retention of protein when compared to unfunctionalised SBA-15. The leaching from the thiol functionalised material is significantly lower than the other materials, indicating a much stronger binding effect between the protein and the support surface. By calculating the total

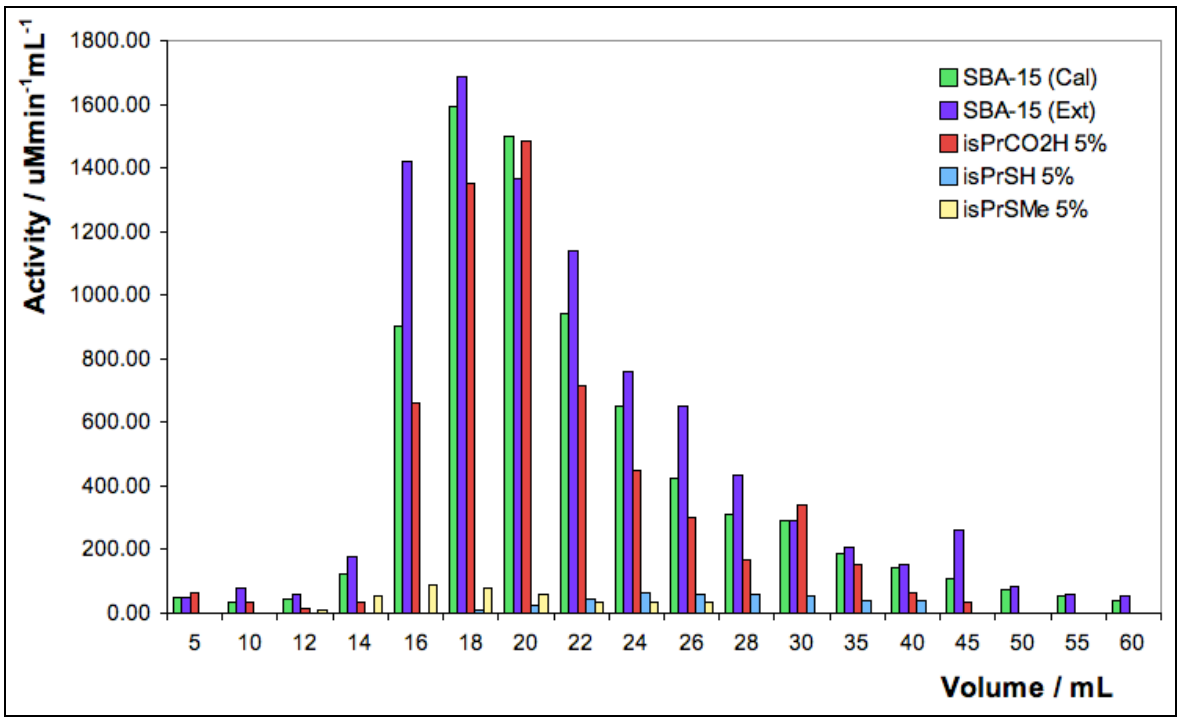

Figure 5.8: Leaching of Immobilised CALB

The investigation of leaching by a continuous flow method shows that the leaching of the enzyme is dependent upon the pH of the buffer used to wash the material. The graph below illustrates the activity of each wash aliquot. It can be seen that there is almost no leaching at pH 6, and considerably more leaching at pH 8. This correlates with the isoelectric point of CALB, which is 6.0, and indicates that the charge on the protein is important. As shown by the zeta potential analysis, it is known that the surface of the support has a net negative charge below pH 4. The protein however, will be neutral at pH 6, and have a negative charge above this pH. The leaching is likely to be due to electrostatic repulsion between the surface of the support and the protein.

5.5 Binding in Thiol Functionalised Supports

5.5.1 Potential Disulfide Bond Formation

The leaching of enzyme from the support at pH 8 is significantly reduced by the incorporation of thiol groups into the material. This could be due to interaction of cysteine residues on the surface of the protein with the free thiols on the surface of the support, resulting in the formation of disulfide bonds. As the six cysteine residues in CALB are

bridged disulfides, the formation of a disulfide between the enzyme and the support would be an exchange reaction, rather than oxidation of two free thiols. This is illustrated below (figure 5.9). Alternatively, the effect could be due to increased van der Waals bonding between the protein and the support.

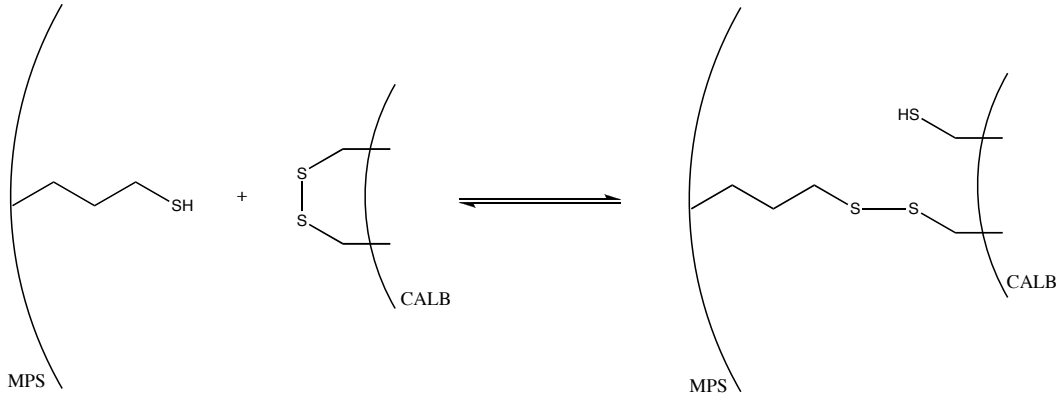

Figure 5.9: Possible Formation of a Disulfide Bond Between Support and CALB

5.5.2 Methylation of Free Thiols

isPrSMe-SBA-15 was synthesised (see section 3.3.3) to investigate the nature of the binding in the thiol functionalised materials, which show good activity and robust binding properties. A thioether is incapable of forming a disulfide bond via oxidation of two free thiol groups, as with a free thiol groups.

5.5.2.1 Immobilisation with isPrSMe-SBA-15 (5%)

The adsorption of CALB at 10 mgg^{-1} with isPrSMe-SBA-15 (5%) is very similar to isPrSH-SBA-15 (5%), with complete uptake after 12 hours (table 5.15). As with the free thiol functionalised material, there is no leaching observed with the pH 7.2 wash.

Table 5.15: Adsorption of CALB by isPrSMe-SBA-15 (5%)

Support	Temp. / °C	Time / h	Immobilised / %	Loading / mg g^{-1}	Wash Act. / mg mL^{-1} (%)
isPrSMe-SBA-15 (5%)	4	5	99.2	9.9	-
isPrSMe-SBA-15 (5%)	4	12	100	10	0 (0%)
isPrSH-SBA-15 (5%)	4	12	100	10	0 (0%)

5.5.2.2 Leaching of CALB from Column Packed Support

The binding properties of CALB on the thioether functionalised sample were investigated as described above (section 5.4.2), by packing of isPrSMe-SBA-15 (5%) supported CALB (0.25 g, 10 mg g^{-1}) within an Omnifit column. The leaching was measured by elution with pH 6 buffer (0 - 10 mL, phosphate, 50 mM), followed by pH 8 buffer (10 - 50 mL, phosphate, 50 mM). The activity was then measured by *p*-NPB hydrolysis, and the activity of these washes are plotted below (figure 5.10).

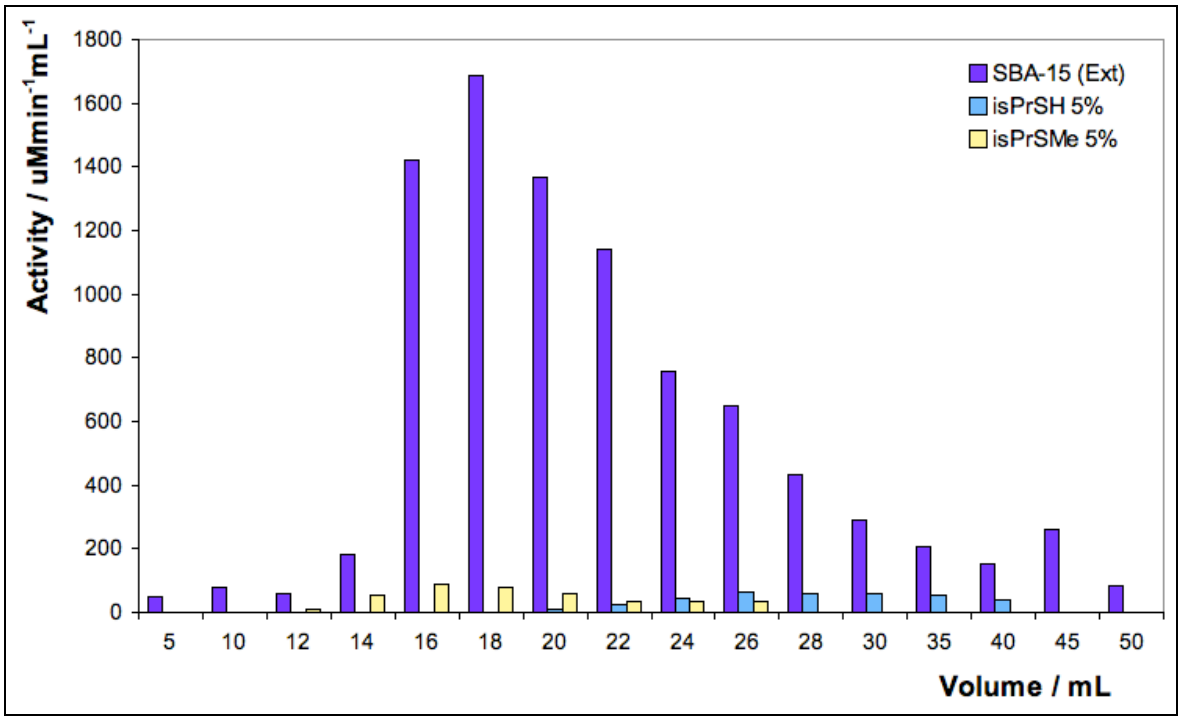

Figure 5.10: Leaching of CALB From Column Packed Supports

It is clear that the thioether has a large effect on the binding of CALB, with a dramatic reduction of the amount of CALB leached at pH 8 when compared to the unfunctionalised materials. The behaviour of this sample is very similar to that of the free thiol functionalised samples, with good uptake and low leaching at pH 8.

5.5.3 CALB Binding in Thiol Functionalised Supports

The incorporation of sulfur containing functional groups dramatically improves the support properties of mesoporous silicas when compared to unfunctionalised materials.

The nature of this binding can either disulfide bond formation, disulfide exchange or van der Wall's bonding. From the data it appears that if a disulfide bond is formed, then it must be reversible, as an irreversible disulfide bond would not show any leaching at pH 8 versus pH 6. Also, the fact that high loading is possible (section 5.3.7.4), albeit at a slower rate of uptake than with unfunctionalised materials, indicates that the enzyme is not binding irreversibly at the entrances to the pore system and blocking access to the internal pore system.

The leaching of CALB at pH 8 for the thioether functionalised support is greatly reduced when compared to the unfunctionalised support, but very similar to the leaching from the thiol functionalised supports. This indicates that if there is any disulfide formation, then it is not essential to the observed properties, which are more likely to be due to increased van der Waals bonding between the enzyme and support.

Any disruption of the cysteine bridges of the enzyme is likely to reduce the stability of the enzyme (from deactivation by unfolding) and may reduce the activity of the enzyme (from deformation of the active site). This is not the case, as thermal stability experiments (section 6.2.6) show a stability enhancement when the material is functionalised with thiol groups. The activity is also not diminished, as shown in section 6.3.3. For other enzymes that have non-bridged cysteine residues on the surface of the protein however, binding via oxidation to disulfide bonds is a reasonable binding mechanism.

5.6 Expanded Pore Mesoporous Silica Supports

5.6.1 Unfunctionalised Expanded Pore SBA-15

The immobilisation of CALB on expanded pore SBA-15 was investigated, and the results are tabulated below (table 5.16). The uptake is very rapid, with complete immobilisation at 50 mg g^{-1} after 12 hours. This is much faster than standard SBA-15, which requires 72 hours to adsorb 97.3% at 50 mg g^{-1}.

Table 5.16: Expanded Pore SBA-15

Support	Temp. / °C	Time / h	Enz. Available / mg g^{-1}	Immobilised / %	Loading / mg g^{-1}
0.4TMB-SBA-15 (Cal)	4	12	10	100	10

0.4TMB-SBA-15 (Cal)	37	12	25	100	25
0.4TMB-SBA-15 (Cal)	37	12	50	100	50

5.6.2 Thiol Functionalised Expanded Pore SBA-15

The adsorption of CALB by thiol functionalised expanded pore SBA-15 was measured (table 5.17). The uptake is much more rapid than for the non-expanded material, with almost complete adsorption after 12 hours at 50 mg g^{-1}. The uptake of CALB for non-expanded isPrSH-SBA-15 (5%) at the same loading is 64.5% after 72 hours, a much slower rate of uptake than for the expanded pore material. The increased rate of uptake with the expanded pore materials is likely due to either faster diffusion of enzyme through the material, or a pore diameter of sufficient size to allow access to the internal pore when an enzyme is bound near the entrance to the pore.

Table 5.17: Expanded Pore isPrSH-SBA-15

Support	Temp. / °C	Time / h	Enz. Available / mg g^{-1}	Immobilised / %	Loading / mg g^{-1}
0.4TMB-isPrSH-SBA-15 (5%)	4	12	10	100	10.0
0.4TMB-isPrSH-SBA-15 (5%)	37	12	25	99.8	24.9
0.4TMB-isPrSH-SBA-15 (5%)	37	12	50	99.4	49.7

5.7 Conclusion

The mesoporous materials described above provide good support materials for the immobilisation of CALB, with rapid uptake of enzyme and high capacities. The enzyme is immobilised within the pore system, rather than on the surface, as shown low uptake of enzyme by unextracted materials and low nitrogen adsorption by immobilised samples.

The immobilisation of CALB on calcined and functionalised materials is very similar, although uptake by amine functionalised materials is poor, and the enzyme is readily washed from the material with pH 7.2 buffer. No differences in the uptake of enzyme by thiol functionalised materials prepared by co-condensation and post-synthesis grafting were observed.

Once adsorbed, the enzyme does not leach readily from most samples, and shows high affinity for samples with thiol functionality incorporated into the structure. However, leaching is a significant problem as the pH of the buffer is removed from the isoelectric point of the protein. This leaching is significantly reduced by the incorporation of sulfur containing groups, which appear to stabilise the protein via van der Waals bonding. The proposed mechanism of enzyme immobilisation has two stages, fast initial binding followed by slower diffusion of enzyme through the pore system. For the thiol functionalised materials which bind the enzyme strongly, the rate of diffusion of enzyme is reduced, resulting in slower uptake at high loading.

The rate of uptake for high loading of CALB can be improved by expansion of the pore size of the mesoporous material, with good uptake and high capacities for the 0.4 TMB materials, both unfunctionalised and with incorporated thiol groups.

References

[1] P. Atkins and J. De Paula, *Atkins' Physical Chemistry*, Oxford University Press, Oxford, 8th Edition, 2006.
[2] G. Ping, J. M. Yuan, M. Vallieres, H. Dong, Z. Sun, Y. Wei, F. Y. Li and S. H. Lin, *J. Chem. Phys.*, 2003, **118**, 8042.
[3] G. Ping, J. M. Yuan, Z. F. Sun and Y. Wei, *J. Mol. Recognit.*, 2004, **17**, 433.
[4] R. Ravindra, Z. Shuang, H. Gies and R. Winter, *J. Am. Chem. Soc.*, 2004, **126**, 12224.

6. Catalysis with Immobilised CALB

6.1 Introduction

Enzymes are highly selective catalysts that operate under very mild conditions when compared to transition metal catalysts.[1] However, the stability of enzymes for catalysis is less than ideal, and purification of the product can be complicated by decomposition and subsequent contamination, especially with proteases.[2] Immobilisation of an enzyme will typically increase the stability of the enzyme, often at the cost of reducing the catalytic rate in aqueous systems.[3] This is offset by numerous advantages to immobilisation including increased stability, easier recovery, facile handling and simplified purification of the product.[4]

The aim of this section is to determine the activity of CALB immobilised within SBA-15, and to investigate the potential applications of mesoporous supported CALB for aqueous and organic catalysis. The sample activity is related to the wash pH to investigate the binding between the enzyme and support for aqueous applications. As part of this study, the effect of the pH on the leaching behaviour of the enzyme under aqueous conditions has been determined and related to the surface chemistry of the enzyme.

6.2 Aqueous Catalysis

6.2.1 Introduction

The hydrolysis of tributyrin (figure 6.1) was selected as a model reaction to measure the activity and stability of CALB in aqueous conditions. Tributyrin is immiscible with water, and the free enzyme hydrolyses the triglyceride on the interface between tributyrin and water.

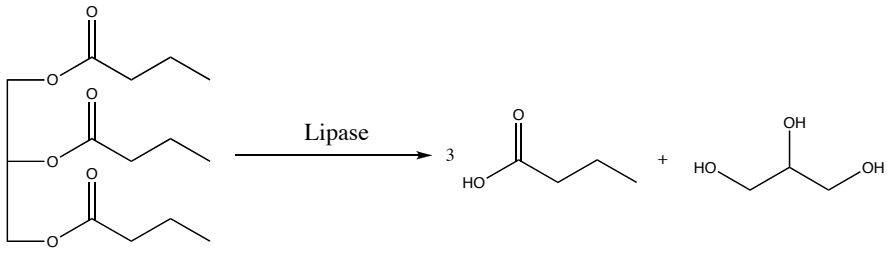

Figure 6.1: Tributyrin Hydrolysis

The rate of tributyrin hydrolysis was followed by measuring the amount of sodium hydroxide required to maintain a constant pH. The rate of tributyrin formation was then calculated from the rate of sodium hydroxide addition. There is a lag phase between 0 - 300 seconds (due to the formation of an emulsion between tributyrin and buffer), and so the rate was calculated from the addition of sodium hydroxide between 600 - 900 seconds. The trace below (figure 6.2) was measured for a sample of CALB immobilised on calcined SBA-15 at a loading of 10 mg g^{-1}, using a Mettler-Toledo DL-21 autotitrator at 25 °C.

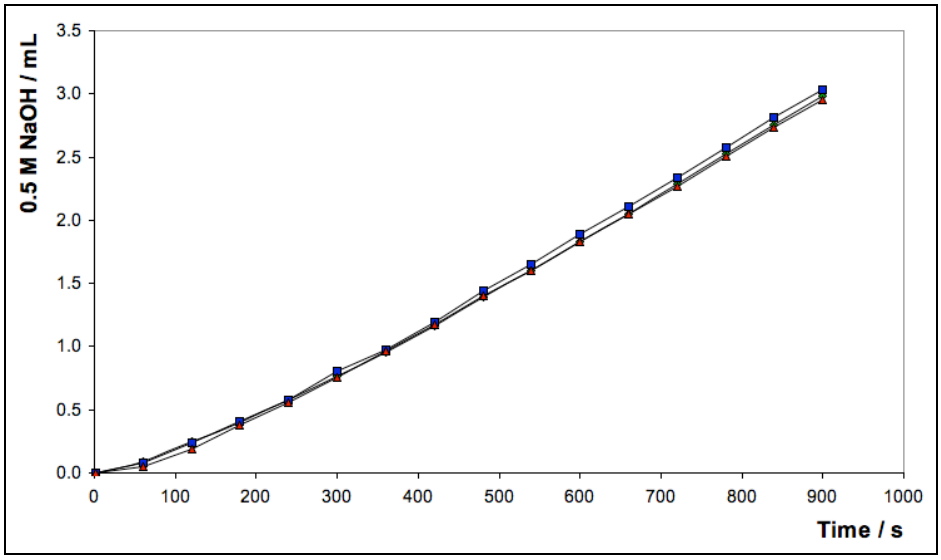

Figure 6.2: Sodium Hydroxide Addition During Tributyrin Hydrolysis

6.2.1 Conditions

The autotitration activity was measured as described in section 4.5. In a typical measurement 100 mg support was suspended in 25 mL buffer, at a pH below that of the static measurement pH (STAT), which was then pre-titrated to the appropriate measurement pH. This avoids errors from additional sodium hydroxide addition due to a starting pH above the STAT pH. For measurement at pH 8, a buffered solution of pH 7.2 (phosphate, 10 mM) was used. For measurement at pH 6 and 7, buffered solutions of pH 5.5 and 6.5 were used (phosphate, 10 mM). The solution was pre-titrated to the appropriate assay pH (static, or STAT pH), then the reaction was initiated by the addition of tributyrin (5 mL (5.16 g), 0.0171 mol). This was repeated three times for each sample and the average rate and standard deviation calculated.

6.2.2 Free Enzyme Activity

To measure activity of the free enzyme for the hydrolysis of tributyrin 25 μL of Novozyme Chirazyme L2 (10 mg mL^{-1}) replaced the solid support in the experimental conditions above (6.2.1), the rate of hydrolysis was measured by autotitration and the results are tabulated below (table 6.1). The enzyme is most active at pH 8, with reduced activity at pH 6 and 7. The activity of immobilised CALB in the subsequent sections was measured primarily at pH 8, with most support materials also measured at pH 6 (section 6.2.6).

Table 6.1: Activity of CALB for the Hydrolysis of Tributyrin

STAT pH	Buffer (10 mM) / mL	Tributyrin / mL	Temperature / °C	Rate / μmol min^{-1} mg^{-1}
6.0	25	5	25	378 ± 8
7.0	25	5	25	406 ± 11
8.0	25	5	25	478 ± 6

6.2.3 Unfunctionalised SBA-15

6.2.3.1 Calcined SBA-15

The activity of CALB immobilised upon calcined SBA-15 is tabulated below (table 6.2). The activity is very high when the support is washed at pH 6, and greatly reduced as the pH of the wash is increased. This supports the results of the leaching study in section 5.4.2, in which the enzyme leaching was observed to increase significantly at pH 8. The results below are due to two effects, firstly, when the sample was washed at pH 6 less enzyme was washed from the material than at pH 8. Secondly, there is expected to be some degree of leaching at an assay pH of 8 (STAT pH), as the enzyme is observed to leach at pH 8 (section 5.4.2), this increases the observed rate as the free enzyme is not subject to diffusion rate limiting effects. The activity of the free enzyme at this pH and at the same concentration is 4780 μmol min^{-1}, therefore the immobilised CALB after washing at pH 8.0 shows 12.6% of the activity of the free enzyme.

Table 6.2: Activity of CALB Supported on Calcined SBA-15

Support	Loading / mg g^{-1}	Wash pH	STAT pH	Rate / µmol min^{-1} g^{-1}
SBA-15 (Cal)	10.0	6.0	8.0	2653 ± 190
SBA-15 (Cal)	10.0	7.2	8.0	1139 ± 13
SBA-15 (Cal)	10.0	8.0	8.0	607 ± 16

6.2.3.2 Comparison of SBA-15 Extraction Methods

The uptake of CALB was observed to be very similar for both extracted and calcined SBA-15 (section 5.2.3), as were the leaching properties (section 5.4.2). The rates of tributyrin hydrolysis for each sample, and rehydrated calcined SBA-15, with washing at pH 6 and pH 8 are tabulated below (table 6.3).

The observed rate is very high when the materials are washed at pH 6, and much lower when washed at pH 8, indicating that a considerable amount of enzyme is washed from the supports at pH 8. The catalytic rate for each sample is very similar, indicating that the residual surfactant in the extracted material neither hinders nor enhances the rate of the reaction, and the binding properties of the enzyme are similar for all materials. The column leaching study showed that the leaching for the extracted and the calcined material share very similar leaching properties, and the surface of the calcined material is expected to be partially hydrolysed during the immobilisation step.

Table 6.3: Activity of CALB Supported on Extracted SBA-15

Support	Loading / mg g^{-1}	Wash pH	STAT pH	Rate / µmol min^{-1} g^{-1}
SBA-15 (Cal)	10.0	6.0	8.0	2653 ± 190
SBA-15 (Cal)	10.0	8.0	8.0	607 ± 16
SBA-15 (Ext)	10.0	6.0	8.0	2822 ± 24
SBA-15 (Ext)	10.0	8.0	8.0	684 ± 42
SBA-15 (Rhd)	10.0	6.0	8.0	2742 ± 87
SBA-15 (Rhd)	10.0	8.0	8.0	622 ± 49

6.2.4 Functionalised Materials

As discussed above, there is a considerable degree of CALB leaching from the support at pH 8, both during washing and during tributyrin hydrolysis. This increases the observed rate for samples in which the enzyme is not bound strongly. In a sample with strong binding between the enzyme and the support the observed rate is expected to be similar for washing at any pH, as the enzyme will not be washed from the support at pH 8 during the assay, as observed for unfunctionalised SBA-15.

6.2.4.1 isPrCO$_2$H-SBA-15

The activity of isPrCO$_2$H-SBA-15 was measured by tributyrin hydrolysis, and the results are tabulated below (table 6.4). The activity is significantly reduced as the pH of the wash is increased from 6.0 to 8.0, indicating that the enzyme is washed from the material and is not strongly bound to the surface. The degree of activity at each wash pH is very similar to the results above for the unfunctionalised materials, indicating that there is no advantage for CALB binding to incorporate carboxylic acid groups into the material.

Table 6.4: Activity of CALB Supported on isPrCO$_2$H-SBA-15

Support	Loading / mg g^{-1}	Wash pH	STAT pH	Rate / μmol min^{-1} g^{-1}
isPrCO$_2$H (5%)	9.8	6.0	8.0	2494 ± 102
isPrCO$_2$H (5%)	9.7	7.2	8.0	1369 ± 67
isPrCO$_2$H (5%)	10.0	8.0	8.0	855 ± 14

6.2.4.2 isPh-SBA-15

The hydrolysis of tributyrin was measured with isPh-SBA-15, and the results are tabulated below (table 6.5). The activity is very similar for the samples washed at pH 6 when compared to the samples washed at pH 8. The large decrease in rate observed with previous samples, due to leaching during the assay is not observed for these materials, indicating a stronger binding between the support and the enzyme. The initial rate for the samples washed at pH 6.0 is low when compared to the unfunctionalised supports due to much lower leaching of the enzyme during the pH 8.0 assay. As the free enzyme is more active than the bound enzyme, any enzyme leaching will significantly increase the observed rate.

Table 6.5: Activity of CALB Supported on isPh-SBA-15

Support	Loading / mg g^{-1}	Wash pH	STAT pH	Rate / µmol min^{-1} g^{-1}
isPh (5%)	9.9	6.0	8.0	938 ± 31
isPh (5%)	9.8	8.0	8.0	866 ± 98

6.2.4.3 Amine Functionalised SBA-15

The tributyrin hydrolysis with the amine functionalised materials, which show low uptake of enzyme and relatively high leaching of enzyme during the post-immobilisation wash (section 5.3.4), was investigated and the results are tabulated below (table 6.6). The activity is generally low, especially when the material is washed at pH 8.0, indicating that the enzyme is not bound and is readily removed from the support. This is likely due to repulsion between the amine groups, which will abstract a proton from the surface to form ammonium ions, and localised regions of the enzyme with a positive charge. The activity measured for the sample washed at pH 6.0 is low, indicating that some of the enzyme immobilised was removed during the washing step.

Table 6.6: Activity of CALB Supported on isPrNH_2-SBA-15

Support	Loading / mg g^{-1}	Wash pH	STAT pH	Rate / µmol min^{-1} g^{-1}
isPrNH_2 (5%)	4.9	6.0	8.0	371 ± 40
isPrNH_2 (5%)	4.9	7.2	8.0	94 ± 24
isPrNH_2 (5%)	4.9	8.0	8.0	115 ± 16
psPrNH_2	4.1	8.0	8.0	191 ± 12

6.2.4.4 isC_3H_5-SBA-15

The tributyrin hydrolysis for CALB supported on allyl-functionalised SBA-15 is tabulated below (table 6.7). There is a considerable change in activity as the wash pH is changed, with more enzyme leaching from the material at higher pH. The activity of the material when washed at pH 6 is much lower than for the unfunctionalised material, due to less leaching during the assay, indicating weak binding between the enzyme and the support.

Table 6.7: Activity of CALB Supported on isC_3H_5-SBA-15

Support	Loading / mg g^{-1}	Wash pH	STAT pH	Rate / µmol min^{-1} g^{-1}
isC_3H_5 (5%)	8.5	6.0	8.0	1472 ± 15
isC_3H_5 (5%)	8.5	7.2	8.0	993 ± 34
isC_3H_5 (5%)	8.5	8.0	8.0	731 ± 27

6.2.4.5 isPrSH-SBA-15

The activity of the in-situ thiol functionalised samples are tabulated below (table 6.8). The activity of the unextracted sample is very low, indicating that any enzyme bound to the surface during the immobilisation step is removed from the material during the pH 7.2 wash. The activity of the sample washed at pH 6.0 is not elevated relative to the other samples, as observed with the unfunctionalised materials above (section 6.2.3.2), indicating that the enzyme is not leached significantly during the assay at pH 8. However, the activity is reduced when the material is washed at pH 8, indicating some leaching of the enzyme from the support at this pH. However, this leaching is significantly lower than observed for unfunctionalised and carboxy-functionalised SBA-15.

Table 6.8: Activity of CALB Supported on Thiol Functionalised Materials

Support	Loading / mg g^{-1}	Wash pH	STAT pH	Rate / µmol min^{-1} g^{-1}
isPrSH (5%) Unextracted	2.4	7.2	8.0	24*
isPrSH (2%)	9.8	7.2	8.0	1432 ± 152
isPrSH (5%)	10.0	6.0	8.0	1138 ± 46
isPrSH (5%)	10.0	7.2	8.0	1139 ± 67
isPrSH (5%)	10.0	8.0	8.0	936 ± 66
isPrSH (7%)	9.9	7.2	8.0	1311 ± 167

*Only 1 sample measured

6.2.4.6 psPrSH-SBA-15

The rates of tributyrin hydrolysis for CALB immobilised within psPrSH-SBA-15 are tabulated below (table 6.9). The rate of reaction is very similar to that of the thiol materials discussed previously, with comparable rates for pH 6 and 7 washing, and a similar reduced rate for the samples washed at pH 8. The observed rate of hydrolysis for

the samples washed at pH 6 and 7.2 is not elevated as with the unfunctionalised materials, indicating the enzyme is not significantly desorbed from the support during the assay. The identical rates of reaction for this material and isPrSH-SBA-15 supported CALB is strong evidence that the residual surfactant present in the co-condensed samples does not reduce or enhance the rate of tributyrin hydrolysis.

Table 6.9: Activity of CALB Supported on psPrSH-SBA-15

Support	Loading / mg g^{-1}	Wash pH	STAT pH	Rate / µmol min^{-1} g^{-1}
psPrSH (HL)	10.0	6.0	8.0	1044 ±79
psPrSH (HL)	9.9	7.2	8.0	1105 ± 30
psPrSH (HL)	9.8	8.0	8.0	897 ± 54

6.2.4.7 isPrSMe-SBA-15

The thioether functionalised SBA-15 shows very similar properties to the free thiol functionalised materials (section 5.5) in both uptake of CALB and leaching of CALB from the support. The tributyrin hydrolysis was measured and the reaction rates are tabulated below (table 6.10). The rate of tributyrin hydrolysis after washing at pH 6.0 is very similar to the rate of reaction observed for the thiol supports above(section 6.2.4.5). The rate of hydrolysis for the sample washed at pH 8.0 is close to the rate of hydrolysis for isPrSH-SBA-15 washed at pH 8.0. This supports the conclusions of the previous section, that the nature of the binding in both materials is very similar, and the enzyme is bound via van der Waals interactions rather than disulfide formation.

Table 6.10: Activity of CALB Supported on isPrSMe-SBA-15

Support	Loading / mg g^{-1}	Wash pH	STAT pH	Rate / µmol min^{-1} g^{-1}
isPrSH (5%)	10	8.0	8.0	936 ± 66
isPrSMe (5%)	10	6.0	8.0	1314 ± 94
isPrSMe (5%)	10	8.0	8.0	895 ± 59

6.2.4.8 isPrSH/isPh-SBA-15

The rate of tributyrin hydrolysis was measured with CALB supported on the mixed functionality support isPrSH/isPh-SBA-15 (2% / 4%) (table 6.11). The activity is very

similar to the rate of reaction obtained with the thiol materials above, with a reduction in activity after pH 8.0 washing due to leaching of enzyme from the material.

Table 6.11: Activity of CALB Supported on isPrSH/isPh-SBA-15 (2%/4%)

Support	Loading / mg g^{-1}	Wash pH	STAT pH	Rate / μmol min^{-1} g^{-1}
isPrSH/isPh	9.7	7.2	8.0	1171 ± 129
isPrSH/isPh	9.8	8.0	8.0	799 ± 76

6.2.4.9 Expanded Pore Supports

The activities of CALB supported on the expanded pore supports are shown below (table 6.12). The 0.4TMB-SBA-15 sample shows very high activity when washed at pH 6.0 and assayed at pH 8, indicating a significant amount of enzyme is leached from the support at pH 8. This is substantiated by the low activity when the material is washed at pH 8.0 prior to activity measurement. The activity after washing at pH 8.0 is lower than observed for calcined SBA-15 under the same conditions, indicating more enzyme is removed from the material during the washing. The thiol functionalised material shows slightly lower activity than the unexpanded thiol functionalised supports.

Table 6.12: Activity of CALB Supported on Expanded Pore Supports

Support	Loading / mg g^{-1}	Wash pH	STAT pH	Rate / μmol min^{-1} g^{-1}
0.4TMB-SBA-15	10	6.0	8.0	2424 ± 231
0.4TMB-SBA-15	10	8.0	8.0	412 ± 6
0.4TMB-isPrSH (5%)	10	6.0	8.0	943 ± 82
0.4TMB-isPrSH (5%)	10	8.0	8.0	723 ±19

6.2.5 Activity of Immobilised CALB at STAT pH 6

To investigate the activity of immobilised CALB without the potential leaching during the assay, the rate of tributyrin hydrolysis was measured at pH 6, these results are tabulated below (table 6.13). The activities of the expanded pore supports are lower than the equivalent unexpanded material, indicating a slower rate of tributyrin diffusion with these materials. The activities for the carboxy and allyl functionalised supports, which showed significant leaching during the assay at STAT pH 8.0, are higher than for the other

samples. It is possible this is due to some leaching during the assay, which is not observed in aqueous systems, but may occur in an emulsion, as the enzyme typically operates on the interface between an oil and water. However, this is not observed for calcined SBA-15, which does not have an elevated rate of hydrolysis.

Table 6.13: Activity of immobilised CALB at STAT pH 6

Support	Loading / mg g^{-1}	Wash pH	STAT pH	Rate / μmol min^{-1} g^{-1}
Free CALB (10 mg)	-	6.0	6.0	3784 ± 82
SBA-15 (Cal)	10.0	6.0	6.0	904 ± 67
isPrCO_2H (5%)	10.0	6.0	6.0	1638 ± 212
isPh (5%)	9.9	6.0	6.0	848 ± 43
isC_3H_5 (5%)	9.8	6.0	6.0	1585 ±132
isPrSH (2%)	9.9	6.0	6.0	1174 ± 92
isPrSH (5%)	10.0	6.0	6.0	735 ± 63
isPrSH (7%)	10.0	6.0	6.0	973 ± 24
psPrSH (Rf)	10.0	6.0	6.0	1150 ± 132
isPrSMe (5%)	10.0	6.0	6.0	660 ± 39
isPrSH/isPh (2/4%)	9.7	6.0	6.0	638 ± 19
0.4TMB-SBA-15	10.0	6.0	6.0	472 ± 12
0.4TMB-isPrSH (5%)	10.0	6.0	6.0	719 ± 54

6.2.6 Thermal Stability

The thermal stability of the immobilised CALB was studied by suspending the immobilised enzyme in buffer (5 mL, phosphate, pH 5.5, 10 mM) and heating at 60 °C. Each sample was removed after a predetermined time and the rate of tributyrin hydrolysis was measured at pH 6 as described previously. The activity with time is plotted below (figure 6.3). The free enzyme shows a significant loss of activity after heating at two hours at 60 °C, with only 5% of the initial activity remaining. This is most likely to be due to thermally induced unfolding of the enzyme.

The stability is improved by immobilisation within SBA-15 (calcined), with 49% of the initial activity retained after 2 hours. This is likely to be a confinement effect when compared to the free enzyme,[5, 6] coupled with some interaction with the surface, resulting in hindered unfolding at elevated temperatures and resulting in a greater retention of

activity. This conclusion is supported by the expanded pore material, 0.4TMB-SBA-15 (calcined), which only retains 21% activity after 2 hours, as the enzyme is not as confined within the larger pores, and the unfolding of the enzyme is less hindered.

The two thiol functionalised samples show excellent retention of activity, with 83% residual activity for the isPrSH-SBA-15 (5%) supported CALB after 8 hours, and no loss of activity observed for the expanded pore 0.4TMB-isPrSH-SBA-15 (5%). This is further evidence for strong bonding between the support and the enzyme, which greatly reduces unfolding at high temperatures. This surface binding effect seems to be more important for enhancement of stability than the confinement effect, as the retention of activity is significantly different for 0.4TMB-SBA-15 and 0.4TMB-isPrSH-SBA-15 (5%).

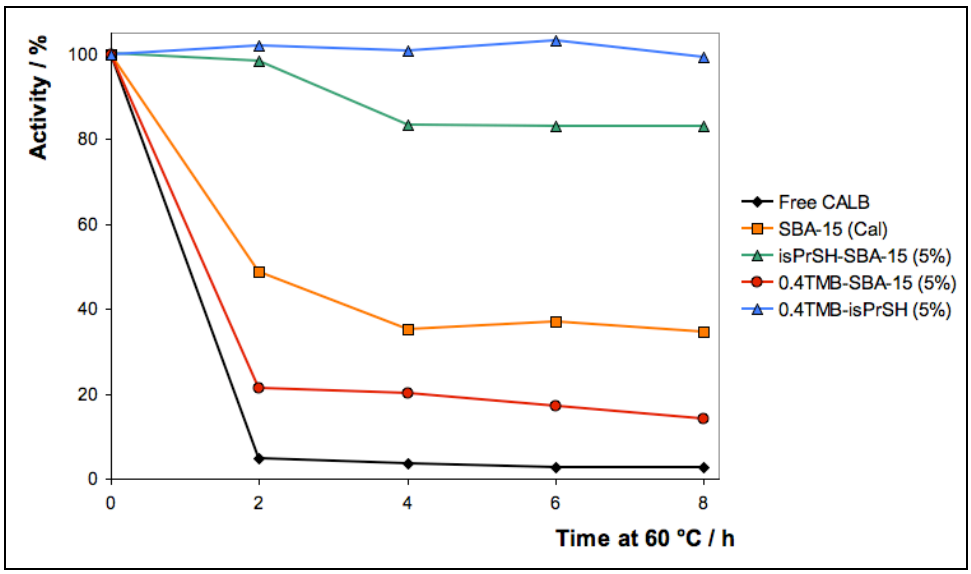

Figure 6.3: Thermal Stability of Immobilised CALB

6.2.7 Reusability

The activity of subsequent re-uses of immobilised CALB supported on SBA-15 (Calcined) and isPrSH-SBA-15 (5%) at a loading of 10 mg g^{-1} are plotted below (figure 6.4). The samples were recovered by filtration after each use, and to remove unreacted tributyrin, which is sparingly soluble in water, washed with propan-1-ol (3 x 5 mL) and phosphate buffer (3 x 10 mL) alternately. In a previous experiment samples washed with acetone to remove excess tributyrin showed complete loss of activity. The unfunctionalised material shows a large activity decrease between each use, which supports the conclusion

above that the activity of CALB on calcined SBA-15 measured above is largely due to free enzyme (section 6.2.3.1). The thiol functionalised material shows some loss of activity, but this is greatly reduced compared to the unfunctionalised material, indicating the enzyme is bound and does not leach significantly during the reaction.

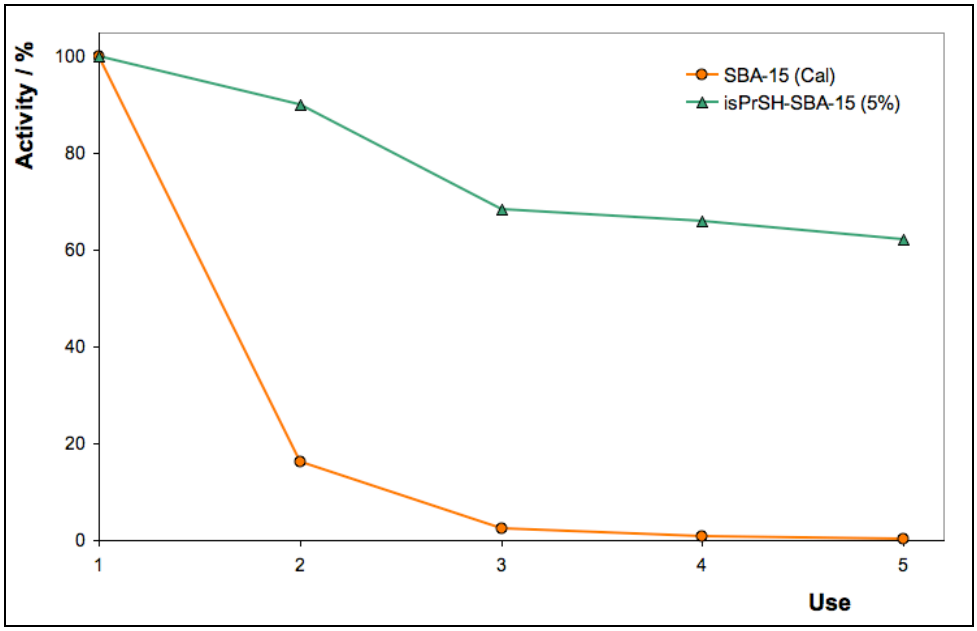

Figure 6.5: Reusability of Immobilised CALB at pH 8.0

6.3 Organic Catalysis

6.3.1 Introduction

Typically, the solubility of enzymes in organic solvents is very low. Enzymes will aggregate and precipitate in organic solvents, greatly reducing their catalytic properties. Practically, this eliminates the problem of leaching of enzyme from support once the immobilised enzyme is transferred into organic media. To transfer the sample to an organic solvent the sample was first washed with propan-1-ol, to remove residual water from the material without deactivation of the enzyme, followed by washing with the organic solvent used in the reaction.

The activity of CALB immobilised within mesoporous supports was compared to the activity of the free enzyme by transesterification of (R)-1-phenylethanol (figure 6.6). The enzyme is selective for the acylation of (R)-1-phenylethanol from a racemic mixture

of 1-phenylethanol, and the reaction conversion is reported as a proportion of the racemic mixture, with a maximum yield of 50%.

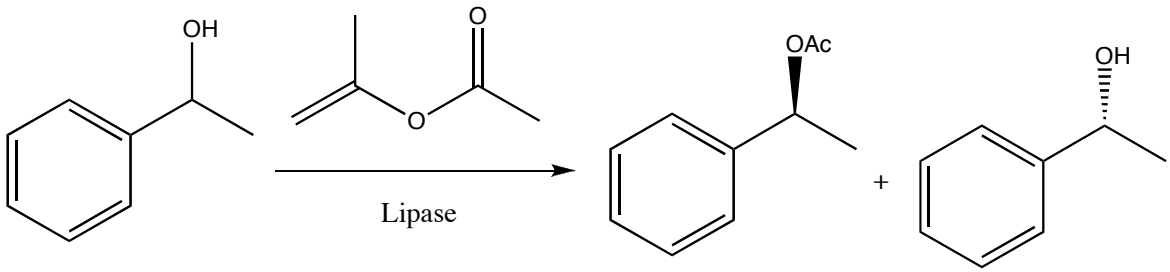

Figure 6.6: Transesterification of (R)-1-Phenylethanol

6.3.2 Conditions

To prepare a sample for transesterification, the support (100 mg) was dispersed in pH 6 buffer (3.9 mL, phosphate, 50 mM) to which the enzyme solution was added (100 μL, 10 mg mL^{-1}, Chirazyme L2). The immobilisation is monitored as previously described (section 5.2.1). The sample was then washed with pH 6 buffer (2 x 5 mL, phosphate, 50 mM) followed by propan-1-ol (2 x 5 mL), then finally with methyl tertiary-butyl ether (MTBE) (2 x 5 mL). The substrate mixture was then added (5 mL MTBE, see section 4.6.3) and the reaction followed by GC.

6.3.3 CALB / SBA-15 Transesterification

The conversion of (R)-1-phenylthanol to (R)-1-phenylethyl acetate with CALB loaded at 10 mg g^{-1} within calcined SBA-15 is shown below (figure 6.7). The reaction was monitored by following the appearance of the acetate peak and the disappearance of the (R)-1-phenylethanol peak. The (S)-1-phenylethanol peak serves as an internal standard, the peak integral of which is equal to the sum of the reactive enantiomer and product peak integrals. The conversion of (S)-1-phenylethanol to (S)-1-phenylethyl acetate is not observed during the measurement period (up to 168 hours).

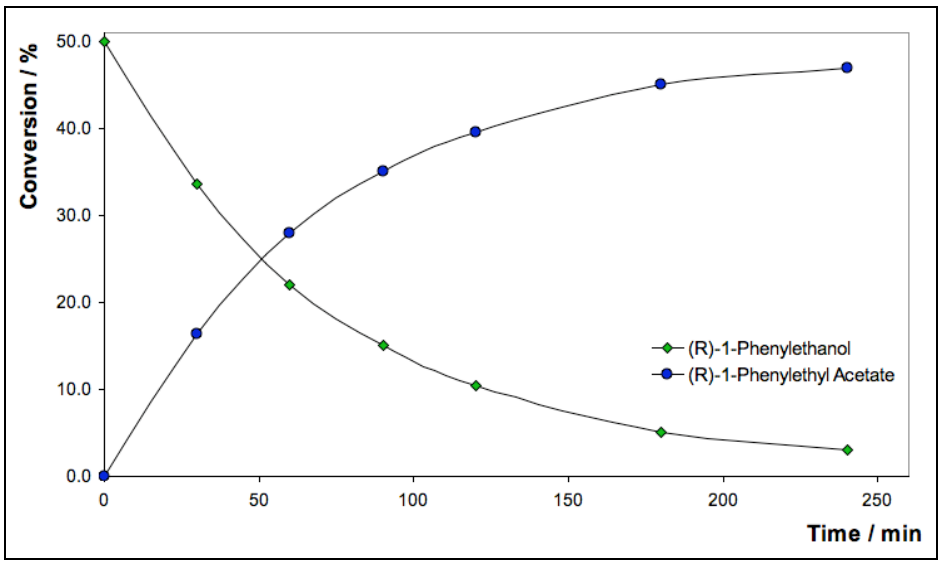

Figure 6.7: (R)-1-Phenylethanol Transesterification by CALB / Calcined SBA-15

The initial rates of the enzyme loaded within unfunctionalised supports are tabulated below (table 6.14). Calcined SBA-15 catalyses the transesterification at a rate of 69.3 μmol min^{-1} g^{-1}, about tenfold slower than the hydrolysis of tributyrin. The addition of 2% distilled water to the reaction mixture causes a significant decrease in the rate of acylation, due to an increase in the competing reverse reaction, the hydrolysis of (R)-1-phenylethyl acetate. The addition of 4A molecular sieves (1 g, dried at 120 °C) to the reaction mixture produces an observable increase in the rate of reaction, despite the drying of the substrate mixture with molecular sieves. This may be due to absorbance of any residual water within the support (from the immobilisation process) by the sieves. Ethanol-extracted SBA-15 shows a significant increase in reaction rate relative to the calcined material. This may be due to incorporation of ethoxide groups on the surface of the silica during ethanol extraction, resulting in improved interface / diffusion properties for the extracted material.

Table 6.14: Transesterification with Unfunctionalised SBA-15 Supported CALB

Support	Loading / mg g^{-1}	Time / min	(R)-1-PE / %	(R)-1-PEA / %	Initial Rate / μmol min^{-1} g^{-1}
SBA-15 (Cal)	10	30	33.3	16.6	69.3 ± 4.7
SBA-15 (Cal) + 2% H_2O	10	30	46.2	3.6	15.2
SBA-15 (Cal) + 4ÅMS	10	30	28.2	21.7	90.5
SBA-15 (Ext)	10	30	23.5	25.8	107.3 ± 9.8

The activities of CALB at higher loadings supported on calcined SBA-15 are shown below (table 6.15). The activity of the calcined SBA-15 samples are much lower than the extracted SBA-15 samples, which show good activity at higher loading. For the extracted materials at higher loading only 50 mg of sample was prepared, due to lack of material, for the other samples 100 mg was prepared.

Table 6.15: CALB at Higher Loading on Calcined SBA-15

Support	Loading / mg g^{-1}	Time / min	(R)-1-PE / %	(R)-1-PEA / %	Initial Rate / μmol min^{-1} g^{-1}
SBA-15 (Cal)	10	30	33.3	16.5	69.3 ± 2.7
SBA-15 (Cal)	25	30	16.3	33.8	140.9
SBA-15 (Cal)	50	30	8.9	41.1	171.4
SBA-15 (Ext)	10.0	30	24.2	25.8	107.3 ± 9.8
SBA-15 (Ext) (50mg)	22.8	30	18.5	31.4	261.7
SBA-15 (Ext) (50mg)	42.0	30	9.5	40.5	337.5

To investigate the leaching of the enzyme from the support during the reaction the support was removed after 90 minutes, and the composition of the reaction mixture monitored by GC (figure 6.8). There is no observed transesterification without the solid support, indicating very low or no leaching of the enzyme during the reaction.

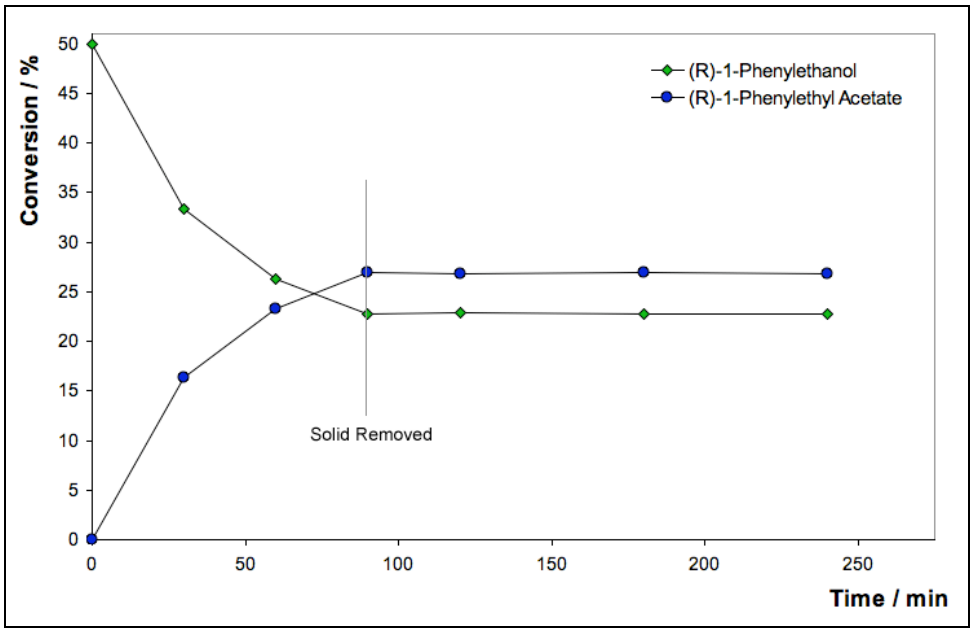

Figure 6.8: Removal of Immobilised Enzyme at 90 Minutes

6.3.4 Free Enzyme Activity

The activity of the free enzyme was investigated by measuring the activity of Chirazyme L2 and a powder dispersion of CALB (table 6.16). The powder dispersion was prepared by suspending 4 mg of CALB powder (0.15 % protein by Bradford's assay) in the substrate mixture (1 mL), and mixing with a Gallenkamp Spinmix. Both samples show very low activity, especially for the Chirazyme sample, which is a liquid preparation and so has low activity due to the high water content (2% by volume). For comparison with the immobilised CALB rates, the initial rate of 10 mg Chirazyme L2 was 1.6 μmol min^{-1} mg^{-1}, and for the powder dispersion the initial rate was 6.1 μmol min^{-1} mg^{-1}. This is 10% of the activity for immobilised CALB supported on calcined SBA-15, and 6% of the activity for immobilised CALB supported on extracted SBA-15. This is due to aggregation of the free enzyme reducing the available enzyme for catalysis. This does not occur for the immobilised enzyme, which has low mobility and does not aggregate.

Table 6.16: Transesterification Activity of Free Enzyme

Support	Enzyme / mg	Time / min	(R)-1-PE / %	(R)-1-PEA / %	Initial Rate / μmol min^{-1} mg^{-1}
Chirazyme L2	1	30	49.7	0.4	0.16
CALB Powder Dispersion	0.615	30	49.1	0.9	0.61

6.3.5 Functionalised Supports

The activity of CALB at a loading of 10 mg g^{-1} was investigated for a range of functionalised supports, the results are tabulated below (table 6.17). With the exception of the amine functionalised sample, which shows low activity due to low enzyme content, the samples show higher activity than CALB supported on calcined silica. This agrees with the higher activity observed for extracted SBA-15 when compared to calcined SBA-15, and may be due to incorporated ethoxide functionalisation of the surface in extracted samples. The allyl and phenyl functionalised samples show very good activity, due to a well supported enzyme and good interface properties with the organic solvent due to the hydrophobic functional groups.

Table 6.17: Acylation by CALB Supported on Functionalised Supports

Support	Loading / mg g^{-1}	Time / min	(R)-1-PE / %	(R)-1-PEA / %	Initial Rate / μmol min^{-1} g^{-1}
isC_3H_5-SBA-15 (5%)	9.8	30	21.0	29.1	121.1 ± 6.4
is$PrCO_2H$-SBA-15 (5%)	10.0	30	25.0	24.8	103.5 ± 7.2
isPh-SBA-15 (5%)	9.8	30	18.5	31.6	131.5 ± 4.7
is$PrNH_2$-SBA-15 (2%)	1.6	28	48.4	1.6	5.9 ± 0.9

6.3.6 Thiol Functionalised Supports

The conversion of (R)-1-phenylethanol by CALB immobilised within isPrSH-SBA-15 (5%) at a loading of 10 mg g^{-1} is shown below (figure 6.9). The conversion is relatively fast, with 80% of the reactive enantiomer converted within 90 minutes, and complete conversion after 18 hours.

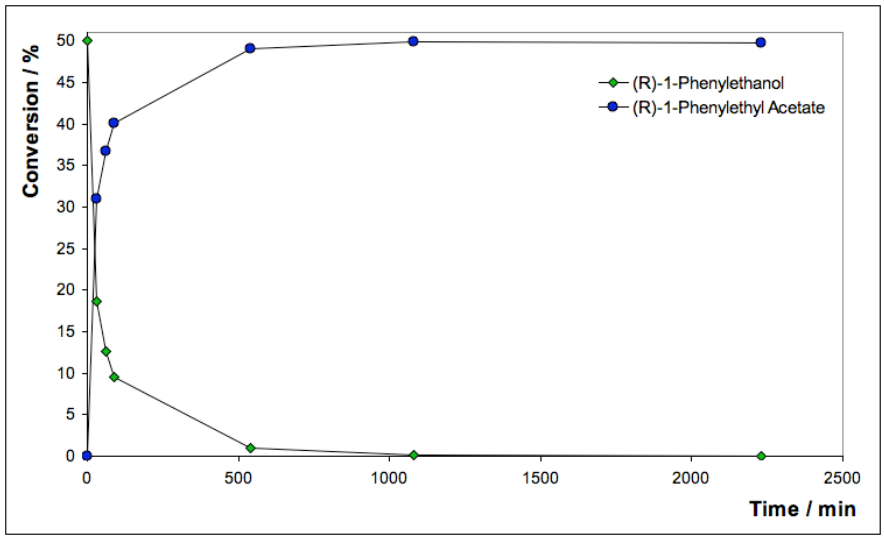

Figure 6.9: Acylation of (R)-1-PE by CALB / isPrSH-SBA-15 (5%)

The initial rates of reaction for the thiol functionalised samples are shown below (table 6.18). The activity of each sample is higher than that of CALB on calcined SBA-15 (69.3 μmol min^{-1} g^{-1}), although the rate with several supports is reduced relative to CALB supported on extracted SBA-15 (107.3 μmol min^{-1} g^{-1}). There is a considerable difference in activity between co-condensed *in-situ* samples with different thiol content. The 2% and 7% samples show reduced activity relative to that of the 5% sample. As these samples contain the same amount of enzyme, and the surface properties of each material should be similar, the morphology of the material must be critical to the rate of reaction. The 5%

sample shows both cubic and hexagonal phases, while the 2% sample is hexagonally ordered and the 7% sample is cubic phase. This indicates that the enzyme active site is more accessible in the 5% sample, possibly due to shorter pore length.

Table 6.18: Conversion of (R)-1-PE by Thiol Supported CALB

Support	Loading / mg g^{-1}	Time / min	(R)-1-PE / %	(R)-1-PEA / %	Initial Rate / µmol min^{-1} g^{-1}
isPrSH-SBA-15 (2%)	9.8	30	30.2	19.9	82.7 ± 1.9
isPrSH-SBA-15 (5%)	10.0	30	18.6	31.4	130.9 ± 4.1
isPrSH-SBA-15 (7%)	9.9	30	30.4	19.6	81.7 ± 3.1
psPrSH-SBA-15 (Rf)	10.0	30	30.5	19.4	80.6 ± 6.2
isPrSMe-SBA-15 (5%)	10.0	30	32.4	17.5	72.9 ± 3.5
isPrSH/isPh-SBA-15 (2/4%)	9.8	30	23.3	26.7	111.2 ± 7.8

To confirm the enzyme does not leach from the support during the reaction, the solid was removed after 60 minutes during the transesterification with isPrSH-SBA-15 (5%) / CALB at 10 mg g^{-1} (figure 6.10). No further conversion of (R)-1-phenylethanol was observed.

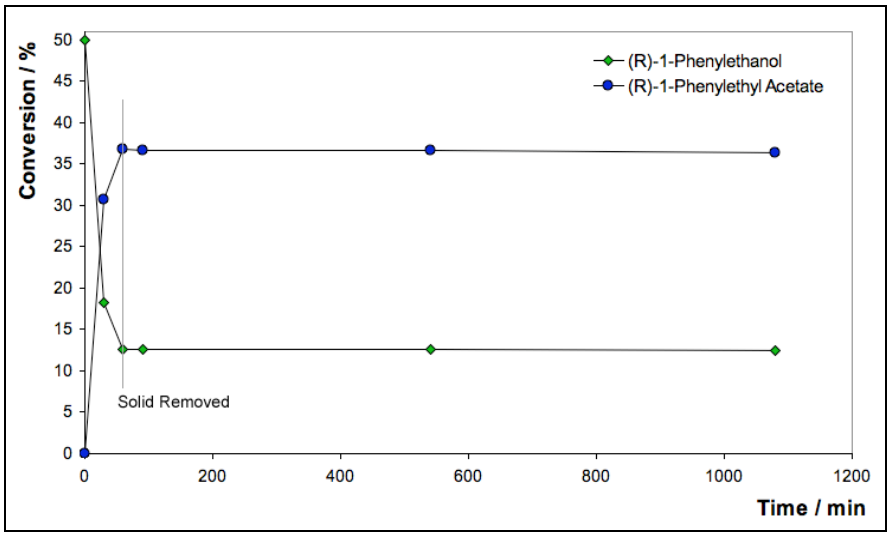

Figure 6.10: Removal of isPrSH-SBA-15 / CALB at 60 Minutes

6.3.7 Expanded Pore Supports

The activity of the expanded pore supports is shown below (table 6.19). The activity of the samples is similar to previously observed, the calcined 0.4TMB-SBA-15 sample shows reduced activity relative to the extracted supports, with a small increase in rate

relative to the calcined SBA-15 support. This is likely to be due to improved diffusion of the substrate through the support with the expanded pore system. The thiol functionalised support shows very good activity, with the highest activity observed at 10 mg g^{-1}, due to improved accessibility of the enzyme within the pore system. The thiol functionalised expanded pore support also shows excellent activity at higher loading, indicating the majority of the bound enzyme is accessible and active.

Table 6.19: Acylation with Expanded Pore Supported CALB

Support	Loading / mg g^{-1}	Time / min	(R)-1-PE / %	(R)-1-PA / %	Initial Rate / μmol min^{-1} g^{-1}
0.4TMB-SBA-15	10	30	37.4	12.4	51.6
0.4TMB-SBA-15	25	15	28.8	21.1	175.8
0.4TMB-SBA-15	50	15	20.4	29.8	248.0
0.4TMB-isPrSH-SBA-15 (5%)	10	30	15.0	35.1	146.3
0.4TMB-isPrSH-SBA-15 (5%)	25	15	14.5	35.6	297.1
0.4TMB-isPrSH-SBA-15 (5%)	50	15	5.9	44.2	368.1

6.3.8 Reusability

The reusability of CALB supported on isPrSH-SBA-15 (5%) at a loading of 7.5 mg g^{-1} was investigated, and subsequent conversions are plotted below (figure 6.11). The sample was recovered and washed twice with MTBE between each use. The activity is the sample is retained after four uses, with 75% of the initial activity (85.0 μmol min^{-1} g^{-1}) observed.

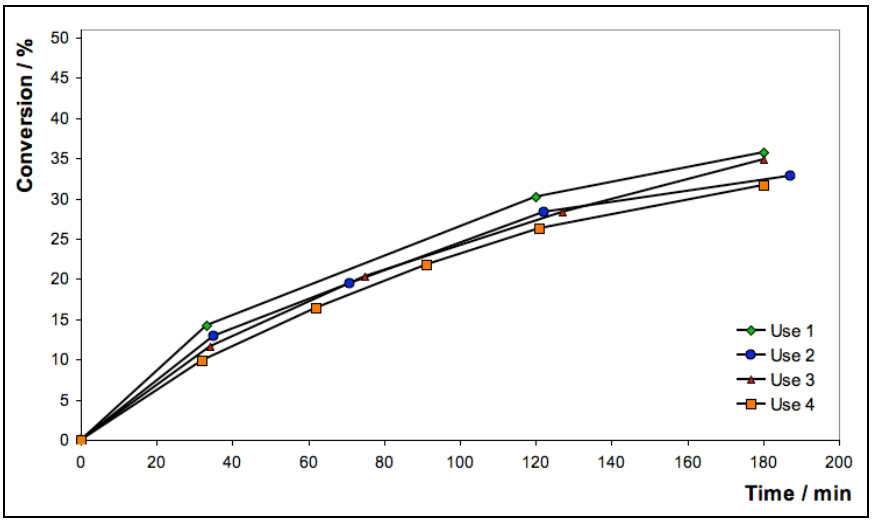

Figure 6.11: Reusability of CALB / isPrSH-SBA-15 (5%)

6.4 Conclusion

6.4.1 Aqueous Catalysis

The activity of CALB immobilised on SBA-15 is reduced relative to the free enzyme, with approximately 12% activity for unfunctionalised samples and 16% for functionalised samples after washing at pH 8. This disadvantage is offset by improved handling properties, improved enzyme stability and simplified purification and reusability.

There is a significant problem with leaching of the immobilised enzyme at pH 8, with poor binding between the enzyme and unfunctionalised materials. There is no observable difference between samples in which the surfactant has been completely removed by calcination or partially removed by ethanol extraction.

This leaching is greatly reduced by the incorporation of organic functional groups, especially sulfur containing groups. The incorporation of amine and carboxylic acid groups has no positive advantages for the binding of CALB, although this may not be the case for other enzymes. There is no observed difference between supports with different thiol concentrations, and between co-condensation or grafting incorporation methods of thiol groups for tributyrin hydrolysis. Samples incorporating a thioether rather than a free thiol showed no observable differences for supporting CALB for tributyrin hydrolysis. The reusability of the thiol functionalised material is also significantly improved relative to the unfunctionalised material, with good retention of activity after reaction at pH 8.

The expansion of the pore size by the addition of trimethylbenzene during synthesis produced did not offer any advantages for tributyrin hydrolysis at 10 mg g^{-1} loading. The unfunctionalised expanded pore support showed reduced activity after washing at pH 8, indicating more enzyme was leached from the support than for the un-expanded SBA-15 sample. CALB supported on expanded thiol functionalised supports showed similar activity to CALB supported on un-expanded thiol functionalised materials.

The stability of the bound enzyme is improved by immobilisation within mesoporous systems, especially for thiol functionalised supports. This is probably due to the strong binding between the surface of the support and the enzyme hindering thermally induced unfolding.

6.4.2 Organic Catalysis

The transfer of CALB immobilised in aqueous conditions to an organic solvent was achieved without loss of activity via a propan-1-ol wash procedure. The immobilised enzyme was highly active for the enantioselective acylation of (R)-1-phenylethanol, without loss of selectivity upon binding.

Unlike aqueous catalysis, the activity of CALB immobilised within mesoporous silica shows a significantly higher activity when compared to the free enzyme. This is due to separation of the catalytic sites throughout the material, and low mobility of the immobilised enzyme preventing activity loss from aggregation.

The method of extraction has an effect on the rate of transesterification, with samples extracted by calcination showing reduced activity relative to ethanol extracted samples. This is probably due to incorporation of hydrophobic groups during the extraction procedure improving the rate of substrate diffusion through the support.

The water content of the samples is important, as the addition of water increases the rate of the competing hydrolysis reaction to produce the alcohol. The rate of reaction is increased by the addition of 4Å molecular sieves, which may be due to removal of residual water from the support.

The incorporation of organic functional groups can improve the rate of reaction, which is probably due to the distribution of the enzyme through the support, the length of the pore system, and the hydrophobicity of the support surface. Supports with hydrophobic groups, especially phenyl groups, show good activity, as do the 5% thiol samples. The reusability of the 5% thiol support is very good, with 75% activity after four uses.

References

[1] H. E. Schoemaker, D. Mink and M. G. Wubbolts, *Science*, 2003, **299**, 1694.
[2] A. Schmid, J. S. Dordick, B. Hauer, A. Kiener, M. Wubbolts and B. Witholt, *Nature*, 2001, **409**, 258.
[3] X. S. Zhao, X. Y. Bao, W. Guo and F. Y. Lee, *Mat. Today*, 2006, **9**, 32.
[4] R. A. Sheldon, *Adv. Synth. Catal.*, 2007, **349**, 1289.
[5] G. Ping, J. M. Yuan, M. Vallieres, H. Dong, Z. Sun, Y. Wei, F. Y. Li and S. H. Lin, *J. Chem. Phys.*, 2003, **118**, 8042.
[6] R. Ravindra, Z. Shuang, H. Gies and R. Winter, *J. Am. Chem. Soc.*, 2004, **126**, 12224.

7. Preliminary Studies on 2nd Generation Catalysts

7.1 Towards BiCatalytic DKR Systems

7.1.1 Introduction

The enzyme catalysed transesterification of a racemic mixture of 1-phenylethanol has a maximum yield of 50%, as the enzyme is enantioselective for only (R)-1-phenylethanol from the racemic mixture. Dynamic kinetic resolution (DKR) involves the racemisation of the unreactive enantiomer by another catalyst in the same system, resulting in a maximum yield of 100% of a racemic mixture to a product comprised of a single enantiomer. This is illustrated in the scheme below (figure 7.1). As the (R)-1-phenylethanol is acetylated, the remaining (S)-1-phenylethanol is converted to a racemic mixture. This racemic mixture will then continue to be acetylated by the enzyme, and this cycle will continue until complete conversion of the racemic starting material is achieved.

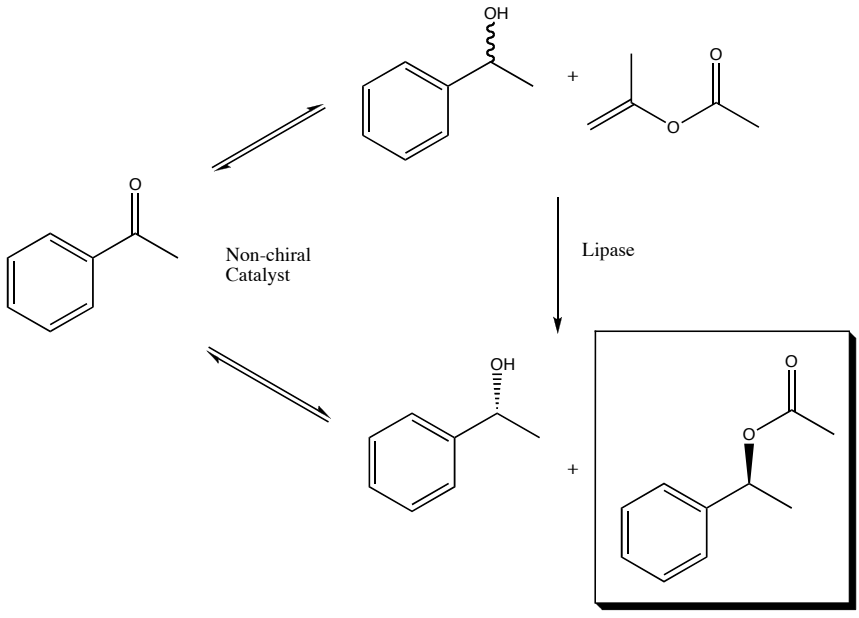

Figure 7.1: Dynamic Kinetic Resolution of (R)-1-Phenylethyl Acetate

There are several catalysts known to catalyse the racemisation of secondary alcohols, and are mostly ruthenium (II) species, although examples exist of palladium[1] and iridium[2] catalysts that can be used. Ruthenium catalysts that have been reported to

racemise secondary alcohols successfully are illustrated below (figure 7.2). These catalysts have been used with immobilised CALB to produce (R)-1-phenylethanol by kinetic resolution,[3] and with Subtilisin Carlsberg to produce (S)-1-phenylethanol by kinetic resolution of 1-phenylethanol.[4]

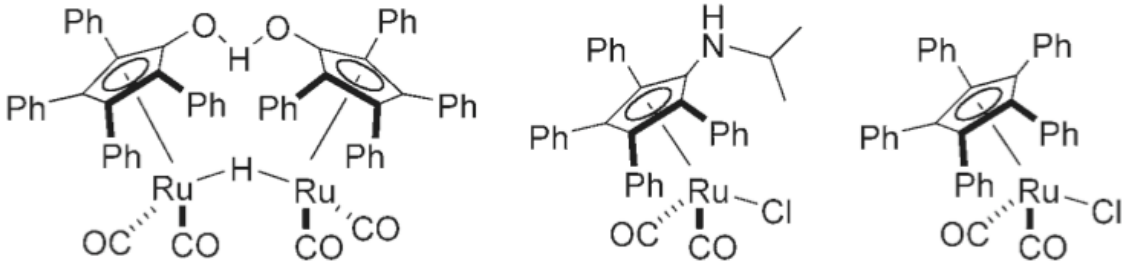

Figure 7.2: Ruthenium (II) Catalysts for Secondary Alcohol Racemisation[4]

Currently, there are many examples in literature of DKR systems that employ two free catalyst systems,[5] or where the racemisation catalyst is free and the lipase is immobilised,[6] but there are few examples of systems in which both catalysts are immobilised (see below for an exception to this). The immobilisation of both catalysts can also prevent a potential problem with these dual catalyst systems, in which one catalyst can be deactivated by the other. By preventing the mobility of both catalysts, a potential deactivation route is removed. A notable system in which both catalysts are immobilised was reported, in which a polymer supported ruthenium (II) catalyst, similar to those illustrated above, was used in conjunction with immobilised CALB for dynamic kinetic resolution (figure 7.3).[7]

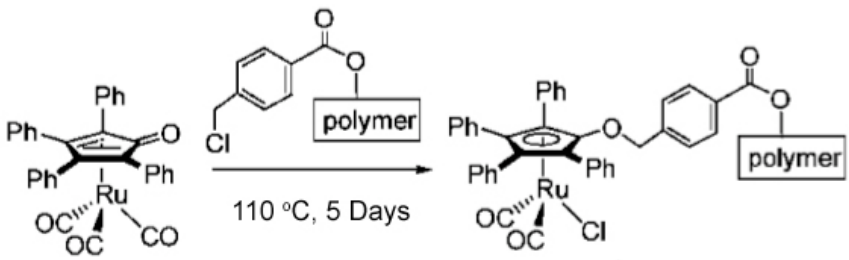

Figure 7.3: Polymer Supported Ruthenium (II) Catalyst[7]

As the enantioselective conversion of (R)-1-phenylethanol with mesoporous SBA-15 supported CALB with a maximum yield of 50% has been previously described (section 6.3), the following experiments describe the attempts to find a suitable immobilised racemisation catalyst for (S)-1-phenylethnol. The catalyst must be selective for the racemisation of secondary alcohols, with no racemisation of (R)-1-phenylethyl acetate.

7.1.2 Racemisation of (S)-1-Phenylethanol by Acidic Zeolites

The racemisation of secondary alcohols has been reported to be catalysed by acidic zeolites.[8, 9] Elevated temperatures were used in the literature reports, which showed a proportional relationship between acid strength and racemisation rate. To investigate the conversion of (S)-1-phenylethanol at temperatures suitable for lipase hydrolysis, a series of acidic zeolites were tested for racemisation activity at room temperature and at 37 °C. The racemisation was investigated by adding 100 mg of each zeolite to a solution of (S)-1-phenylethanol (1.25×10^{-3} mol) and (R)-1-phenylethyl acetate (1.25×10^{-3} mol) in MTBE (5 mL), mixing and measuring the conversion by chiral GC. The results are tabulated below (table 7.1). The conversion of (S)-1-phenylethanol to (R)-1-phenylethanol was poor, with very little conversion observed at room temperature, and only 3.7% conversion by the boron-β sample after 48 hours at 37 °C (85.2% e.e.).

Table 7.1: Racemisation with Acidic Zeolites

Zeolite	Temp. / °C	Time / h	(R)-1-PE	(S)-1-PE	(R)-1-PEA	(S)-1-PEA
Zeolite β	22	48	-	50	50	-
Zeolite β	37	48	0.2	49.8	50	-
Boron-β	22	48	0.5	49.5	50	-
Boron-β	37	48	3.7	46.3	48.8	0.2
USY	22	48	-	50	50	-
USY	37	48	-	50	50	-
ZSM-5	22	48	-	50	50	-
ZSM-5	37	48	0.2	49.8	50	-

To explore the possibility of using a biphasic system for DKR, the zeolite samples were tested for racemisation activity in aqueous conditions. In each experiment, the zeolite (100 mg) was added to distilled water (5 mL) containing (S)-1-phenylethanol (1.25×10^{-3}

mol) and (R)-1-phenylethyl acetate (1.25 x 10^{-3} mol). To measure the extent of conversion, the zeolite was removed by filtration, and the filtrate extracted with diethyl ether (3 x 5 mL), which was dried with magnesium sulfate before analysis by chiral GC. The results are tabulated below (table 7.2). The extraction process does not extract all of the 1-phenylethanol, so the relative intensity of this peak is reduced, resulting in an increase in the relative concentration of 1-phenylethyl acetate in the table below. The zeolite β sample converted the (S)-1-phenylethanol well, with 10% e.e. after 48 hours. However, the zeolite also racemised the product, with only 62% e.e. for the (R)-1-phenylethyl acetate.

Table 7.2: Racemisation with Acidic Zeolites in Aqueous Conditions

Zeolite	Temp. / °C	Time / h	(R)-1-PE	(S)-1-PE	(R)-1-PEA	(S)-1-PEA
No Zeolite	22	48	0	46.4	53.6	0
Zeolite β	22	48	26.0	32.3	33.8	7.9
Boron-β	22	48	3.3	46.1	50.2	0.4
USY	22	48	0	49.5	50.5	0
ZSM-5	22	48	0.2	48.7	51.1	0

A biphasic DKR system comprised of zeolite β and immobilised CALB in a water : MTBE mixture was then tested, and the results are tabulated below (table 7.3). The CALB immobilised on calcined SBA-15 (100 mg, 10 mg g^{-1} CALB) was added to the substrate, in a mixture of distilled water and MTBE (according to the table below), with racemic 1-phenylethanol (2.5 x 10^{-3} mol) and isopropenyl acetate (5.0 x 10^{-3} mol). Each sample was mixed at 37 °C, and the conversion measured by chiral GC. The conversion with both samples was very low, and much slower than without the addition of water. This is because the rate of the competing hydrolysis reaction is increased with the additional water. No racemisation was observed for either sample.

Table 7.3: Transesterification with Immobilised CALB and Acidic Zeolites

Water / mL	MTBE / mL	Time	(R)-1-PE	(S)-1-PE	(R)-1-PEA	(S)-1-PEA
5.0	5.0	24	45.2	50.0	4.7	0.0
5.0	5.0	92	45.8	50.1	4.0	0.0
0.5	5.0	24	46.5	50.0	3.5	0.0
0.5	5.0	92	41.1	50.0	8.9	0.0

7.1.3 Racemisation of (S)-1-Phenylethanol by Ru^{II}-SBA-15

The racemisation of (R)-1-phenylethanol has been reported in literature to be catalysed by ruthenium II complexes.[10, 11] A diphenylphosphine functionalised SBA-15 material was synthesised to incorporate a ruthenium II complex within the mesoporous material, which was then mixed with immobilised CALB to prepare a bicatalytic immobilised DKR system. There is an example in the literature of a ruthenium complex incorporated into SBA-15 using a diphenylphosphine group, which was employed for the racemisation of allylic secondary alcohols.[12]

7.1.3.1 Synthesis of isDPP-SBA-15

The surfactant P123 (4.0 g, 6.86 x 10^{-4} mol)($EO_{20}PO_{70}EO_{20}$, BASF) was dissolved in a solution of HCl (148 mL, 0.8 M) at 40 °C. Tetraethylorthosilicate (7.98 g, 0.0383 mol) and 2-(diphenylphosphino)ethyltriethoxysilane (0.76 g, 2.02 x 10^{-3} mol) were mixed, then added drop-wise to the surfactant mixture and stirred at 40 °C for 24 h. The mixture was then transferred to a thick walled Teflon flask and heated at 100 °C for 48 h. The white solid was collected by filtration, washed with distilled water and the surfactant was removed by Soxhlet extraction with ethanol (250 mL, HPLC Grade). The sample was labelled isDPP-SBA-15.

The nitrogen adsorption / desorption traces are shown below (figure 7.4), which exhibit a type IV isotherm. The surface area by BET was calculated as 598 m^2 g^{-1} and the average pore size as 35.4 Å by BJH analysis.

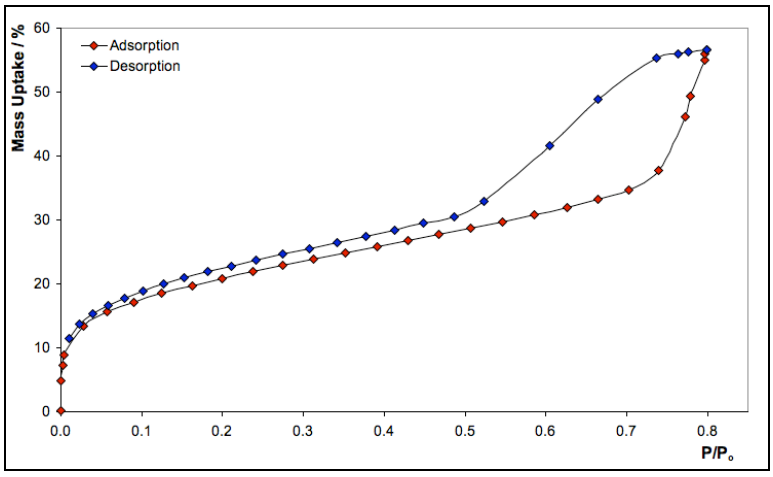

Figure 7.4: isDPP-SBA-15 Nitrogen Adsorption

7.1.3.2 Synthesis of Ru^{II}-SBA-15

The strategy for incorporating a ruthenium (II) complex into the material was to introduce an existing complex with a relatively weak binding η^2 ligand, which would exchange with the phosphines in the solid. Under an inert atmosphere, with dry glassware, $Ru(DMSO)_4Cl_2$ (40 mg, 8.26 x 10^{-5} mol) was added to isDPP-SBA-15 (100 mg) in toluene (10 mL), which was then mixed at room temperature for 12 hours. The solid was then removed by filtration and the ruthenium content of the filtrate measured by ICP, which showed no remaining ruthenium in solution.

7.1.3.3 Racemisation of (S)-1-Phenylethanol by Ru^{II}-SBA-15

The racemisation properties of $isRu^{II}$-SBA-15 were investigated by adding 100 mg to a solution of (S)-1-phenylethanol (1.25 x 10^{-3} mol), (R)-1-phenylethyl acetate (1.25 x 10^{-3} mol) and isopropenyl acetate (5.0 x 10^{-3} mol) in MTBE (5 mL). The relative concentration of each component was measured, and this is tabulated below (table 7.4). The relative concentration of (R)-1-phenylethyl acetate increases during the course of the reaction, this may be due to a side reaction of (S)-1-phenylethanol decreasing the concentration relative to (R)-1-phenylethyl acetate. No other compounds are observed by GC, so the reaction would have to yield an insoluble or fully adsorbed product. No racemisation is observed of (S)-1-phenylethanol.

Table 7.4: Racemisation with $isRu^{II}$-SBA-15

Sample	Temp. / °C	Time / h	(R)-1-PE	(S)-1-PE	(R)-1-PEA	(S)-1-PEA
$isRu^{II}$-SBA-15	22	12	0.0	45.0	55.0	0.0
$isRu^{II}$-SBA-15 + ^{t}OBu	22	12	0.0	47.9	51.9	0.2
$isRu^{II}$-SBA-15 + IPA	22	48	0.0	37.1	62.8	0.1

7.1.3.4 DKR with Immobilised CALB and Ru^{II}-SBA-15

To investigate the stability of immobilised CALB to the presence of the ruthenium complex and the isDPP-SBA-15 support, the transesterification properties of CALB immobilised on calcined SBA-15 were measured. The immobilised CALB (100 mg, 10 mg g^{-1}) and $isRu^{II}$-SBA-15 (100 mg) were added to a solution of (S)-1-phenylethanol (1.25 x 10^{-3} mol), (R)-1-phenylethyl acetate (1.25 x 10^{-3} mol) and isopropenylacetate (5.0 x 10^{-3} mol). The reaction was monitored by GC, and the results are shown below (table 7.5). The

rate of conversion is 39.4 μmol min^{-1} g^{-1}, compared to 69.3 μmol min^{-1} g^{-1} for CALB without the $isRu^{II}$-SBA-15. This reduction in rate may be due to a competing side reaction, or possibly due to adsorption of a reactive species by the phosphate.

Table 7.5: Transesterification with $isRu^{II}$-SBA-15 and Immobilised CALB

Sample	Time / h	(R)-1-PE	(S)-1-PE	(R)-1-PEA	(S)-1-PEA
$isRu^{II}$-SBA-15 + CALB	1	30.9	50.1	18.9	0.0
$isRu^{II}$-SBA-15 + CALB	12	12.3	49.8	37.9	0.0

7.1.4 Conclusion

The dynamic kinetic resolution of 1-phenylenthanol requires a suitable catalyst for the racemisation step. The catalyst must be selective for the alcohol and not the acetate. A catalyst that will operate in organic media is required as a biphasic system is not efficient for transesterification. The synthetic strategy discussed above to incorporate a ruthenium catalyst into a mesoporous support via a diphenylphosphine functional group may be a valid route to a working catalyst, as the enzyme will still operate under these conditions, but further research is required to prepare a successful DKR system.

7.2 Encapsulating CALB in SBA-15

7.2.1 Introduction

To understand the advantages of an encapsulation system for the immobilisation of CALB, or any small globular protein, it is useful to review the advantages and disadvantages of the adsorption systems discussed previously. The adsorption systems typically retain the enzyme in the active form, unlike covalent methods, which can denature the enzyme upon binding.[13, 14] However, the fact that the enzyme can be removed from the material is a significant problem, as both the activity is reduced and the product of a reaction can be contaminated by protein impurities.[15]

To address these problems, an encapsulation method is described below that consists of two distinct steps. Firstly, the enzyme is adsorbed into the mesoporous material as previously described at a loading of 10 mg g^{-1}, this is followed by the addition of an encapsulating agent which reacts with the support and prevents the leaching of the enzyme from the material. There are some challenges inherent in this approach. Firstly, the enzyme

must remain active during the encapsulation step, and secondly, the enzyme must remain accessible to the substrate. As the degree to which the enzyme is entrapped within the material has an inverse relationship with the accessibility to substrate, the conditions must be carefully controlled. Mesoporous systems in which the pore size is very close to the diameter of the enzyme have a significant advantage over alternative systems, as the support does not require a great deal of modification to prevent leaching of the enzyme.

7.2.2 Encapsulating CALB With Tetraethoxysilane

In this experiment an organic solvent (MTBE) was added after immobilisation and washing (2 x 5 mL, pH 6, phosphate). Propan-1-ol was not used as an intermediate solvent in order to maintain the aqueous environment within the pore system, with MTBE as the bulk phase. The encapsulating agent added was tetraethoxysilane, which was added slowly by a syringe pump to the stirred mixture. The hypothesis is that the TEOS will hydrolyse upon contact with the aqueous environment of the pore system, followed by condensation with the silica support, reducing the effective pore diameter and preventing leaching of CALB. The condensation will be localised within the pore system and the surface of the support, due to the organic solvent, and slow addition, will minimise the self-condensation of TEOS.

7.2.3 Conditions

Calcined SBA-15 (0.25g, 4.16 x 10^{-3} mol) was added to a CALB solution (10 mL, 0.25 mg mL^{-1}) at pH 6 (phosphate, 50 mM), this mixture was stirred at 4 °C for 12 h. The solid was recovered by centrifugation and the activity of the supernatant measured by *p*-NPB hydrolysis. The immobilised CALB was transferred to MTBE (20 mL, > 98%) and stirred with a magnetic follower. Tetraethoxysilane (0.087 g, 4.16 x 10^{-4} mol) in MTBE (5 mL), was added to the immobilised CALB with a syringe pump at a rate of 0.5 mL h^{-1}. The solid was collected by centrifugation, then packed within an adjustable Omnifit column (see section 5.4) and washed with pH 6 buffer (10 mL, 50 mM, phosphate), followed by pH 8 buffer (40 mL, 50 mM, phosphate). Aliquots were collected and measured for protein content by Bradford's assay.

7.2.4 Leaching and Activity of CALB

The leaching of CALB from the TEOS encapsulated sample is compared to the leaching of adsorbed CALB from calcined SBA-15 below (table 7.6). No leaching of enzyme was observed when washing at pH 8, indicating successful condensation of the TEOS to the support surface, preventing the enzyme from leaching from the support.

Table 7.6: Enzyme Content of Wash Aliquots

Wash Volume / mL	Adsorbed Leaching / mg mL^{-1}	Encapsulated Leaching / mg mL^{-1}
5	0.04	0
10	0.02	0
12	0.03	0
14	0.09	0
16	0.67	0
18	1.18	0
20	1.11	0
22	0.70	0
24	0.48	0
26	0.32	0

The sample was then measured for tributyrin hydrolysis activity as previously described (section 4.5) at STAT pH 8.0. However, no activity was observed for the sample, indicating that either the enzyme was denatured during the addition of TEOS or that the active site of the enzyme is inaccessible to substrate.

7.2.5 Encapsulating CALB With 3-Mercaptopropyltriethoxysilane

To further investigate the encapsulation of CALB a similar experiment as described above was carried out with 3-mercaptopropyltriethoxysilane (9.9 mg, 4.16 x 10^{-5} mol) as the encapsulating agent at a lower concentration (1 molar percent) rather than TEOS. It was thought that the thiol group of the triethoxysilane may bind to the enzyme, followed by condensation to the surface, preventing the enzyme from leaching from the pore system.

After mixing with the encapsulating agent for 12 hours, the sample was recovered by centrifugation. To measure the leaching the sample was suspended in aliquots of 5 mL pH 8.0 buffer and mixed, followed by separation by centrifugation and analysis by

Bradford's assay (30 mL total volume). No enzyme was measured in any of the washes by Bradford's assay, indicating no leaching of the enzyme, either active or denatured. The tributyrin hydrolysis activity of the sample was measured at 22 μmol min^{-1} g^{-1}, much lower than the average activity for unencapsulated CALB on SBA-15 after washing at pH 8.0, which was 607 μmol min^{-1} g^{-1}. As above, it is not clear if this is due to an inaccessibility of the enzyme active site, or due to the denaturation of the enzyme during the encapsulation process. However, the addition of 1 molar percent of 3-mercaptopropyltriethoxysilane is unlikely to completely block access the enzyme active site, and it is probable that the enzyme has been denatured.

7.2.6 Encapsulation in Aqueous Conditions

In order to try and minimise the enzyme denaturation the encapsulation was investigated in aqueous buffer rather than MTBE, although this increases the probability of self-condensation by the encapsulating agent. To minimise self-condensation, the addition of the encapsulation agent was immediate, rather than slowly with a syringe pump, and the system was buffered at pH 6, which greatly reduces the rate of alkoxysilane hydrolysis, as the hydrolysis is catalysed by acids and bases. The buffer should also stabilise the protein, and prevent deactivation by overloading the buffer, as may have occurred in the MTBE system described above.

7.2.7 Encapsulation with 3-Mercaptopropyltriethoxysilane at pH 6

CALB was immobilised at 10 mg g^{-1} within calcined SBA-15 (0.25 g) as discussed previously, and washed with pH 6 buffer (2 x 5 mL, phosphate). The sample was suspended in pH 6 buffer (10 mL, 50 mM, phosphate) to which 3-mercaptopropyltriethoxyilane (9.9 mg, 4.16 x 10^{-5} mol) was added. The mixture was then stirred for 12 hours at 4 °C. The sample was recovered by centrifugation and washed with pH 6 buffer (2 x 5 mL) followed by pH 8 buffer (6 x 5 mL), the enzyme content of which was measured by Bradford's assay.

As above, no enzyme leaching at either pH 6 or pH 8 was observed, indicating successful entrapment of the enzyme within the support. The activity was measured by tributyrin hydrolysis at pH 8, and a rate of 301 μmol min^{-1} g^{-1} was recorded. This is approximately half of the initial rate observed for CALB adsorbed by calcined SBA-15 at

the same loading after washing at pH 8. Encouragingly, reusability of the material was very good, with no loss of activity after five assays, and is compared to the reusability for adsorbed CALB below (figure 7.5).

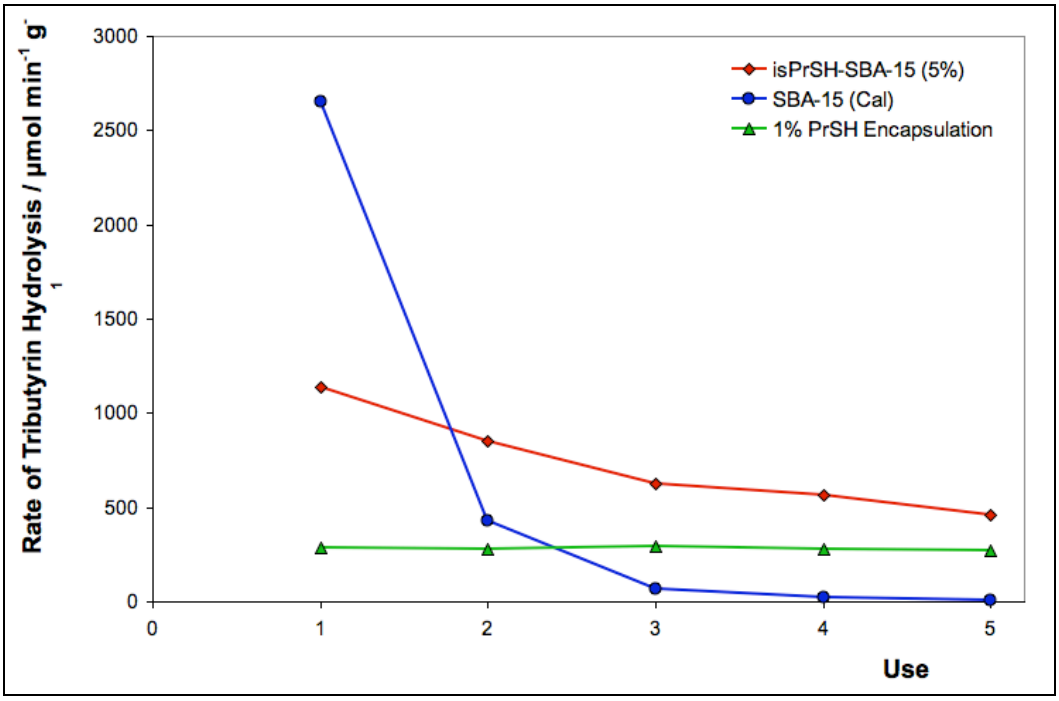

Figure 7.5: Reusability of 1% PrSH Encapsulated CALB

7.2.8 Alternative Encapsulating Agents and Concentrations

To investigate the encapsulation system, and to determine if the reduction in activity is due denaturation or inaccessibility, the experiment above was repeated for a series of concentrations and different encapsulation agents (table 7.7). Octyltriethoxysilane ($C_8H_{17}Si(OEt)_3$) was added to investigate the effect of non-thiol containing groups. Chloro(dimethyl)thexylsilane ($((CH_3)_2CHC(CH_3)_2Si(CH_3)_2Cl$) was used to investigate the effect of a chlorosilane encapsulating agent, which binds to the surface of the support, eliminating HCl, and removing the possibility of self-condensation. Hexadimethrine bromide was added in an attempt to prevent the release of CALB from the support via electrostatic interactions.

The thiol encapsulated samples show a clear relationship between the concentration of the encapsulating agent and initial activity, with higher concentrations resulting in lower activity. This may be due to denaturation of the enzyme, as by increasing the mixing time

to 72 hours at 1% encapsulation, the enzyme activity is reduced almost completely. It is unlikely that complete attachment to the surface will completely prevent substrate access at this concentration of 3-mercaptopropyltriethoxysilane.

Table 7.7: Encapsulation Data

Encapsulation Agent	Amount / mol. %	Time / h	Activity / μmol min^{-1} g^{-1}
$(OEt)_3SiPrSH$	0.5	12	555
$(OEt)_3SiPrSH$	1.0	12	301
$(OEt)_3SiPrSH$	1.0	72	1
$(OEt)_3SiPrSH$	2.0	12	238
$(OEt)_3SiPrSH$	5.0	12	56
$(OEt)_3SiC_8H_{17}$	1.0	12	543
Chloro(dimethyl)thexylsilane $(CH_3)_2CHC(CH_3)_2Si(CH_3)_2Cl$	1.0	12	542
Hexadimethrine Bromide $C_{13}H_{30}N_2Br_2$	1.0	12	176

The reusability of these samples is shown below (figure 7.6), where chloro(dimethyl)thexylsilane is labelled R_3SiCl. The hexadimethrine bromide and octylsilane encapsulations show poor reusability, indicating that the enzyme is leached during the pH 8 assay, and thus is not entrapped within the support. It is not clear why the bulky octyltriethoxysilane does not prevent leaching of the enzyme, as condensation of the bulky group is expected to block the pore system. There may be some aggregation of the hydrophobic alkyl chains in aqueous media, and subsequent self-condensation, although this has not been investigated. The 0.5% propylthiol encapsulation sample shows reasonably good reusability, with 81% activity retained after five uses. The 1% and 2% propylthiol encapsulation samples show excellent reusability with very little activity loss after five uses (97% and 92% activity retained).

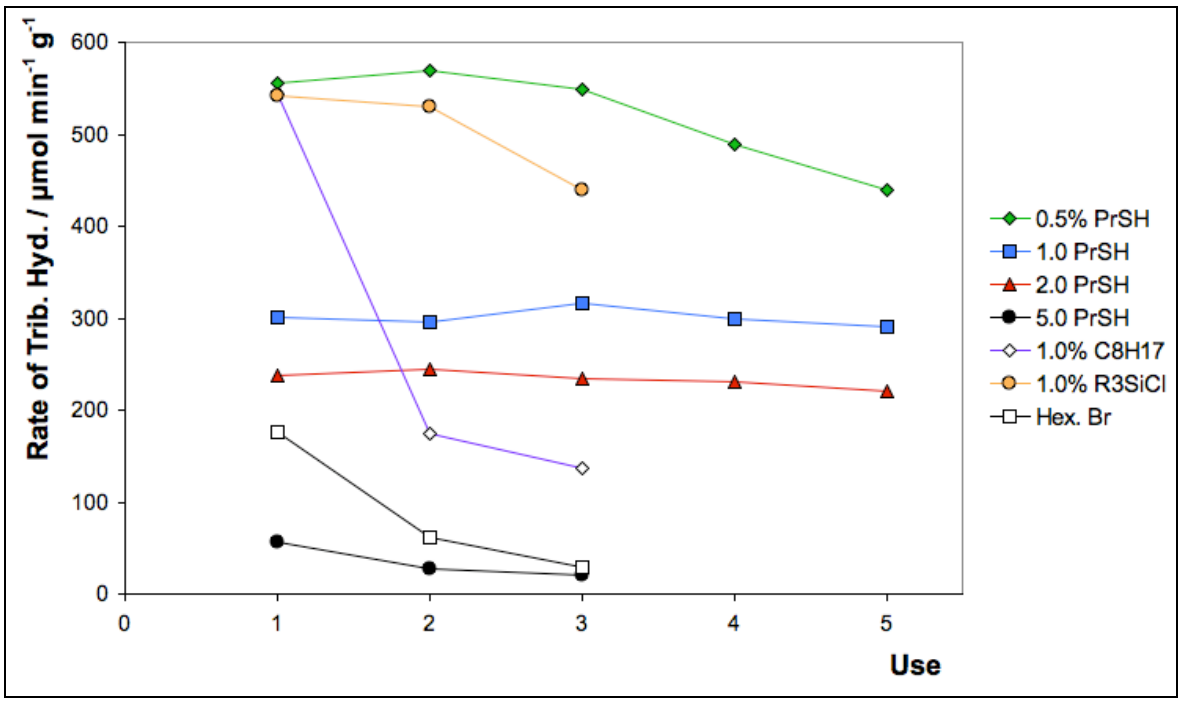

Figure 7.6: Reusability of Encapsulated CALB

7.3 Conclusion

CALB has been successfully encapsulated within mesoporous silica by the addition of 3-mercaptopropyltriethoxysilane to immobilised CALB on calcined SBA-15. The reusability of encapsulated CALB is excellent, with much lower leaching than comparable adsorption systems. This is an effective and simple method for immobilisation of CALB for catalysis in aqueous systems. The encapsulation does not require large structural changes to the material to prevent the leaching of enzyme, even at a pH removed from the isoelectric point of the enzyme. There is potential for development of these systems as an excellent route to immobilised enzymes, which require little modification of the enzyme or the support to prepare a robust immobilised enzyme that can be used repeatedly for aqueous catalysis.

References

[1] R. Sturmer, *Angew. Chem., Int. Ed.*, 1997, **36**, 1173.
[2] Y. Y. Li, X. Q. Zhang, Z. R. Dong, W. Y. Shen, G. Chen and J. X. Gao, *Org. Lett.*, 2006, **8**, 5565.
[3] B. A. Persson, F. F. Huerta and J. E. Backvall, *J. Org. Chem.*, 1999, **64**, 5237.

[4] L. Boren, B. Martin-Matute, Y. M. Xu, A. Cordova and J. E. Backvall, *Chem. Eur. J.*, 2005, **12**, 225.
[5] N. J. Turner, *Curr. Opin. Chem. Biol.*, 2004, **8**, 114.
[6] F. F. Huerta, A. B. E. Minidis and J. E. Backvall, *Chem. Soc. Rev.*, 2001, **30**, 321.
[7] N. Kim, S. B. Ko, M. S. Kwon, M. J. Kim and J. Park, *Org. Lett.*, 2005, **7**, 4523.
[8] S. Wuyts, K. De Temmerman, D. E. De Vos and P. A. Jacobs, *Chem. Eur. J.*, 2004, **11**, 386.
[9] Y. Z. Zhu, K. L. Fow, G. K. Chuah and S. Jaenicke, *Chem. Eur. J.*, 2007, **13**, 541.
[10] J. H. Choi, Y. H. Kim, S. H. Nam, S. T. Shin, M. J. Kim and J. Park, *Angew. Chem., Int. Ed.*, 2002, **41**, 2373.
[11] T. H. Riermeier, P. Gross, A. Monsees, M. Hoff and H. Trauthwein, *Tetrahedron Lett.*, 2005, **46**, 3403.
[12] H. X. Li, F. Zhang, Y. Wan and Y. F. Lu, *J. Phys. Chem. B*, 2006, **110**, 22942.
[13] X. S. Zhao, X. Y. Bao, W. Guo and F. Y. Lee, *Materials Today (Oxford, United Kingdom)*, 2006, **9**, 32.
[14] U. T. Bornscheuer, *Angew. Chem., Int. Ed.*, 2003, **42**, 3336.
[15] R. A. Sheldon, *Adv. Synth. Catal.*, 2007, **349**, 1289.

8. General Conclusions and Further Work

8.1 General Conclusions

The synthesis and characterisation of a range of mesoporous materials based on SBA-15 have been described. The materials are thick-walled and stable to heat treatment in aqueous conditions. The material was templated by surfactant, which resulted in a hexagonal structure (p6mm) with a narrow pore size distribution. The surfactant was removed, either by calcination or extraction by solvent. The surface of a calcined material is fully condensed, and this surface is hydrolysed in aqueous conditions without disruption of the structure, to generate a surface comprised largely of silanol groups.

The incorporation of organic functional groups was demonstrated by co-condensation and by post-synthesis grafting. These functional groups can alter the morphology of the structure when incorporated by co-condensation, and a change from hexagonal to cubic symmetry was observed with increasing propyl thiol concentration. A wide range of functional groups were incorporated, although incorporation of basic amine groups resulted in a poorly ordered material at high concentration. The pore size of the material was increased with the addition of trimethylbenzene during synthesis, which also changed the morphology of the material to a foam-like structure.

The immobilisation of CALB within the mesoporous materials synthesised was rapid, and a high uptake of enzyme was possible, with a maximum loading of 450 mg g^{-1} measured. The uptake of the enzyme was poor when the surfactant template was not extracted, indicating that the enzyme is located within the pore system of the support. This was supported by nitrogen adsorption experiments on immobilised CALB samples, with lower adsorption of nitrogen as the enzyme content was increased. However, the leaching of enzyme at a pH removed from the isoelectric point of the protein was a significant problem with unfunctionalised systems. This leaching was significantly reduced by the incorporation of sulfur containing groups on the surface of the material, which stabilise the enzyme via van der Waal's interactions. The uptake of enzyme by thiol functionalised materials is described by a two step model, in which the enzyme is quickly adsorbed by the support and then diffuses through the pore system at a slower rate. Once the enzyme was

adsorbed within thiol functionalised materials, it was not readily removed, with very low levels of leaching measured after washing with pH 8 phosphate buffer. CALB was also immobilised successfully on expanded pore supports, with rapid uptake at high levels of enzyme incorporation.

The rate of reaction in aqueous conditions for the hydrolysis of tributyrin was complicated by the leaching of enzyme from unfunctionalised supports that bind the enzyme poorly. The reusability with these supports was poor, with very low activity after only five reuses. For the supports which bind CALB strongly, including the thiol functionalised materials, little difference in hydrolysis activity was observed when the sample was washed with pH 8 buffer. The thiol supported CALB samples showed good reusability over successive reactions. CALB supported within thiol functionalised supports showed higher stability toward thermal degradation than unfunctionalised supports, and all supported CALB samples showed a large improvement over the free enzyme. This is due to strong binding to the surface of the support hindering unfolding of the enzyme at high temperature.

The enantioselective acylation of (R)-1-phenylethanol was catalysed by immobilised CALB in organic solvents, with much higher activity measured for the mesoporous supported enzyme than for a powder dispersion of free enzyme. The activity of the immobilised enzyme was higher with calcined supports, which may be due to the incorporation of ethoxide groups on the surface of the material during extraction, resulting in faster substrate diffusion. The incorporation of organic functional groups has a direct effect on the rate of the reaction, with hydrophobic organic groups increasing the initial rate, due to improved substrate diffusion. There is no leaching of enzyme observed from the mesoporous supports, with good reusability properties of the immobilised enzyme.

The encapsulation of CALB within mesoporous silica was also demonstrated, although retaining the activity of the enzyme was challenging. Although the initial rate of reaction was reduced relative to adsorbed CALB, the reusability properties were excellent, with no activity loss observed after five uses when the enzyme was encapsulated by 3-mercaptopropyltriethoxysilane.

8.2 Further Work

There is considerable scope for further study and modification of the experiments previously described. The modification of the support material morphology is possible, with the properties of larger pore supports holding considerable interest, as larger pore supports not only have potentially better substrate diffusion properties, they can also potentially accommodate larger enzymes, such as cytochrome P450 or glycosidases.

As good reusability and low enzyme leaching from the thiol functionalised supports was demonstrated, the nature of binding for enzymes that have unbridged cysteine residues on the surface of the protein can be studied, and the potential formation of disulfide bonds can be investigated. This could be compared with established methods for covalent attachment, although attempts at binding CALB via glutaraldehyde and other covalent binding methods (not reported) were unsuccessful.

The preliminary studies on mesoporous systems for DKR could be explored further, as immobilised CALB within mesoporous support shows good activity and excellent selectivity for the kinetic resolution of secondary alcohols. This would require a study of racemisation catalysts, and the ruthenium catalysts described in section 7.1.1 may provide good targets for immobilisation studies.

The encapsulation methods described above are very promising methods for maintaining the advantages of adsorption systems, with very little enzyme leaching in aqueous conditions. Investigation with a smaller substrate may elucidate the reason for the activity loss during encapsulation. The development of alternative encapsulation methods, and a detailed study of the kinetics and stability of the encapsulated enzyme would be an interesting study. The adaptation of these methods to larger support materials and alternative enzymes could lead to simple methods of immobilisation that would produce highly robust heterogeneous catalysts. One potential route to encapsulation of an enzyme without deactivation would be to first immobilise the enzyme on a thiol functionalised support. The surface of the catalyst could then be reacted with a bulky compound incorporating a free thiol group, to encapsulate the enzyme via disulfide formation between the support and the bulky thiol.